

SYSTEMATIC INVESTIGATION OF CELLULAR RESPONSE TO NANOPARTICLE  
SURFACE CHEMISTRY



by  
Melike Sarıçam

Submitted to Graduate School of Natural and Applied Sciences  
in Partial Fulfillment of the Requirements  
for the Degree of Doctor of Philosophy in  
Biotechnology

Yeditepe University

2019

SYSTEMATIC INVESTIGATION OF CELLULAR RESPONSE OF NANOPARTICLE  
SURFACE CHEMISTRY

APPROVED BY:

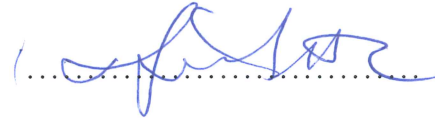
Prof. Dr. Mustafa Çulha  
(Thesis Supervisor)  
(Yeditepe University)



Prof. Dr. Gamze Torun Köse  
(Yeditepe University)



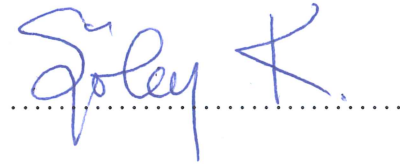
Assist. Prof. Dr. Hüseyin Çimen  
(Yeditepe University)



Assist. Prof. Dr. Sultan Sibel Erdem  
(İstanbul Medipol University)



Assist. Prof. Dr. Şölen Kınayyigit  
(Gebze Technical University)



DATE OF APPROVAL: .... / .... / 2019



*Dedicated to my lovely sister,  
offering unconditional love...*

## ACKNOWLEDGMENTS

During my lovely five-year journey with challenges and learning, I have met a lot of brilliant people, who touched my life, taught me, helped me to improve myself and encouraged me to do the best. Let me “cite” them before crying.

I would like gratefully thanks to my supervisor, Prof. Dr. Mustafa Çulha, to accept me in his group as a member, force me improve myself and give me the chance to work as a researcher in two important projects, COST Action (MP1302) funded by TUBITAK (Project no: 113Z554) and TUBITAK 1001 project (Project no: 214Z224). On his coattails, I learned how to think like a scientist. If I can identify myself as a “junior” scientist, this is thanks to his support and teaching. In addition, I will never forget his funny speech he did in the first day of Ramadan.

I would like to express my gratitude to two precious members of my thesis monitoring jury, Assist. Prof. Sibel Sultan Erdem and Assist. Prof. Hüseyin Çimen, for allocated their valuable time and providing constructive comments throughout the thesis monitoring meetings.

My sincere thanks go to kind members of Pharmacy Department of Yeditepe University, Prof. Dr. Meriç Köksal Akkoç, Prof. Dr. Mine Yarım Yüksel and Technical specialist Bilal Şenkal, thanks to provide laboratory facilities for me to thiolate carbohydrates.

When considered the five-year journey, the first following paragraph must be reserved for my “second crazy apla” as Dr. Gamze Kuku. At least two years, we worked together, we grown up together, we cried together, we laughed together, we were exhausted in the lab together and we shared too many precious moments. Only she can know what happens to me in the lab after 4:00 pm. Thanks to her excellent Excel skills, first I was illuminated and then I grown up new junior Gamziis. It would be impossible to write everything I feel about her, but I could tell that she has an important place in my heart.

The next paragraph goes to... “Meğmeeeee”, M.S. Merve Ercan, who is my second partner came from The British royal family. I feel grateful to know her and spend time together. We accomplished a tough project together, yes, we did! I will never forget her, her calmness, her vintage style, our song, “Shape of you, Ed Sheeran” and adventure of İTK .

My heart forced me to open a new paragraph for PhD. Can. Deniz Uzunoğlu, “Uzunummm”, who is my secret soul mate. Most probably she would have been my next lovely partner in Nanolab if I had had enough time before graduation. Even though she had no specific reason, she always gave me her spiritual support. No one can fill her place in my heart and no one can cause me to forget her.

I am appreciated to meet my sweet sisters and friends, M.S. Hamide Özeydin Murtezaoğlu “scorpion”, Hande Duru “The romantic Kızıl, one over one million”, Phd. Can. Zeynep Işık “Movie queen and mom of Ayşe”, Phd. Can. Zehra Çobandede “The body shape of mercy, Zehyaaa, mom of Furkii, the best mom”, Ayşe Çinkılıç “new born Nanolab member, the most atarlı after me”, Dr. Sevda Deniz Mert “The Bro”, Dr. Seda Keleştemur “The mom of nanaks”, Dr. Fatma Özen “The business women, who cannot let you pick up the bill in her presence”, Dr. Bahar Hazal Yalçinkaya “The best friend ever”, Dr. Mine Altunbek “my first teacher in Nanolab and pretty partner of Macera Dolu Amerika”, Dr. Cansu Ümran Taş Tunç “Origami lady, nice Budgie”, Dr. Pınar Akkuş Süt “Big origami lady, the one found best carbohydrate thiolation procedure and I am appreciated for this”, Dr. Hülya Yılmaz “Post. Doc. of Hülya Avşar”, PhD. Std. Nurselin Kaya “The traveller”, M.S. Gizem Uçankuş “Oligonucleotide lady”, M.S. Deniz Yaşar Öztaş “Tweety”, Dr. Melis Emanet and Dr. Özlem Şen “The BNNT girls”, PhD. Can. İnci Kurt Celeb “Minnie” and Phd. Can. Zeynep Büşra Bolat “The best supporter for thesis completion”. Finally, I would like say my thanks to Dr. Şaban Kalay “USS, KSS, ASS and unique male member of Nanolab” and PhD Can. Ertuğ Avcı “SERS man”.

My pretty “ponçık” friends from high school, Alev Pöke, Kübra Kaya ve Yağmur Şengül... I am glad to encounter with you and live enormously perfect time during and after school. Who is marrying first? Ouch, I remember, she is Alev, the one is the against of marriage!

People say: “Behind each successful person there is a strong woman”. No one deserves a greater thankfulness than you, my strong woman, Gülsen Sariçam. I am appreciated that you support me either morally or financially. I have no idea what I would do in your absence.

I would like present my gratitude to my lovely mom, Emriye Sariçam, and my brother, Murat Sariçam, for their endless support and blessings. Moreover, I am grateful to all my relatives, who supported me, felt proud of me and prayed for me.

As last sentences, I would like to say my thanks to my dad and my brother, Abdülkadir and Suat Sariçam, since they grown me up as a strong, fair and honest girl by creating an invisible wall behind me. I am sure you always watch me from somewhere and be proud of me. Keep watching, your babe will reach the top!

## ABSTRACT

### SYSTEMATIC INVESTIGATION OF CELLULAR RESPONSE TO NANOPARTICLE SURFACE CHEMISTRY

The interface between nanoparticles (NPs) and living systems is one of the most important determinants of cellular responses. The well-understanding of the interaction between the NP surface chemistry and living systems makes possible to design safer NPs to be used in medical and technological areas. In this study, it was aimed to systematically investigate the cellular response of living cells to subtle surface chemistry changes on AuNPs conjugated with specially designed carbohydrates and peptides. In order to create small differences on AuNP surfaces, spherical AuNPs of 13 nm diameter size were modified with four carbohydrates, D-Glucose, D-Mannose, Lactose and Mannose, and fourteen peptides different in charge, length, isoelectric point, sequence with or without RGD and free end terminus -NH<sub>2</sub> or -COOH. The cellular responses of A549, BEAS-2b and MDA-MB-231 cells were investigated by considering cellular uptake, cytotoxicity and cell cycle arrest. Before modification of AuNP surfaces, carbohydrates were thiolated using Lawesson reagent. Then, AuNPs with an average size of 13 nm were conjugated with carbohydrates and peptides in appropriate conditions. The naked AuNPs and AuNP conjugates were characterized with UV/Vis spectroscopy, DLS, agarose gel electrophoresis, FTIR and SERS to understand the nature of the interactions of the used biomacromolecules on the AuNPs surfaces. The peptides designed by placing cysteine to -NH<sub>2</sub> or -COOH end showed significantly different binding affinity to AuNPs surfaces. Then, the cellular response of the conjugates were investigated using several molecular techniques including WST-1 cell proliferation assay, Apoptosis/Necrosis assay, Clonogenic assay and cell cycle evaluation assay. It was found that small changes on the surfaces of AuNPs caused varying significant cellular responses depending on surface chemistry, NP concentration and cell line type.

## ÖZET

### NANOPARÇACIK YÜZEY KİMYASINA HÜCRENİN VERDİĞİ TEPKİNİN SİSTEMATİK ARAŞTIRILMASI

Nanopartiküller (NP'ler) ve canlı sistemler arasındaki arayüz, canlı sistemlerin verdiği tepkilerin en önemli belirleyicilerinden biridir. NP yüzey kimyası ve canlı sistemler arasındaki etkileşimin iyi anlaşılması, tıbbi ve teknolojik alanlarda kullanılacak daha güvenli NP'lerin tasarlanmasını mümkün kılar. Bu çalışmada, özel olarak tasarlanmış karbonhidratlar ve peptidlerle konjuge edilmiş AuNP'lerin yüzeyindeki küçük yüzey kimyası değişikliklerine hücrelerin verdiği tepkinin sistematik olarak araştırılması amaçlanmıştır. AuNP yüzeylerinde küçük farklılıklar oluşturmak için, 13 nm boyutlu AuNP'ler dört farklı karbonhidrat, D-Glikoz, D-Mannoz, Laktoz ve Mannoz, ve yük, uzunluk, izoelektrik noktası, RGD'li veya RGD'siz dizilime sahip oluşu ve  $-NH_2$  veya  $-COOH$  serbest uca sahip oluşuna göre farklı olan on dört tane peptit ile modifiye edilmiştir ve A549, BEAS-2b ve MDA-MB-231 hücrelerinin hücresel cevapları hücresel alınım, sitotoksositeye ve hücre döngüsüne olan etkileri dikkate alınarak incelenmiştir. AuNP yüzeylerine modifikasyon yapılmadan önce, karbonhidratlar Lawesson reaktifi kullanılarak tiollenmiştir. Ardından, ortalama 13 nm boyutta AuNP'ler karbonhidratlar ve peptitler uygun koşullarda işlevleştirilmiştir. Çıplak AuNP'ler ve AuNP konjugatları, yüzeydeki biyomakromoleküllerin etkileşimlerinin doğasını anlamak için UV/Vis spektroskopisi, DLS, Agaroz jel elektroforezi, FTIR ve SERS ile karakterize edilmiştir. Örneğin, sisteinin peptitlerin  $-NH_2$  ya da  $-COOH$  uçlarındna olması, AuNP yüzeylerine önemli ölçüde farklı bağlanma eğiliminde olduğunu göstermiştir. Daha sonra, AuNP konjugatlarının hücrelerde meydana getirdiği tepkiler, WST-1 hücre çoğalma, Apoptosis/Necrosis, Klonojenik ve hücre döngüsü belirleme deneyi gibi çeşitli deneylerle incelenmiştir. AuNP'lerin yüzeylerindeki küçük değişikliklerin, NP konsantrasyonuna ve hücre tipine bağlı olarak değişen hücresel tepkilere neden olduğu bulunmuştur.



## TABLE OF CONTENTS

ACKNOWLEDGMENTS .....	iv
ABSTRACT.....	vii
ÖZET .....	viii
LIST OF FIGURES .....	xiv
LIST OF TABLES.....	xxv
LIST OF SYMBOLS/ABBREVIATIONS.....	xxvii
1. INTRODUCTION .....	1
1.1. NANOPARTICLES .....	1
1.2. NANOPARTICLE-BIOCONJUGATE CHEMISTRY .....	3
1.2.1. Challenges in Bioconjugation of Nanoparticles .....	4
1.2.2. Criteria for Ideal Bioconjugation Chemistry .....	5
1.2.3. General Bioconjugation Strategies .....	7
1.2.3.1. Electrostatic Adsorption .....	7
1.2.3.2. Direct Attachment.....	10
1.2.3.3. Covalent Attachment .....	10
1.2.3.4. Ligand-Receptor Interaction .....	11
1.2.3.5. Encapsulation.....	12
1.3. GOLD NANOPARTICLES.....	13
1.3.1. History .....	13
1.3.2. Synthesis.....	15
1.3.3. Properties .....	17
1.3.4. Surface Chemistry and Bioconjugation.....	19
1.3.5. Characterization of AuNP-Biomolecule Conjugates.....	23
1.4. NANOTOXICITY .....	23
1.4.1. Surface Chemistry and Nanotoxicity.....	25
1.4.2. Gold Nanoparticle Toxicity .....	27
1.4.3. How to Determine Toxicity of Nanoparticles .....	30
2. OBJECTIVES OF THE STUDY.....	32

3. MATERIALS AND METHODS.....	33
3.1. MATERIALS .....	33
3.1.1. Chemicals .....	33
3.1.2. Cell Lines.....	33
3.1.3. Cell Culture Reagents.....	33
3.1.4. Kits .....	34
3.2. METHODS .....	34
3.2.1. AuNP Synthesis.....	34
3.2.2. Surface Modification of AuNPs with Carbohydrates.....	35
3.2.2.1. Thiolation of Carbohydrates .....	35
3.2.2.2. Purification of Thiolated Carbohydrates.....	36
3.2.2.3. Characterization of Thiolated Carbohydrates .....	37
3.2.2.4. AuNP-Carbohydrate Conjugation Process .....	38
3.2.3. Surface Modification of AuNPs with Peptides .....	38
3.2.4. Characterization of Naked AuNPs and AuNP Conjugates.....	40
3.2.4.1. Transmission Electron Microscope (TEM) .....	40
3.2.4.2. UV/Vis spectrometer .....	40
3.2.4.3. Dynamic Light Scattering (DLS).....	41
3.2.4.4. Agarose Gel Electrophoresis .....	41
3.2.4.5. Fourier Transform Infrared Resonance (FTIR) .....	42
3.2.4.6. Surface Enhanced Raman Scattering (SERS).....	42
3.2.5. Cell Culture .....	43
3.2.5.1. Nanoparticle Exposure to Cells .....	43
3.2.5.2. Cellular Uptake .....	44
3.2.5.3. WST-1 Cell Proliferation Assay .....	45
3.2.5.4. Apoptosis/Necrosis Assay .....	45
3.2.5.5. Clonogenic Assay .....	46
3.2.5.6. Cell Cycle Evaluation .....	47
4. RESULTS AND DISCUSSION .....	49

4.1. AuNPs SYNTHESIS AND CHARACTERIZATION.....	49
4.1.1. Characterization.....	49
4.1.2. Determination of Concentration .....	49
4.2. SURFACE MODIFICATION OF AuNPs WITH BIOMOLECULES .....	51
4.2.1. Surface Modification of AuNPs with Carbohydrates.....	51
4.2.1.1. Thiolation of Carbohydrates and Their Characterization .....	53
4.2.1.2. Optimization of AuNP-Lactose and AuNP-Maltose Conjugates and Their Characterization .....	55
4.2.1.3. Optimization of AuNP-Glucose and AuNP-Mannose Conjugates and Their Characterization .....	59
4.2.1.4. Conjugation of AuNPs with Carbohydrates and Their Characterization .....	64
4.2.2. Surface Modification of AuNPs with Peptides .....	70
4.2.2.1. Optimization of AuNP Conjugation with Pep1 and Pep8 and Their Characterization .....	83
4.2.2.2. Optimization of AuNP Conjugation with Pep2 and Pep9 and Their Characterization .....	87
4.2.2.3. Optimization of AuNP Conjugation with Pep3 and Pep10 and Their Characterization .....	91
4.2.2.4. Optimization of AuNP Conjugation with Pep4 and Pep11 and Their Characterization .....	94
4.2.2.5. Optimization of AuNP Conjugation with Pep5 and Pep12 and Their Characterization .....	97
4.2.2.6. Optimization of AuNP Conjugation with Pep6 and Pep13 and Their Characterization .....	101
4.2.2.7. Optimization of AuNP Conjugation with Pep7 and Pep14 and Their Characterization .....	105
4.2.2.8. Conjugation of AuNPs with Peptides and Their Characterization ...	109
4.3. INVESTIGATION OF CELLULAR RESPONSE.....	119

4.3.1. Cellular Response to AuNPs Modified With Carbohydrates .....	121
4.3.1.1. Uptake Studies .....	122
4.3.1.2. WST-1 Cell Proliferation Assay .....	124
4.3.1.3. Apoptosis/Necrosis Assay .....	126
4.3.1.4. Clonogenic Assay .....	127
4.3.1.5. Cell Cycle Evaluation .....	130
4.3.1.6. Summary of Cellular Response to Carbohydrate Modified AuNPs .	131
4.3.2. Cellular Response to AuNPs Modified with RGD Sequenced Peptides ....	133
4.3.2.1. Uptake Studies .....	134
4.3.2.2. WST-1 Cell Proliferation Assay .....	136
4.3.2.3. Apoptosis/Necrosis Assay .....	138
4.3.2.4. Clonogenic Assay .....	139
4.3.2.5. Cell Cycle Progression.....	142
4.3.2.6. Summary of Cellular Response to AuNPs Modified with RGD Sequenced Peptides.....	143
4.3.3. Cellular Response to AuNPs Modified Glycine Rich Peptides.....	145
4.3.3.1. Uptake Studies .....	146
4.3.3.2. WST-1 Cell Proliferation Assay .....	148
4.3.3.3. Apoptosis/Necrosis Assay .....	150
4.3.3.4. Clonogenic Assay .....	151
4.3.3.5. Cell Cycle Progression.....	154
4.3.3.6. Summary of Cellular Response to AuNPs Modified with Glycine Rich Peptides.....	155
4.3.4. Cellular Response to AuNPs Modified with Glutamic Acid Rich Peptides	157
4.3.4.1. Uptake Studies .....	158
4.3.4.2. WST-1 Cell Proliferation Assay .....	161
4.3.4.3. Apoptosis/Necrosis Assay .....	163
4.3.4.4. Clonogenic Assay .....	164
4.3.4.5. Cell Cycle Progression.....	167

4.3.4.6. Summary of Cellular Response to AuNPs Modified with Glutamic Acid Rich Peptides.....	168
4.3.5. Cellular Response to AuNPs Modified with Histidine Rich Peptides .....	170
4.3.5.1. Uptake Studies .....	171
4.3.5.2. WST-1 Cell Proliferation Assay .....	174
4.3.5.3. Apoptosis/Necrosis Assay .....	176
4.3.5.4. Clonogenic Assay .....	177
4.3.5.5. Cell Cycle Progression.....	180
4.3.5.6. Summary of Cellular Response to AuNPs Modified with Histidine Rich Peptides .....	181
5. CONCLUSION AND FUTURE PERSPECTIVES .....	185
REFERENCES .....	190

## LIST OF FIGURES

Figure 1.1. Schematic showing physical and chemical composition of uniform NPs and core-shell NPs. ....	2
Figure 1.2. Schematic representation of various NP types used in nanomedicine .....	3
Figure 1.3. Schematic representation of NP-bioconjugates .....	4
Figure 1.4. Schematic showing of six generalized principles for controlling the attachments of proteins or other biomolecules on NP surfaces .....	7
Figure 1.5. NP-biomolecule conjugation strategies .....	9
Figure 1.6. Electron microscopy images of AuNPs in various shapes. ....	16
Figure 1.7. Basics of SPR of AuNPs .....	17
Figure 1.8. AuNPs owing different SPR properties.....	18
Figure 1.9. Schematic description of AuNP curvature. ....	21
Figure 1.10. Schematic representation of biochemical mechanisms associated with nanotoxicity.....	25
Figure 1.11. Illustrative scheme about AuNPs and their interaction with biological systems either <i>in vitro</i> or <i>in vivo</i> .....	28

Figure 3.1. Scheme showing thiolation process of Glucose, Mannose, Lactose and Maltose by Lawesson reagent.....	35
Figure 3.2. Image of the carbohydrate thiolation set up. ....	36
Figure 3.3. White light image of purification setup of thiolated carbohydrates. ....	37
Figure 4.1. Characterization of colloidal suspension containing 13 nm AuNPs .....	49
Figure 4.2. Determination of AuNP numbers in 1 ml suspension .....	51
Figure 4.3. Scheme of orientation differences between Glucose and Mannose and free monosaccharide differences between Lactose and Maltose after conjugation. ....	52
Figure 4.4. Scheme of AuNP-Carbohydrate conjugation process .....	53
Figure 4.5. Comparative FTIR spectra of Thiolated Glucose, Thiolated Mannose, Thiolated Lactose and Thiolated Maltose. ....	54
Figure 4.6. While light images of suspensions of naked AuNP and AuNP-Maltose conjugates, and naked AuNP and AuNP-Lactose conjugates.. ....	55
Figure 4.7. Comparative UV/Vis spectra of naked AuNPs and AuNPs modified with increasing concentrations of thiolated Maltose and Lactose. ....	56
Figure 4.8. Intermolecular interaction between the free citrate ions and -OH groups of carbohydrates on AuNP surfaces. ....	57

Figure 4.9. White light image of agarose gel loaded naked AuNPs and AuNPs modified with increasing concentrations of thiolated Maltose and Lactose. ....	58
Figure 4.10. While light images of suspensions of naked AuNP and AuNP-Glucose conjugates, and naked AuNP and AuNP-Mannose conjugates. ....	59
Figure 4.11. Comparative UV/Vis spectra of naked AuNPs and AuNPs modified with increasing concentrations of thiolated Glucose and Mannose. ....	60
Figure 4.12. White light image of agarose gel loaded naked AuNPs and AuNPs modified with increasing concentrations of thiolated Glucose and Mannose. ....	61
Figure 4.13. White light images of suspensions of naked AuNP and AuNP-Glucose conjugates, and naked AuNP and AuNP-Mannose conjugates. ....	62
Figure 4.14. Comparative UV/Vis spectra of naked AuNPs and AuNPs modified with increasing concentrations of thiolated Glucose and Mannose. ....	62
Figure 4.15. White light image of agarose gel loaded naked AuNPs and AuNPs modified with increasing concentrations of thiolated Glucose and Mannose. ....	64
Figure 4.16. White light image of suspensions of naked AuNPs and AuNP-Carbohydrate conjugates. ....	65
Figure 4.17. Comparative UV/Vis spectra of naked AuNPs and AuNP-Carbohydrate conjugates. ....	66
Figure 4.18. White light image of Agarose gel, in which the naked AuNPs and AuNP-Carbohydrate conjugates were loaded. ....	67



Figure 4.19. Comparative FTIR spectra of naked AuNPs and AuNP-Carbohydrate conjugates. ....	68
Figure 4.20. Comparative SERS spectra of naked AuNPs and AuNP-Carbohydrate conjugates. ....	69
Figure 4.21. Color differences of AuNP suspension after addition of Pep1 and Pep8. ....	72
Figure 4.22. AuNP suspensions at several pHs. ....	73
Figure 4.23. AuNP suspension color change after addition of Pep1 solution. ....	74
Figure 4.24. AuNP suspension color change after addition of Pep2 solution. ....	74
Figure 4.25. AuNP suspension color change after addition of Pep3 solution. ....	75
Figure 4.26. AuNP suspension color change after addition of Pep4 solution. ....	76
Figure 4.27. AuNP suspension color change after addition of Pep5 solution. ....	76
Figure 4.28. AuNP suspension color change after addition of Pep6 solution. ....	77
Figure 4.29. AuNP suspension color change after addition of Pep7 solution. ....	78
Figure 4.30. AuNP suspension color change after addition of Pep8 solution. ....	78
Figure 4.31. AuNP suspension color change after addition of Pep9 solution. ....	79
Figure 4.32. AuNP suspension color change after addition of Pep10 solution. ....	80

Figure 4.33. AuNP suspension color change after addition of Pep11 solution. ....	80
Figure 4.34. AuNP suspension color change after addition of Pep12 solution. ....	81
Figure 4.35. AuNP suspension color change after addition of Pep13 solution. ....	82
Figure 4.36. AuNP suspension color change after addition of Pep14 solution. ....	82
Figure 4.37. White light images of suspensions of naked AuNPs and AuNPs modified with Pep1 at pH 11.0, at pH 11.5 and naked AuNPs and AuNPs modified with Pep8 at 5.9. ....	84
Figure 4.38. Comparative UV/Vis spectra of naked AuNPs, AuNP-Pep1 and AuNP-Pep8 conjugates. ....	85
Figure 4.39. White light image of agarose gel loaded naked AuNPs, AuNP-Pep1 and AuNP-Pep8 conjugates. ....	87
Figure 4.40. White light images of suspensions of naked AuNPs and AuNPs modified with Pep2 at pH 11.0 and naked AuNPs and AuNPs modified with Pep9 at 5.9. ....	88
Figure 4.41. Comparative UV/Vis spectra of naked AuNPs, AuNP-Pep2 and AuNP-Pep9 conjugates. ....	89
Figure 4.42. White light image of agarose gel loaded naked AuNPs, AuNP-Pep2 and AuNP-Pep9 conjugates. ....	90
Figure 4.43. White light images of suspensions of naked AuNPs and AuNPs modified with Pep3 at pH 6.7, at pH 8.6, at pH 10.5 and naked AuNPs and AuNPs modified with Pep10 at pH 5.9. ....	91

Figure 4.44. Comparative UV/Vis spectra of naked AuNPs, AuNP-Pep3 and AuNP-Pep10 conjugates. ....	92
Figure 4.45. White light images of agarose gels loaded naked AuNPs, AuNP-Pep3 and AuNP-Pep10 conjugates. ....	94
Figure 4.46. White light image of suspensions of naked AuNPs and AuNPs modified with either Pep4 and Pep11 pH at 11.0 and pH at 11.5.. ....	95
Figure 4.47. Comparative UV/Vis spectra of naked AuNPs, AuNP-Pep4 and AuNP-Pep11 conjugates. ....	95
Figure 4.48. White light image of agarose gel loaded naked AuNPs, AuNP-Pep4 and AuNP-Pep11 conjugates. ....	97
Figure 4.49. White light images of suspensions of naked AuNPs and AuNPs modified with Pep5 at pH 10.5, 11.0 and 11.5 and naked AuNPs and AuNPs modified with Pep12 at pH 5.9, 10.5, 11.0 and 11.5.....	98
Figure 4.50. Comparative UV/Vis spectra of naked AuNPs, AuNP-Pep5 and AuNP-Pep12 conjugates. ....	99
Figure 4.51. White light image of agarose gel loaded naked AuNPs, AuNP-Pep5 and AuNP-Pep12 conjugates. ....	101
Figure 4.52. White light image of suspensions of naked AuNPs and AuNPs modified with either Pep6 or Pep13 at pH 5.9, 9.5 and 11.5.....	102

Figure 4.53. Comparative UV/Vis spectra of naked AuNPs, AuNP-Pep6 and AuNP-Pep13 conjugates. ....	103
Figure 4.54. White light image of agarose gel loaded naked AuNPs, AuNP-Pep6 and AuNP-Pep13 conjugates. ....	105
Figure 4.55. White light images of suspensions of naked AuNPs and AuNPs modified with Pep7 at pH 10.5, 11.0 and 11.5 and naked AuNPs and AuNP modified with Pep14 at pH 8.4, 9.5 and 10.5.....	106
Figure 4.56. Comparative UV/Vis spectra of naked AuNPs, AuNP-Pep7 and AuNP-Pep14 conjugates. ....	107
Figure 4.57. White light image of agarose gel loaded naked AuNPs, AuNP-Pep7 and AuNP-Pep14 conjugates. ....	109
Figure 4.58. White light image of naked AuNPs and AuNP-Peptide conjugate suspensions.. ....	110
Figure 4.59. Comparative UV/Vis spectra of naked AuNPs and AuNP-Peptide conjugates.	111
Figure 4.60. Schematic representation of interaction between the free citrate ions and reactive groups of neutrally charged peptides, negatively charged peptides and positively charged peptides on AuNP surfaces. ....	113
Figure 4.61. White light image of agarose gel, in which naked AuNPs and AuNP-Peptide conjugates were loaded. ....	115
Figure 4.62. Comparative FTIR spectra of naked AuNPs and AuNP-Peptide conjugates.	116

Figure 4.63. Comparative SERS spectra of naked AuNPs and AuNP-Peptide conjugates.	117
Figure 4.64. Subtle differences on AuNP surfaces after functionalization with thiolated Glucose, Mannose, Lactose and Maltose. ....	122
Figure 4.65. SSC graphs of A549, BEAS-2b and MDA-MB-231 cells treated with 0.1, 0.5, 1.0 and 2.5 nM naked 13 nm AuNPs and Glucose, Mannose, Lactose and Maltose Functionalized AuNPs. ....	123
Figure 4.66. WST-1 Cell Proliferation result of A549, BEAS-2b and MDA-MB-231 cells treated with 0.1, 0.5, 1.0 and 2.5 nM of naked 13 nm AuNPs and Glucose, Mannose, Lactose and Maltose Functionalized AuNPs .....	125
Figure 4.67. Apoptosis/necrosis assay result of A549, BEAS-2b and MDA-MB-231 cells treated with 0.1, 0.5, 1.0 and 2.5 nM of naked 13 nm AuNPs and Glucose, Mannose, Lactose and Maltose Functionalized AuNPs.. ....	127
Figure 4.68. Clonogenic assay result of A549, BEAS-2b and MDA-MB-231 cells treated with 0.1, 0.5, 1.0 and 2.5 nM of naked 13 nm AuNPs and Glucose, Mannose, Lactose and Maltose Functionalized AuNPs. ....	129
Figure 4.69. Cell cycle progression of A549, BEAS-2b and MDA-MB-231 cells treated with 0.1, 0.5, 1.0 and 2.5 nM of naked 13 nm AuNPs and Glucose, Mannose, Lactose and Maltose Functionalized AuNPs. ....	131
Figure 4.70. Subtle differences on AuNP surface after functionalization with Pep1 and Pep8.....	134
Figure 4.71. SSC graphs of A549, BEAS-2b and MDA-MB-231 cells treated with 0.1, 0.5, 1.0 and 2.5 nM of naked 13 nm AuNPs and Pep1 and Pep8 Functionalized AuNPs.....	135

Figure 4.72 . WST-1 cell proliferation assay results of A549, BEAS-2b and MDA-MB-231 cells treated with 0.1, 0.5, 1.0 and 2.5 nM of naked 13 nm AuNPs and Pep1 and Pep8 Functionalized AuNPs. ....	137
Figure 4.73. Apoptosis/Necrosis assay results of A549, BEAS-2b and MDA-MB-231 cells treated with 0.1, 0.5, 1.0 and 2.5 nM of naked 13 nm AuNPs and Pep1 and Pep8 Functionalized AuNPs. ....	139
Figure 4.74. Clonogenic assay results of A549, BEAS-2b and MDA-MB-231 cells treated with 0.1, 0.5, 1.0 and 2.5 nM of naked 13 nm AuNPs and Pep1 and Pep8 Functionalized AuNPs.....	141
Figure 4.75. Cell cycle progression of A549, BEAS-2b and MDA-MB-231 cells treated with 0.1, 0.5, 1.0 and 2.5 nM of naked 13 nm AuNPs and Pep1 and Pep8 Functionalized AuNPs.....	143
Figure 4.76. Subtle differences on AuNP surface after functionalization with Pep2, Pep5, Pep9 and Pep12.....	146
Figure 4.77. SSC graphs of A549, BEAS-2b and MDA-MB-231 cells treated with 0.1, 0.5, 1.0 and 2.5 nM of naked 13 nm AuNPs and Pep2, Pep5, Pep9 and Pep12 Functionalized AuNPs.....	147
Figure 4.78. WST-1 cell proliferation assay results of A549, BEAS-2b and MDA-MB-231 cells treated with 0.1, 0.5, 1.0 and 2.5 nM of naked 13 nm AuNPs and Pep2, Pep5, Pep9 and Pep12 Functionalized AuNPs.. ....	149
Figure 4.79. Apoptosis/Necrosis assay results of A549, BEAS-2b and MDA-MB-231 cells treated with 0.1, 0.5, 1.0 and 2.5 nM of naked 13 nm AuNPs and Pep2, Pep5, Pep9 and Pep12 Functionalized AuNPs. ....	151

Figure 4.80. Clonogenic assay results of A549, BEAS-2b and MDA-MB-231 cells treated with 0.1, 0.5, 1.0 and 2.5 nM of naked 13 nm AuNPs and Pep2, Pep5, Pep9 and Pep12 Functionalized AuNPs .....	153
Figure 4.81. Cell cycle progression of A549, BEAS-2b and MDA-MB-231 cells treated with 0.1, 0.5, 1.0 and 2.5 nM of naked 13 nm AuNPs and Pep2, Pep5, Pep9 and Pep12 Functionalized AuNPs. ....	155
Figure 4.82. Subtle differences on AuNP surface after functionalization with Pep3, Pep6, Pep10 and Pep13.....	158
Figure 4.83. SSC graphs of A549, BEAS-2b and MDA-MB-231 cells treated with 0.1, 0.5, 1.0 and 2.5 nM of naked 13 nm AuNPs and Pep3, Pep6, Pep10 and Pep13 Functionalized AuNPs.....	160
Figure 4.84. WST-1 cell proliferation assay results of A549, BEAS-2b and MDA-MB-231 cells treated with 0.1, 0.5, 1.0 and 2.5 nM of naked 13 nm AuNPs and Pep3, Pep6, Pep10 and Pep13 Functionalized AuNPs.. ....	162
Figure 4.85. Apoptosis/Necrosis assay results of A549, BEAS-2b and MDA-MB-231 cells treated with 0.1, 0.5, 1.0 and 2.5 nM of naked 13 nm AuNPs and Pep3, Pep6, Pep10 and Pep13 Functionalized AuNPs. ....	164
Figure 4.86. Clonogenic assay results of A549, BEAS-2b and MDA-MB-231 cells treated with 0.1, 0.5, 1.0 and 2.5 nM of naked 13 nm AuNPs and Pep3, Pep6, Pep10 and Pep13 Functionalized AuNPs. ....	166

Figure 4.87. Cell cycle progression of A549, BEAS-2b and MDA-MB-231 cells treated with 0.1, 0.5, 1.0 and 2.5 nM of naked 13 nm AuNPs and Pep3, Pep6, Pep10 and Pep13 Functionalized AuNPs. ....	168
Figure 4.88. Subtle differences on AuNP surfaces after functionalization with Pep4, Pep7, Pep11 and Pep14.....	171
Figure 4.89. SSC graphs of A549, BEAS-2b and MDA-MB-231 cells treated with 0.1, 0.5, 1.0 and 2.5 nM of naked 13 nm AuNPs and Pep4, Pep7, Pep11 and Pep14 Functionalized AuNPs.....	173
Figure 4.90. WST-1 proliferation assay results of A549, BEAS-2b and MDA-MB-231 cells treated with 0.1, 0.5, 1.0 and 2.5 nM of naked 13 nm AuNPs and Pep4, Pep7, Pep11 and Pep14 Functionalized AuNPs.....	175
Figure 4.91. Apoptosis/Necrosis assay results of A549, BEAS-2b and MDA-MB-231 cells treated with 0.1, 0.5, 1.0 and 2.5 nM of naked 13 nm AuNPs and Pep4, Pep7, Pep11 and Pep14 Functionalized AuNPs. ....	177
Figure 4.92. Clonogenic assay results of A549, BEAS-2b and MDA-MB-231 cells treated with 0.1, 0.5, 1.0 and 2.5 nM of naked 13 nm AuNPs and Pep4, Pep7, Pep11 and Pep14 Functionalized AuNPs. ....	179
Figure 4.93. Cell cycle progression of A549, BEAS-2b and MDA-MB-231 cells treated with 0.1, 0.5, 1.0 and 2.5 nM of naked 13 nm AuNPs and Pep4, Pep7, Pep11 and Pep14 Functionalized AuNPs. ....	181



## LIST OF TABLES

Table 3.1. Properties of peptides used in the study. ....	39
Table 4.1. Average hydrodynamic sizes and zeta potentials of naked AuNPs and AuNPs modified with increasing concentrations of Maltose and Lactose.....	57
Table 4.2. Average hydrodynamic sizes and zeta potentials of naked AuNPs and AuNPs modified with increasing concentrations of Glucose and Mannose. ....	60
Table 4.3. Average hydrodynamic sizes and zeta potentials of naked AuNPs and AuNPs modified with increasing concentrations of Glucose and Mannose. ....	63
Table 4.4. SPR, average hydrodynamic sizes and zeta potentials of naked AuNPs and AuNP-Carbohydrate conjugates. ....	66
Table 4.5. Length, sequence, isoelectric point, charge and codes of fourteen peptides used to functionalize AuNP surfaces. ....	71
Table 4.6. Best conjugation pH condition of each peptides. ....	83
Table 4.7. Average hydrodynamic sizes and zeta potentials of naked AuNPs, AuNP-Pep1 and AuNP-Pep8 conjugates. ....	86
Table 4.8. Average hydrodynamic sizes and zeta potentials of naked AuNPs, AuNP-Pep2 and AuNP-Pep9 conjugates. ....	90
Table 4.9 Average hydrodynamic sizes and zeta potentials of naked AuNPs, AuNP-Pep3 and AuNP-Pep10 conjugates. ....	93

Table 4.10. Average hydrodynamic sizes and zeta potentials of naked AuNPs, AuNP-Pep4 and AuNP-Pep11 conjugates. ....	96
Table 4.11. Average hydrodynamic sizes and zeta potentials of naked AuNPs, AuNP-Pep5 and AuNP-Pep12 conjugates. ....	100
Table 4.12. Average hydrodynamic sizes and zeta potentials of naked AuNPs, AuNP-Pep6 and AuNP-Pep13 conjugates. ....	104
Table 4.13. Average hydrodynamic sizes and zeta potentials of naked AuNPs, AuNP-Pep7 and AuNP-Pep14 conjugates. ....	107
Table 4.14. SPR on UV/Vis spectra, average hydrodynamic sizes and zeta potentials of naked AuNPs and AuNP-Peptide conjugates. ....	112
Table 4.15. Peak assignments of SERS spectra of AuNP-Peptide conjugates. ....	118

## LIST OF SYMBOLS/ABBREVIATIONS

°C	Degrees Celsius
cm <sup>-1</sup>	Wavenumber
cm <sup>2</sup>	Square centimeter
h	Hour
mg	Milligram
ml	Milliliter
nm	Nanometer
nM	Nanomolar
S	Surface area
S/V	Ratio of surface area and volume
V	Volume
$\alpha$	Alpha
$\beta$	Beta
$\mu$ l	Microliter
$\mu$ M	Micromolar
$\mu$ m	Micrometer
<sup>198</sup> Au	Gold, isotope of mass 198
3D	Three dimensional
a. u.	Arbitrary units
aa	Amino acid
A549	Human lung carcinoma cell line
AFM	Atomic Force Microscopy
AsO-FeO NP complex	Arsenic oxide-Ferrite oxide nanoparticle complex
ATO	Arsenic trioxide
ATP	Adeninde triphosphate

ATR	Attenuated total reflectance
Au	Gold
AuNPs	Gold nanoparticles
Au-SH	Gold-Thiol
BEAS-2b	Human bronchial epithelial cell line
BSA	Bovine serum albumin
C	Cysteine
C-CH <sub>3</sub>	Carbon methyl bond
C=O	Carbon oxygen bond
C2	Second carbon
C4	Fourth carbon
Ca <sup>+2</sup>	Calcium ion
CaF <sub>2</sub>	Calcium fluoride
CD	Circular dichorism
CE	Capillary electrophoresis
C-H	Carbon hydrogen bond
C-N	Carbon nitrogen bond
CO <sub>2</sub>	Carbon dioxide
COOH	Carboxylic acid
C-S	Carbon sulfur bond
D	Aspartic acid
DCFH-DA	Dichloro-dihydro-fluorescein diacetate
DLS	Dynamic light scattering
DMEM	Dulbecco's Modified Eagle's medium
DMEM-F12	Dulbecco's Modified Eagle Medium/Nutrient Mixture F-12
DMSO	Dimethyl sulfoxide
DNA	Deoxyribonucleic acid
Dox	Doxorubicin
E	Glutamic acid

EDC	1-ethyl-3-(3-dimethylaminopropyl)carbodiimide hydrochloride
EDTA	Ethylenediaminetetraacetic acid
EDX	Energy Dispersive X-ray Spectroscopy
FBS	Fetal bovine serum
Fe <sub>3</sub> O <sub>4</sub> /Mn <sub>x</sub> Fe <sub>3-x</sub> O <sub>4</sub> NPs	Ferrite oxide/Manganate-ferrite core/shell nanoparticles
FeO magnetic NPs	Ferrite oxide magnetic nanoparticles
FITC	Fluorescein isothiocyanate
FM	Fluorescence microscopy
FRET	Förster resonance energy transfer
FTIR	Fourier transmittance infrared resonance
G	Glycine
G0/G1	Gap 0/Gap 1
G2/M	Gap 2/Mitosis
Glu	Glucose
GSH	Glutathione
H	Histidine
H <sub>2</sub>	Hydrogen
H <sub>2</sub> O	Hydrogen dioxide, Water
HAuCl <sub>4</sub> .3H <sub>2</sub> O	Gold (III) chloride trihydrate
HeLa	HeLa cell line
HPLC	High pressure liquid chromatography
HSF	Human skin fibroblast cell line
ICP	Inductively coupled plasma
IMR-90	Human lung fibroblast cell line
IR	Infrared
J774A.1	Mouse alveolar macrophages
Lac	Lactose
LDH	Lactate dehydrogenase
Mal	Maltose

Man	Mannose
MDA-MB-231	Human breast cancer cell line
MTS	3-(4,5-dimethylthiazol-2-yl)-5-(3-carboxymethoxyphenyl)-2-(4-sulfophenyl)-2H-tetrazolium
MTT	3-(4,5-dimethylthiazol-2-yl)-2,5-diphenyltetrazolium bromide
n	Replicate number
NaCit	Sodium citrate
N-H	Nitrogen Hydrogen bond
NH <sub>2</sub>	Amino group
NHS	N-hydroxysuccinimide
NIR	Near infrared
NMR	Nuclear magnetic resonance
NMs	Nanomaterials
NP-bioconjugates	Nanoparticle-Bioconjugates
NPs	Nanoparticles
OH	Hydroxyl
PEG	Poly ethylene glycol
Pen/Strep	Penicillin-Streptomycin
Pep	Peptide
PI	Propidium iodide
QDs	Quantum dots
R	Arginine
RAW 264.7	Phagocytic cell line
RGD	Arginine, Glycine, Aspartic acid
RNA	Ribonucleic acid
ROS	Reactive oxygen species
S	Synthesis
SAM	Self assembled monolayer
SANS	Small angle neutron scattering
SAXS	Small angle X-ray scattering

SEM	Scanning electron microscopy
SERS	Surface enhanced Raman scattering
SKOV3	Human ovarian carcinoma cell line
SPR	Surface plasmon resonance
S-S bond	Disulphite bond
SSC	Side-scattered light
TAE	Tris-acetate buffer
TEM	Transmission electron microscopy
TGA	Thermal gravimetric analysis
TP-DNA	Triangular pyramid DNA nanostructures
U251	Human glioblastoma cell line
UV/Vis	Ultraviolet/Visible spectroscopy
UV/Vis/NIR	Ultraviolet/Visible/Near Infrared spectroscopy
WST-1	Water-soluble tetrazolium-1
WST-8	Water-soluble tetrazolium-8
XRD	X-ray diffraction
Zn <sup>+2</sup>	Zinc ion

# 1. INTRODUCTION

## 1.1. NANOPARTICLES

Nanoparticles (NPs) are described as any particulate material with at least one dimension in the range of 1-100 nm [1]. NPs can be divided into two groups based on the material prepared through synthetic approach. The first group are prepared from metals, alloys, semiconductors, carbon allotropes, or polymers whereas the second group has a biological origin containing viral particles, bacteriophages, liposomes, or biopolymers [2]. NPs can be synthesized in various shapes such as spheres [3], rods [4], wires [5], planes [6], stars [7], cages [8] and multipods [9]. The synthesis of NPs in the nanometer scale is managed by nanochemistry, which have a critical role in modifying physical and chemical properties of NPs [10, 11]. The unique properties of NPs, which cannot be found in their bulk counterparts, can be aligned as high surface-to-volume ratio (S/V ratio), unique electrical, optical, magnetic, mechanical and thermal behaviors and high surface energy [12, 13]. These unique properties enable them to be used in a wide variety of applications, which can be simplified as electronics [14], energy harvesting and storage [15, 16], communications [17], biology and medicine [18]. In order to suit NPs for a specific application, their surfaces are modified with desired functional groups to arrange the chemical reactivity and dispersibility in different solvents [19].

The composition of NPs diversifies their structures, which are directly associated with their surface chemistry. To begin with, some NPs include only one type of material in their structure and they are called as uniform NPs, such as Gold Nanoparticles (AuNPs) as seen in Figure 1.1a. In the other cases, NPs are designed as core-shell structures so as to protect inner layers by outer shells and named as core-shell NPs such as core-shell  $\text{Fe}_3\text{O}_4/\text{Mn}_x\text{Fe}_{3-x}\text{O}_4$  NPs [20] as seen in Figure 1.1b. However, the problem behind the usage of core-shell NPs in biomedical applications is that some of them have hydrophobic and complex core-shell surfaces and are required to tune from hydrophobic to hydrophilic surfaces by



chemical modifications as ligand chemistry [21-22]. Moreover, in order to make hydrophobic NPs stably dispersed in aqueous systems, NPs surface chemistry can be tuned from hydrophobicity to hydrophilicity with phospholipid-micelle technology, pegylation and additional free reactive moieties depending on the intended application [23, 24]. Nevertheless, it should be known that these free reactive groups can cause toxicity. For example, NPs having high cationic surface charge can connect with anionic groups on cell membranes and creates severe damage on membrane, named as lipid peroxidation [25]. Therefore, it is worth pointing out that conjugation protocols should be carefully analyzed to prohibit toxicity of surface modified NPs [26].

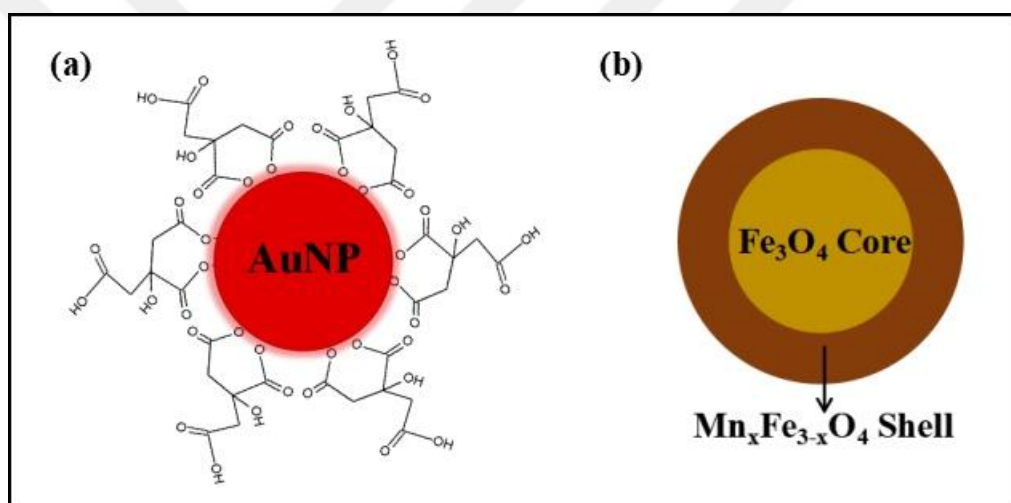


Figure 1.1. Schematic showing physical and chemical composition of (a) uniform NPs and (b) core-shell NPs. Concept partially adopted from ref 20.

Nanomedicine is the application of NPs in medicine [27]. The NPs used in Nanomedicine are lipid-based nanocarriers, viral particles, polymeric nanocarriers, drug conjugates and inorganic nanoparticles, as schemed in Figure 1.2 [28]. The use of NPs in medical application has been inspired from natural NPs in the body, which are nanosized vesicles, lipids, proteins, and complex biomacromolecules [29]. For sustained and targeted drug delivery, lipid or polymer based nanocarriers have been used in medicine as first attempts [30]. The interest of smaller inorganic-based NPs has developed nanoprobes to diagnose illnesses and then be utilized for novel therapies [31]. Recently, theranostics, which is a

combination of therapy and diagnosis are being recognized as modern medical techniques in nanomedicine [32].

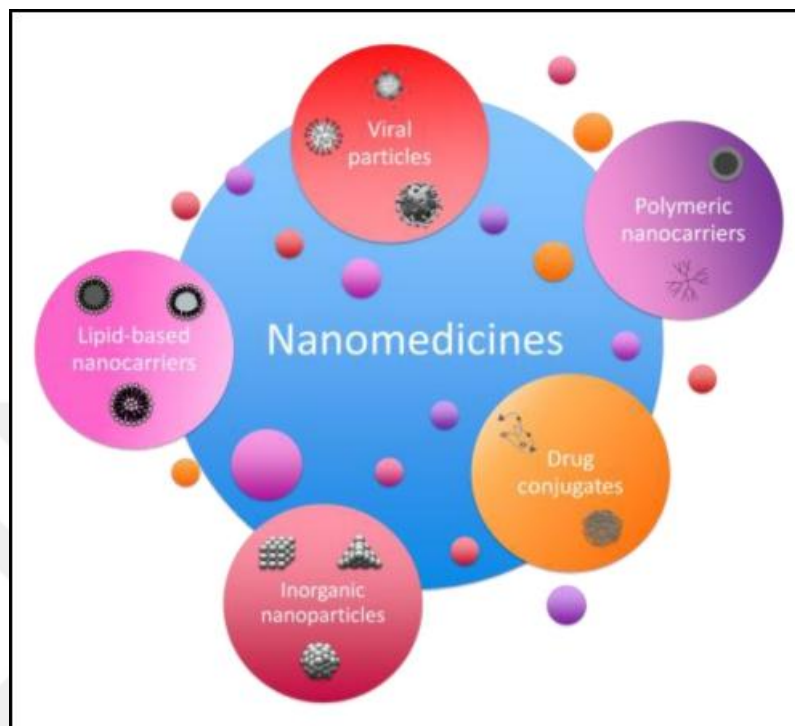


Figure 1.2. Schematic representation of various NP types used in nanomedicine [28].

## 1.2. NANOPARTICLE-BIOCONJUGATE CHEMISTRY

For specific biomedical applications such as labeling, tracking and detection, the surfaces of NPs can be tailored with a variety of molecules such as peptides [33], proteins/enzymes [34-35], antibodies [36], oligonucleotides [37], aptamers [38], carbohydrates [39], lipids [40], drugs [41], biologically active small molecules [42], reporter molecules [43], radiolabeled or fluorescent dyes [44] as schemed in Figure 1.3. The bioconjugation between NP surface and biomolecules occurs via coordinate covalent bonding, electrostatic interactions and van der Waals interactions [45]. Moreover, the functional group selection for surface modification is directly related to the NP surface. For instance, amines, thiols, disulfides and phosphines can anchor to the surface of quantum dots (QDs) and noble metal NPs [46], whereas carboxylic acids and phosphonic acids can interact with the

surfaces of metal oxide NPs [47]. Notably, the strength of surface modification takes importance in biomedical applications because a proper surface coating prevents NP aggregation.

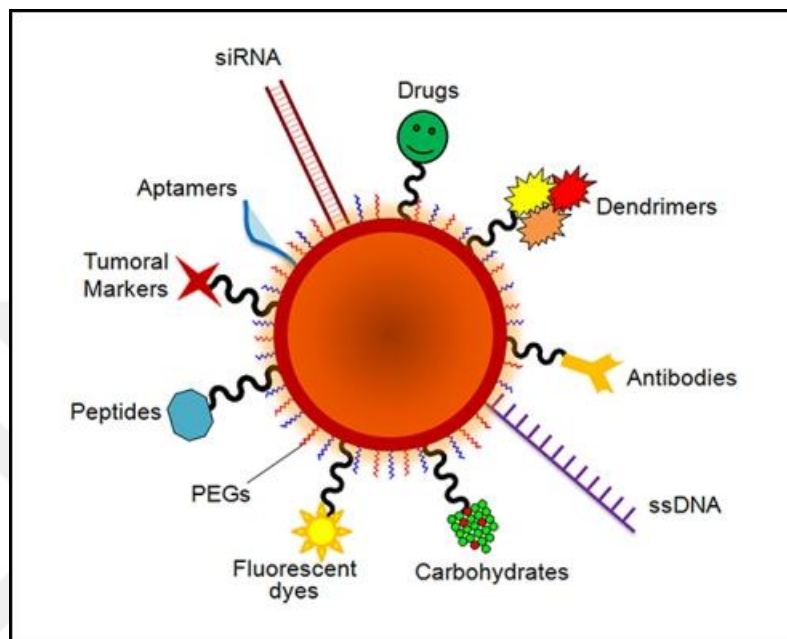


Figure 1.3. Schematic representation of NP-bioconjugates [28].

### 1.2.1. Challenges in Bioconjugation of Nanoparticles

Since the NPs are synthesized from various materials in several shapes and dimensions as described above, there exists the challenges related to bioconjugation of NPs. Therefore, the following factors should be considered when one attempts to control the modification of NP surfaces [48-49]:

- Since NPs are synthesized in various dimensions (1-100 nm), they have a wide range of surface areas (S), volumes (V) and pertaining to S/V ratios.
- The tendency of heterogeneity or polydispersity of NPs in population exists.

- NPs cannot dissolve in the suspension however they are adequately small to be modified with molecules for colloidal dispersibility and have ability to diffuse in aqueous media.
- The sizes of NPs should be larger than the sizes of biomolecules to be conjugated, except large protein complexes.
- The choice of bioconjugation chemistry is limited due to the fact that the reactive groups on inorganic NP surfaces may not create a new covalent formation.
- The surfaces of NPs might not be applicable for the desired functionalization.
- Most bioconjugation reactions may induce heterogeneity or polydispersity of NP-Bioconjugates even though naked NPs have nonaggregated nature and homogeneous dispersion.
- Some properties of NPs such as charge density, electrostatic repulsion, reduced colloidal stability, lead to produce low yields of NP-Bioconjugates.

### 1.2.2. Criteria for Ideal Bioconjugation Chemistry

There are six generalized criteria to describe the ideal bioconjugation chemistry of NPs [21] as demonstrated in Figure 1.4. These six criteria, which are difficult to accomplish in practice, are explained below:

- Controlling **average number of biomolecules on a NP** ( $NP_1:biomolecule_n$ ). The NP surfaces' coating with biomolecules in different concentrations for distinctive biomedical applications results in different valencies [50]. For instance, monovalency ( $NP_1 : biomolecule_1$ ) determines the single binding issues whereas higher valency ( $NP_1:biomolecule_{n>1}$ ) displays the avidity and binding interactions. Nonetheless, the overconjugation on NP surfaces can cause crowding and so mitigate the NPs' function [51]. Therefore, it must be considered to control over the valency of biomolecules on a NP in suspension.

- Determining **the orientation of biomolecules on a NP**. Biomolecules like proteins, peptides, enzymes and antibodies, are required not to lose their activities after binding on NP surface. Their activities are dependent on the reactive groups on the binding sites. Any nonspecific and electrostatic interactions between reactive groups inhibit homogeneous attachment of biomolecules on NP surfaces and reduce the activity of biomolecules.
- Controlling **the distance from NP surface to binding site of biomolecules**. In some cases, it is necessary to have a rigid distance between NP and biomolecules, e.g. Förster resonance energy transfer (FRET) [52].
- Controlling **the attachment affinity between NP and biomolecules**. The linkage between NP and biomolecules should be stable or labile under several conditions, like temperature, and pH [53]. The linkage may be either rigid or easy breakable and this is a key for some NP-mediated drug delivery systems [54].
- Pursuing **the optimum activity and function of either NP or biomolecules**. For all cases, the applied chemistry may change the own unique properties of both participants, for instance loss of protein activity, loss of NP stability in suspension.
- Lastly, **the reproducibility of aforementioned five criteria** among experiments, distinct types and synthesis batches of NPs and with other biological molecules [2].

In conclusion, the controlling of the biomolecule attachment on NP surface is nontrivial. Even though aforementioned six criteria are claimed to be satisfied by all bioconjugation experiments, **most of them can be achieved in practice.**

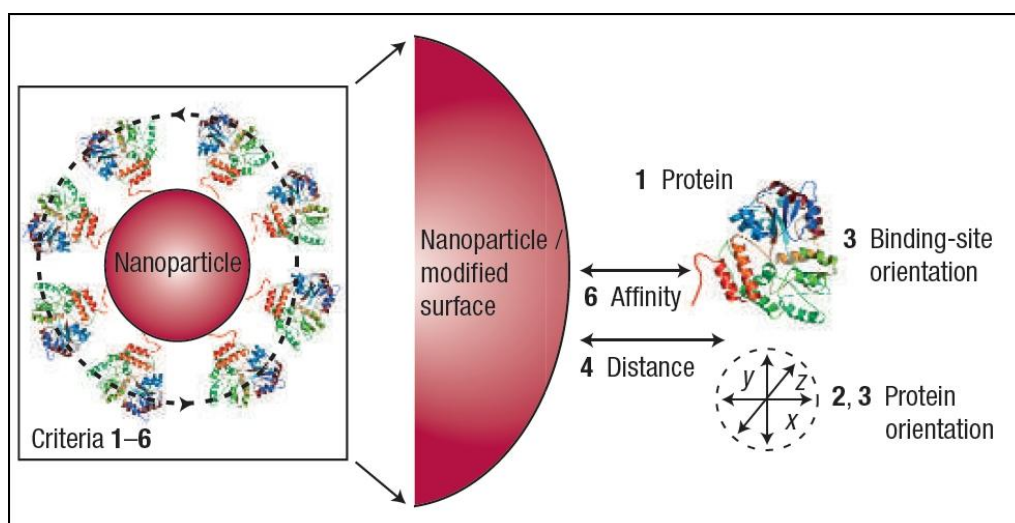


Figure 1.4. Schematic showing of six generalized principles for controlling the attachments of proteins or other biomolecules on NP surfaces [50].

### 1.2.3. General Bioconjugation Strategies

The choice of bioconjugation strategy is dependent on the factors of both NPs and biomolecules. These factors of NPs are defined as size, shape, surface chemistry and structure, material composition, surface ligands and functional groups on the surface while the factors of biomolecules are pointed out as size, chemical composition, affinity, activity, binding sites on active reagents, and utility [55]. The bioconjugation strategies may be divided into five main approaches, as electrostatic adsorption, direct attachment, covalent chemical attachment, ligand-receptor interaction, and encapsulation as shown in Figure 1.5 [21]. It is also worth noting that these conjugation approaches should not necessitate additional cross-linking and should be stable under desired conditions.

#### 1.2.3.1. Electrostatic Adsorption

Electrostatic adsorption, the simplest and most widely utilized approach to conjugate NPs with biomolecules, necessitates no chemical reactions. The electrostatic interaction

between charges on NP surfaces or charges on ligands of NPs with oppositely charged biomolecules to mediate charge-charge based NP-biomolecule conjugates, as schemed in Figure 1.5a. It can be exemplified that Song et al. discovered AuNP assembled triangular pyramid DNA nanostructures (TP-DNA), having unique Surface Plasmon Resonance (SPR) properties in the NIR region, which enable them deep-tissue penetration, to be utilized in photothermal cancer therapy, Raman imaging, drug delivery and photoacoustic imaging [56]. The citrate reduced AuNPs were coated with quaternary ammoniums by ligand exchange reactions to make positively charged surface. Positively charged AuNPs were interacted with negatively charged TP-DNA structures via electrostatic attraction and finally nanocomposites possessed three or four AuNPs accumulated on a TP-DNA. Furthermore, Guo et al. attached positively charged cellulose nanofibrils on the surfaces of citrate reduced AuNPs via electrostatic interactions in order to bio-inorganic hybrid materials based on renewable biopolymers to be used in industry [57]. On the other side, it must be considered that at the nanoscale, some factors may affect the formation of desired NP-biomolecule conjugates via electrostatic adsorption, such as amount of reagents, ionic strength, the type and magnitude of the charge [58]. That interaction may be arranged by pH or ionic strength.

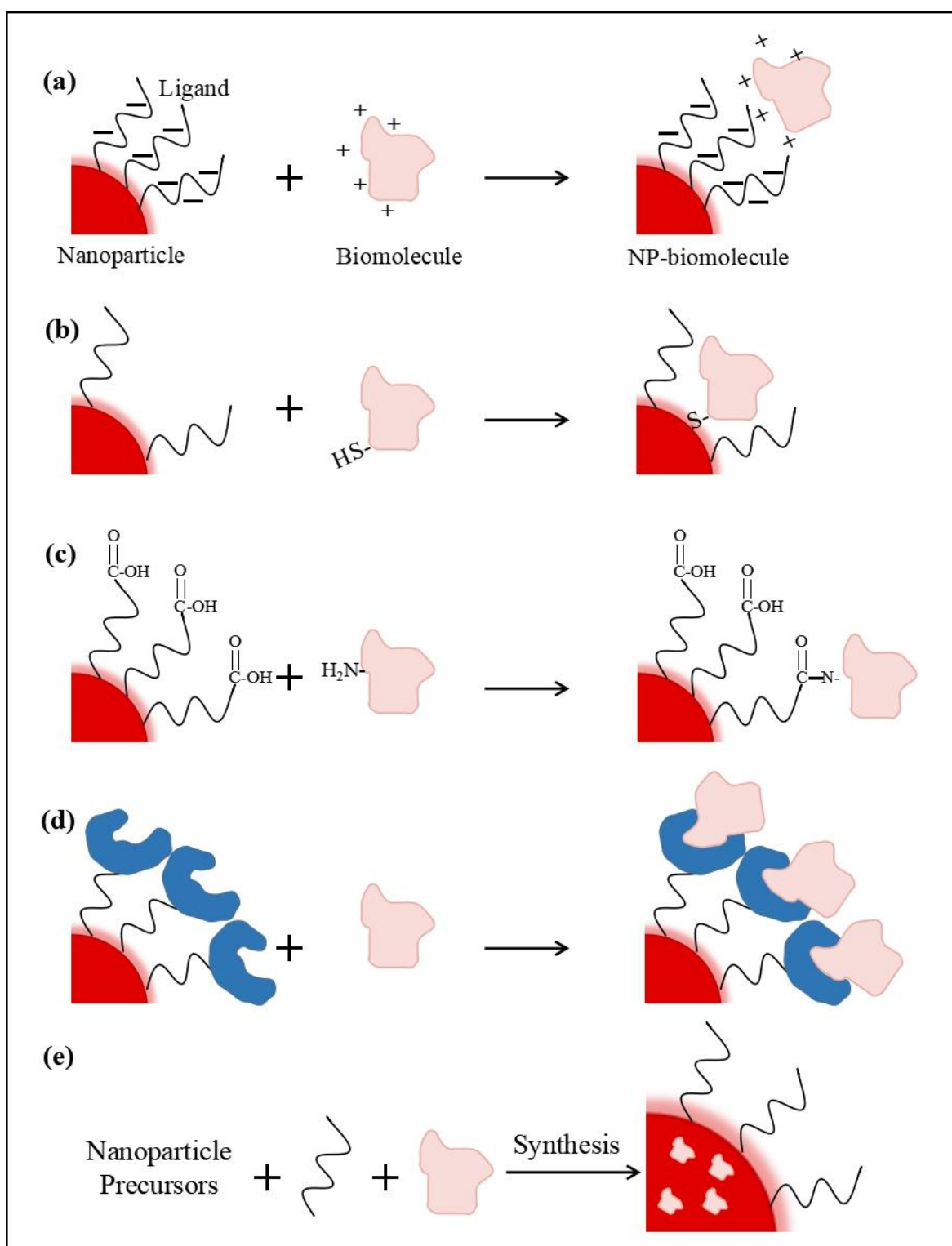


Figure 1.5. NP-biomolecule conjugation strategies. (a) electrostatic adsorption, (b) direct attachment, (c) covalent chemical attachment, (d) ligand-receptor interaction and (e) encapsulation. Figure was adapted from ref 21.



### ***1.2.3.2. Direct Attachment***

The biological molecules can be directly attached to the surface of NPs and this process is named as direct attachment, as seen in Figure 1.5b. Direct attachment is managed by coordinate covalent bonds, which are a shared pair of electrons where both electrons originate from the same atom [59]. These bonds are also known as having longer bond lengths, higher polarities and less energy when compared to covalent bonds. These bonds are not classified as strong as covalent bonds, since they can be broken by alteration of bioconjugation conditions, such as pH [60]. Coordinate covalent bonds can be exemplified with metal ions' chelation and Gold-thiol (Au-SH) chemisorption. Au-SH chemistry can be gained in the case of the fact that sulphur atoms of thiol groups in biomolecules, generally cysteine in proteins, enable a lone pair of electrons to unoccupied orbitals of gold atoms [21]. This type of conjugation only requires an overnight incubation of AuNPs and biomolecules including -SH groups due to form Au-SH bond. First Au-SH chemisorption study was reported by Mirkin and Alivisatos. Based on their studies, AuNPs were conjugated with thiolated oligonucleotides to generate nanoscaffolds to able to detect DNA [61]. Furthermore, sulphur atoms can also directly attach to the surfaces of ZnS/CdSe QDs by forming disulphite (S-S) bonds at interface [62]. In addition, His tags can directly link to the surfaces of NPs having transition metals in their compositions such as Zn, Ni, Cu, Fe and Mn atoms, either [63]. It must be mentioned that there are some concerns in direct attachment such as steric crowding on the surface of NPs since the ligands on NPs can be so densely or long that biomolecules may not reach to the NP surface to adsorb directly.

### ***1.2.3.3. Covalent Attachment***

Another common strategy to conjugate NPs with biomolecules is covalent chemical attachment, in which the ligands on NPs are linked with biomolecules via covalent bonds, as schemed in Figure 1.5c. This type of bioconjugation strategy can be illustrated with EDC/NHS reaction. EDC (1-ethyl-3-(3-dimethylaminopropyl) carbodiimide

hydrochloride) activates the carboxylic acids on NPs. Then, it is necessary to add NHS (N-hydroxysuccinimide) to the reaction to form a stable intermediate. The biomolecules including amino group link to the intermediate by creating a stable amide bond. In this reaction, the ratio of EDC and NHS is very crucial and the pH conditions of the reaction must be acidic. Kelestemur and coworkers used EDC/NHS reaction to bind BSA (bovine serum albumin) to the surface of silica coated zinc oxide NPs in order to observe their possible cytotoxic effects on human lung cancer (A549) and human skin fibroblast (HSF) cells [64]. Moreover, Giorgi-Coll et al., prepared Heparin functionalized AuNPs as cytokine capture agents in the way of enhancing microdialysis sampling to be applied in clinics [65]. In their study, Heparin-AuNPs were created with bifunctional Polyethylene glycol linker (PEG), by its thiol functional group was attached to the surface of AuNPs and the terminal amine groups were linked to Heparin via EDC/NHS reaction. By contrast, the only problem about covalent chemical attachment of biomolecules on the ligands of NPs is that the choice of chemistry type is limited because of the reactive groups on NP ligands to form a new covalent bond.

#### ***1.2.3.4. Ligand-Receptor Interaction***

As an alternative, the surfaces of NPs can be covered with biomolecules via specific labeling strategies, in other words, biomolecules can recognize and bind to the ligands on NP surfaces. The most common biolabeling strategy is biotin-avidin binding, as shown in Figure 1.5d. The avidin was discovered by E. E. Snell in 1940 and the structure of isolated biotin was determined by du Vigneaud. Then, du Vigneaud and coworkers revealed that avidin-biotin system can be used in various biological applications as so powerful tool [66]. The avidin is a glycoprotein found in white egg, stable at extreme condition, has high carbohydrate content at basic conditions and homotetrametric structure to bind biotin [67]. Nonetheless, the basic conditions and carbohydrates resulted in nonspecific binding of avidin to several substances. As an alternative, streptavidin, which is isolated from bacteria *Spteytomycetes avidinii*, is a homotetrametric like avidin, stable at extreme conditions, but is

not a glycoprotein, and this enables lower nonspecific binding. Since the avidin-biotin is one of the strongest noncovalent interaction to be used in biological studies, several companies offered numerous streptavidin and biotin derivatives and their functionalized and fluorescent labeled forms by claiming less nonspecific binding of avidin to other substances and high specifically binding of avidin to biotin, such as NeutrAvidin (Thermo Scientific Pierce), NeutraLite (Belovo), ExtrAvidin (Sigma-Aldrich), Texas red, thiosulfate functionalized biotin, BSA conjugated biotin, AlexaFluor (488, 546, 594) and IgG conjugated avidin [21]. Indeed, this makes avidin-biotin complex so attractive to link biomolecules on NP surfaces. There are two ways to conjugate NP surfaces with biomolecules via actin-biotin chemistry. The first one is that avidin functionalized NPs are conjugated with biotinylated molecules and the second one is that polymer-based NPs and biotinylated biomolecules are crosslinked with avidin intermediate. For example, van der Meer et al., created covalently avidin conjugated calcium phosphate NPs, which were covered with a thin silica layer and then functionalized with sulfhydryl groups so as to link any biotinylated biomolecules to be utilized as a versatile NP system [68]. As an second example, Veszelka et al., created neutravidin functionalized fluorescent NPs linked with biotin and biotinylated glutathione to pass through the blood brain barrier with high uptake and no valuable toxicity [69]. As a consequence, the existence of a wide range of avidin derivatives linking to biotin provides extensively utility in NP bioconjugation in foreseeable future.

#### ***1.2.3.5. Encapsulation***

One of the most utilized bioconjugation chemistry, especially for NP-mediated drug delivery, is encapsulation, in which biomolecules are placed inside of NPs during NP synthesis or after NP formation, as seen in Figure 5e. Relevant NPs can consist of several materials like metals oxides [70], liposomes [71], dendrimers [72], micelles [73] and natural or artificial polymeric NPs [74]. During encapsulation process, either size and function of encapsulated NPs or drug loading and its efficient release from NPs must be

considered. Banga et al., loaded polymeric NPs with cancer drug doxorubicin and modified with oligonucleotides to create stable 65 nm size Dox-loaded polymeric spherical nucleic acid nanostructures to be utilized in nanomedicine [75]. Thanks to surface functionalization with DNA, these specific NPs could be uptaken more by SKOV3 cancer cells and resulted high cytotoxicity. In addition, especially anti-cancer drug loaded magnetic NPs have an importance in cancer studies. These magnetic NPs provide hyperthermia in tumor tissues since NPs absorb energy and transfer all energy to heat and so burst tumor cells. Healthy cells surrounded tumor cells are not affected by this heat owing to localized point of heat in tumor cells. It can be exemplified that Du et al., synthesized FeO magnetic NPs with arsenic trioxide using co-precipitation and impregnation techniques to obtain AsO-FeO NP complexes [76]. These NPs were injected into xenograft cancer tissue of HeLa cells in nude mice. It was seen that these NPs were internalized by cancer cells more and after applying heat, the cancer cells were destroyed. Overall, encapsulation will continue to be one of the most common method in future NP-bioconjugate studies due to its wide materials made of and versatile application processes.

### **1.3. GOLD NANOPARTICLES**

#### **1.3.1. History**

Gold, a noble metal, was discovered in Bulgaria five hundred years ago and the history of its studies and applications spread over two hundred years [77]. The treatises among Arabian, Indian and Chinese scientists in the fifth-fourth centuries BC can be approved as first information about colloidal gold. “Liquid gold” by Indian scientists and “Golden solution” by Chinese scientists were used for medical purposes [78]. The ancient colloidal was first appeared in China and Egypt for medical and decorative purposes. Colloidal gold was seen in alchemist laboratories in Europe in the Middle Age. Paracelsus, a German-Swiss physician and alchemist, found out the reduction of gold chloride by vegetable dig outs in alcohols or oils. He utilized “potable gold” as cure for several metal diseases and

syphilis. His contemporary, Giovanni Andrea used “aurum potabile” as the treatment of lepra, ulcer, epilepsy and diarrhea. The first book about preparation of colloidal gold and its applications was written by Francisco Antonii, philosopher and doctor of medicine, in 1618 and was presented till today [79]. In 1633, David de Planis-Campy, the alchemist, was entrusted as the doctor to Louis XIII of France and he advised his “longevity elixir”, colloidal gold solution [80]. A complete summary of medical usages of gold was published by Hans Heicher in 1712 [81]. It was defined that gold could be stabilized with boiled starch. This study may be accepted as first colloidal gold stabilization with ligands.

In 1857, Faraday shifted the paradigm of colloidal gold to a modern view by publishing an article about synthesis methods and properties of colloidal gold [82] and Mie developed the visible absorption of colloidal gold by using Maxwell’s electromagnetic equations in 1908 [83]. For the first time, Faraday mentioned about agglomeration of colloidal gold in the presence of electrolytes and he was possibly prior to experience that colloidal gold has different properties than bulk gold [84]. In 1898, Richard Zsigmondy firstly synthesized different sizes of colloidal gold by reducing with hydrogen peroxide, formaldehyde and white phosphorous and reported their physicochemical and optical properties [85]. Moreover, Zsigmondy and Siedentopf invented ultramicroscope, whose main experimental item was colloidal gold. In 1925, Zsigmondy was remunerated the Nobel Prize in Chemistry “for his demonstration of the heterogenous nature of colloid solutions and for the methods he used, which have since become fundamental in modern colloid chemistry”. Furthermore, Theodor Svedberg was awarded in the Nobel Prize in Chemistry in 1926 “for his work on disperse systems”. In his study, Svedberg examined reduction kinetics of gold halides and formulated main notions of chemical condensation mechanisms of colloidal gold [86].

Gold colloids have been advised to treat several diseases over the centuries and until recently. Rheumatoid arthritis patients have been treated with colloidal gold until 1920s [87]. In 1927, colloidal gold was firstly applied as a cure for patients suffering from inoperable cancer [88]. In addition, the colloidal solution of the  $^{198}\text{Au}$  isotope, having 65 h

half-life time, was utilized as treatment for cancer [89]. During 1970s, Faulk and Taylor discovered a technique to conjugate gold colloids with antibodies to visualize *Salmonella* surface antigens under electron microscopy [90]. This study firstly showed that colloidal gold conjugate was benefited as an immunochemical marker. The tendency of colloidal gold biomolecule conjugates usage in numerous fields of nanomedicine for therapeutic and diagnostic purposes has raised thanks to this study and numerous studies in the literature showed that gold colloids could be functionalized with various biomolecules such as proteins, enzymes, oligo or polypeptides, oligonucleotides, DNA, antisense or sense RNA molecules, antibodies, cell surface receptors to be used in gene delivery [91-92], targeted drug delivery [93-94], cancer diagnostics [95], biosensors [96], metal sensors [97], detection of biological molecules [98], enzyme immobilization [99], immunoassay [100] and single nucleotide polymorphisms detection [101].

### 1.3.2. Synthesis

AuNPs can be synthesized in various sizes and shapes such as spherical [102], rod [103], triangular [104], star [105], cage [106], cube [107], wire [108], diamond [109] and popcorn [110] as seen in Figure 1.6. AuNPs firstly was synthesized by Turkevich in 1951 as monodisperse spherical gold nanoparticles suspended in water [102]. This simple method is based on the reaction of chloroauric acid ( $\text{HAuCl}_4$ ) and sodium citrate solution. Acting citrate ions either a reducing agent or a capping agent generates the colloidal gold. AuNPs in sizes between 10-100 nm are synthesized by using this general procedure. The red-wine solution includes 10-20 nm sized negatively charged AuNPs. By changing the ratio of citrate to gold in the reaction, the sizes of AuNPs are grown up to 150 nm and the color of the suspension alters from red to blue [111]. The Turkevich method for spherical AuNPs was later developed by Brust and Schiffrin in 1990 in terms of AuNPs suspended in organic liquids [112], by Perrault and Chan in 2009 in the way of using hydroquinone as a reducing agent [113], by Martin and Eah in 2010 as nearly monodispersed naked AuNPs in

water [114], by Navarro et al. in 2013 as creating one pot protocol [115]. The AuNPs synthesis protocol changes due to reaction conditions and the reason of AuNPs usage.

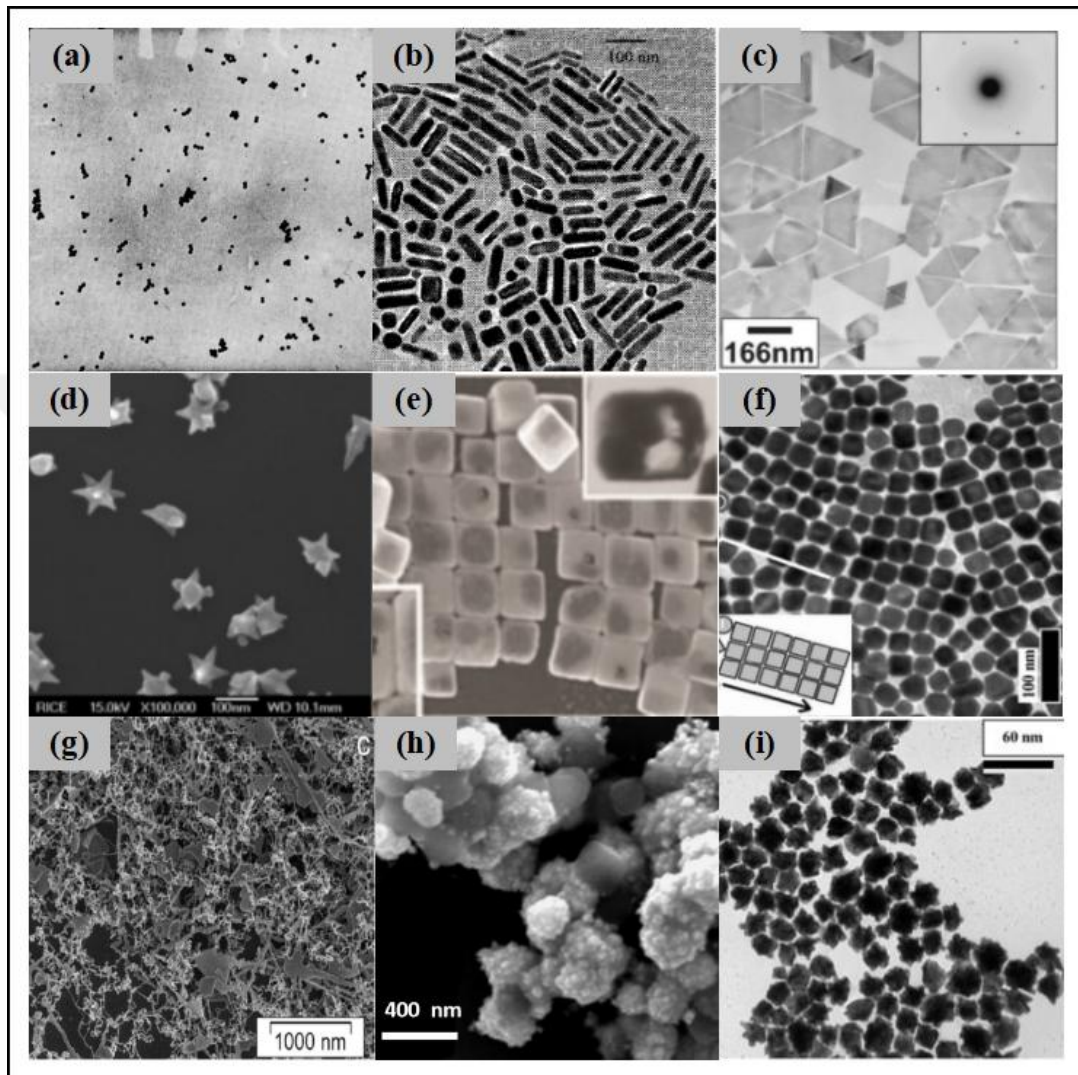


Figure 1.6. Electron microscopy images of AuNPs in various shapes. (a) spherical, (b) rod, (c) triangular, (d) star, (e) cage, (f) cube, (g) wire, (h) diamond and (i) popcorn.

In addition to wet chemical synthesis, AuNPs can be synthesized with natural and low-cost products by biosynthesis due to minimize the usage of chemicals and their possible environmental hazards. The materials in plant extracts were used as a reducing agent to reduce Au (III) precursors, such as sugar in the extract of *Eucalyptus globulus Labill* [116]. Furthermore, microorganisms are utilized to synthesize AuNPs in case of playing reducing

and stabilizing agents of amino acids in proteins or enzymes in microorganisms for instance *Lactobacillus strains*, *Shewanella algae* or *Rhodopseudomonas capsulate*, [117]. Despite of promising inventions for AuNPs biosynthesis, the controlling of sizes and shapes of AuNPs is still a handicap.

### 1.3.3. Properties

AuNPs are one of the most studied and promising metal NPs for therapy and diagnosis in medical and biomedical fields because of their unique physical and optical properties [118]. The most essential physical property of AuNPs is surface plasmon resonance (SPR) [119]. Along with irradiation of light, the electrons of conduction band on AuNP surfaces commence to oscillate collectively, which is called SPR, as seen in Figure 1.7. This results in strong absorption and scattering of light by colloidal AuNPs within the visible region of the electromagnetic spectrum [120]. In addition, the agglomeration of AuNPs cause a red-shifting in SPR frequency and altering the color of AuNP suspension from red to blue because of interparticle plasmon coupling [121].

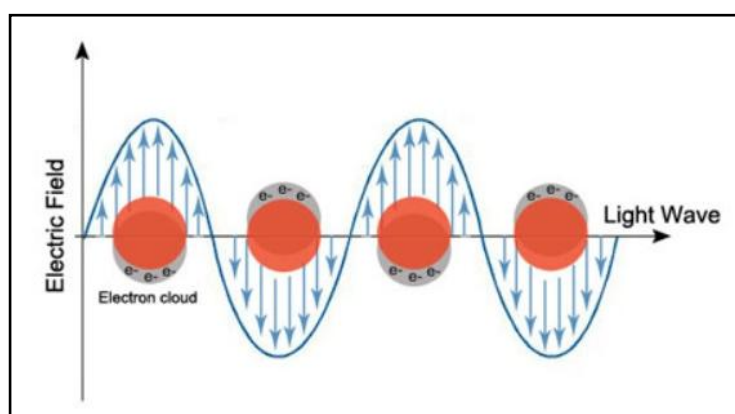


Figure 1.7. Basics of SPR of AuNPs [122].

The SPR absorption peak can be tunable within the visible to NIR range by changing their size, shape, solvent, surface chemistry, agglomeration and refractive index of surrounding



medium [123]. This SPR absorption peak can be monitored by UV/Vis spectroscopy as seen in Figure 1.8 [124]. Approximately 5-15 nm diameter sized spherical AuNPs have this SPR peak as a unique peak close to 520 nm and this peak shifts through red with respect to the size increase such as 50 nm AuNPs have SPR peak around 530 nm. The rod shaped colloidal gold (AuNRs), however, have two distinct peaks as transverse peak around 520-530 nm representing width of AuNRs and longitudinal peak around 600-1200 nm representing length of AuNRs [125]. Therefore, the alteration of the aspect ratio of length to diameter of colloidal gold, different AuNPs owing multiple transverse and longitudinal peaks can be prepared, which is exploited in several applications, and these tuned AuNPs can be monitored by UV/Vis spectroscopy thanks to their SPR effect.

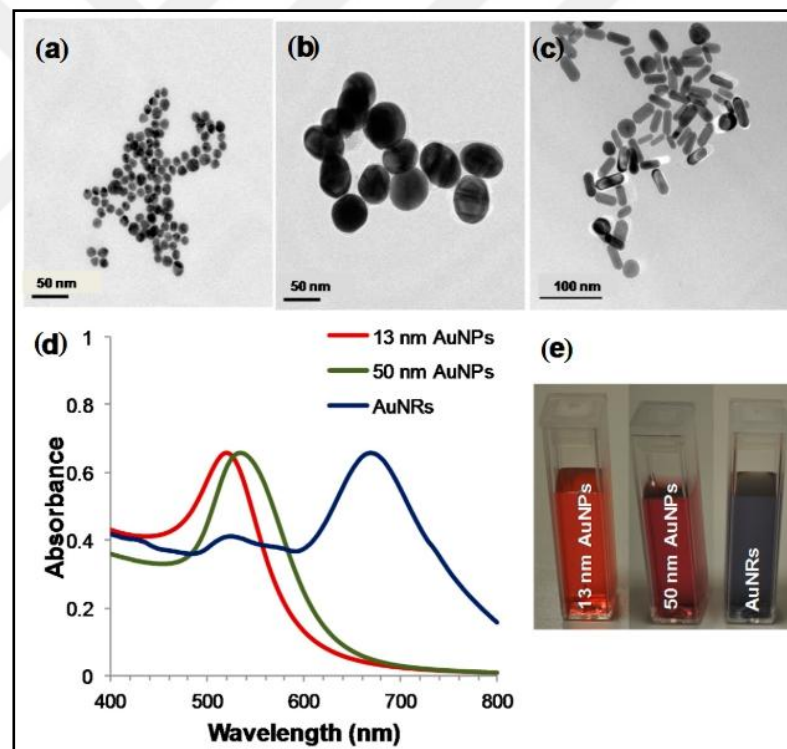


Figure 1.8. AuNPs owing different SPR properties. TEM images of (a) 13 nm spherical AuNPs, (b) 50 nm spherical AuNPs and (c) rod shaped AuNRs, (d) their UV/Vis spectra and (e) images of color of suspensions [124].

There exist several other properties of AuNPs, which can be utilized in bio-imaging and diagnosis. Thanks to their light scattering and high electron density, AuNPs can be used as contrast agent in live cells using dark-field imaging and X-ray computed tomography imaging [126]. In addition, AuNPs have great potential to be used in *in vivo* imaging such as two photon optical luminescence imaging [127], optical coherence tomography imaging [128] and photoacoustic tomographic imaging [129]. Furthermore, in the realm of single cell analysis, AuNPs have significant applications in surface-enhanced Raman scattering (SERS) since they enhance Raman signal and enable to detect small biological molecules in living cells [70]. Finally, AuNPs have been widely used in photothermal therapy for cancer as targeted drug carriers because they can convert optical absorption in heat energy to destroy cancer cells in living organisms [107].

#### **1.3.4. Surface Chemistry and Bioconjugation**

One of the reasons why AuNPs are widely utilized metal NPs for biomedical and technological applications is that their stability and performance needed for the application can be improved by functionalization of their surface chemistry. Functionalization of AuNPs with biomolecules, which is strictly related to NP surfaces itself, stabilizing ligands and functional groups of biomolecules, provides high stability and low or no aggregation at biological conditions. Biomolecules the most used in functionalization of AuNP surfaces are peptides [130], proteins/enzymes [131-132], DNA [133] and carbohydrates [134]. Owing to the fact that these biomolecules are fundamental components of living organisms and have various functions, AuNPs are functionalized with them to possess enhanced properties to be employed in biomedical and technological fields. Moreover, these biomolecules are regarded as ideal to adsorb to AuNP surfaces thanks to their sizes within the range of 2 to 20 nm [135]. High stability in biological conditions and advanced optical properties can be achieved by building AuNP-Biomolecule hybrids consisting of the benefits of either AuNPs or biomolecules. The most chosen surface functionalization

process to enable a stable monolayer of these biomolecules on AuNP surfaces are chemisorption, electrostatic interaction and hydrophobic interaction.

Undoubtedly, the first and most studied bioconjugation strategy to functionalize AuNP surfaces with biomolecules is thiolate chemisorption on gold, simply named as **chemisorption**. The principle of this strategy is that various organosulfur compounds, which are known as alkyl thiols, dialkyl sulfides, dialkyl disulfides, alkylxanthates and dialkylthiocarbamates, create a monolayer on metal NP substances [136]. Additionally, alkyl thiols and dialkyl disulfides are predominantly chosen for AuNP surface functionalization. These types of thiol compounds chemisorp to Au as gold (I) thiolates by reductive elimination of the thiol hydrogen to either H<sub>2</sub> or H<sub>2</sub>O. During chemisorption, citrate ligands used as stabilizing agent during AuNP synthesis are exchanged with thiol compounds without disturbing structure and function of NPs thanks to high affinity of sulfur for gold and then form a strong coordinate covalent bond S-to-Au atoms, whose strength is estimated as 40-50 kcal/mol [137]. Furthermore, in order to increase solubility of NPs in aqueous environment and to enable a chemical handle for a following bioconjugation with another biomolecules, the terminal functional group on thiol derivatives can be particularly designated [138]. During monolayer formation of thiol ligands on spherical AuNP surfaces, the curvature of NP structure takes a remarkable role [139]. Three-dimensional structure and function of proteins, especially enzymes, are required to be conserved after conjugation. This curvature of NPs provides a less contact area between thiol groups and Au surface and eliminates conformational changes associated with function loss [51]. AuNPs owing larger size than 0.8 nm are estimated to possess a truncated octahedral or cubooctahedral shape, which is correlated with the number of gold atoms in core, as seen Figure 9a [140]. Based on Thermal Gravimetric Analysis (TGA) results, AuNPs increased as a truncated octahedron more than 4.4 nm have mostly surface atoms consisted of flat terraces instead of edges and vertices. Thus, the increment on AuNPs size provides that the thiolate ligand layer have similar properties with planar SAM [141]. Therefore, thiol ligands cover densely AuNP surfaces, which is similar to a planar SAM. Moreover, to possess a high radius of curvature of thiol ligand is

also important for SAM as this curvature results in less conjugated thiol chain density on the surface of the core, as shown in Figure 9b. The decreasing of number of alkanethiols density consequences improved mobility of terminal methyl group. The alkyl chain completely fits into the volume of a cone encircling an area for each chain conjugation on a NP, however, cannot occupy the higher end of the cone, as demonstrated in Figure 9c [142]. For instance, methyl group density of fully conjugated 2.4 nm sized AuNPs with an octanethiol decreased to one-fourth that of Au-S groups situated on the core surface [143].

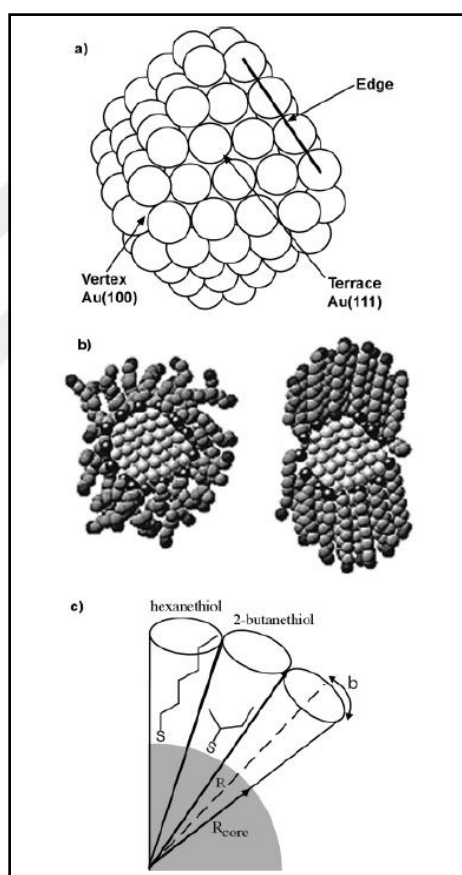


Figure 1.9. Schematic description of AuNP curvature. (a) Model of Au<sub>140</sub> nanoclusters with a truncated octahedral geometry, (b) equilibrium configurations of Au<sub>140</sub> nanoclusters conjugated with dodecanethiol gained by a molecular dynamic simulation as 350K (left) and 200K (right), and (c) scheme of a  $R_{core}$  sized Au nanocluster modified with a branched and unbranched alkanethiolate [138].

Regarding thiol chemisorption, the surfaces of AuNPs are also tailored with biomolecules via other reactive groups on biomolecules, such as amino, carboxyl and hydroxyl groups from lysine, glutamic or aspartic acid, and tyrosine or serine residues of proteins [144]. The affinity of amino and carboxyl groups to Au results in an adsorption of proteins on AuNP surfaces. Moreover, in particular pH conditions, protein residues at opposite charge can adsorb to the ligands on AuNPs surfaces through electrostatic interaction [60]. For instance, as carboxyl groups are negative above pH 4, they can be electrostatically linked to positive ligands on AuNPs surfaces. It should be paid attention that simple adsorption of biomolecules on AuNPs may be a weak interaction for a desired application, especially the case required medium condition alteration. In order to form a strong conjugation, biomolecules are covalently cross-linked on the AuNP surfaces, such as EDC/NHS chemistry to conjugate COOH with NH<sub>2</sub> or vice versa [145].

Even though thiol chemisorption has been used the first and most preferred bioconjugation strategy for AuNP surface functionalization, other non-thiolated organic and inorganic substances have been also utilized to coat AuNP surfaces for a specific biological applications [146]. The use of amino or carboxy terminated polyethylene glycol (PEG) ligands is prevalent for AuNP functionalization due to significantly improve their stability in *in vivo* and *in vitro* studies [147]. Furthermore, several non-thiolated polymers have been applied to stabilize and modify AuNPs, such as poly-N-vinylpyrrolidone (PVP) [148], poly(2-aminothiophenol) [149], polyethyleneimine (PEI) [150] and chitosan [151]. Among inorganic materials, silica coating is one of the most chosen functionalization strategies in order to enhance stability and surface function of AuNPs. The silica shell on AuNP surfaces enables an easy conjugation with diverse functional groups via silane coupling agents.

### 1.3.5. Characterization of AuNP-Biomolecule Conjugates

The characterization of AuNP-Biomolecule conjugates is an essential step to confirm the construction of the targeted structure, which is necessary for well-controlled and reproducible performance and safety in desired application [152-154].

In order to characterize AuNP-Biomolecule conjugates, several physicochemical norms are particularly considered and these norms can be listed as size and size distribution, shape and aspect ratio, zeta potential, surface area and surface chemistry, chemical composition, stability, solubility, purity and aggregation state [155]. Several techniques can be used to characterize not only bare AuNPs but also AuNP-Biomolecule conjugates, which are transmission electron microscopy (TEM) [45], scanning electron microscopy (SEM) [156], dynamic light scattering (DLS) [157], zeta potential [158], UV/Vis/NIR spectroscopy [159], fluorescence microscopy (FM) [160], inductively coupled plasma (ICP) [161], atomic force microscopy (AFM) [162], small angle X-ray scattering (SAXS) [37], small angle neutron scattering (SANS) [163], surface enhanced Raman scattering (SERS) [164], X-ray diffraction (XRD) [165], energy dispersive X-ray spectroscopy (EDX) [166], agarose gel electrophoresis [130], circular dichroism (CD) [167], Fourier transform infrared resonance (FTIR) [168] and nuclear magnetic resonance (NMR) [169].

## 1.4. NANOTOXICITY

The developed NPs, before using them in medical applications, should undergo several toxicity tests to check their possible risks associated with their interactions with biological systems. Theoretically, NPs are delivered into the body in a medical intent to represent their function, and then are excreted from the body without any hazard effects [46]. On the other hand, it was revealed either *in vitro* studies or clinical observations that NPs create minor or major toxic effects on a biological system [26]. Therefore, it is very critical to understand behavior of NPs from toxicological perspective.

NPs are recognized by biological systems as foreign materials. Thus, some undesirable effects caused by them can be seen on the host. The degree of the hazard depends on the dosage of NPs, extent and type of physical, chemical or immunological host-guest interactions [170]. These physical and chemical interactions trigger nanotoxicity via several mechanisms such as oxidative stress [171], DNA damage [172], immunogenicity [173], apoptosis and necrosis [70] and inflammation [174]. In addition, in order to be able to safely use of NPs in medicine, it is important to determine the correct dosage of NPs associated with specific threshold concentration of each NPs above which they show toxic effects [175].

NPs have the ability to enter into various tissues, cells and biological compartments [176]. Toxicity can be caused because of these overcrowded biological compartments. For instance, occupation-related NP exposure in miners results critical lung toxicity by producing inflammatory cytokines, fibrosis and carcinogenesis [26]. The internalization of NPs can result several toxicity mechanisms in cells such as ROS [177], interference with cell signaling proteins [178], glutathione (GSH) depletion [179] and increase of  $\text{Ca}^{+2}$  uptake [180] by inducing damage on organelles and mitochondria and finally cell death (Figure 10). The excretion of NPs from body and its route have not been clear yet.

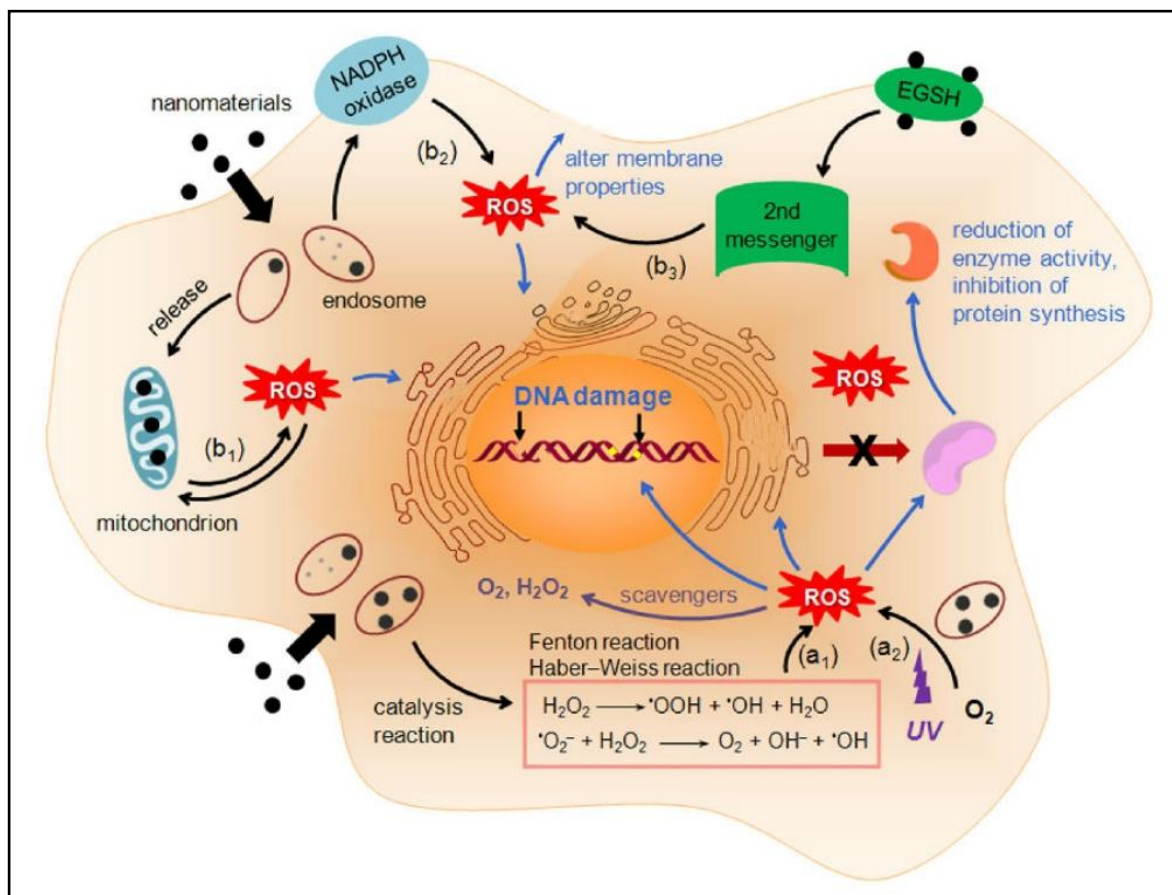


Figure 1.10. Schematic representation of biochemical mechanisms associated with nanotoxicity [181].

#### 1.4.1. Surface Chemistry and Nanotoxicity

The physical effects of NPs uptake on tissues, cells and biological compartments are related to several biochemical mechanisms activated by several physical and chemical properties of NPs such as size, shape, chemical composition and surface chemistry. The surface chemistry of NPs is the most controllable property of NPs as it controls their behavior in biological systems. These behaviors, directly related to their toxicological profiles, can be itemized as aggregation tendency, pharmacodynamics, biochemical reactivity, immunogenicity, biodistribution, cell entry and intracellular localization, biodegradability, and excretion [26]. The primary reason of NP toxicity is their high



surface energy in comparison to their bulk forms. This high surface energy can be gained by modification of NP surfaces with several biomolecules having reactive end(s). Due to the fact that the strength and nature of the modification is essential from their toxicological perspective, a proper surface functionalization can prohibit NP aggregation in aqueous media.

For specific applications, NPs must possess cationic, anionic or zwitterionic surfaces. Therefore, the NP surfaces are functionalized with free reactive moieties such as amines, carboxylic acids or proteins [46]. Nevertheless, it must be kept in mind that these reactive groups on surfaces can cause toxicity. For instance, the strong interaction between cationic NP surfaces and anionic functional groups of biomolecules on cellular membrane lead to severe damage to the membrane such as lipid peroxidation [25], to lose entrance control of ions and other biomacromolecules to the cytosol [182], to mitochondrial dysfunction [183], to activate defensive signaling pathways [184], to induce ROS [185] and genotoxicity [186]. Additionally, positively charged AuNPs showed severe cytotoxicity and genotoxicity to HeLa cells by inducing ROS [187]. It is noteworthy that the toxicity of NPs is altered based on the type of hydrophobic ligand on their surfaces. In another study, it was demonstrated that ultrasmall NPs having cationic surface passed through nuclear membrane and then inhibited gene expression by interacting with negatively charged DNA [188]. Furthermore, it was determined that starch functionalized silver NPs decrease ATP in either IMR-90 (human lung fibroblast) or U251 (human glioblastoma cells) and cause mitochondrial damage. Additionally, these NPs arrested cell cycle of both cell lines at G2/M phase, and the arrest content was concentration dependent [189]. It must be kept in mind that the reason why various cell lines showed different cytotoxic effects to the same NPs is that the each cell type gave unique cellular responses, which were cell type dependent [190]. As a consequence, the choice of free reactive group on NP surfaces plays an essential role to be able to avoid the cytotoxic effects on each cell type.

### 1.4.2. Gold Nanoparticle Toxicity

The utilization of several forms of AuNPs in a wide range of application such as imaging, drug and gene delivery, photothermal therapy and sensing revealed a concern about their possible toxicity in biological systems and so their toxicity has been comprehensively studied both *in vitro* and *in vivo* [18]. Many researchers have studied to understand cellular uptake, localization and trafficking, cell cycle progression, cell viability, DNA damage, circulation, aggregation, and excretion of AuNPs and their possible effects on immune system and the toxicity mechanisms, as schemed in Figure 11 [191]. Many reviews have been clearly published to evaluate the toxicity of AuNPs either *in vitro* or *in vivo* conditions and a deep and meaningful discussion by overviewing the all published reports on this topic [192]. On the other hand, all the previous studies determined two contradicting consequences as some researchers claimed that AuNPs are non-toxic while the most others claimed significantly high toxicity of AuNPs [193]. The discrepancy among AuNP toxicity studies was caused by several parameters of AuNPs such as size, shape and surface chemistry, interactions between AuNPs and biological systems and experimental conditions. In spite of these conflicting reports, there is a general concurrence about their size dependent cytotoxicity in a such way that AuNPs having less than 5 nm size caused more toxicity than those of having larger size than 15 nm [194]. The reason behind is that small AuNPs penetrated through nucleus and induce genotoxicity while larger AuNPs do not have the ability to do it because of steric effect. Moreover, thanks to surface modification of AuNPs, their toxicity can be diminished or even eliminated. For example, cationic AuNPs determined an important toxicity whereas anionic AuNPs were non-toxic [195]. Furthermore, it must be kept in mind that each group perform the studies under their own facilities and the variety of experimental conditions among groups also lead to different and even opposite conclusions.

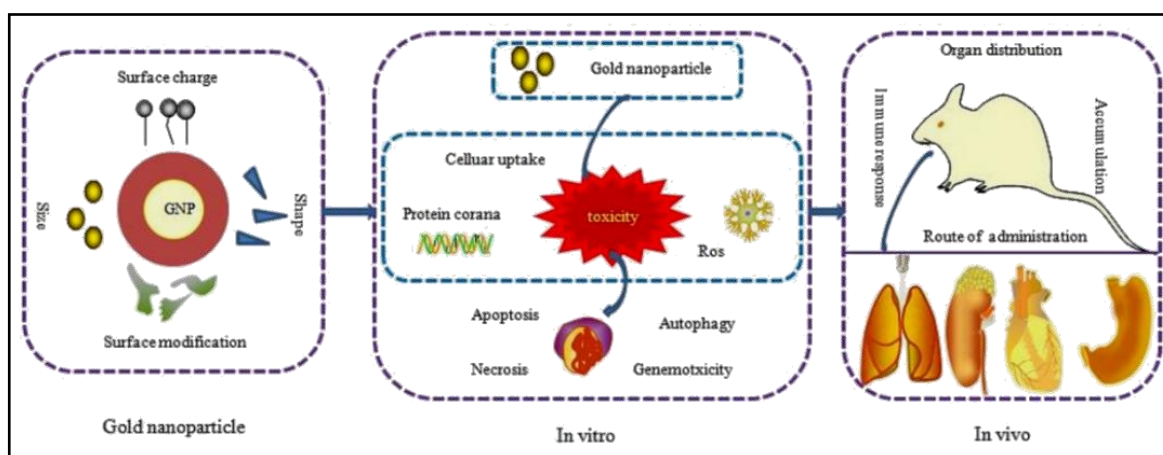


Figure 1.11. Illustrative scheme about AuNPs and their interaction with biological systems either *in vitro* or *in vivo* [191].

The carbohydrates on mammalian cell surfaces play critical roles in several cellular processes such as cell-cell recognition, inflammation, infection, cancer, tumors and metastasis [196-198]. For protein-carbohydrate and carbohydrate-carbohydrate interactions, it was demonstrated that carbohydrate functionalized AuNPs can be utilized as an effective therapeutic agent [199]. In a study, AuNPs were modified with lactose, maltose and glucose neoglycoconjugate as specific tumor associated carbohydrate antigens. The carbohydrate functionalized AuNPs having diameter below 2 nm were tested in mouse melanoma model (B16F10) for *ex vivo* investigation of the possible providing antiadhesion therapy and prohibition of lung metastasis [200]. The Glucose and Maltose functionalized AuNPs were used as negative inhibitor while The Lactose modified AuNPs was potential inhibitor of adhesion of melanoma cells to endothelium cells. According to the results, it was demonstrated that the AuNP-Lactose conjugates showed a strong protective effect to lung metastasis. Moreover, for designing a potential carbohydrate based anticancer vaccines, AuNPs were conjugated with T-cell helper peptides and sialylTn and Lewis antigens, which were tumor associated carbohydrate antigens overexpressed in several cancer types [201]. In another study, the utilization of thio-glucose modified 13 nm AuNPs with megavoltage X-ray enhanced the radiation affect and induced apoptosis in A549 cells [202]. At last but not least, Suvarna et al. have developed

a novel 2-deoxy-D-glucose (2DG) capped AuNPs as a theranostic candidate [203]. The synthesized 2DG-AuNPs and Glucose-AuNPs induced no toxicity in three cancer cell lines (HeLa, HepG2 and HCT116), however 2DG-AuNPs maintained the survival ability of all cancer cells. Therefore, 2DG-AuNPs were claimed as a better candidate for theranostic studies since they were a new targeting agent for glucose-dependent cancer cell types and a perfect candidate to AuNPs as a drug to be delivered to the interested sites. At that point, it must be confessed that even though there existed some studies about the effects of AuNP-Carbohydrate conjugates on cancer cells, a systematic investigation of cellular response to them is a requirement to solve the relation between the cellular response and AuNP surface chemistry in either healthy cells or cancer cells.

In addition to AuNP-Carbohydrate studies, there existed several studies in the literature to investigate the relation between surface chemistry of AuNPs and cellular response. For example, Kawazoe and Guoping claimed that AuNPs with different charges and moieties resulted in various cell responses in mesenchymal stem cell osteogenesis [204]. In order to search the interactions of surface modified AuNPs with the cells, AuNP surfaces were functionalized with differently charged alkanethiols, which were aminoethanethiol for amine group modification, mercaptoethanoic acid for carboxylic acid group modification and mercaptoethanol for hydroxyl group modification. No significant cytotoxicity was seen surface modified AuNPs treated mesenchymal cells, but amine group modified AuNPs induced higher cellular uptake. Moreover, carboxylic acid group functionalized AuNPs induced upregulation of growth factors, and thus increased the cell proliferation. In another study, the role of surface charge of AuNPs on membrane potential of either malignant or nonmalignant cell lines was investigated [205]. The surfaces of AuNPs were covered with alkanethiols different in charge and reactive free ends such as amine, hydroxyl, carboxylic acid and sulfonic acid groups. The findings showed that the positive, negative, neutral and zwitterionic AuNP surfaces modulated membrane potential of the cells affected cellular uptake. In another study, the toxicity of the quaternary ammonium and carboxylate functionalized AuNPs was investigated in Cos-1 cells, red blood cells and *E. coli* [206]. Interestingly, the AuNP surfaces were coated with an alkanethiol mix

consisting of approximately 70 charged thiols and 30 unsubstituted thiols. Based on results, only cationic AuNPs showed cytotoxicity and this was associated with strong electrostatic attraction to negatively charged bilayer. At that point, it must be mentioned that the common similarity between these studies was the explicit differences on surface chemistry of AuNPs and the anticipated different cellular responses to them. On the other hand, a systematic investigation of cellular response to the subtle differences on NP surface chemistry such as free reactive group orientation, order of peptide sequence, free terminus of peptide, remained unclear.

### **1.4.3. How to Determine Toxicity of Nanoparticles**

In order to elucidate the possible cytotoxic effects of NPs on cell cultures, several conventional *in vitro* cytotoxicity assays can be applied. These assays can be listed as tetrazolium based cell proliferation assays such as WST-1, WST-8, MTT, MTS, which measure the enzymatic activity of cellular mitochondria and are accepted as gold standard for *in vitro* cytotoxicity studies, Annexin V-FITC/PI assay or caspase substrates, which detect apoptosis/necrosis in cells, lactate dehydrogenase (LDH) lipid peroxidation assay, which measures LDH released from cells to cell culture medium and is accepted as a best sign for cell membrane disruption, DCFH-DA ROS detection assay, which detects intracellular hydrogen peroxide and oxidative stress, tryphan blue and PI staining, which detect cell membrane permeability, and finally calcein AM assay, which determines intracellular esterase activity [207]. The cytotoxicity of NPs should be cross-checked with at least two different assays mentioned above because of eliminating misconception of results. As a general advise, the results of different cytotoxicity *in vitro* assays cannot be compared with each other since each assay detects discrete parameter of toxicity [208]. Moreover, all these *in vitro* cytotoxicity assays mentioned above cannot give accurate results for all types of NPs, because the unique properties of NPs can change emission, absorbance and fluorescence characteristics of active molecules in the assays and occur the false negative or false positive results. For example, metal ions like  $Zn^{+2}$  ions interfered

with MTT and resulted the alteration on absorption spectrum of MTT and so false negative results were acquired [209]. Furthermore, single-walled carbon nanotubes (SWCNTs) can interact with free MTT and then cause false negative results [210]. As the last example, metal NPs such as copper NPs interfere with LDH and lead to false results [211]. On the other hand, the cytotoxicity of AuNPs has been investigated by all these cytotoxicity *in vitro* assays for several studies [70]. Since the well-developed protocols to test the cytotoxicity of AuNPs were generated, interference of AuNPs with reagents in the assays is nearly negligible and the toxicity assay consequences are reliable [212].



## **2. OBJECTIVES OF THE STUDY**

The interfaces between the NP surfaces and living systems have a critical role to explain the cellular response to the NP surfaces. Therefore, the nature of these interactions should be determined to design safer NPs to be used in medicine and other application fields. In all previous studies, the cellular responses to quite different chemistry changes on NPs were investigated and predictable results were obtained. With these studies two contradicting results were determined such as some researchers claimed AuNPs were non-toxic while the most others argued their significantly high toxicity. When considered these contradictory results, it is clear that a systematic investigation of cellular response to small changes on NP surface chemistry is absolutely needed. Therefore, in this thesis, it was aimed to systematically investigate the cellular response of living cells to subtle surface chemistry changes on AuNPs conjugated with custom designed carbohydrates and peptides. In order to systematically find out the effects of functionalized AuNPs, their cellular uptake and the possible effects on cytotoxicity, reproductive integrity and cell cycle phases were investigated and the relationship between the cellular response and NP surface chemistry was aimed to understand better.

## **3. MATERIALS AND METHODS**

### **3.1. MATERIALS**

#### **3.1.1. Chemicals**

D-(+)-Glucose (powder,  $\geq 99.5\%$ ), D-(+)-Mannose (powder,  $\geq 99.0\%$ ),  $\alpha$ -Lactose monohydrate (powder,  $\geq 96.0\%$ ), D-(+)-Maltose monohydrate (powder,  $\geq 98.0\%$ ), 1,4-dioxane (anhydrous,  $\geq 99.8\%$ ), dichloromethane (anhydrous,  $\geq 99.8\%$ ), Lawesson reagent ( $\geq 97.0\%$ ), methanol (for HPLC,  $\geq 99.9\%$ ), hydrochloric acid (36.5-38.0%), sodium hydroxide (BioXtra,  $\geq 98.0\%$ ), gold (III) chloride trihydrate ( $\geq 99.9\%$  trace metals basis), agarose (powder), Trizma base (powder,  $\geq 99.0\%$ ), EDTA (anhydrous,  $\geq 98.5\%$ ), acetic acid (anhydrous,  $\geq 99.0\%$ ), Triton X-100 (for molecular biology) and ethanol (anhydrous,  $\geq 99.5\%$ ) were purchased from Sigma-Aldrich (Darmstadt, Germany). Crystal violet (powder) and tri-sodium citrate (powder) was purchased from Merck Millipore (Germany). Peptides were synthesized by Alpha DNA (Montreal, Canada).

#### **3.1.2. Cell Lines**

A549 (human caucasian lung carcinoma), BEAS-2b (human bronchial epithelial cell) and MDA-MB-231 (human breast cancer cell) cell lines were purchased from the American Type Culture Collection (ATCC).

#### **3.1.3. Cell Culture Reagents**

Dulbecco's Modified Eagle Medium (1x DMEM, 4500 mg/L Glucose, L-glutamine, sodium pyruvate, Phenol red), Dulbecco's Modified Eagle Medium/Nutrient Mixture F-12 (DMEM/F-12, 4500 mg/L Glucose, L-glutamine, sodium pyruvate, Phenol red), fetal



bovine serum (FBS), Penicillin (10,000 Units/ml), Streptomycin (10,000  $\mu\text{g/ml}$ ), L-glutamine (200 mM), 1x Trypsin-EDTA (0.25 percent Trypsin- 0.02 percent EDTA) and HyClone™ phosphate buffered saline (10x PBS) were purchased from Gibco, USA. Colchicine ( $\geq 95$  percent HPLC purified, powder) and dimethyl sulfoxide (anhydrous,  $\geq 99.9$  percent) were purchased from Sigma-Aldrich (USA). Tissue culture flasks, well plates, falcon tubes, serological pipettes and cryotubes were purchased from TPP, Switzerland.

#### **3.1.4. Kits**

WST-1 cell proliferation reagent was purchased from Roche Diagnostic GmbH (CELLPRO-RO, Germany). Annexin V-FITC-/PI apoptosis necrosis detection kit was taken from Calbichem (Germany). Propidium iodide solution (10 mg/ml in water) and Ribonuclease A were purchased from Sigma-Aldrich (USA).

### **3.2. METHODS**

#### **3.2.1. AuNP Synthesis**

The 13 nm sized spherical AuNPs were synthesized by Turkevich method or also called citrate reduction method [102]. 80 mg gold (III) chloride trihydrate ( $\text{HAuCl}_4 \cdot 3\text{H}_2\text{O}$ ) in 200 ml deionized water ( $\text{dH}_2\text{O}$ ) was heated with continuous stirring at 1000 rpm by using a hot plate with magnetic stirrer. Then, 228.22 mg sodium citrate in 20 ml  $\text{dH}_2\text{O}$  was rapidly added into the boiling mixture. Finally, the resulting mixture was shaken for another 15 minutes. The synthesized AuNPs suspension was cooled down at room temperature for characterization.

The concentration of AuNPs was calculated by Beer-Lambert's Law [213]. Firstly the serial dilutions (1:2, 1:4, 1:8 and 1:16 v/v) of the AuNP suspension were prepared in

deionized water to determine concentration of the AuNPs ( $n=3$ ). The samples were scanned from 200 to 800 nm in quartz cuvette by UV/Vis spectrometer. The SPR absorptions of diluted AuNP suspensions were recorded. The concentration of AuNP suspension was calculated using resulting values. Moreover, the number of AuNPs in 1 ml suspension was calculated via a formula advanced by Haiss et al., by considering absorbance value of AuNP suspension at 450 nm [213].

### 3.2.2. Surface Modification of AuNPs with Carbohydrates

#### 3.2.2.1. Thiolation of Carbohydrates

In order to conjugate carbohydrates to AuNPs, the carbohydrates needed to be functionalized with thiol groups to enable Au-S bond. Therefore, the carbohydrates were thiolated with sufficient yields by Lawesson reagent [214] as schemed in Figure 3.1.

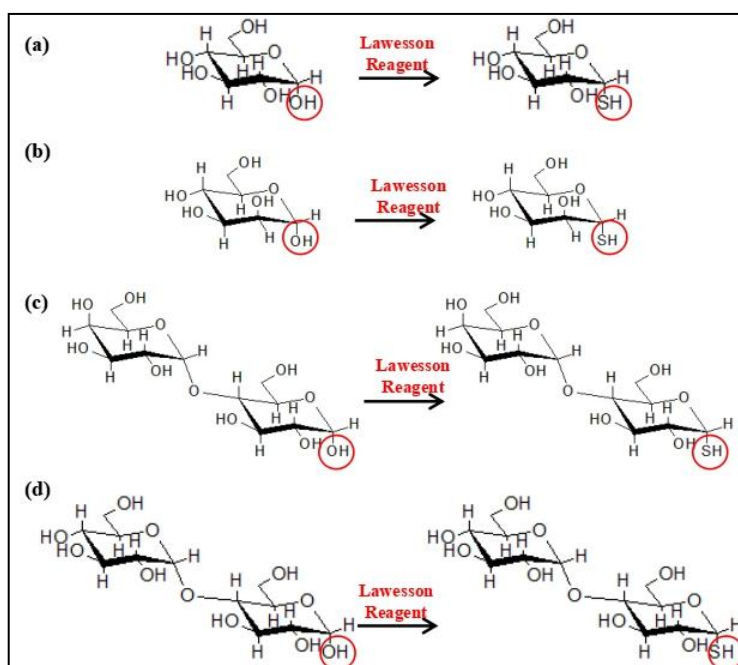


Figure 3.1. Scheme showing thiolation process of (a) Glucose, (b) Mannose, (c) Lactose and (d) Maltose by Lawesson reagent.

A 500 mg of carbohydrate and the Lawesson reagent (1.2 mol equivalents of carbohydrate) were dissolved in 30 mL of 1,4-dioxane. The resulting mixture was stirred at 110<sup>0</sup> C for 48 hours without any intervention under argon gas, as seen in Figure 3.2.

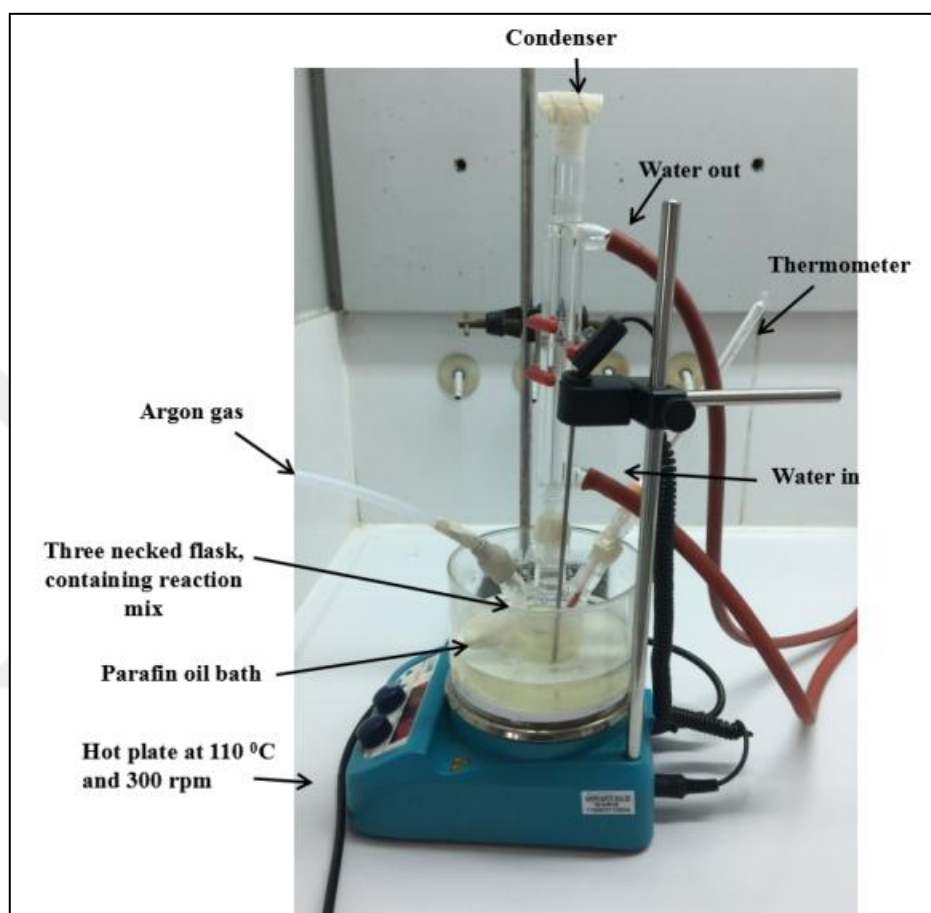


Figure 3.2. Image of the carbohydrate thiolation set up.

#### 3.2.2.2. Purification of Thiolated Carbohydrates

The cooled reaction mixture was filtered through a filter paper using 20 ml of 1,4-dioxane. The filtered mixture was concentrated using a rotary evaporator. The concentrated sample was dissolved in a mixture of 50 ml dichloromethane and 80 ml water. This mixture was transferred to a separatory funnel as shown in Figure 3.3. After adding a few drops of methanol, two distinct layers were visible in the funnel. While the top aqueous layer

contained thiolated carbohydrates, the bottom layer included unreacted reaction residues. The bottom layer was discarded. The upper aqueous phase was divided into about 10 ml fractions and frozen at  $-80^{\circ}\text{C}$ , then dried using a Freeze-Dryer.

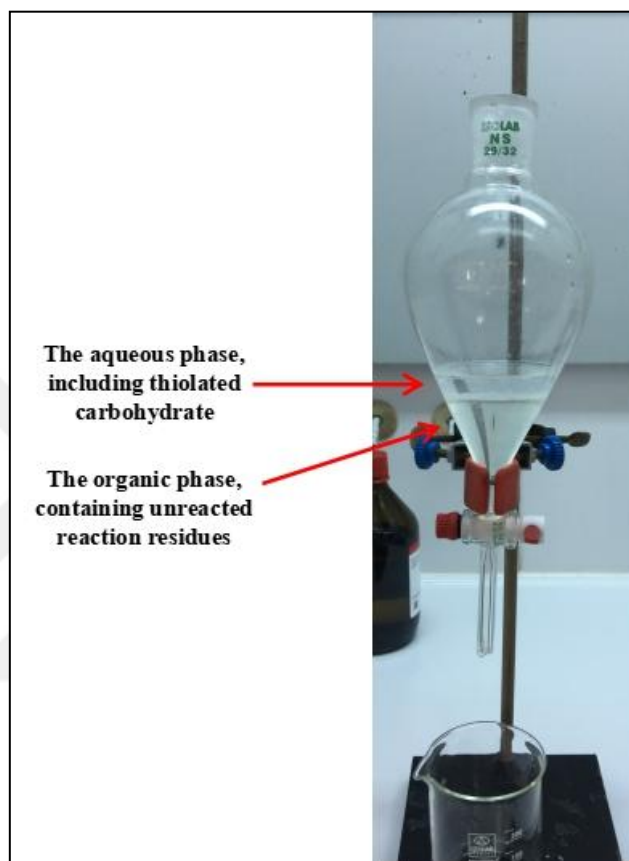


Figure 3.3. White light image of purification setup of thiolated carbohydrates.

### ***3.2.2.3. Characterization of Thiolated Carbohydrates***

The thiolated carbohydrates were characterized with FT-IR spectroscopy (Thermo NICOLET IS50, Massachusetts, USA) in attenuated total reflectance (ATR) mode.

#### **3.2.2.4. AuNP-Carbohydrate Conjugation Process**

For a direct attachment of thiolated carbohydrates on AuNP surfaces, the modified carbohydrates were dissolved in water by bringing the concentration to 10 mg/ml. The 13 nm AuNP suspension (10 nM, 1ml) was mixed with increasing concentrations of thiolated carbohydrate solutions (10 mg/ml) in 1.5 ml eppendorf tubes (n=3). The conjugation mix was shaken overnight at room temperature on a 3D Laboratory mini-shaker (Biosan Multi Bio 3D, Programmable mini-shaker). The optimization studies indicated that 150  $\mu$ l of 10 mg/ml of thiolated Glucose and Mannose solutions, and 75  $\mu$ l of 10 mg/ml thiolated Lactose and Maltose solutions was enough to functionalize 1 ml of 10 nM 13 nm AuNPs.

#### **3.2.3. Surface Modification of AuNPs with Peptides**

In order to create subtle differences on NP surface, 14 peptides different in length, sequence and charge were designed (Table 3.1). The lyophilized peptides (4 or 7 aa in length) were obtained from manufacturer (Alpha DNA, Montreal, Canada) and dissolved in deionized water based on manufacturer's instructions. The 7 aa length peptides were designed as addition of RGD sequence in the 4 aa length peptides. The peptides were designed as peptide couples, which meant that two peptides possessed same amino acid sequence but the sequence was either from -COOH to -NH<sub>2</sub> or -NH<sub>2</sub> to -COOH end. Cysteine was the first amino acid in all peptide sequences. The peptides were coded from 1 to 14 according to the free end of the peptide sequence where Cysteine was located on. Therefore, in Pep1 to Pep7, Cysteine was located at -NH<sub>2</sub> end while in Pep8 to Pep14, it was located at -COOH end. The 14 peptides were grouped by considering their charge and sequence. The first group was 4 aa length neutrally charged RGD peptides, which were Pep1 and Pep8. The second group was neutrally charged glycine rich peptides, which were Pep2, Pep5, Pep9 and Pep12. Pep2 and Pep9 were 4 aa length glycine rich peptide couples while Pep5 and Pep12 were 7 aa length glycine rich peptide couples including RGD sequence. The third group was negatively charged glutamic acid rich peptides, which were

Pep3, Pep6, Pep10 and Pep13. Pep3 and Pep10 were 4 aa length glutamic acid rich peptide couples while Pep6 and Pep13 were 7 aa length glutamic acid rich peptide couples including RGD sequence. The last group was positively charged histidine rich peptides, which were Pep4, Pep7, Pep11 and Pep14. Pep4 and Pep7 were 4 aa length histidine rich peptide couples while Pep7 and Pep14 were 7 aa length histidine rich peptide couples including RGD sequence.

Table 3.1. Properties of peptides used in the study.

Code	Length(aa)	Sequence (from NH <sub>2</sub> to COOH)	Isoelectric point	Charge
Pep1	4	DGRC	6.09	0
Pep2	4	GGGC	5.33	0
Pep3	4	EEEC	3.08	-3
Pep4	4	HHHC	7.40	+3
Pep5	7	DGRGGGC	6.09	0
Pep6	7	DGREEEC	3.83	-3
Pep7	7	DGRHHHC	7.40	+3
Pep8	4	CRGD	6.09	0
Pep9	4	CGGG	5.33	0
Pep10	4	CEEE	3.08	-3
Pep11	4	CHHH	7.40	+3
Pep12	7	CGGGRGD	6.09	0
Pep13	7	CEEERGD	3.83	-3
Pep14	7	CHHRGD	7.40	+3

D: Aspartic acid, G: Glycine, R: Asparagine, E: Glutamic acid, H: Histidine.

The 13 nm AuNP suspension (10 nM, 1ml) was mixed with increasing concentration of peptide solutions (1 mg/ml, 5-30  $\mu$ l). Based on the optimization studies, it was determined that 20  $\mu$ l of peptide solution was adequate to cover the surfaces of all AuNPs in suspension. On the other hand, it was found out that AuNPs immediately precipitated after addition of peptides having free -NH<sub>2</sub> terminus (Pep8-14) although AuNPs were remained as suspended in the suspension after addition of peptides having -COOH surfaces (Pep1-7).

Since it is known that protein residues at particular pH conditions can bind to oppositely charged AuNPs surfaces through electrostatic interactions, the effects of pH on AuNP functionalization was investigated [60]. As a first step, the pH values of AuNP suspension, where AuNPs were stable, was determined. The natural pH of AuNP suspension was measured as 5.9. The pH of the suspension was adjusted from 1.0 to 5.5 by adding 0.05 M HCl and from 6.0 to 12.0 by adding 0.05 NaOH. It was found that AuNPs in suspension at pH 3.0-11.8 were stable. 18 AuNP suspensions different in pH were prepared (from 3.0 to 11.8 at 0.5 increment). For each peptide, 20  $\mu$ l was added into 1 ml of each 18 AuNP suspensions (n=3), then the reaction tubes were shaken for overnight. The white light images of AuNP-Peptide suspensions were taken. AuNP-Peptide conjugates were stable in different pH intervals and these intervals changed according to the charge, length and free terminus of peptides. In order to find the optimum pH condition for each peptide conjugation, AuNPs were modified with peptides at randomly chosen pHs at that interval (n=3). They were shaken for overnight. Based on characterization results, the best pH condition for each AuNP-Peptide conjugates were determined.

### **3.2.4. Characterization of Naked AuNPs and AuNP Conjugates**

#### ***3.2.4.1. Transmission Electron Microscope (TEM)***

The synthesized 13 nm AuNPs were characterized by TEM to observe size, shape and uniformity of AuNPs in suspension. A few microliters of AuNP suspension was spotted onto TEM grids. Images were taken at different magnifications by using a JEOL JEM 100C TEM with a 70  $\mu$ m lens operating at 100 kV and with 2.0 Å point to point resolution.

#### ***3.2.4.2. UV/Vis spectrometer***

AuNPs and surface functionalized AuNPs were characterized by UV/Vis spectrometer (Lambda 25, Perkin Elmer, Foster City, CA, USA). The characteristic SPR absorption of

1:10 diluted AuNP suspension in deionized water was obtained over the range 200 to 800 nm using 1 cm path length quartz cuvette.

#### ***3.2.4.3. Dynamic Light Scattering (DLS)***

AuNPs and surface functionalized AuNPs were characterized by DLS (ZetaSizer Nano ZS, Malvern Instruments, Malvern, UK). The hydrodynamic sizes and zeta potentials of 1:10 diluted AuNP suspensions were measured in polystyrene cuvettes and disposable capillary cuvettes, respectively. The measurements were applied with a  $173^{\circ}$  scattering angle using 4 mW He-Ne laser at room temperature.

#### ***3.2.4.4. Agarose Gel Electrophoresis***

The density of biomolecules on AuNPs in suspension was monitored by 1 percent Agarose gel electrophoresis. The AuNP suspensions were centrifuged at 13000 rpm for 20 min. The supernatants were discarded, and the pellets were dissolved in 1 ml deionized water. The samples were centrifuged again at same speed for same time. The 0.98 ml of supernatants were removed, and the pellets were resuspended in the remaining 20  $\mu$ l supernatants by soft vortexing. An 80 mg agarose powder was melted in 80 ml 1x TAE buffer solution (40 mM Tris-Acetate and 1 mM EDTA) by microwaving. Since AuNP suspension has red color, no Ethidium bromide (EtBr) was added into the gel. The hot agarose was poured into comb placed gel cassette and allowed for solidification. After removing comb from the gel, the suspended samples were loaded into the wells. The gel cassette was placed into electrophoresis chamber and 1x TAE buffer solution as running buffer was dropped into the chamber up to cover up the gel. The chamber was fitted with Pt electrodes of DC supply (PowerPac Basic Power Supply, BioRad). The gel was run at 100V for 1.5 h. The white image of agarose gel was taken.



#### **3.2.4.5. Fourier Transform Infrared Resonance (FTIR)**

In order to identify chemical composition of AuNP surfaces, naked AuNP and modified AuNP suspensions were characterized via FTIR (Thermo NICOLET IS50, Massachusetts, USA) in attenuated total reflectance (ATR) mode. The naked AuNPs and surface functionalized AuNPs suspensions were centrifuged at 13000 rpm for 20 min. The supernatants were removed, and the pellets were suspended in 1 ml deionized water. This washing process was repeated twice. After last washing, the pellets were resuspended in 300  $\mu$ l deionized water. The samples were frozen at  $-80^{\circ}\text{C}$  and then dried by using Freeze-dryer (Laboratory Freeze-Dryer, C-Gen Biotech, Maharashtra). The dried samples were scanned in the transmission mode by FTIR from 400 to  $4000\text{ cm}^{-1}$ .

#### **3.2.4.6. Surface Enhanced Raman Scattering (SERS)**

Thanks to SPR properties of AuNPs, both naked AuNPs and surface modified AuNPs were characterized by SERS (Renishaw inVia Reflex Raman spectrometer equipped with a high speed encoded Streamline™ stage, UK), which could obtain the information about biomolecules chemically bound on AuNP surfaces. Both the naked AuNPs and surface modified AuNPs suspensions were centrifuged at 13000 rpm for 20 min. The pellets were dissolved in 1 mL deionized water. The dispersed NP suspensions were centrifuged at same speed and for same time. This washing process was repeated one more time. The acquired pellets were dissolved in 100  $\mu$ l double distilled water and 2  $\mu$ l of the suspended samples were dropped on Calcium Fluoride ( $\text{CaF}_2$ ) slides, then waited to dry. For each sample, at least ten areas of  $10 \times 10\text{ }\mu\text{m}^2$  with a laser spot size of  $1.5\text{ }\mu\text{m}$  were mapped under 50x objective (Leica DM2500 upright microscope) with a 830 nm photodiode laser source with 1200 line/mm grating by applying 4s laser exposure and 150 mV laser power. The mapped areas were preprocessed as subtract baseline, cosmic ray removal, smoothing. Then, the spectra obtained from the mapped area were averaged and normalized..

### 3.2.5. Cell Culture

A549 cell line (adenocarcinomic human alveolar basal epithelial cells) was cultured in DMEM/F-12 (with 4500 mg/L) supplemented with 10 percent FBS, 100 unit/ml Penicilin, 100 µg/ml Streptomycin and 2 mM L-Glutamine, BEAS-2b cell line (human bronchial epithelial cell line) was cultured in DMEM (with 4500 mg/L) supplemented with 5 percent FBS, 100 unit/ml Penicilin, 100 µg/ml Streptomycin and 2 mM L-Glutamine and MDA-MB-231 cell line (breast cancer cell line) was cultured in DMEM (with 4500 mg/L) supplemented with 10 percent FBS, 100 unit/ml Penicilin, 100 µg/ml Streptomycin and 2 mM L-Glutamine in an incubator at 37°C with five percent CO<sub>2</sub> humidified atmosphere.

When A549 and MDA-MB-231 cells reached to 90-95 percent confluency and BEAS-2b cells reached to 75-80 percent confluency, they were passaged. Firstly, culture medium on flasks was discarded and the cells on flasks were washed with 1x PBS. After removing PBS, 0.5 ml trypsin-EDTA solution for T25 flasks, 2 ml for T75 flasks and 5 ml for T150 flasks was added and incubated at 37°C under 5 percent atmosphere to detach cells. The detaching was checked by inverted microscope (Nikon Eclipse, TS100). When all cells were detached, trypsin was inactivated by addition of culture medium into flask (double volume of trypsin). The detached cells were collected into 15 ml sterile falcon tubes. The cells were counted by hemocytometer (Hemocytometer Bright Line). The 500,000 cells were seeded into T75 flasks and incubated at 37°C and 5 percent CO<sub>2</sub> humidified incubator.

#### 3.2.5.1. Nanoparticle Exposure to Cells

The cells were treated with either naked AuNPs or surface modified AuNPs with increasing concentrations as 0.1, 0.5, 1.0 and 2.5 nM for 24h. Before treatment, AuNP conjugates suspensions were washed with deionized water once by centrifuging at 13,000 rpm for 20 min. Then, 970 µl of supernatant was discarded and 950 µl of deionized water

was added and so all NPs were suspended in totally 1 ml suspension. Additionally, 1 ml of 13 nm AuNPs (10 nM) and AuNP conjugates included approximately  $5.37 \times 10^{12}$  particles. The cells were incubated with 100  $\mu$ l of AuNPs suspension ( $5.37 \times 10^{11}$  NPs) for WST-1 assay, with 1 ml of that ( $5.37 \times 10^{12}$  NPs) for Apoptosis Necrosis Assay, cell cycle determination and NP uptake studies, and 2 ml of that ( $10.74 \times 10^{12}$  NPs) for clonogenic assay.

### ***3.2.5.2. Cellular Uptake***

Cellular uptake of NPs was examined using flow cytometry. A549 cells (50,000), BEAS-2b cells (42,000) and MDA-MB-231 cells (50,000) were seeded in each well of 24 well plates and incubated at 37°C in humidified atmosphere under 5 percent CO<sub>2</sub> for 24h. The cells were exposed to increasing concentrations of NPs and incubated for 24 h in humidified incubator. After incubation, the cell culture medium in wells were collected into 1.5 ml eppendorf tubes. The attached cells were incubated with 200  $\mu$ l of trypsin-EDTA solution for 5 min at 37°C in humidified incubator. In order to finish trypsin activity, 400  $\mu$ l of collected medium was added in the wells. The detached cells were harvested into same eppendorf tubes and agitated at 2500 rpm for 5 min. After centrifugation, the cells were suspended in 1x PBS and immediately analyzed by flow cytometry. The quadrant gate on SSC vs FSC plot was used to determine the cellular uptake of NPs. Based on calculation of quadrant percentages by software, the results were drawn as a clustered column graph and were analyzed with two paired Student's t-test statistically to examine the cellular uptake of cells treated with increasing concentrations of NPs in comparison to negative control cells. The samples with a  $p \leq 0.05$  were marked with one-star sign (\*), with a  $p \leq 0.01$  were marked with two-star signs (\*\*), and with  $p \leq 0.001$  were marked with three-star signs (\*\*\*)).

### **3.2.5.3. WST-1 Cell Proliferation Assay**

A549 cells (10,000), BEAS-2b cells (8,000) and MDA-MB-231 cells (10,000) were seeded into the wells of 96 well plate and incubated for 24 h in an incubator at 37°C with 5 percent CO<sub>2</sub> humidified atmosphere (n=6). After 24 h incubation, the culture medium on cells were aspirated and washed with 1x PBS. When considered the controls, just 100 µl of culture medium was added into wells for negative control and 100 µl of culture medium containing 10 percent DMSO was added into wells as positive control. In addition, 100 µl of culture medium dispersed either naked AuNPs or surface modified AuNPs were added into the wells. After 24h incubation, the culture media were aspirated and the cells were washed with 1x PBS. The 100 µl of 5 percent WST-1 reagent containing culture medium was added into cells and incubated for 1h for A549 cells, 1.5 h for BEAS-2b cells and 2h for MDA-MB-231 cells in the incubator. Moreover, WST-1 reagent containing culture media were added into empty wells as blank. At the end of the incubation, 80 µl of medium into each wells were transferred to a new 96 well plate in order to prohibit positive wrong results caused by NP interference during measurement [215]. Then, the absorbance values of transferred WST-1 reagent containing media were recorded at 450 nm by using a microplate reader (ELx808, BioTek, Winooski, VT, USA). The results were drawn as percent viability graph and were analyzed with two paired Student's t-test statistically to investigate the cell viability of cells treated with increasing concentrations of NPs in comparison to negative control cells. The samples with a  $p \leq 0.05$  were marked with one star sign (\*), with a  $p \leq 0.01$  were marked with two star signs (\*\*), and with  $p \leq 0.001$  were marked with three star signs (\*\*\*)

### **3.2.5.4. Apoptosis/Necrosis Assay**

In order to determine the rate of apoptotic and necrotic cells of the cell population upon NP exposure, Annexin V-FITC apoptosis and necrosis detection kit from Calbiochem (Merck Millipore) was applied according to the manufacturer's instruction. A549 cells (50,000),

BEAS-2b cells (42,000) and MDA-MB-231 cells (50,000) were seeded into 24 well cell culture plates (n=3) and incubated for 24 h in the incubator at 37°C with 5 percent humidified atmosphere. After 24 h, the cells were treated with either 10 percent DMSO as positive control or 0.1, 0.5, 1.0 and 2.5 nM medium dispersed NPs and incubated for 24 h. Upon NP exposure, the cell culture medium containing detached cells in the wells were collected into 1.5 ml eppendorf tubes. The attached cells were incubated with 200 µl of trypsin for 5 min at incubator. A 400 µl of collected cell culture medium was added into trypsinized cells due to inactivate trypsin. The detached cells were collected in the same tubes including cell culture medium. The samples were agitated at 2500 rpm for 5 min at 4°C to obtain cells. After centrifuge, supernatant of samples were aspirated and they were washed with 1x PBS. They were centrifuged at 2500 rpm for 5 min, again. Based on manufacturer's instruction, 1x binding buffer was prepared from 10 x binding buffer with deionized water. 0.5 µl Annexin V-FITC reagent and 1 µl PI reagent per sample was added into 1 x binding buffer to prepare the dye mix. After washing with 1x PBS, one negative control was not stained with any dyes to analyze unstained cells, one negative control was stained with only Annexin V-FITC in order to set up green detector voltage, one negative control was stained with only PI due to adjust red detector voltage, and finally the other negative control samples, positive control samples and NP treated samples were stained with both dyes in 200 µl 1x binding mix for the purpose of apoptosis and necrosis detection. All stained cells were incubated with dyes at dark for 15 min. The samples were kept on at 4°C until analysis. For each sample, 20 000 cells were counted and analyzed by using on Guava easy-Cyte™ 5 (Merck Millipore) benchtop flow cytometer. According to calculation of the quadrants ratio of cell population by software, the results were drawn as a 2-D stacked column graph.

#### **3.2.5.5. Clonogenic Assay**

Due to observe survival ability of cells after NP exposure, their colony formation ability was visualized by clonogenic assay. For this assay, 100 cells for A549, BEAS-2b and

MDA-MB-231 cell lines were seeded into each wells of 6 well plates (n=3) and waited for cell's attachment for 24 h at 37°C and 5 percent CO<sub>2</sub> humidified incubator. After 24 h, the cells were treated with 2 ml either 10 percent DMSO as positive control or medium dispersed 0.1, 0.5, 1.0 and 2.5 nM NPs. A549 and MDA-MB-231 cells were incubated for seven days whereas BEAS-2b cells were for 10 days at humidified incubator until each seeded single cells formed colonies including at least 50 cells. During 7-10 days incubation at incubator, the media on cells were not changed and the plates were not moved anywhere to make able to create a steady condition. In the final days of the incubation, the colonies of negative controls were observed under microscope and the cells in each colonies were counted. If the number of cells in colonies were close to 50, the incubation was stopped. The media into the wells were removed and the colonies were stained with crystal violet by incubating with dye for 15 min. Then, the dye was taken away and the plates were washed with water until all dye was removed from the plate. The washed plates were left to dry. The violet colored colonies were counted. The results were drawn a clustered column graph and were analyzed with two paired Student's t-test statistically to investigate the survival ability of cells exposed to increasing concentrations of NPs in comparison to negative control cells by forming colonies. The samples with a  $p \leq 0.05$  were marked with one star sign (\*), with a  $p \leq 0.01$  were marked with two star signs (\*\*), and with  $p \leq 0.001$  were marked with three star signs (\*\*\*)).

#### ***3.2.5.6. Cell Cycle Evaluation***

The cell cycle progression of A549, BEAS-2b and MDA-MB-231 cells were analyzed for 24 h treatment with either naked AuNPs or surface functionalized AuNPs by flow cytometry. A549 cells (50,000), BEAS-2b cells (42,000) and MDA-MB-231 cells (50,000) were seeded in each well of 24 well plates (n=3) and incubated for 24h in an incubator 37°C with 5 percent CO<sub>2</sub> humidified atmosphere. After cell attachment, the cells were treated with 0.1  $\mu$ M colchicine as a positive control and 0.1, 0.5, 1.0 and 2.5 nM of medium dispersed NPs for 24 h. At the end of 24h incubation, the cell culture media in

wells were collected into 1.5 ml eppendorf tubes. The attached cells were incubated with 200  $\mu$ l of trypsin-EDTA solution for 5 min at 37°C in humidified incubator. 400  $\mu$ l of collected medium was added into detached cells to terminate trypsin activity. The collected cells were centrifuged at 2500 rpm for 5 min at 4°C. The supernatant was aspirated, and the cells were suspended in 1x PBS. After centrifugation at same speed and time, the cells were fixed with 500  $\mu$ l of 70 percent ice-cold ethanol (v/v, ethanol in water) by gently mixing and kept at -20°C at least overnight. The fixed cells were agitated at 2500 rpm for 5 min at 4°C. The supernatant was aspirated and the cells were suspended in 500  $\mu$ l of 0.1 percent ice-cold Triton X-100 (v/v, Triton X-100 in 1x PBS) and incubated for 20 min at room temperature to make cells permeabilized. After incubation with Triton X-100, the cells were centrifuged and the cells were suspended in 200  $\mu$ l of 100  $\mu$ g/ml of RNase solution (v/v, RNase solution in 1x PBS) and incubated for 30 min at 37°C to prevent attachment of propidium iodide (PI) to RNAs, which gave positive wrong results. Finally, PI staining was carried out as the cells were stained with 1  $\mu$ g/ml for 15 min at dark, except one negative control, which called as unstained. Then, their cell cycle progressions were analyzed on Red Width vs Red Area plot on flow cytometry software. The cell cycle phases as G0/G1, S and G2/M, were adjusted by considering those of negative and positive controls. According to the calculation of cell cycle phase percents by software, the results were drawn as a 2-D stacked column graph.

## 4. RESULTS AND DISCUSSION

### 4.1. AuNPs SYNTHESIS AND CHARACTERIZATION

#### 4.1.1. Characterization

Spherical AuNPs of 13 nm diameter size were synthesized by Turkevich method as monodisperse and suspended in water [102]. The synthesized AuNPs were characterized by Transmission Electron Microscopy (TEM), UV/Vis spectroscopy and Dynamic Light Scattering (DLS) as shown in Figure 4.1. The TEM images showed that the AuNPs were in 13 nm average diameter. UV/Vis and DLS spectra were typical for the AuNPs colloidal suspension synthesized with the method.

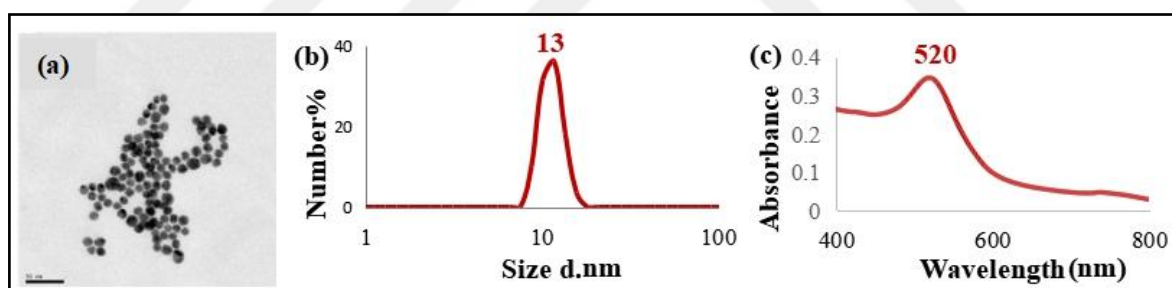


Figure 4.1. Characterization of colloidal suspension containing 13 nm AuNPs. (a) TEM image, (b) UV/Vis spectrum, and (c) DLS spectrum.

#### 4.1.2. Determination of Concentration

The size and concentration are the key points of AuNPs in their applications. Since the AuNPs can be synthesized in a wide range of sizes by several synthesis protocols, their concentration determination becomes troublesome. Thus, the concentration of synthesized spherical AuNPs in suspension is determined by Beer-Lambert's Law. In this approach,



the concentration of AuNPs in suspension can be estimated by measuring the SPR value of AuNPs by UV/Vis spectroscopy [203]. Therefore, the diluted AuNP suspensions in water were prepared as 1:2, 1:4, 1:8 and 1:16 in triplicates. Then, their absorbance values at SPR peak, 519 nm, were recorded three times. The obtained nine measurements for each dilution factors were averaged. Beer-Lambert's law is referred as depicted in Equation 4.1:

$$A = C \times \epsilon \times l \quad (4.1)$$

where A is absorbance of AuNPs suspension, C is the concentration of AuNPs in suspension,  $\epsilon$  is extinction coefficient of AuNPs and l is the path length of cuvette, which was 1 cm. The slope of absorbance vs dilution factor graph of AuNPs was calculated as 3.49 and this slope was equal to  $\epsilon$  of AuNPs in suspension from formula  $\epsilon = A/DF$ . By referring  $\epsilon$  values from literature,  $\epsilon$  of around 13 nm sized AuNPs has  $10^8 \text{ M}^{-1} \text{ cm}^{-1}$  unit [213]. Moreover,  $A_{\text{SPR}}/A_{450}$  ratios discussed by Haiss et al. to determine the concentration of 12 and 14 nm AuNP suspension were 1.56 and 1.61 respectively. The ratio of synthesized 13 nm AuNPs was calculated as 1.57, which is consisted with the literature values above. Therefore,  $\epsilon$  was assessed as  $3.49 \times 10^8 \text{ M}^{-1} \text{ cm}^{-1}$ .

After the determination of  $\epsilon$ , the concentration of AuNP suspension was calculated with Beer-Lambert's Law. The absorbance values at SPR peak and  $\epsilon$  of 13 nm AuNPs were placed in the formula and the concentration of synthesized 13 nm AuNPs suspension was found as 10 nM.

As a next step, the AuNP numbers in 1 ml suspension was determined by using a formula, suggested by Haiss et al., as shown in Figure 4.2 [213]. Based on this formula, absorbance value at 450 nm was crucial to designate the AuNP numbers in suspension. As a result,  $5.37 \times 10^{12}$  13 nm sized AuNPs were suspended in 1 ml suspension.

<p><b>The number of AuNPs in 1 ml colloidal suspension:</b></p> $N = \frac{A_{450} \times 10^{14}}{d^2 [-0.295 + 1.36 \exp(-(\frac{d-96.8}{78.2})^2)]}$ <p style="color: red; text-align: center;"><b><math>N = 5.37 \times 10^{12}</math> AuNPs in 1 ml suspension</b></p>
---

Figure 4.2. Determination of AuNP numbers in 1 ml suspension.  $A_{450}$  was 1.1026 of 1:10 diluted AuNP suspension and  $d$  was equal to 6.5 nm.

As a result, the concentration and  $\epsilon$  of synthesized 13 nm AuNPs was calculated as 10 nM and  $3.49 \times 10^8 \text{ M}^{-1} \text{ cm}^{-1}$ . The number of 13 nm sized AuNPs in 1 ml suspension was estimated as  $5.37 \times 10^{12}$ . In addition, the concentration of AuNP-Biomolecule suspensions was assumed as much as that of 13 nm AuNPs suspension. The reason behind of this is that the determination of AuNP concentration by UV/Vis spectroscopy depends on the color of the suspension and the color of AuNP-Biomolecule suspensions were darker than naked AuNPs suspension. Moreover, during surface modification process, only biomolecules were added into AuNP suspension to cover the surfaces of AuNPs and this did not result to decrease the AuNP number in reaction tube. Therefore, it was assumed that the concentration of AuNP conjugates and NP numbers in suspension was equal to that of naked AuNP suspension.

## 4.2. SURFACE MODIFICATION OF AuNPs WITH BIOMOLECULES

### 4.2.1. Surface Modification of AuNPs with Carbohydrates

Carbohydrates have been used for surface modification of AuNPs since they are a major targeting molecules due to their unique molecular characteristics and actions in living systems [216]. Many types of carbohydrates have been conjugated with AuNPs to study carbohydrate-carbohydrate and carbohydrate-protein interactions *ex vivo* [217] and *in vivo* [218] or *in vitro* diagnostics [219]. Carbohydrates cannot link AuNP surfaces directly, thus

the linkage between carbohydrates and AuNPs can be established through a thiol group -SH [220]. In this study, it was aimed to conjugate AuNPs with carbohydrates via Au-S bond formation. Glucose, Mannose, Lactose and Maltose were chosen in the study. The reason why they were selected was that Glucose and Mannose were epimers at the second carbon, and the free units of Lactose and Maltose were Galactose and Glucose, which were epimers at C4 as shown in Figure 4.3. The mentioned differences would be helpful to investigate the cellular response of living cells to subtle surface chemistry changes on the NP surfaces.

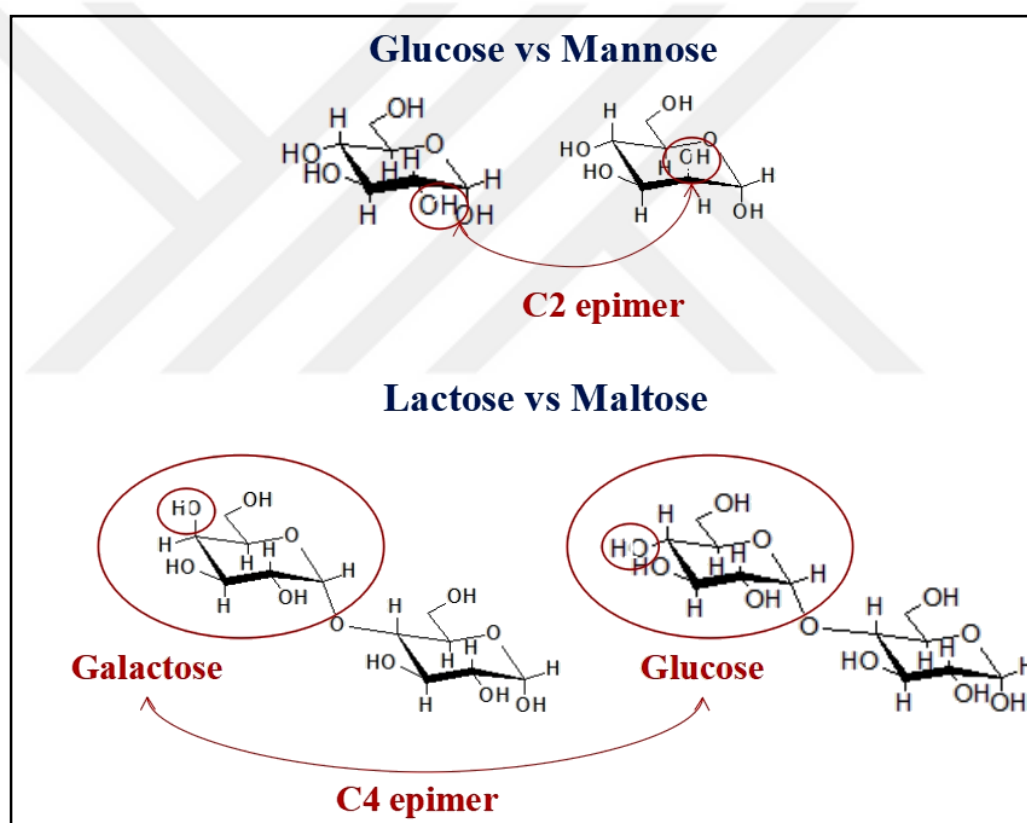


Figure 4.3. Scheme of orientation differences between Glucose and Mannose and free monosaccharide differences between Lactose and Maltose after conjugation.

#### 4.2.1.1. Thiolation of Carbohydrates and Their Characterization

For the purpose of linking carbohydrates with AuNPs, the carbohydrates initially were thiolated by Lawesson reagent to create C-S bond formation at first carbon, and then the surface of AuNPs were coated with them, as schemed in Figure 4.4 [214]. The reason for using this reagent was its ability to thiolate only -OH group of the first carbon of carbohydrates as shown in the figure.

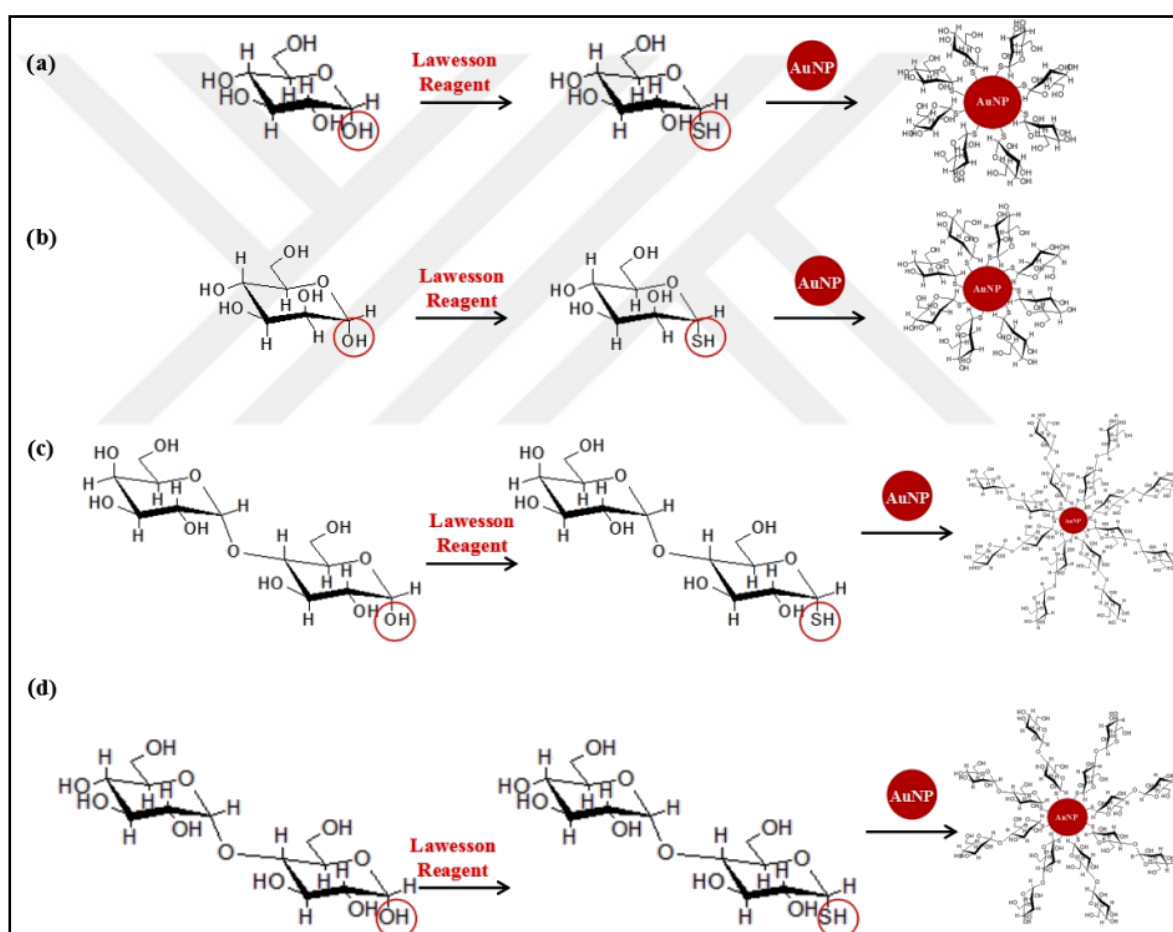


Figure 4.4. Scheme of AuNP-Carbohydrate conjugation process. **(a)** Glucose, **(b)** Mannose, **(c)** Lactose and **(d)** Maltose.

The thiolated carbohydrates powders were characterized by FTIR. The comparative FTIR spectra of unprotected and thiolated carbohydrates were seen in Figure 4.5. The weak

peaks around  $2550\text{-}2650\text{ cm}^{-1}$  and  $1650\text{ cm}^{-1}$  on the spectra of thiolated carbohydrates represented -SH bond vibration and C-S vibration, respectively, however a broad peak around  $3200\text{ cm}^{-1}$  representing -OH bond was observed only on the spectra of unprotected carbohydrates [221]. By considering these weak peaks representing thiol functionalization, it was concluded that carbohydrates were thiolated by using Lawesson reagent.

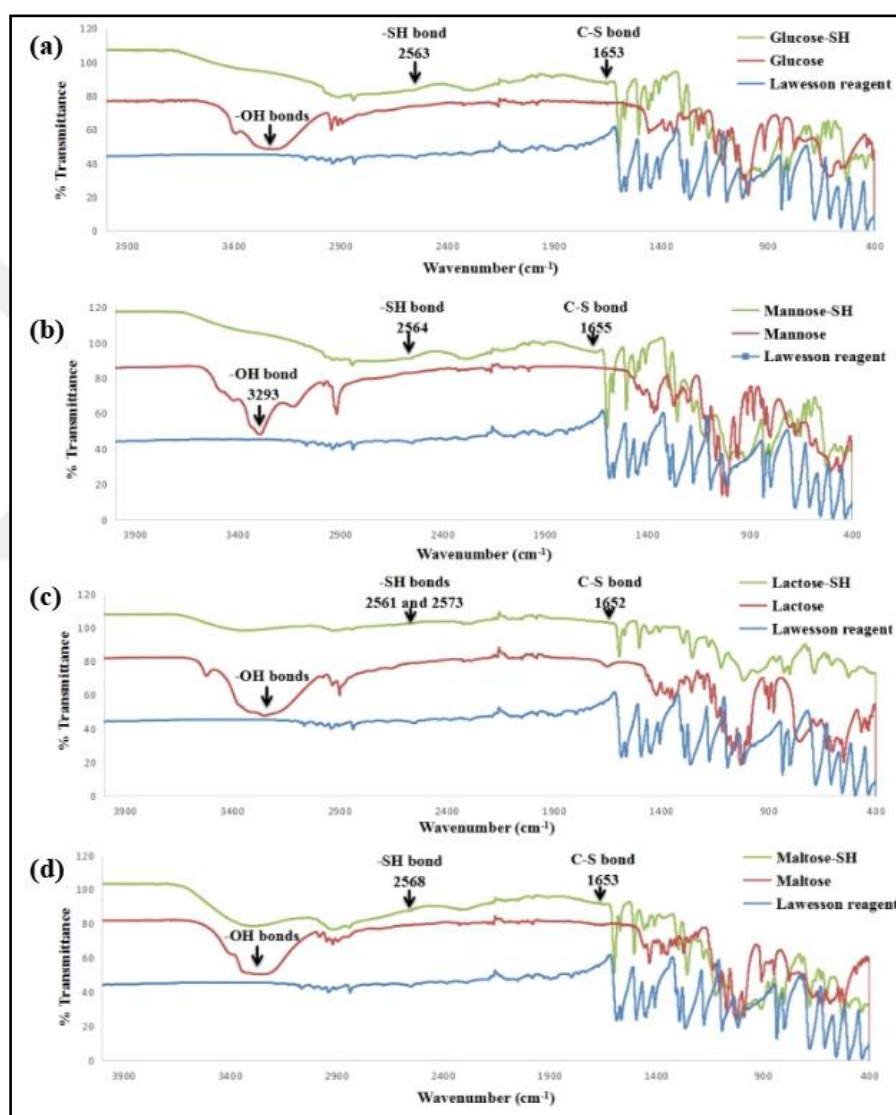


Figure 4.5. Comparative FTIR spectra of (a) Thiolated Glucose, (b) Thiolated Mannose, (c) Thiolated Lactose and (d) Thiolated Maltose.

#### 4.2.1.2. Optimization of AuNP-Lactose and AuNP-Maltose Conjugates and Their Characterization

The spherical AuNPs of 13 nm diameter size (10 nM, 1ml) were mixed with 25, 50, 75 and 250  $\mu$ l of 10 mg/ml thiolated Maltose and Lactose solutions (n=3). The reaction tubes were shaken for overnight. The photo of naked AuNPs and AuNP-Saccharide conjugates was given in Figure 4.6. No AuNP aggregation was observed after the conjugation indicating the stability of the suspension.

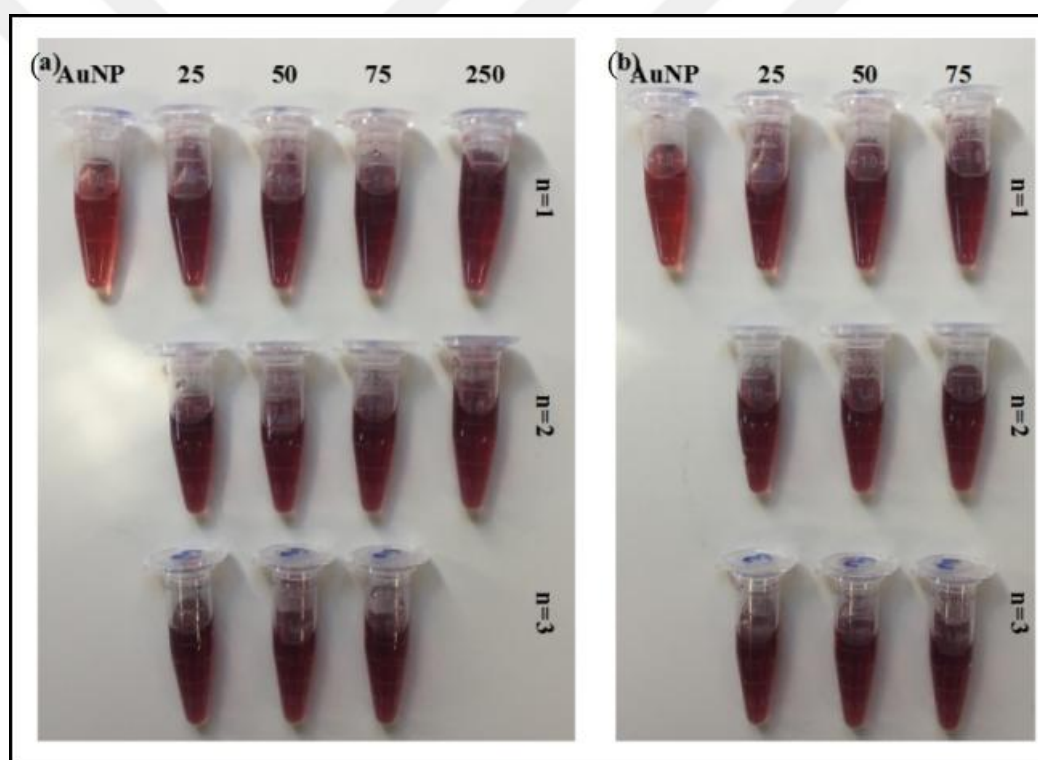


Figure 4.6. While light images of suspensions of (a) naked AuNP and AuNP-Maltose conjugates, and (b) naked AuNP and AuNP-Lactose conjugates. “n” indicates replicate number.

The naked AuNPs and AuNP-Maltose and AuNP-Lactose conjugates were characterized using UV/Vis spectroscopy and their spectra were presented in Figure 4.7. The SPR band

of naked 13 nm AuNPs was at 519 nm whereas AuNP-Maltose conjugates had it at 525 nm, and AuNP-Lactose conjugates at 524 nm. A 5-6 nm redshift on UV/Vis spectra indicates that conjugation of thiolated Lactose and Maltose to AuNP surfaces.

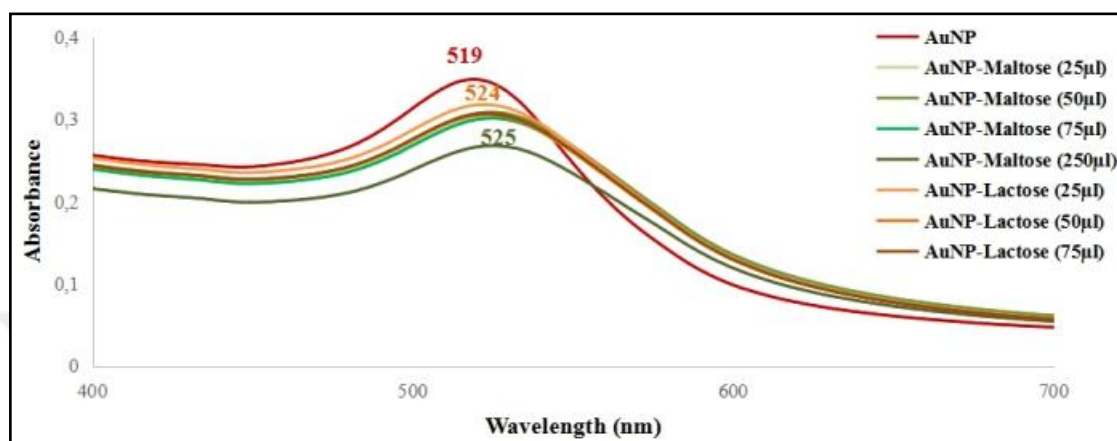


Figure 4.7. Comparative UV/Vis spectra of naked AuNPs and AuNPs modified with increasing concentrations of thiolated Maltose and Lactose.

The naked AuNPs, AuNP-Lactose and AuNP-Maltose conjugates were characterized by DLS. The hydrodynamic sizes and zeta potentials of triplicates were measured three times. The collected nine measurement was averaged, and the average values of size and zeta potentials of naked AuNPs, AuNP-Lactose and AuNP-Maltose conjugates were given in Table 4.3. Based on the results, the naked AuNPs had an average 12.2 nm size, however after the conjugation the sizes of conjugates were larger. Moreover, the zeta potential of AuNPs were more negative after conjugation with thiolated Lactose and Maltose.

Table 4.1. Average hydrodynamic sizes and zeta potentials of naked AuNPs and AuNPs modified with increasing concentrations of thiolated Maltose and Lactose.

Sample	Size (nm)	Zeta potential (mV)
AuNPs	12.2 ± 0.3	-13.3 ± 0.2
AuNP-Maltose(25µl)	13.4 ± 0.5	-21.4 ± 2.6
AuNP-Maltose (50µl)	13.3 ± 0.7	-16.1 ± 1.0
AuNP-Maltose (75µl)	13.9 ± 0.6	-26.9 ± 6.6
AuNP-Maltose (250µl)	13.8 ± 0.4	-23.7 ± 2.4
AuNP-Lactose (25µl)	13.3 ± 0.3	-20.4 ± 4.9
AuNP-Lactose (50µl)	13.0 ± 0.7	-26.2 ± 3.4
AuNP-Lactose (75µl)	13.2 ± 0.2	-22.1 ± 5.7

The zeta potentials of AuNP-Lactose and AuNP-Maltose was measured as negative although Lactose and Maltose was neutrally charged. The reason behind that can be explained as after the replacement between the citrate ions and carbohydrates on AuNP surface, the free citrate ions were strongly interacted with -OH groups on carbohydrates and made the AuNP surface negative, as schemed in Figure 8. In addition, this intermolecular interaction can be claimed as strong since the citrate ions and the -OH groups on the carbohydrates remained as interacted after they were washed twice.

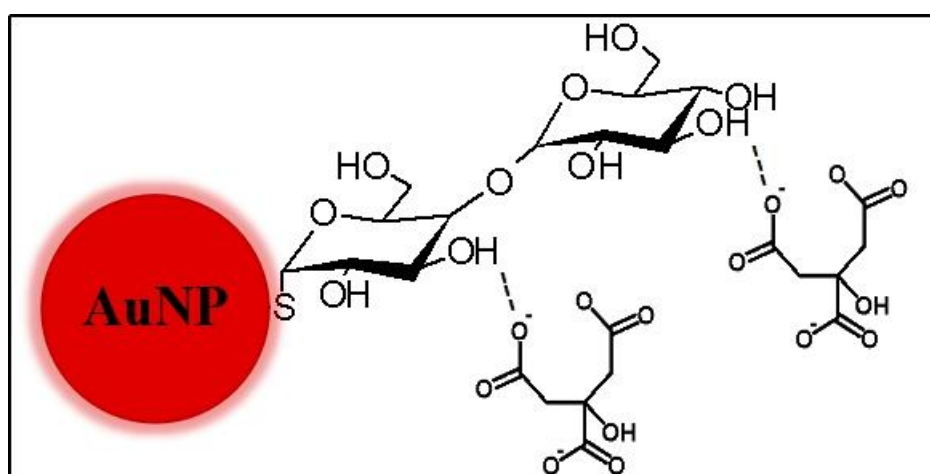


Figure 4.8. Intermolecular interaction between the free citrate ions and -OH groups of carbohydrates on AuNP surfaces.



In order to check the carbohydrate density on AuNPs and observe the conjugation between carbohydrates and AuNPs, the naked AuNPs and AuNP-Maltose and AuNP-Lactose conjugates were also characterized by 1 percent Agarose gel electrophoresis as seen in Figure 4.9. The naked AuNPs could not run because the precipitation of AuNPs caused by TAE buffer. The all conjugates run through the gel and the bands were seen dense. When compared the bands in each conjugation group, the best conjugation of AuNPs with thiolated Lactose and Maltose was successful in the addition of 75  $\mu$ l of 10 mg/ml solution.

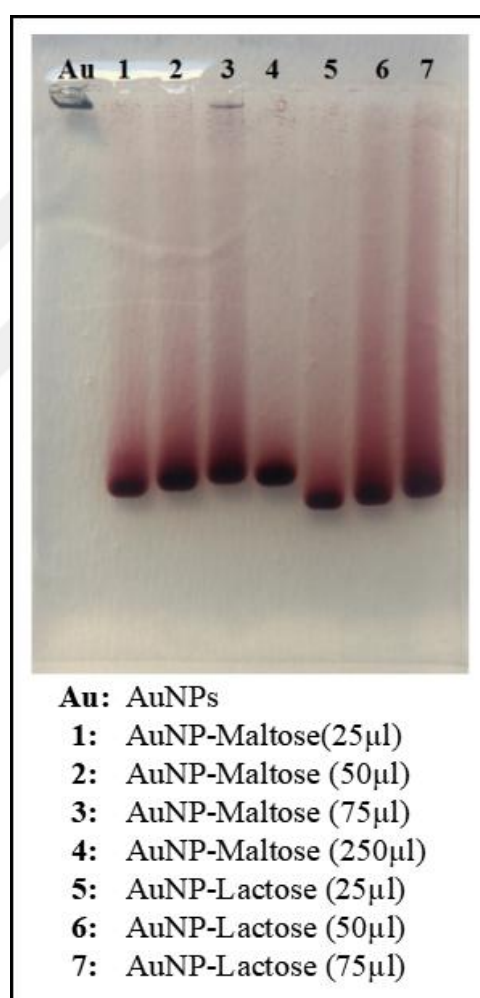


Figure 4.9. White light image of agarose gel loaded naked AuNPs and AuNPs modified with increasing concentrations of thiolated Maltose and Lactose.

#### ***4.2.1.3. Optimization of AuNP-Glucose and AuNP-Mannose Conjugates and Their Characterization***

The spherical AuNPs of 13 nm diameter size (10 nM, 1ml) were coated with 25, 50 and 75  $\mu$ l of 10 mg/ml Glucose and Mannose, as same as AuNP-Lactose and AuNP-Maltose conjugates. The photo of naked AuNPs and AuNP conjugates was given in Figure 4.10. No AuNP aggregation was observed in the reaction tubes after conjugation indicating the stability of the suspension.

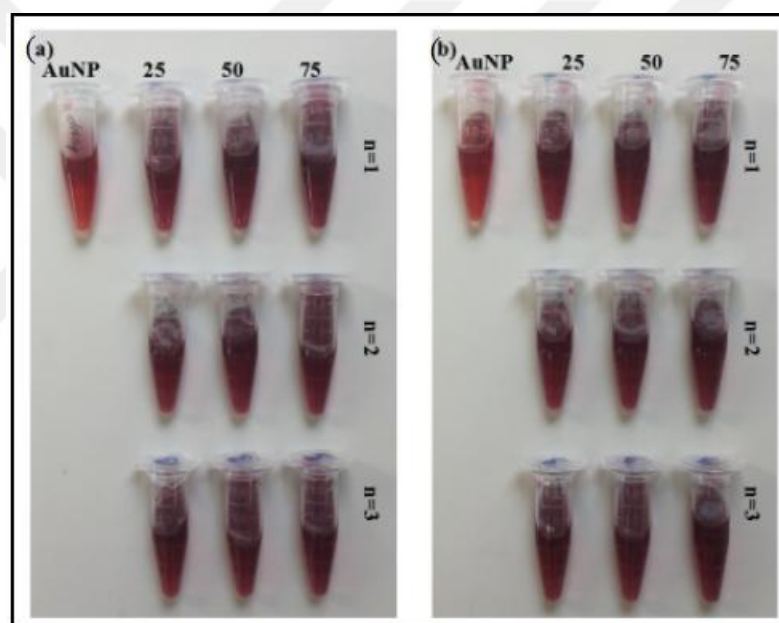


Figure 4.10. While light images of suspensions of (a) naked AuNP and AuNP-Glucose conjugates, and (b) naked AuNP and AuNP-Mannose conjugates. “n” indicates replicate number.

The naked AuNPs and AuNP-Glucose and AuNP-Mannose conjugates were characterized by UV/Vis, as seen in Figure 4.11. The SPR of naked AuNPs was at 519 nm while that of the conjugates was 4-6 nm redshifted. The shift increased with respected to the concentration increase of Glucose or Mannose in the conjugation. Thus, the most red-shift

was observed on the spectra of AuNP-Glucose and AuNP-Mannose spectra, which were functionalized with 75  $\mu\text{l}$  of 10 mg/ml mono saccharide solution.

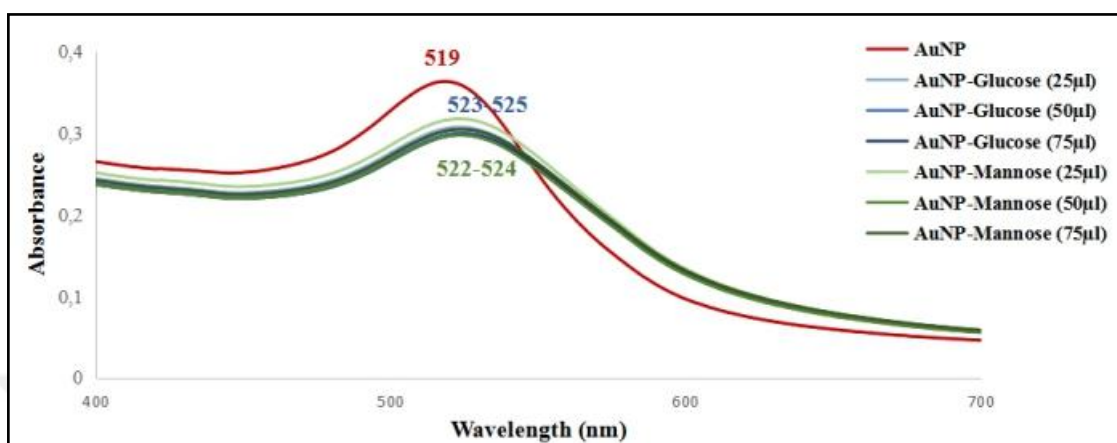


Figure 4.11. Comparative UV/Vis spectra of naked AuNPs and AuNPs modified with increasing concentrations of thiolated Glucose and Mannose.

The hydrodynamic sizes and zeta potentials of naked AuNPs and functionalized AuNPs were measured by DLS three times and the average size and zeta potentials were listed in Table 4.2. The size of naked AuNPs were approximately 11.7 nm while the conjugates were larger. Furthermore, the zeta potential on AuNP surfaces got more negative after conjugation with mono saccharides.

Table 4.2. Average hydrodynamic sizes and zeta potentials of naked AuNPs and AuNPs modified with increasing concentrations of thiolated Glucose and Mannose.

Sample	Size (nm)	Zeta potential (mV)
AuNPs	11.7 $\pm$ 0.4	-20.0 $\pm$ 1.3
AuNP-Glucose (25 $\mu\text{l}$ )	12.9 $\pm$ 0.5	-31.3 $\pm$ 8.0
AuNP-Glucose (50 $\mu\text{l}$ )	13.0 $\pm$ 0.4	-45.3 $\pm$ 4.6
AuNP-Glucose (75 $\mu\text{l}$ )	13.0 $\pm$ 0.8	-34.0 $\pm$ 9.5
AuNP-Mannose (25 $\mu\text{l}$ )	12.6 $\pm$ 0.5	-42.3 $\pm$ 6.0
AuNP-Mannose (50 $\mu\text{l}$ )	12.5 $\pm$ 0.5	-36.0 $\pm$ 11.0
AuNP-Mannose (75 $\mu\text{l}$ )	12.1 $\pm$ 0.8	-26.6 $\pm$ 6.4

The naked AuNPs and AuNP-Maltose and AuNP-Lactose conjugates were characterized by 1 percent Agarose gel in order to check the density of mono saccharides on AuNP surfaces, as seen in Figure 4.12. The result of Agarose gel showed that the conjugation between AuNPs and mono saccharides in those concentrations was not successful. Therefore, it was decided that AuNPs could be conjugated with higher concentration of thiolated Glucose and Mannose solutions.

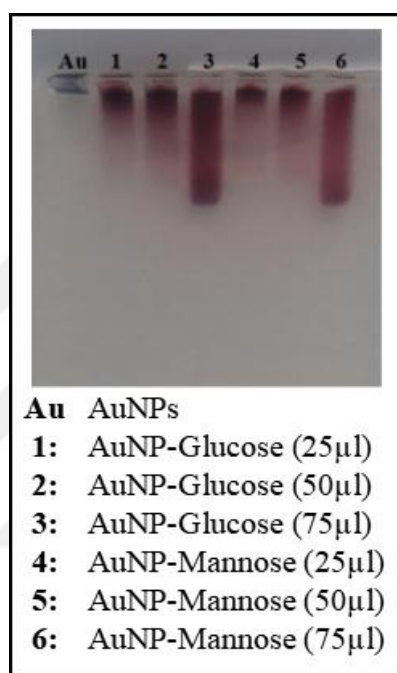


Figure 4.12. White light image of agarose gel loaded naked AuNPs and AuNPs modified with increasing concentrations of thiolated Glucose and Mannose.

AuNPs were functionalized with higher concentrations of thiolated Glucose and Mannose solutions. The spherical AuNPs of 13 nm diameter size (10 nM, 1ml) were conjugated with 100, 150 and 200  $\mu$ l of 10 mg/ml thiolated Glucose and Mannose solutions (n=3). They were shaken for overnight. The suspensions of naked AuNPs and AuNP-Glucose and AuNP-Mannose conjugates were seen in Figure 4.13. No AuNP aggregation was observed after the functionalization indicating the stability of the suspension.

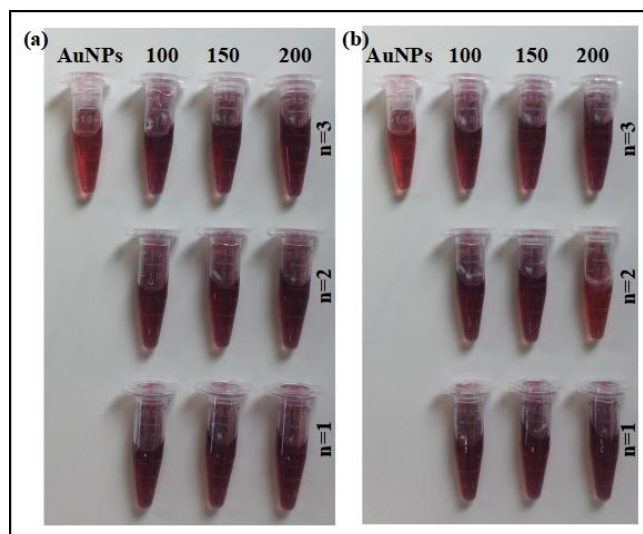


Figure 4.13. White light images of suspensions of (a) naked AuNP and AuNP-Glucose conjugates, and (b) naked AuNP and AuNP-Mannose conjugates. “n” indicates replicate number.

The naked AuNPs, AuNP-Glucose and AuNP-Mannose conjugates were characterized by UV/Vis spectroscopy. The comparative UV/Vis spectra of naked AuNPs, AuNP-Glucose and AuNP-Mannose was given in Figure 4.14. The SPR of naked AuNPs was observed at 519 nm while the whole conjugates had SPR at 524 nm. The 5 nm redshift can be considered as a proof that AuNPs were functionalized with thiolated Glucose and Mannose.

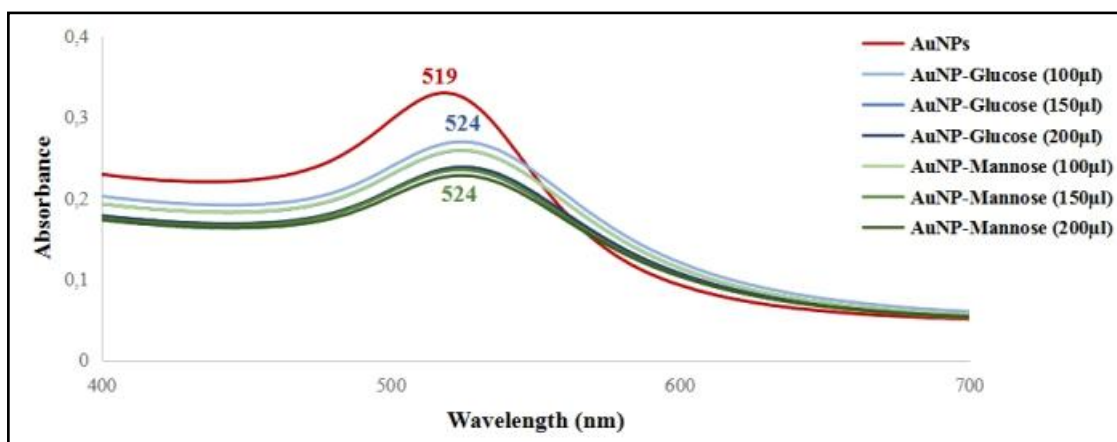


Figure 4.14. Comparative UV/Vis spectra of naked AuNPs and AuNPs modified with increasing concentrations of thiolated Glucose and Mannose.

The naked AuNPs and AuNP-Glucose and AuNP-Mannose conjugates were characterized by DLS. The hydrodynamic sizes and zeta potentials of the triplicates were measured three times. The acquired nine measurement was averaged. The average size and zeta potential of naked AuNPs and AuNP-Glucose and AuNP-Mannose conjugates was given with the standard deviations in Table 4.3. The hydrodynamic size of naked AuNPs was approximately 11.9 nm. After conjugation with thiolated Glucose and Mannose, the sizes were grown. When discussed the zeta potentials, the naked AuNPs had -6.1 mV surface charge while the conjugates had more negative surface charge. However, the zeta potentials of AuNP-Glucose and AuNP-Mannose, conjugated with 100  $\mu$ l of 10 mg/ml mono saccharides, did not have valuable surface charge alteration. This could imply that the surface coverage of mono saccharides was not dense in this concentration. As a result, the size growth and more negative surface determined that AuNPs were conjugated with thiolated Glucose and Mannose.

Table 4.3. Average hydrodynamic sizes and zeta potentials of naked AuNPs and AuNPs modified with increasing concentrations of thiolated Glucose and Mannose.

Sample	Size (nm)	Zeta potential (mV)
AuNPs	11.9 $\pm$ 0.3	-6.1 $\pm$ 1.7
AuNP-Glucose (100 $\mu$ l)	12.2 $\pm$ 0.8	-10.8 $\pm$ 3.1
AuNP-Glucose (150 $\mu$ l)	12.6 $\pm$ 0.5	-32.2 $\pm$ 8.3
AuNP-Glucose (200 $\mu$ l)	12.7 $\pm$ 0.5	-26.2 $\pm$ 1.7
AuNP-Mannose (100 $\mu$ l)	12.2 $\pm$ 0.9	-9.4 $\pm$ 0.4
AuNP-Mannose (150 $\mu$ l)	12.3 $\pm$ 0.7	-13.8 $\pm$ 1.7
AuNP-Mannose (200 $\mu$ l)	12.6 $\pm$ 0.7	-22.7 $\pm$ 1.8

To observe the mono saccharide density on AuNP surfaces, the naked AuNPs, AuNP-Glucose and AuNP-Mannose conjugates were characterized by 1 percent Agarose gel electrophoresis. The gel image was given in Figure 4.15. The smear-like running in the 1st and 4th wells of the gel indicated that the AuNPs could not be functionalized by 100  $\mu$ l of 10 mg/ml mono saccharides. On the other hand, AuNP-Glucose and AuNP-Mannose, coated with 150  $\mu$ l of 10 mg/ml, seen in the 2nd and 5th wells, were the best conjugations in terms of denser bands. Consequently, it was clearly understood that 1 ml AuNPs should

be functionalized with 150  $\mu\text{l}$  of 10 mg/ml thiolated Glucose and Mannose to obtain dense coating.

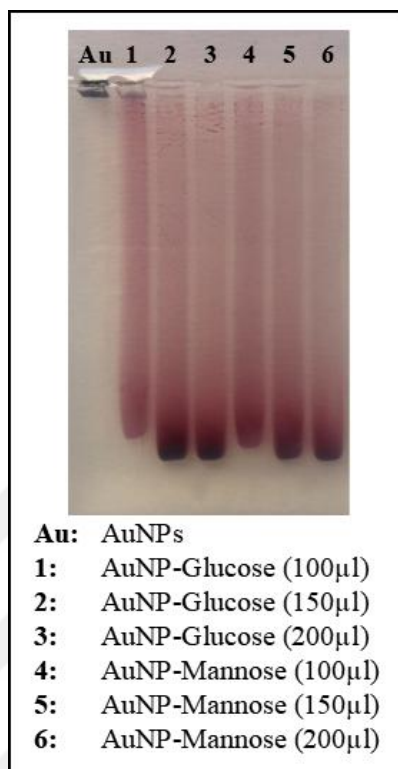


Figure 4.15. White light image of agarose gel loaded naked AuNPs and AuNPs modified with increasing concentrations of thiolated Glucose and Mannose.

#### ***4.2.1.4. Conjugation of AuNPs with Carbohydrates and Their Characterization***

Based on optimization data, 1 ml of 10 nM 13 nm AuNPs were conjugated with 75  $\mu\text{l}$  of 10 mg/ml thiolated Lactose and Maltose, 150  $\mu\text{l}$  of 10 mg/ml thiolated Glucose and Mannose solutions. The naked AuNPs and AuNP-Carbohydrate conjugates were characterized by UV/Vis, DLS, 1 percent Agarose gel electrophoresis, FTIR and SERS. The image of suspensions of naked AuNPs and AuNP-Carbohydrate conjugates was given in Figure 4.16. There was no AuNP aggregation in the reaction tubes after conjugation and the colors were red and clear. In addition, the color of AuNP conjugates were slightly darker than that of naked AuNPs.

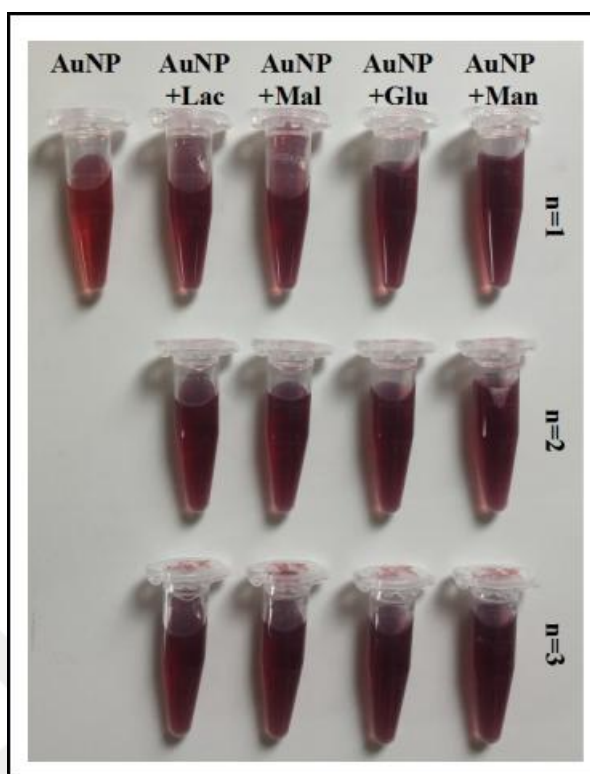


Figure 4.16. White light image of suspensions of naked AuNPs and AuNP-Carbohydrate conjugates. “n” indicates the replicate number.

The naked AuNPs and AuNP-Carbohydrate conjugates were characterized with UV/Vis spectroscopy to analyze their optical characteristics. The comparative UV/Vis spectra of naked AuNPs and AuNP-Carbohydrate conjugates were given in Figure 4.17. The SPR of naked 13 nm AuNPs were seen at 518 nm while the conjugates had it at 524 or 525 nm. The SPR of monosaccharide coated AuNPs was at 525 nm whereas that of disaccharides were at 524 nm. These red-shifts on their SPR values represented that the surface of AuNPs were coated with carbohydrates.



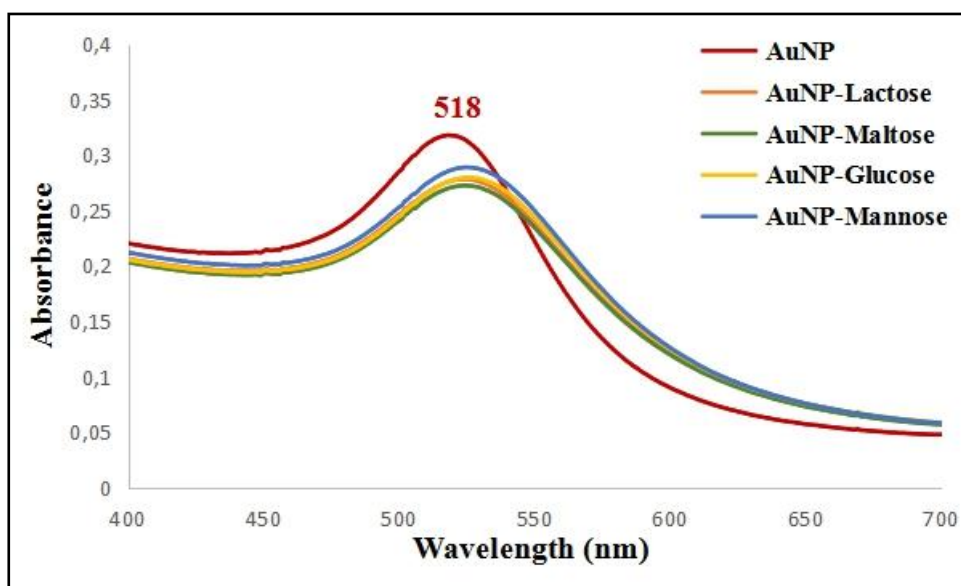


Figure 4.17. Comparative UV/Vis spectra of naked AuNPs and AuNP-Carbohydrate conjugates.

The naked AuNPs and AuNP-Carbohydrate conjugates were characterized by DLS. The hydrodynamic sizes and zeta potentials of naked AuNPs and AuNP-Carbohydrate conjugate triplicates were measured three times and the total nine measurements were averaged. The average hydrodynamic sizes and zeta potentials of naked AuNPs and AuNP-Carbohydrate conjugates were given in Table 4.4. The naked AuNPs had 10.7 nm average size and -10.5 mV average zeta potential. After conjugation with mono and disaccharides, the sizes were larger and the zeta potentials were more negative.

Table 4.4. SPR, average hydrodynamic sizes and zeta potentials of naked AuNPs and AuNP-Carbohydrate conjugates.

Sample	SPR (nm)	Size (nm)	Zeta Potential (mV)
<b>AuNP</b>	518	10.7 ± 0.5	-10.5 ± 0.3
<b>AuNP-Glucose</b>	525	12.6 ± 0.5	-18.2 ± 1.9
<b>AuNP-Mannose</b>	525	12.6 ± 0.9	-15.5 ± 1.9
<b>AuNP-Lactose</b>	524	12.3 ± 0.6	-16.8 ± 2.2
<b>AuNP-Maltose</b>	524	12.3 ± 0.6	-13.5 ± 1.8

The naked AuNPs and AuNP-Carbohydrate conjugates were also characterized by 1 percent Agarose gel electrophoresis to examine carbohydrate density on AuNPs in suspension, as seen in Figure 4.18. The naked AuNPs precipitated whenever loaded into the gel due to salt content of TAE buffer, however the conjugates run through gel since their surfaces were covered with adequate amount of carbohydrates and so they could not be affected by salt. The bands of the conjugates were denser, except AuNP-Maltose in the 2<sup>nd</sup> well. Only AuNP-Maltose conjugates moved through the gel as smear-like because of bad sampling. Through this result, it was claimed that the surfaces of all AuNPs in 1 ml suspension were covered with carbohydrates in added amounts and also it was argued that most AuNPs in the suspension had similar carbohydrate number on their surfaces when interpreted their band densities.

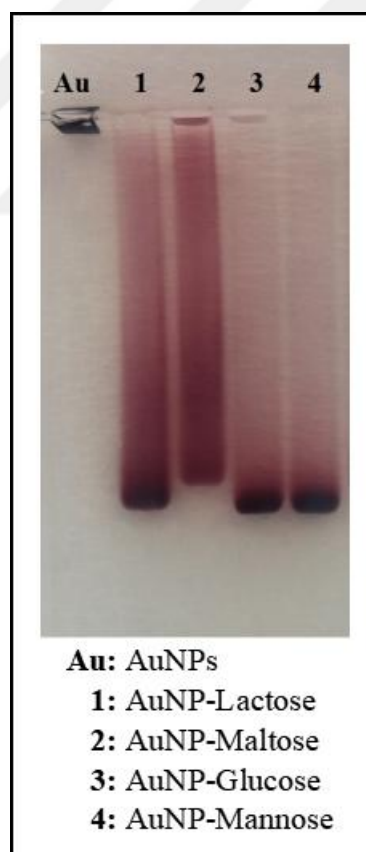


Figure 4.18. White light image of Agarose gel, in which the naked AuNPs and AuNP-Carbohydrate conjugates were loaded.

The naked AuNPs and AuNP-Carbohydrate conjugates were characterized by FTIR to obtain information about surface chemistry. The comparative FTIR spectra of naked AuNPs and AuNP-Carbohydrate conjugates were shown in Figure 4.19. On the FTIR spectrum of naked AuNPs, no valuable information could be obtained, as expected, because they had only citrate reduced surfaces. On the other hand, on the spectra of AuNP conjugates, some chemical properties were investigated, such as C-H stretching at 2850-2900  $\text{cm}^{-1}$ , O-C stretching at 1472  $\text{cm}^{-1}$ , C-H plane bending  $\text{cm}^{-1}$ , C-C stretching at 1090-1250  $\text{cm}^{-1}$  and C-O plane bending at 719 and 548  $\text{cm}^{-1}$ . These all peaks were related to the chemical composition of carbohydrates [221]. As a result, it was shown that carbohydrates were located onto the AuNP surfaces since the chemical changes on the surface were monitored by FTIR.

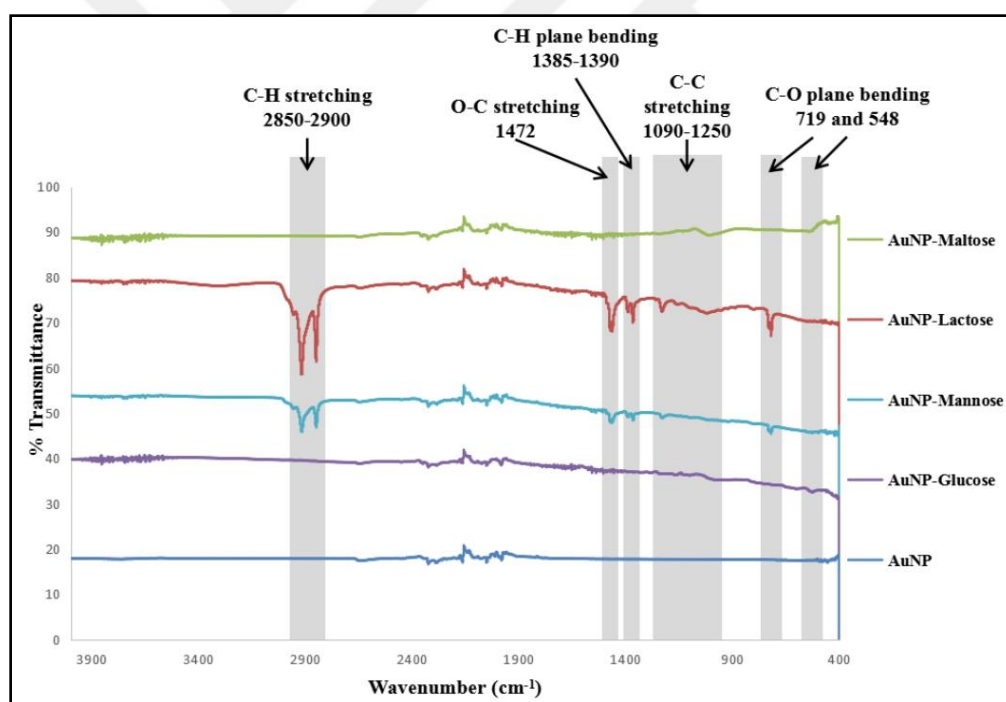


Figure 4.19. Comparative FTIR spectra of naked AuNPs and AuNP-Carbohydrate conjugates.

The naked AuNPs and AuNP-Carbohydrate conjugates were finally characterized with SERS in order to determine chemical identity and structural information of AuNP surfaces after the conjugation. The comparative SERS spectra of naked AuNPs and AuNP-Carbohydrate conjugates were presented in Figure 4.20. The SERS spectra analysis

indicated that there was not a noteworthy chemical species present on the AuNP surfaces. However, the characteristic peaks originating from carbohydrate on the AuNP-Carbohydrate conjugates were observed such as C-O stretching at  $492\text{ cm}^{-1}$ , C-C stretching at  $555, 605, 1031, 1054, 1140$  and  $1178\text{ cm}^{-1}$ , C-S stretching at  $635, 654, 665$  and  $750\text{ cm}^{-1}$ , C-H stretching at  $82, 823, 946, 1260, 1287$  and  $1325\text{ cm}^{-1}$ , C-CH<sub>2</sub> stretching at  $515\text{ cm}^{-1}$ , and C-H<sub>2</sub> stretching at  $1407$  and  $1429\text{ cm}^{-1}$  [222]. Furthermore, the similar spectral pattern and common peak intensities were observed on the spectra of AuNP-Glucose and AuNP-Mannose, and AuNP-Lactose and AuNP-Maltose. On the spectra of AuNPs conjugated with monosaccharides, C-S stretching at  $635\text{ cm}^{-1}$ , C-C stretching at  $1054\text{ cm}^{-1}$ , C-H stretching at  $1325\text{ cm}^{-1}$  and C-H<sub>2</sub> stretching at  $1407\text{ cm}^{-1}$  were dominant peaks. Nevertheless, C-H stretching at  $802$  and  $823\text{ cm}^{-1}$ , C-C stretching at  $1031, 1140$  and  $1178\text{ cm}^{-1}$  were dominant on the spectra of AuNPs conjugated with disaccharides. In conclusion, the SERS spectra of the conjugates supported the binding of ligand bound to the AgNP surfaces.

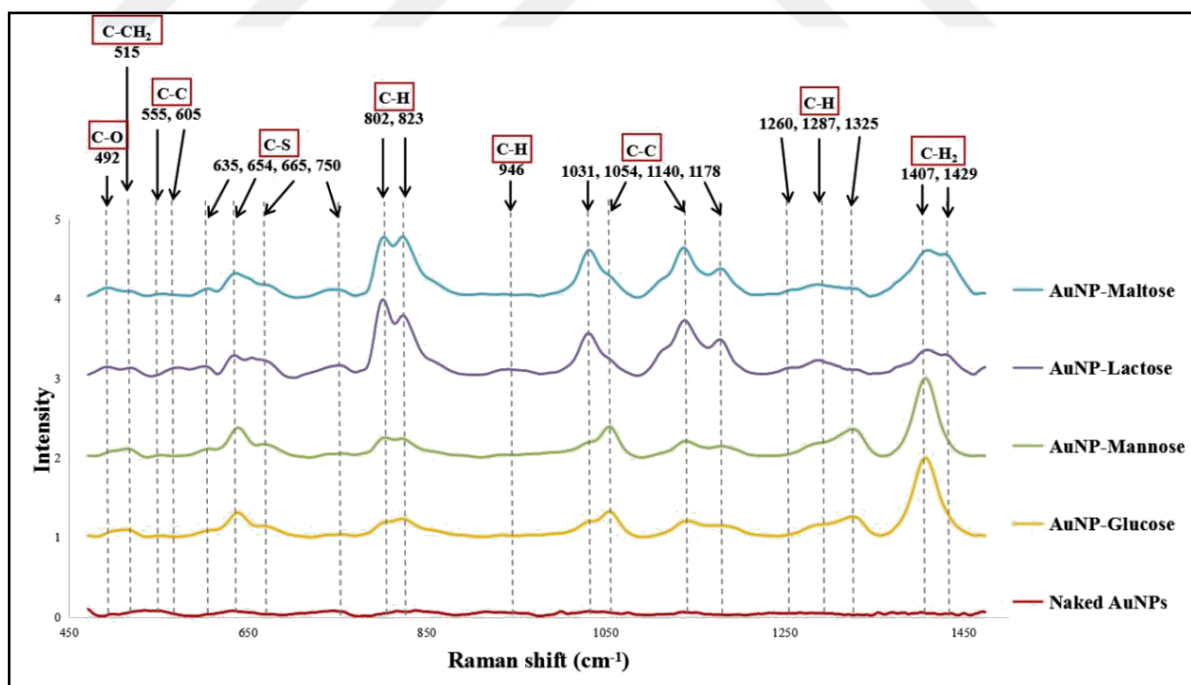


Figure 4.20. Comparative SERS spectra of naked AuNPs and AuNP-Carbohydrate conjugates.

#### 4.2.2. Surface Modification of AuNPs with Peptides

Functionalized AuNPs with especially peptides, proteins and enzymes are emerging and promising NPs in therapeutic and diagnostic applications and have demonstrated crucial progress in cancer therapy and diagnosis [223]. These biomolecules are fundamental components of living organisms and their abundance and various functionalities enable several ways to manipulate their properties in order to be used in medicine [224]. Peptide functionalized AuNPs are one of the most favorable therapeutic application due to small size, ease of synthesis, tumor-penetrating ability, bioavailability, and good biocompatibility of peptides [120].

In this study, it was aimed to functionalize AuNP surfaces with fourteen different peptides, which are different from each other in the conditions of length, sequence and charge, in order to investigate the cellular response of living cells to subtle surface chemistry changes on the NP surface. The codes, lengths, sequences, isoelectric points and charges of these fourteen peptides were listed in Table 4.5. These peptides had four or seven amino acid lengths. The seven amino acid length peptides were designed as addition of RGD sequence in the end of four amino acid length peptides. The first amino acid in the peptide sequences was cysteine (C) because it had thiol groups and assisted the chemisorption on AuNP surfaces [225]. In the half of these fourteen peptides, C was located at -COOH end of the peptides coded as Pep1-Pep7 and in the other peptides, C was located -NH<sub>2</sub> end of the peptides coded as Pep8-Pep14. In other words, two of peptides had same sequence but the order from -COOH to -NH<sub>2</sub> end was vice verse. Furthermore, these peptides were designed as glycine (neutral), glutamic acid (negatively charged) or histidine (positively charged) rich peptides. By this way, it was aimed to examine at which end side of the peptides AuNPs would be conjugated and to analyze the differences caused by length, sequence, charge, free end side and also binding position of peptides on AuNPs. In addition, only RGD sequence with C amino acid and glycine, glutamic acid and histidine rich peptides with RGD sequence were also designed to investigate the role of RGD sequence to cellular response.

Table 4.5. Length, sequence, isoelectric point, charge and codes of fourteen peptides used to functionalize AuNP surfaces.

Code	Length(aa)	Sequence (from NH <sub>2</sub> to COOH)	Isoelectric point	Charge
Pep1	4	DGRC	6.09	0
Pep2	4	GGGC	5.33	0
Pep3	4	EEEC	3.08	-3
Pep4	4	HHHC	7.40	+3
Pep5	7	DGRGGGC	6.09	0
Pep6	7	DGREEEC	3.83	-3
Pep7	7	DGRHHHC	7.40	+3
Pep8	4	CRGD	6.09	0
Pep9	4	CGGG	5.33	0
Pep10	4	CEEE	3.08	-3
Pep11	4	CHHH	7.40	+3
Pep12	7	CGGGRGD	6.09	0
Pep13	7	CEEERGD	3.83	-3
Pep14	7	CHHHRGD	7.40	+3

D: Aspartic acid, G: Glycine, R: Asparagine, E: Glutamic acid, H: Histidine.

Based on published studies, 10-15 nm AuNPs were conjugated with 10-30  $\mu$ l of 1 mg/ml peptides [30]. The conjugation studies were started with CRGD peptide couple, Pep1 (NH<sub>2</sub>-DGRC-COOH) and Pep8 (NH<sub>2</sub>-CRGD-COOH). AuNP suspension was filtered by 0.22  $\mu$ m filter to remove the large impurities and then 20-25  $\mu$ l of 1 mg/ml Pep1 and Pep8 was added into 1 ml of 10 nM AuNP suspension, sequentially. As a result, the color of AuNP suspension immediately turned blue as soon as Pep1 was added. This meant that AuNPs in the suspensions aggregated because of Pep1 addition, as seen Figure 4.21a. On the other hand, there existed no color change on AuNP suspension after addition of Pep8, as seen in Figure 4.22b.

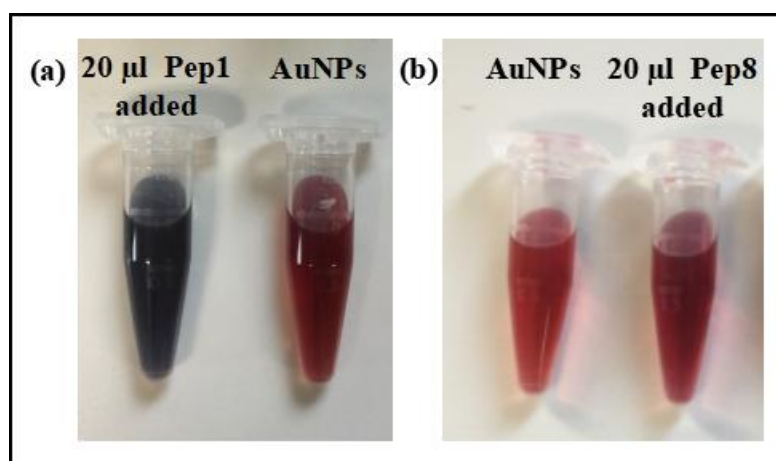


Figure 4.21. Color differences of AuNP suspension after addition of (a) Pep1 and (b) Pep8.

In the several studies about the conjugation of NPs with peptides or proteins, it was demonstrated that the isoelectric point of peptides and the pH of suspension played significant role during conjugation and claimed that when the pH of AuNP suspension is close to the pI of the protein, the electrostatic repulsion between NP and protein is reduced. After the adsorption, peptide or protein can be irreversibly immobilized on the NP surfaces. The pH of synthesized 13 nm AuNP suspension was measured as 5.9. The isoelectric point of Pep1 and Pep8 was 5.82. Therefore, it was expected that AuNPs should be conjugated with Pep1 at 5.9. Consequently, all AuNPs in suspension agglomerated as soon as 20 µl of 1 mg/ml Pep1 was added, but they could be conjugated with Pep8 in same concentration. This indicated that the different end sides of Pep1 and Pep8 interacted with AuNP surfaces and the position of cysteine in peptide affected the conjugation.

In order to find the optimum pH for AuNP-Peptide conjugation, I adjusted the pH of AuNP suspension before addition of peptides. Firstly, I determined the stability of bare 13 nm sized AuNPs at different pHs. The pH of AuNP suspension was measured as 5.9, so 0.1 NaOH or 0.1 HNO<sub>3</sub> was dropwise added into AuNP suspension and the pH was measured by pH meter. Between pH 3.0 and 11.8, the AuNP suspension was clear, AuNPs in suspension was stable and no AuNPs aggregated, as seen in Figure 4.22.

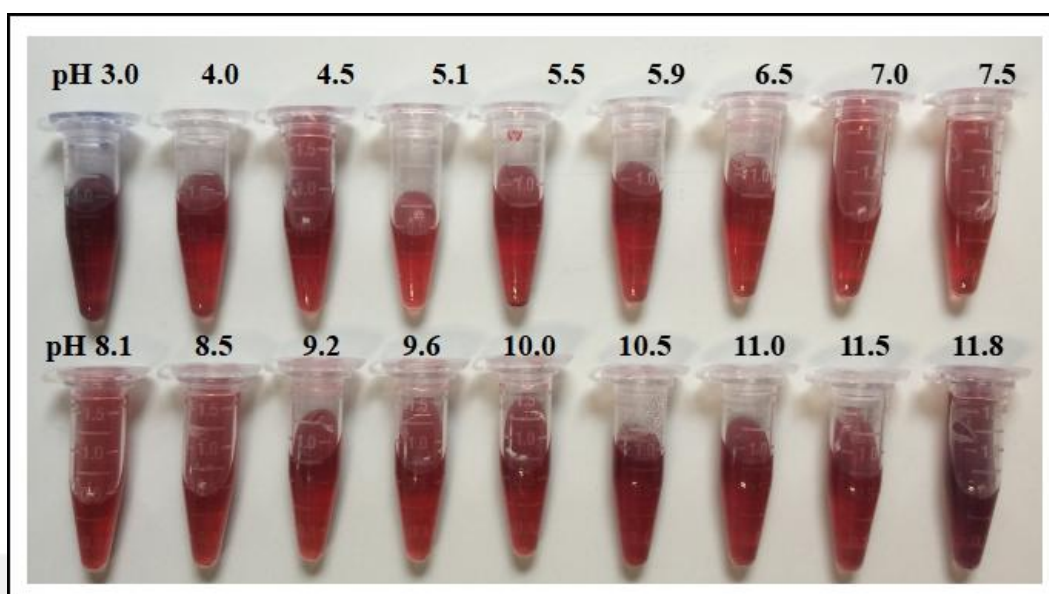


Figure 4.22. AuNP suspensions at several pHs.

After the determination at which pHs AuNPs were stable, 20  $\mu$ l of 1 mg/ml Peptide solution was added into each pH adjusted AuNPs suspensions. Then, the image of suspensions were taken after overnight incubation and the pH range where AuNPs were conjugated with peptides was designated.

A 20  $\mu$ l of 1 mg/ml Pep1 was added into 1 ml of 10 nM 13 nm AuNP suspensions, whose pHs were in the range of 3.0 to 11.8. After the overnight shaking, the suspension colors changed as seen in Figure 4.23. A precipitation at pHs lower than 10.0 was observed indicating that AuNPs were possibly functionalized with the Pep1 at pHs higher than 10.0.



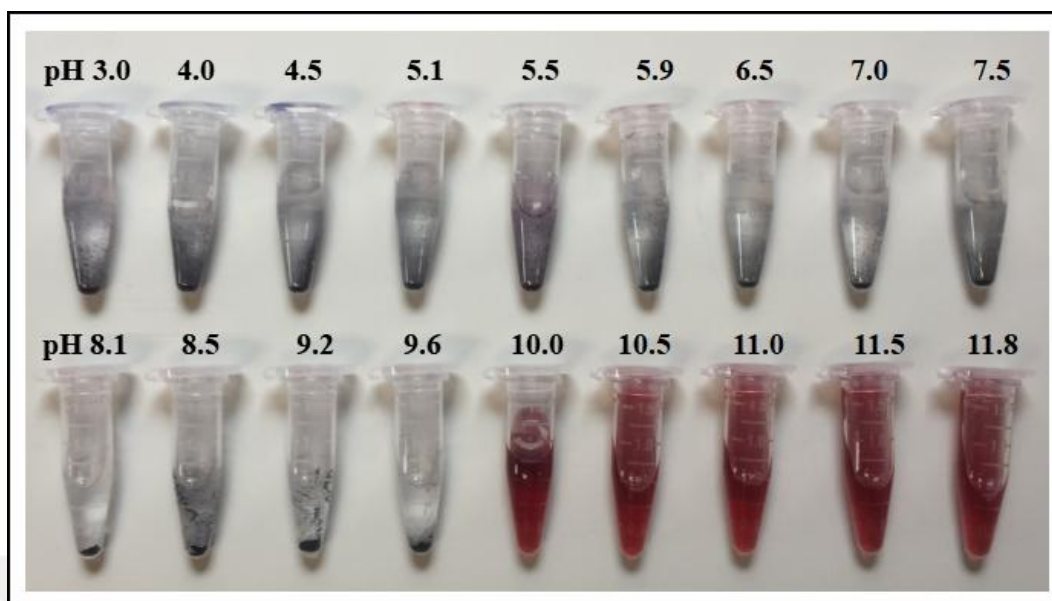


Figure 4.23. AuNP suspension color change after addition of Pep1 solution.

A 20  $\mu$ l of 1 mg/ml Pep2 was added into 1 ml of 10 nM 13 nm AuNP suspensions, whose pHs were ranged from 3.0 to 11.8. After overnight shake, the suspension colors changed as seen in Figure 4.24. The suspension was stable at pHs higher than 10.5 indicating possible conjugation of AuNPs with Pep2.

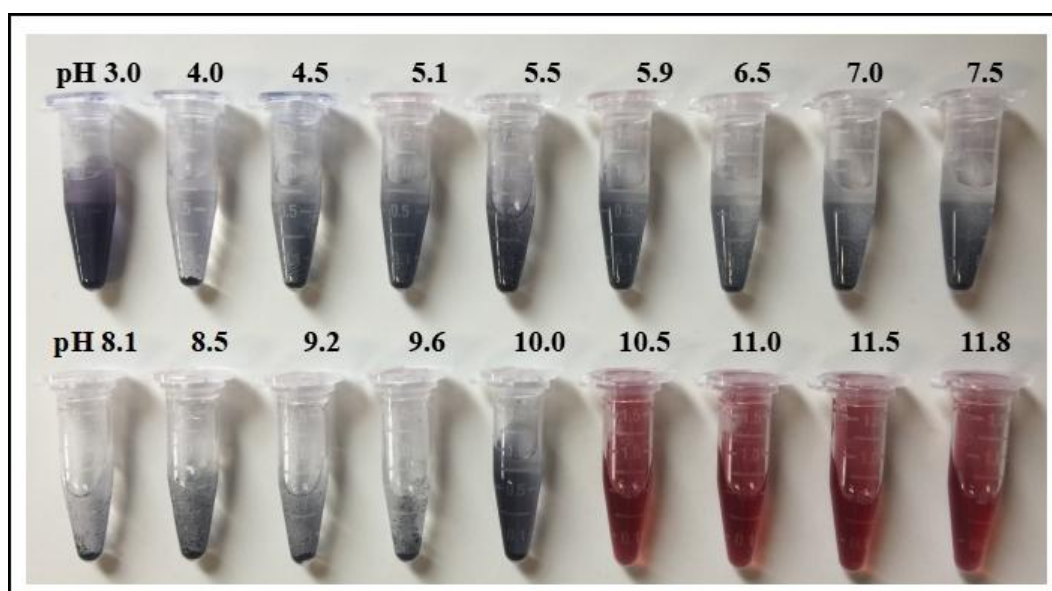


Figure 4.24. AuNP suspension color change after addition of Pep2 solution.

A 20  $\mu\text{l}$  of 1 mg/ml Pep3 was added into 1 ml of 10 nM 13 nm AuNP suspensions, whose pHs were in the range of 3.0 to 11.8. After overnight shake, the suspension colors changed as seen in Figure 4.25. The suspension was stable at pHs higher than 5.5 indicating possible conjugation of AuNPs with Pep3.

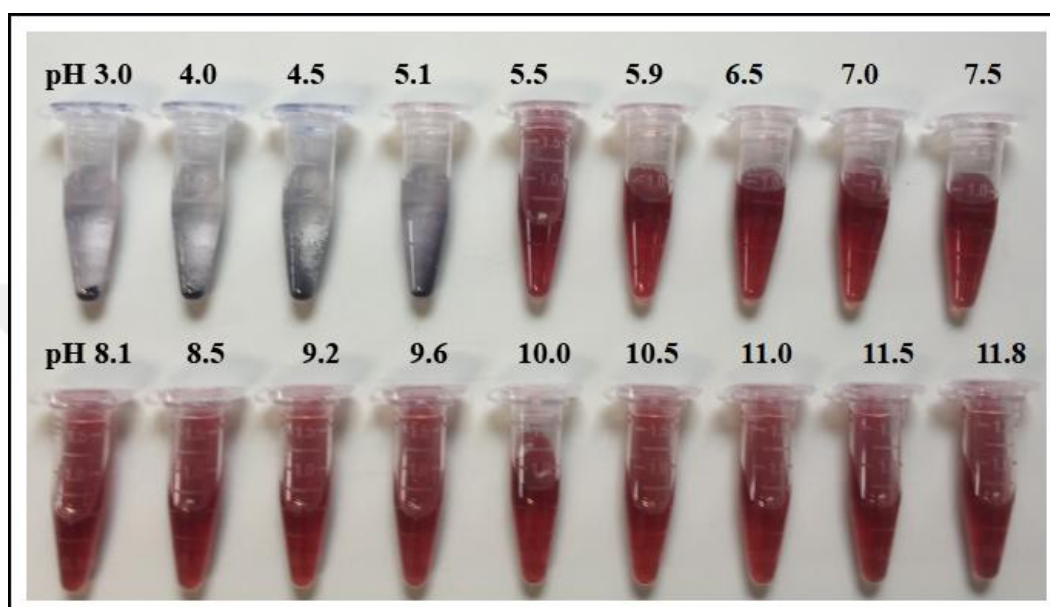


Figure 4.25. AuNP suspension color change after addition of Pep3 solution.

A 20  $\mu\text{l}$  of 1 mg/ml Pep4 was added into 1 ml of 10 nM 13 nm AuNP suspensions, whose pHs were from 3.0 to 11.8. After overnight shake, the suspension colors changed as seen in Figure 4.26. A precipitation at pHs lower than 10.5 was observed indicating that AuNPs were possibly modified with the Pep4 at pHs higher than 10.5.

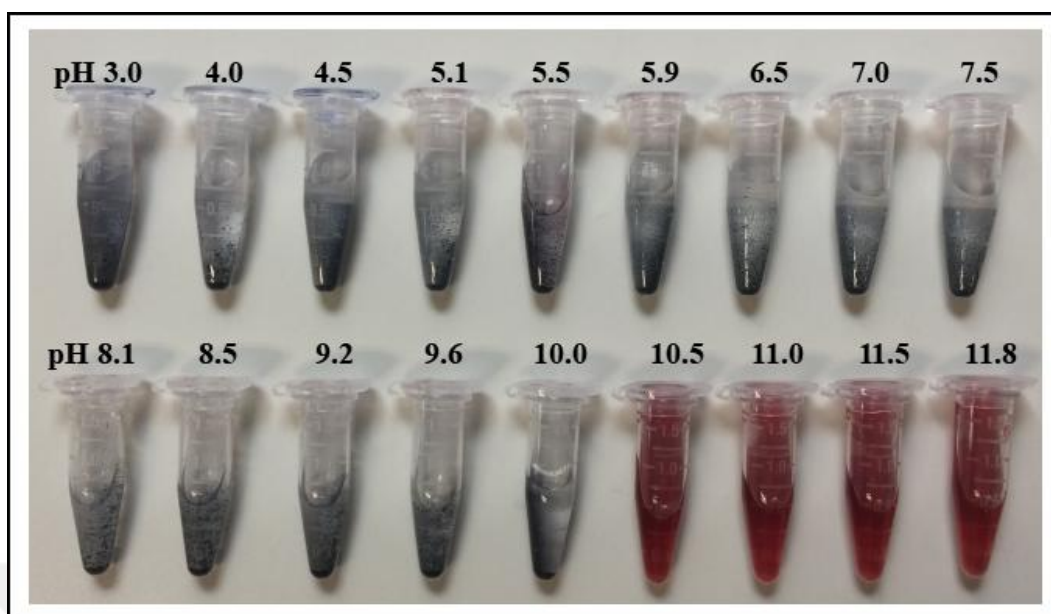


Figure 4.26. AuNP suspension color change after addition of Pep4 solution.

A 20  $\mu$ l of 1 mg/ml Pep5 was added into 1 ml of 10 nM 13 nm AuNP suspensions, whose pHs were from 3.0 to 11.8. After overnight shake, the suspension colors changed as seen in Figure 4.27. A precipitation at pHs lower than 10.0 was observed indicating that AuNPs were possibly conjugated with the Pep5 at pHs higher than 10.0.

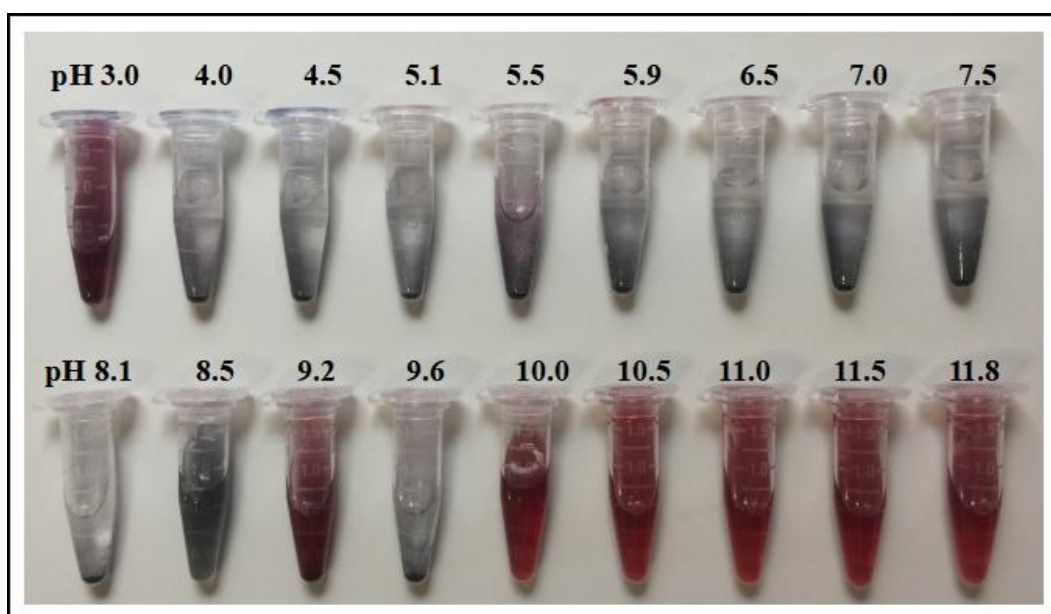


Figure 4.27. AuNP suspension color change after addition of Pep5 solution.

A 20  $\mu$ l of 1 mg/ml Pep6 was added into 1 ml of 10 nM 13 nm AuNP suspensions, whose pHs were in the range of 3.0 to 11.8. After overnight shaking, a precipitation was observed at pHs lower than 5.5 as seen in Figure 4.28. The suspension was stable at pHs higher than 5.5 indicating possible conjugation of AuNPs with Pep6.

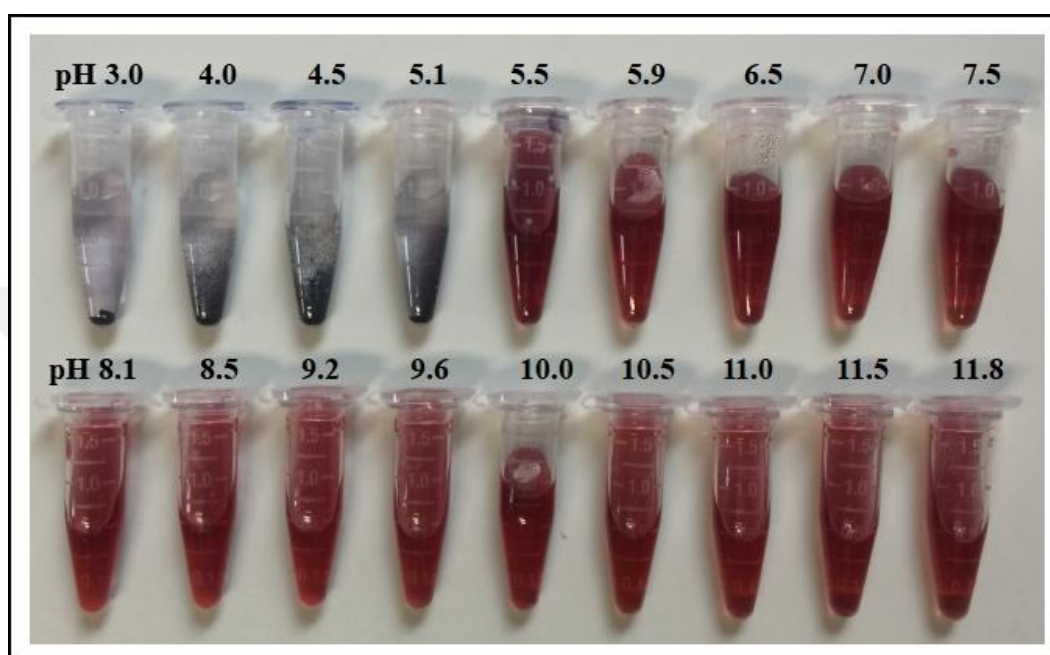


Figure 4.28. AuNP suspension color change after addition of Pep6 solution.

A 20  $\mu$ l of 1 mg/ml Pep7 was added into 1 ml of 10 nM 13 nm AuNP suspensions, whose pHs ranged from 3.0 to 11.8. After overnight shaking, the suspension colors changed as seen in Figure 4.29. A precipitation at pHs lower than 10.5 was observed indicating that AuNPs were possibly conjugated with the Pep7 at pHs higher than 10.5.

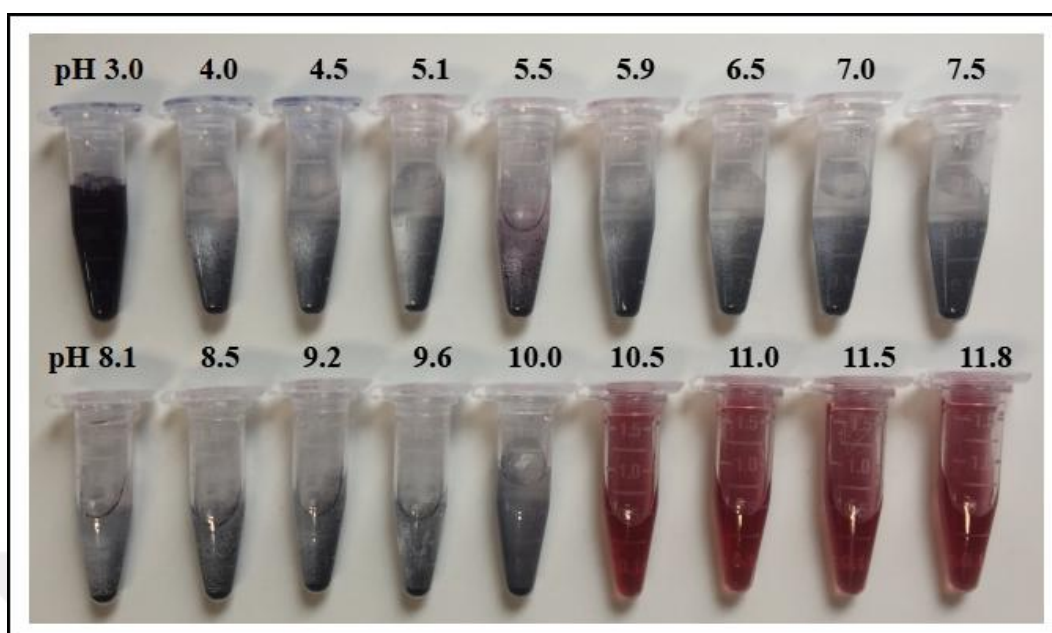


Figure 4.29. AuNP suspension color change after addition of Pep7 solution.

A 20  $\mu\text{l}$  of 1 mg/ml Pep8 was added into 1 ml of 10 nM 13 nm AuNP suspensions, whose pHs were from 3.0 to 11.8. After overnight shake, the suspension colors changed as seen in Figure 4.30. The suspension was stable at pHs higher than 5.5 indicating possible conjugation of AuNPs with Pep8.

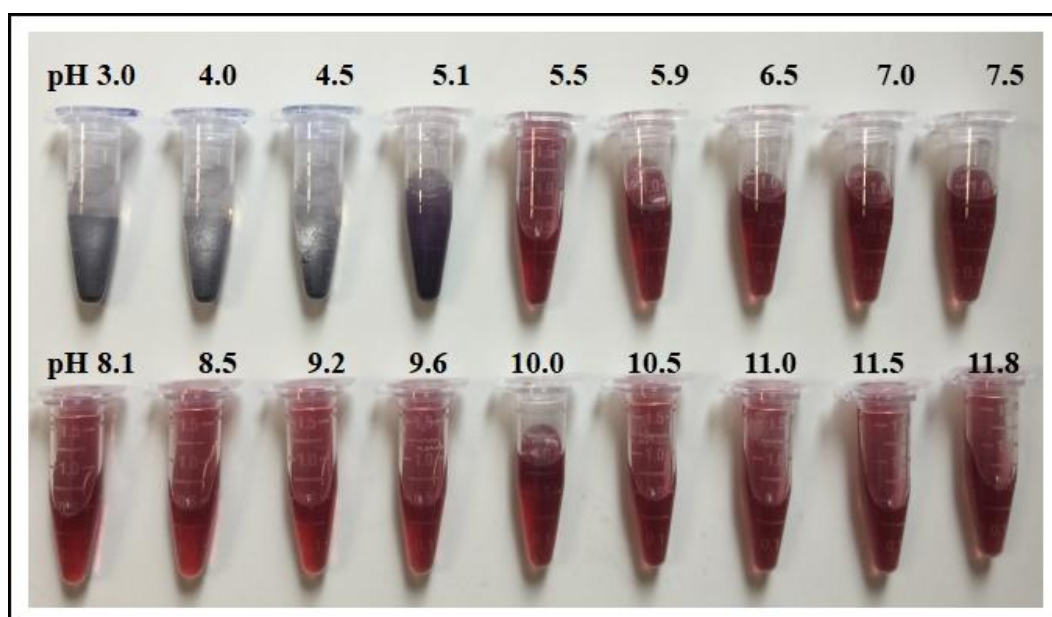


Figure 4.30. AuNP suspension color change after addition of Pep8 solution.

A 20  $\mu$ l of 1 mg/ml Pep9 was added into 1 ml of 10 nM 13 nm AuNP suspensions, whose pHs were from 3.0 to 11.8. After overnight shake, the suspension colors changed as seen in Figure 4.31. A precipitation at pHs lower than 4.5 was observed indicating that AuNPs were possibly tailored with the Pep9 at pHs higher than 4.5.

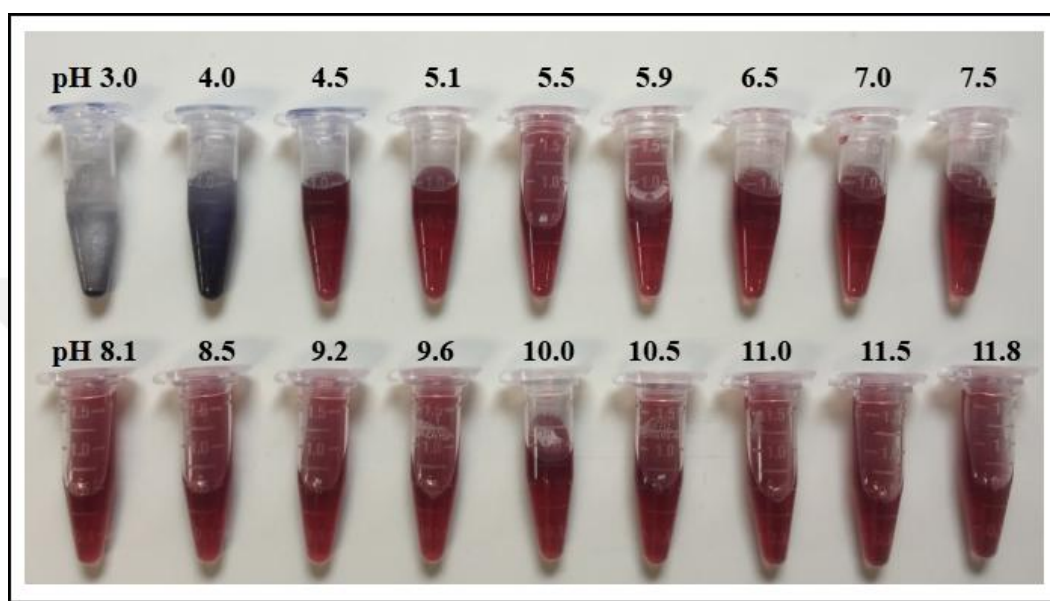


Figure 4.31. AuNP suspension color change after addition of Pep9 solution.

A 20  $\mu$ l of 1 mg/ml Pep10 was added into 1 ml of 10 nM 13 nm AuNP suspensions, whose pHs were from 3.0 to 11.8. After overnight shake, the suspension colors changed as seen in Figure 4.32. The suspension color was seen as clear after pH 4.0, therefore it was understood that the suspension was stable at pHs higher than 4.0 indicating possible conjugation of AuNPs with Pep10.

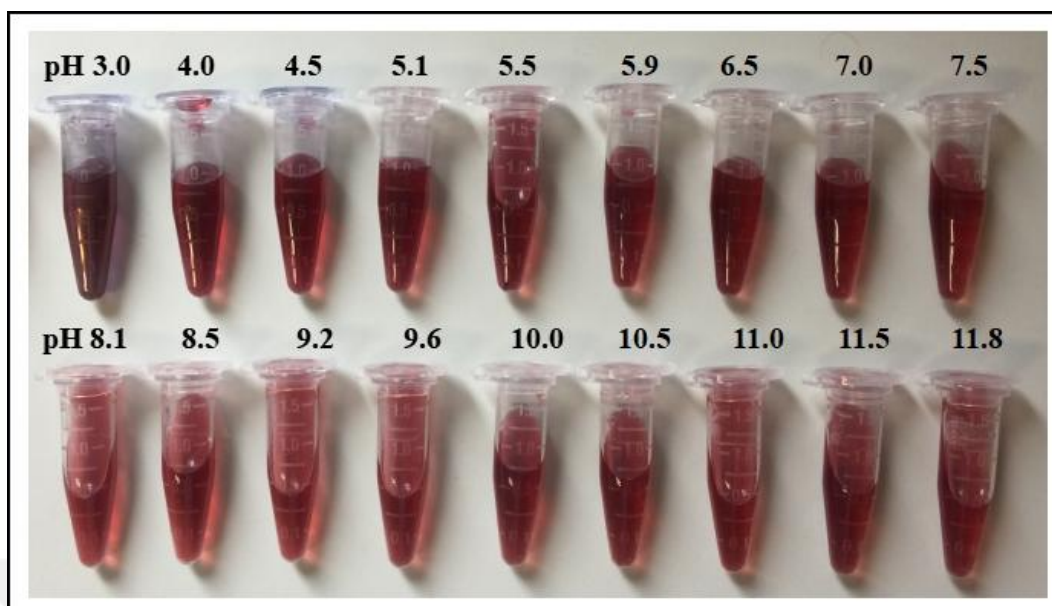


Figure 4.32. AuNP suspension color change after addition of Pep10 solution.

A 20  $\mu$ l of 1 mg/ml Pep11 was added into 1 ml of 10 nM 13 nm AuNP suspensions, whose pHs were from 3.0 to 11.8. After overnight shake, the suspension colors changed as seen in Figure 4.33. A precipitation at pHs lower than 10.0 was observed indicating that AuNPs were possibly conjugated with the Pep11 at pHs higher than 10.0.

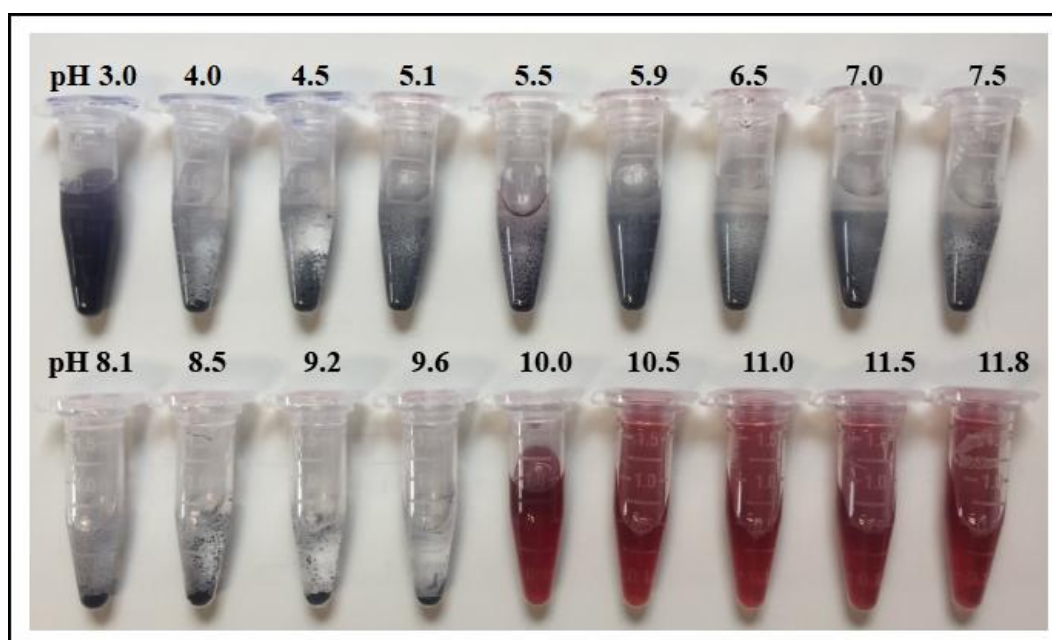


Figure 4.33. AuNP suspension color change after addition of Pep11 solution.

A 20  $\mu$ l of 1 mg/ml Pep12 was added into 1 ml of 10 nM 13 nm AuNP suspensions, whose pHs were from 3.0 to 11.8. After overnight shake, the suspension colors changed as seen in Figure 4.34. The suspension was stable at pHs higher than 5.5 indicating possible conjugation of AuNPs with Pep12.

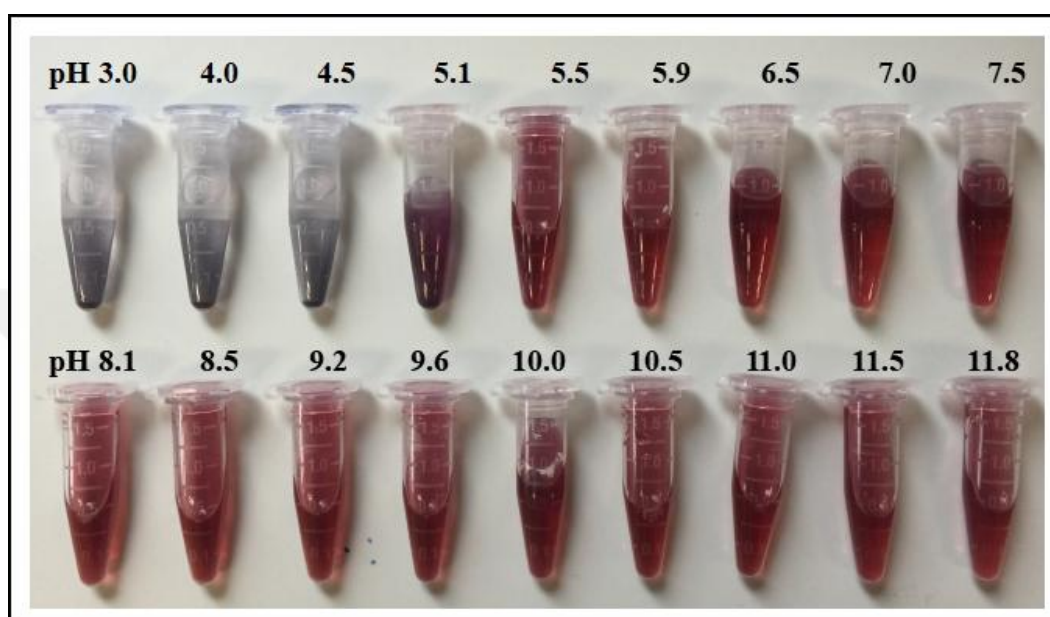


Figure 4.34. AuNP suspension color change after addition of Pep12 solution.

A 20  $\mu$ l of 1 mg/ml Pep13 was added into 1 ml of 10 nM 13 nm AuNP suspensions, whose pHs were from 3.0 to 11.8. After overnight shake, the suspension colors changed as seen in Figure 4.35. A precipitation at pHs lower than 5.5 was observed indicating that AuNPs were possibly tailored with the Pep13 at pHs higher than 5.5.



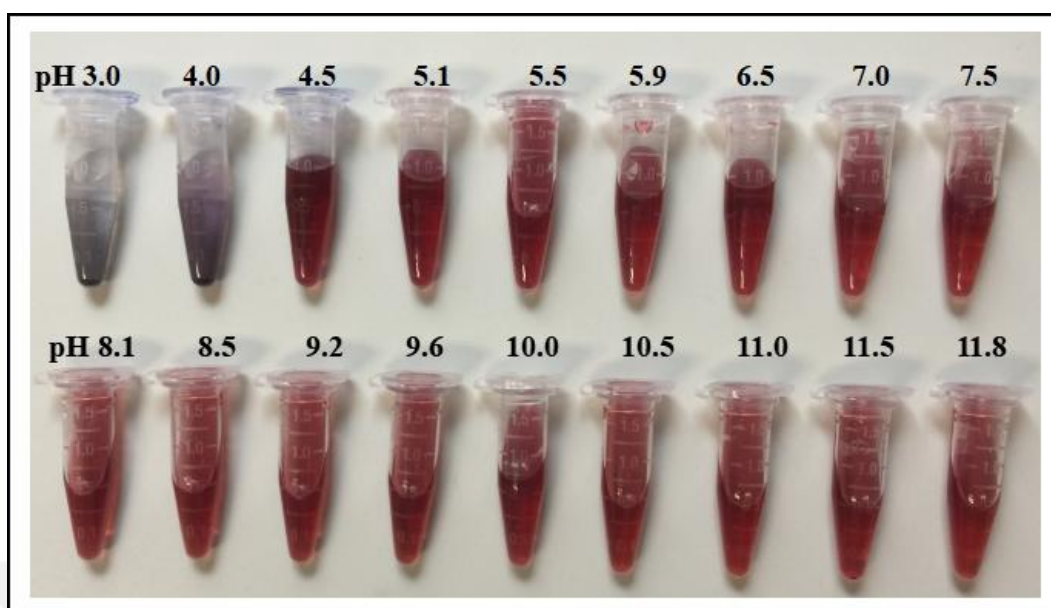


Figure 4.35. AuNP suspension color change after addition of Pep13 solution.

A 20  $\mu\text{l}$  of 1 mg/ml Pep14 was added into 1 ml of 10 nM 13 nm AuNP suspensions, whose pHs were from 3.0 to 11.8. After overnight shake, the suspension colors changed as seen in Figure 4.36. The suspension was stable at pHs higher than 8.1 indicating possible conjugation of AuNPs with Pep14.

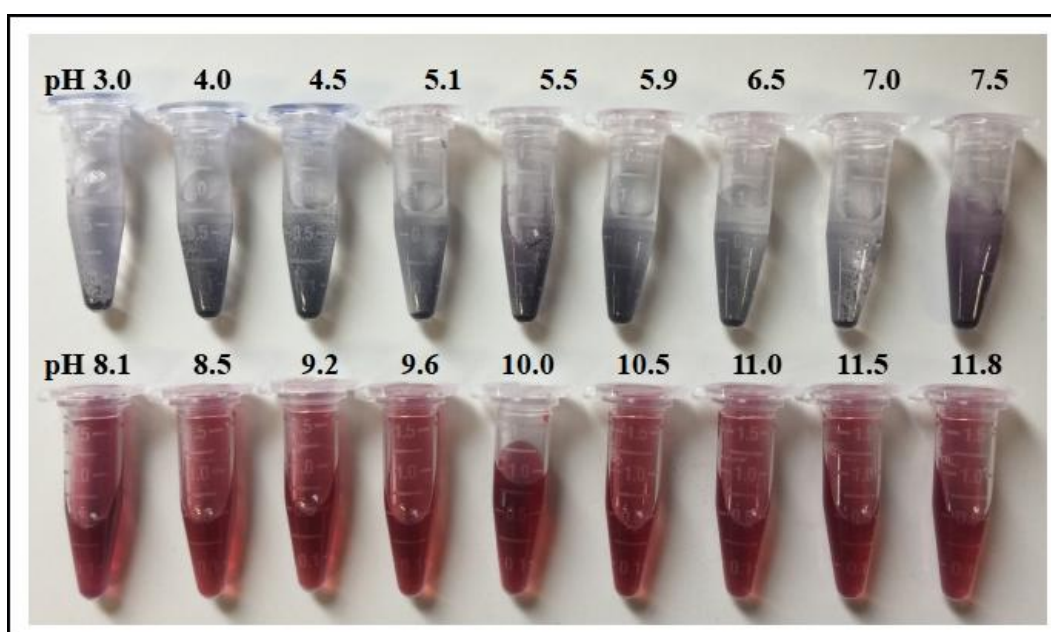


Figure 4.36. AuNP suspension color change after addition of Pep14 solution.

In the light of these results, the pH ranges where AuNPs could be conjugated with each peptides were determined. Then, it was pointed out to find the best conjugation pH condition for each AuNP-Peptide conjugates. To solve this, randomly pH values in those pH ranges were chosen for each peptide, and then AuNPs were modified with peptides in these pH conditions and characterized by several techniques. Based on characterization results, the best conjugation pHs for each peptide were specified and these values were listed in Table 4.6. As a consequence, the suspension pHs of AuNPs were adjusted to these pH values, then their surfaces were modified with each peptides.

Table 4.6. Best conjugation pH condition of each peptides.

Code	NH <sub>2</sub> to COOH	Isoelectric point	Conjugation pH
Pep1	DGRC	6.1	11.0
Pep2	GGGC	5.3	11.0
Pep3	EEEC	3.1	8.6
Pep4	HHHC	7.4	11.0
Pep5	DGRGGGC	6.1	10.5
Pep6	DGREEEC	3.8	6.0
Pep7	DGRHHHC	7.4	11.5
Pep8	CRGD	6.1	6.0
Pep9	CGGG	5.3	6.0
Pep10	CEEE	3.1	6.0
Pep11	CHHH	7.4	11.0
Pep12	CGGGRGD	6.1	6.0
Pep13	CEEERGD	3.8	6.0
Pep14	CHHRGD	7.4	8.6

#### *4.2.2.1. Optimization of AuNP Conjugation with Pep1 and Pep8 and Their Characterization*

When considered the results of AuNP suspension color change after addition of Pep1 (NH<sub>2</sub>-DRGC-COOH) and Pep8 (NH<sub>2</sub>-CRGD-COOH), whose isoelectric points were 6.1, AuNPs could be coated with Pep1 at basic conditions, especially after pH 10.0, and with

Pep8 without changing the pH of the suspension. Thus, 1 ml of 10 nM 13 nm AuNPs were conjugated with 20 and 25  $\mu$ l of 1 mg/ml Pep1 either at pH 11.0 or at pH 11.5 whereas they were functionalized with Pep8 at only pH 5.9. The conjugates were shaken for overnight. The photos of the suspensions of naked AuNPs, AuNP-Pep1 and AuNP-Pep8 conjugates were shown in Figure 4.37. As seen in the photo, there was no AuNP aggregation after conjugation with either Pep1 or Pep8, and so the color of the suspensions were clear and red.

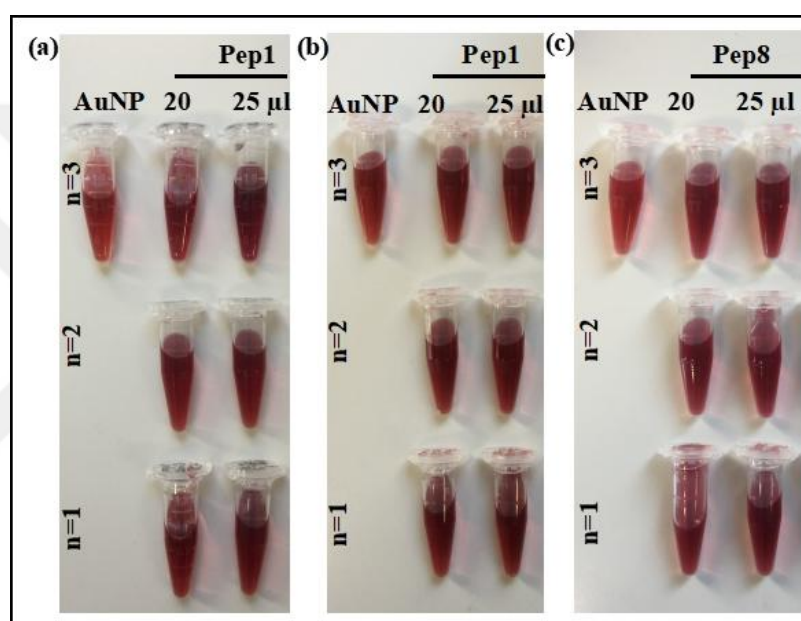


Figure 4.37. White light images of suspensions of naked AuNPs and AuNPs modified with Pep1 (a) at pH 11.0 (b) at pH 11.5 and (c) naked AuNPs and AuNPs modified with Pep8 at 5.9. “n” indicates replicate number.

The naked AuNPs, AuNP-Pep1 and AuNP-Pep8 conjugates were characterized by UV/Vis spectroscopy and the comparative UV/Vis spectra of AuNP-Pep1 and AuNP-Pep8 conjugates were given in Figure 4.38. The SPR of naked AuNPs was at 519 nm. When considered the SPR of AuNP-Pep1 conjugates, AuNP-Pep1 conjugated at pH 11.0 had 2 nm red-shift in SPR while AuNP-Pep1 conjugated at pH 11.5 had 3 nm red-shift. On the other hand, AuNP-Pep8 conjugates had SPR at 522 nm. The shifts of SPR represented the successful functionalization.

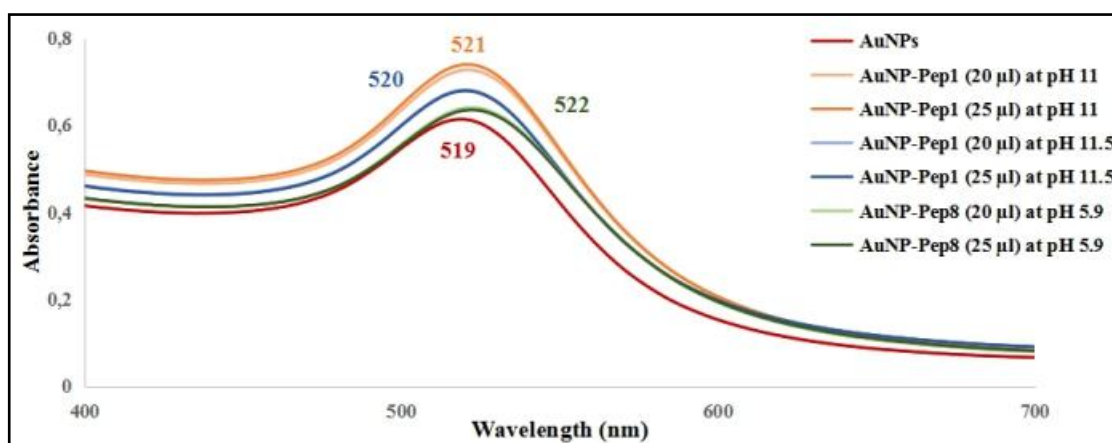


Figure 4.38. Comparative UV/Vis spectra of naked AuNPs, AuNP-Pep1 and AuNP-Pep8 conjugates.

The naked AuNPs, AuNP-Pep1 and AuNP-Pep8 conjugates were also characterized by DLS. The hydrodynamic sizes and zeta potentials of the triplicates were measured three times and total collected nine measurements were averaged. The average hydrodynamic size and zeta potentials of naked AuNPs and AuNP conjugates were given with standard deviations in Table 4.7. The average hydrodynamic size of naked AuNPs was 11.0 nm and their average zeta potential was -11.9 mV. After conjugation, it was observed that the sizes were grown and the surface charges were more negative when compared to naked AuNPs. The sizes of AuNP-Pep1 conjugates were 1-2 nm larger and AuNP-Pep8 conjugates were 2 nm larger than naked AuNPs. The zeta potentials of AuNP-Pep1 were more negative than AuNP-Pep8.

Table 4.7. Average hydrodynamic sizes and zeta potentials of naked AuNPs, AuNP-Pep1 and AuNP-Pep8 conjugates.

Sample	Size (nm)	Zeta Potential (mV)
AuNPs	11.1 ± 0.4	-11.9 ± 0.3
AuNP-Pep1 (20 µl) at pH 11.0	12.1 ± 0.9	-35.9 ± 1.8
AuNP-Pep1 (25 µl) at pH 11.0	11.8 ± 0.8	-35.0 ± 3.2
AuNP-Pep1 (20 µl) at pH 11.5	12.7 ± 0.9	-32.8 ± 2.9
AuNP-Pep1 (25 µl) at pH 11.5	13.4 ± 1.2	-22.4 ± 3.0
AuNP-Pep8 (20 µl) at pH 5.9	13.2 ± 0.8	-17.6 ± 2.1
AuNP-Pep8 (25 µl) at pH 5.9	13.0 ± 0.5	-18.3 ± 3.9

The naked AuNPs, AuNP-Pep1 and AuNP-Pep8 conjugates were also characterized by 1 percent Agarose gel electrophoresis. The images of the agarose gels after run was seen in Figure 4.39. In the 1st and 2nd wells of the first gel, AuNP-Pep1, conjugated at pH 11, were loaded, in the 3rd and 4th wells, AuNP-Pep1, conjugated at 11.5, were loaded. According to the result, it was clearly seen that Pep1 could cover AuNP surfaces at both pH conditions, but interestingly the bands of AuNP-Pep1 at pH 11.0 were denser and AuNP-Pep1 at pH 11.5 run through the gel faster. This can imply that more AuNPs in the suspension could be functionalized with Pep1 equally and better in the condition of pH 11.0. Moreover, the concentrations of Pep1, 20 and 25 µl of 1 mg/ml, were sufficient to cover the surfaces of whole AuNPs in the suspension. In order to compare AuNP-Pep1 and AuNP-Pep8 conjugates, they were loaded and run in the same gel, as seen in the second gel. In the 5th and 6th wells, AuNP-Pep1 at pH 11.5 were loaded and in the 6th and 7th wells, AuNP-Pep8 were loaded. The bands of AuNP-Pep1 at pH 11.5 were seen broad whereas the bands of AuNP-Pep8 were denser and run through the gel faster. Moreover, the bands of the same conjugates were parallel to each other, so they coat the AuNP surfaces with less difference. As a result, it can be decided that 20 µl of 1 mg/ml peptides were enough to cover the surfaces of whole AuNPs in the suspension, AuNPs should be conjugated with Pep1 at pH 11, and AuNP-Pep8 run through the gel faster than AuNP-Pep1.

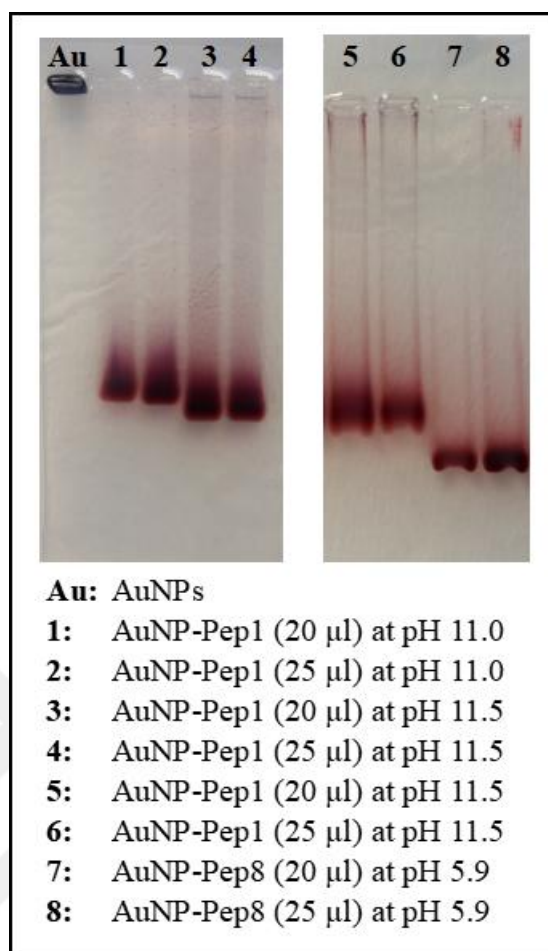


Figure 4.39. White light image of agarose gel loaded naked AuNPs, AuNP-Pep1 and AuNP-Pep8 conjugates.

#### ***4.2.2.2. Optimization of AuNP Conjugation with Pep2 and Pep9 and Their Characterization***

The spherical AuNPs of 13 nm diameter size were functionalized with either Pep2 (NH<sub>2</sub>-GGGC-COOH) and Pep9 (NH<sub>2</sub>-CGGG-COOH) with increasing concentration as 20 or 25  $\mu$ l (n=3). Based on the results of AuNP suspension color change after addition of Pep2 and Pep9, AuNPs could be coated with Pep2 at basic conditions, especially after pH 10.5, and with Pep9 after pH of the suspension was 4.5. The isoelectric point of Pep2 and Pep9 was 5.3, which was close to the isoelectric point of Pep1 and Pep8. So, it was decided to conjugate AuNPs with Pep2 in the condition of pH 11.0 and with Pep9 in original pH

without any adjustment. Therefore, the pH of AuNP suspension was adjusted at 11.0 with 0.1 NaOH due to functionalize AuNPs surfaces with only Pep2. As a result, 1 ml 13 nm AuNPs were conjugated with 20 and 25  $\mu\text{l}$  of 1 mg/ml Pep2 at pH 11.0 and with 20 and 25  $\mu\text{l}$  of 1 mg/ml Pep9 at pH 5.9, as triplicates. The conjugates were shaken for overnight. The image of the suspensions of naked AuNPs, AuNP-Pep2 and AuNP-Pep9 conjugates were shown in Figure 4.40. As seen in the image, there was no AuNP aggregation after conjugation with either Pep2 or Pep9, and the color of the AuNP suspensions were clear and red, which indicated the stability of the suspension.

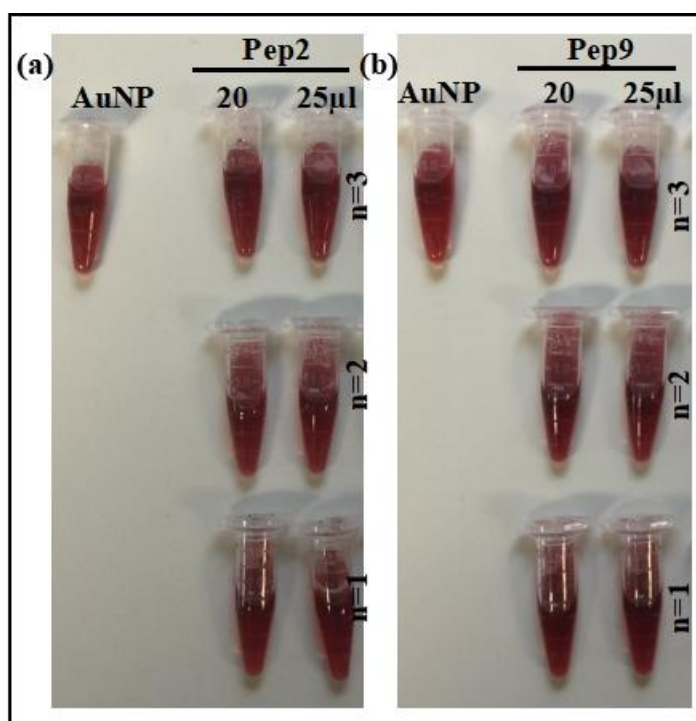


Figure 4.40. White light images of suspensions of (a) naked AuNPs and AuNPs modified with Pep2 at pH 11.0 and (b) naked AuNPs and AuNPs modified with Pep9 at 5.9. “n” indicates replicate number.

The naked AuNPs, AuNP-Pep2 and AuNP-Pep9 conjugates were characterized by UV/Vis spectroscopy. The comparative UV/Vis spectra was given in Figure 4.41. After functionalization of naked AuNPs with Pep2, the SPR peak was 1 nm redshifted from 519 to 520 nm while after conjugation with Pep9, it was 3 nm redshifted from 519 to 522 nm. These shifts were proved that peptides were bound on the surface of AuNPs. Although the

sequence of Pep2 and Pep9 was same, the binding site and position of the peptides influenced the shift.

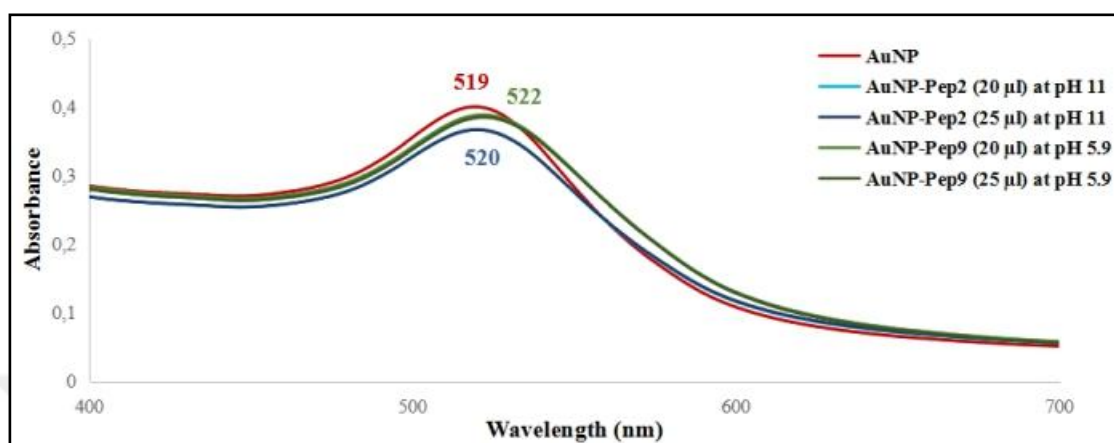


Figure 4.41. Comparative UV/Vis spectra of naked AuNPs, AuNP-Pep2 and AuNP-Pep9 conjugates.

The naked AuNPs and AuNP-Pep2 and AuNP-Pep9 conjugates were characterized by DLS. The hydrodynamic sizes and zeta potentials of 1:10 diluted triplicates were measured three times. The total nine measurements were averaged and the values of average sizes and zeta potentials were shown in Table 4.8. The average hydrodynamic size of naked AuNPs was 12.7 nm while the sizes of conjugates were grown as 1 nm for AuNP-Pep2 and 3 nm for AuNP-Pep9 conjugates. The growth in conjugates' sizes proved the successful functionalization. When discussed the zeta potentials, after conjugation, the surface charge of AuNP-Pep2 were more negative than naked AuNPs while no valuable alteration was measured on the surface of AuNP-Pep9. When considering the amino acids in peptides, glycine was neutral amino acid and cysteine was negatively charged amino acid because of sulphur group. This can explain that AuNP surfaces were interacted with  $\text{NH}_2$  end of Pep2, so cysteine created more negatively on AuNP surfaces. On the other hand, AuNPs were covered with Pep9 via Au-S bonds, created by cysteine, so glycine amino acids were at outside of the conjugate and could not change the zeta potential of AuNPs.



Table 4.8. Average hydrodynamic sizes and zeta potentials of naked AuNPs, AuNP-Pep2 and AuNP-Pep9 conjugates.

Sample	Size (nm)	Zeta Potential (mV)
AuNP	12.7 ± 1.0	-21.6 ± 3.0
AuNP-Pep2 (20 µl) at pH 11.0	14.0 ± 0.8	-33.0 ± 0.7
AuNP-Pep2 (25 µl) at pH 11.0	13.8 ± 0.6	-28.9 ± 1.1
AuNP-Pep9 (20 µl) at pH 5.9	15.3 ± 0.6	-19.3 ± 1.7
AuNP-Pep9 (25 µl) at pH 5.9	15.6 ± 0.6	-18.1 ± 1.0

The naked AuNPs, AuNP-Pep2 and AuNP-Pep9 conjugates were also characterized by 1 percent Agarose gel electrophoresis and the image of the Agarose gels after run was seen in Figure 4.42. In the 1<sup>st</sup> and 2<sup>nd</sup> wells of the first gel, AuNP-Pep2, conjugated at pH 11.0, were loaded and in the 3<sup>rd</sup> and 4<sup>th</sup> wells, AuNP-Pep9, conjugated at pH 5.9, were loaded. Being founded on the dense bands of conjugates on Agarose gel, it can be said that 1 ml 13 nm 10 nM AuNPs were conjugated with 20 µl of 1 mg/ml Pep2 and Pep9, and AuNP-Pep9 conjugates run faster than AuNP-Pep1.

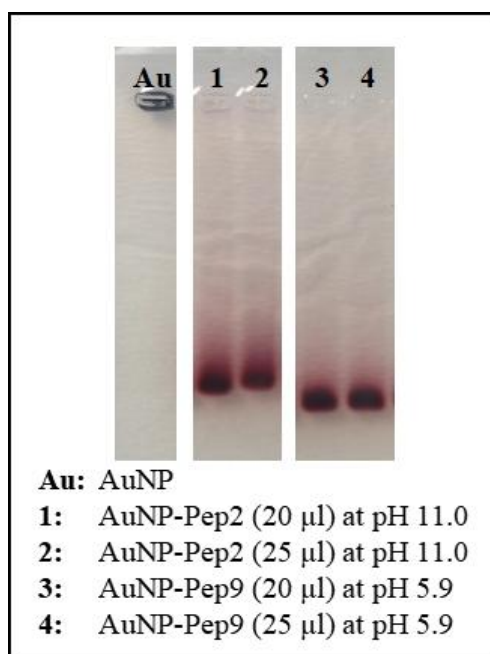


Figure 4.42. White light image of agarose gel loaded naked AuNPs, AuNP-Pep2 and AuNP-Pep9 conjugates.

#### 4.2.2.3. Optimization of AuNP Conjugation with Pep3 and Pep10 and Their Characterization

The spherical AuNPs of 13 nm diameter size were functionalized with either Pep3 (NH<sub>2</sub>-EEEE-COOH) and Pep10 (NH<sub>2</sub>-CEEE-COOH) with increasing concentration in three repeats. Based on the results of AuNP suspension color change after addition of Pep3 and Pep10, 13 nm AuNPs could be coated with Pep3 after the pH of AuNP suspension was 5.5, and with Pep10 after 4. The isoelectric point of Pep3 and Pep10 was 3.1, which was different than that of Pep1, Pep2, Pep8 and Pep10's. Thus, I decided to conjugate AuNPs with Pep3 in the condition of several pHs and with Pep10 in original pH without any adjustment. As a first step, the pH of AuNP suspension was adjusted at 6.7, 8.6, 10.8 with 0.05 and 0.1 NaOH. Then, 1 ml 13 nm 10 nM AuNPs were conjugated with 20 and 25  $\mu$ l of 1 mg/ml Pep3 at pH 6.7, 8.6, 10.8 and with 20 and 25  $\mu$ l of 1 mg/ml Pep10 at pH 5.9, as triplicates. The conjugates were shaken for overnight. The photos of the suspensions of naked AuNPs, AuNP-Pep3 and AuNP-Pep10 conjugates were shown in Figure 4.43. As seen in the image, the colors of the suspensions were clear and there existed no AuNP aggregation after addition of peptides, which showed the stability of the suspension.

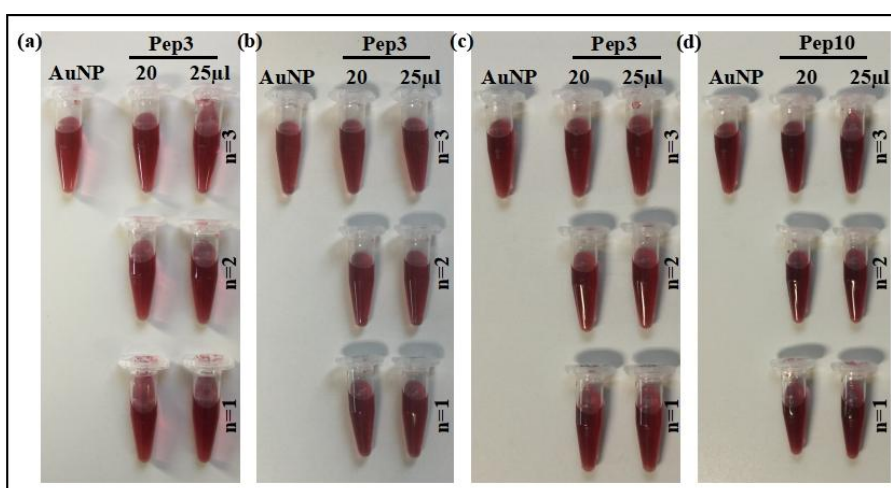


Figure 4.43. White light images of suspensions of naked AuNPs and AuNPs modified with Pep3 (a) at pH 6.7 (b) at pH 8.6 (c) at pH 10.5 and (d) naked AuNPs and AuNPs modified with Pep10 at pH 5.9. “n” indicates replicate number.

The naked AuNPs and AuNP-Pep3 and AuNP-Pep10 conjugates were characterized by UV/Vis spectroscopy. The comparative UV/Vis spectra of naked AuNPs and conjugates were given in Figure 4.44. The SPR of naked 13 nm AuNPs was observed at 519 nm. The AuNP-Pep3, functionalized at pH 6.7 and 10.8, had no valuable shift on spectra while those of conjugated at pH 8.6 had it at 520 nm. This indicated that Pep3 coating on the AuNP surfaces was not successful in the case of the pH of AuNP suspension at 6.7 and 10.8. The conjugation of AuNP with Pep3 could be succeed at pH 8.6. In addition, the SPR of AuNP-Pep10 conjugates were 3 nm redshifted.

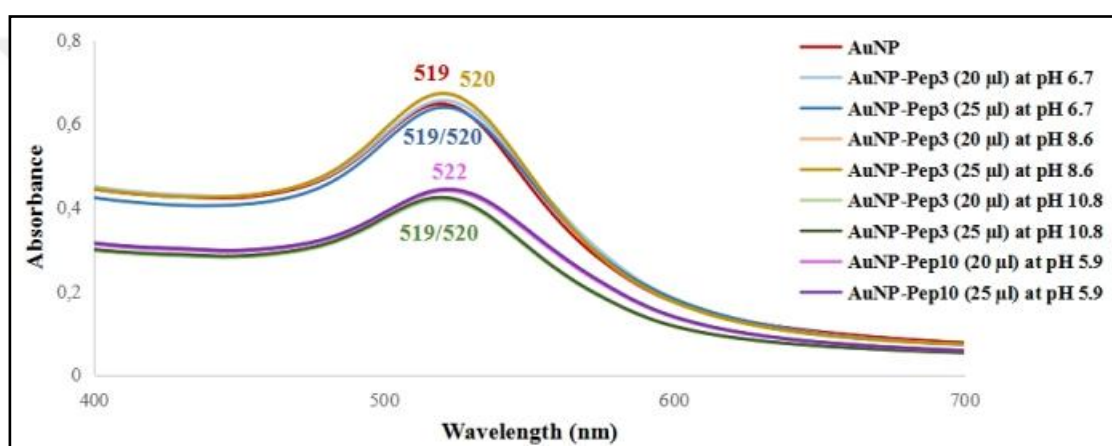


Figure 4.44. Comparative UV/Vis spectra of naked AuNPs, AuNP-Pep3 and AuNP-Pep10 conjugates.

The hydrodynamic sizes and zeta potentials of naked AuNPs and AuNP-Pep3 and AuNP-Pep10 conjugates were measured by DLS. Each triplicates of AuNP conjugates were measured three times. The average of nine measurements were calculated with standard deviations and they were listed in Table 4.9. The average hydrodynamic size of naked AuNPs was measured as 13.8 nm. The most size increase was observed in AuNP-Pep3, conjugated at pH 8.6 and when considered the standard deviations, no impressive size growth could be seen in the other AuNP-Pep3 conjugates. In addition, the sizes of AuNP-Pep10 conjugates were larger, more than 15 nm. When discussing the zeta potentials, the naked AuNPs had -16.5 mV as average. After all conjugations, the conjugates had more negative surface.

Table 4.9. Average hydrodynamic sizes and zeta potentials of naked AuNPs, AuNP-Pep3 and AuNP-Pep10 conjugates.

Sample	Size (nm)	Zeta potential (mV)
AuNP	13.8 ± 0.5	-16.5 ± 0.1
AuNP-Pep3 (20 µl) at pH 6.7	14.3 ± 1.2	-32.8 ± 2.9
AuNP-Pep3 (25 µl) at pH 6.7	14.4 ± 1.0	-31.1 ± 3.8
AuNP-Pep3 (20 µl) at pH 8.6	14.6 ± 0.8	-22.1 ± 1.9
AuNP-Pep3 (25 µl) at pH 8.6	14.5 ± 0.5	-24.7 ± 2.3
AuNP-Pep3 (20 µl) at pH 10.8	14.3 ± 0.7	-21.7 ± 2.0
AuNP-Pep3 (25 µl) at pH 10.8	14.0 ± 0.5	-20.9 ± 2.1
AuNP-Pep10 (20 µl) at pH 5.9	15.4 ± 0.7	-17.3 ± 1.5
AuNP-Pep10 (25 µl) at pH 5.9	15.9 ± 0.5	-19.2 ± 4.2

To understand the surface density of peptides on AuNPs, they were characterized by 1 percent Agarose Gel Electrophoresis assay. The images of the agarose gels after run was seen in Figure 4.45. The bands of AuNP-Pep3, conjugated at pH 6.7 and 8.6, seen in the 1<sup>st</sup>, 2<sup>nd</sup>, 3<sup>rd</sup> and 4<sup>th</sup> wells, were denser. However, AuNP-Pep3, conjugated at pH 10.8, run through the gel as seen in the 5<sup>th</sup> and 6<sup>th</sup> wells. The reason why they did not have a dense bands was that AuNPs in the suspension could not be equally conjugated with Pep3 at pH 10.8. Moreover, AuNP-Pep10 conjugates, in the 7<sup>th</sup> and 8<sup>th</sup> wells, were dense. Consequently, it was decided that AuNPs should be functionalized with Pep3 at pH 8.6 by considering the whole characterization results.

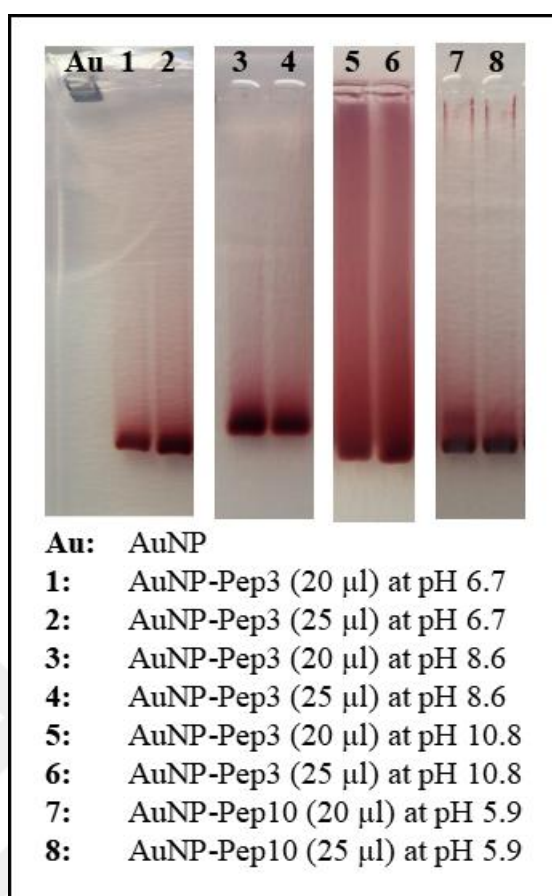


Figure 4.45. White light images of agarose gels loaded naked AuNPs, AuNP-Pep3 and AuNP-Pep10 conjugates.

#### ***4.2.2.4. Optimization of AuNP Conjugation with Pep4 and Pep11 and Their Characterization***

The spherical AuNPs of 13 nm diameter size were coated with 20 µl of 1 mg/ml either Pep4 (NH<sub>2</sub>-HHHC-COOH) or Pep11 (NH<sub>2</sub>-CHHH-COOH) in three repeats. The isoelectric point of Pep4 and Pep11 was 7.4. When investigated the AuNP conjugation issue based on pHs, AuNPs could be conjugated with Pep4 after pH 10.5 whereas they can be covered with Pep11 after pH 10.0. Therefore, it was decided that AuNPs would be conjugated with both peptides at either pH 11.0 or pH 11.5. 1 ml of 10 nM 13 nm AuNPs were functionalized with 20 µl of 1 mg/ml Pep4 and Pep10 as triplicates, as seen Figure 4.46. The suspensions' colors were seen as clear and there was no AuNP aggregates in the

suspension after addition of peptides. This indicated that the suspensions after functionalization were stable.

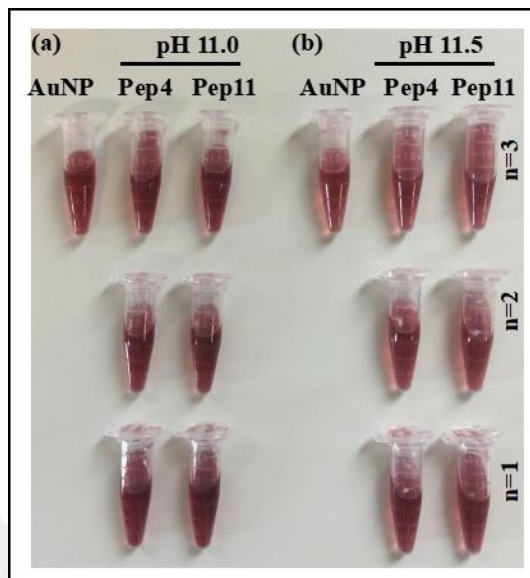


Figure 4.46. White light image of suspensions of naked AuNPs and AuNPs modified with either Pep4 and Pep11 (a) pH at 11.0 and (b) pH at 11.5. “n” indicates replicate number.

The naked AuNPs, AuNP-Pep4 and AuNP-Pep11 conjugates were characterized by UV/Vis spectroscopy, as given in Figure 4.47. The naked AuNPs had SPR at 519 nm while the whole conjugates had it at 521 nm. The 2 nm redshift indicated the conjugation between AuNPs and peptides.

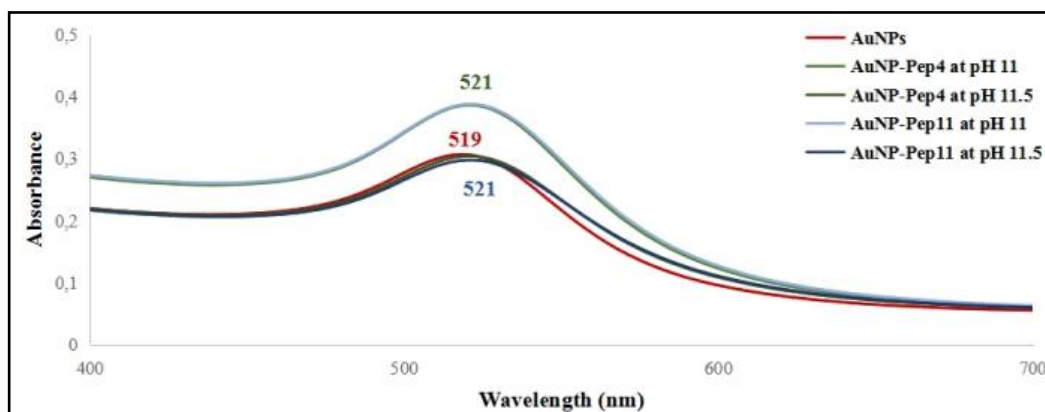


Figure 4.47. Comparative UV/Vis spectra of naked AuNPs, AuNP-Pep4 and AuNP-Pep11 conjugates.

The hydrodynamic sizes and zeta potentials of naked AuNPs, AuNP-Pep4 and AuNP-Pep11 conjugates were measured three times by DLS and the average values were given in Table 4.10. The average hydrodynamic size of naked AuNPs was measured as 12.6 nm. Only AuNP-Pep11 conjugated at pH 11.0 had larger size when compared to naked AuNPs. The others had no valuable size growth. In terms of zeta potentials, AuNP-Pep4 conjugated at pH 11.5 and AuNP-Pep11 conjugated at pH 11.0 were more negative than naked AuNPs.

Table 4.10. Average hydrodynamic sizes and zeta potentials of naked AuNPs, AuNP-Pep4 and AuNP-Pep11 conjugates.

Sample	Size (nm)	Zeta Potential (mV)
AuNPs	12.6 ± 0.3	-21.0 ± 1.7
AuNP-Pep4 at pH 11.0	12.3 ± 0.9	-13.6 ± 1.6
AuNP-Pep4 at pH 11.5	12.8 ± 0.6	-31.4 ± 5.8
AuNP-Pep11 at pH 11.0	13.9 ± 0.8	-33.4 ± 0.9
AuNP-Pep11 at pH 11.5	12.6 ± 0.6	-24.1 ± 5.5

In order to observe the density of peptides on AuNPs, AuNP-Pep4 and AuNP-Pep11 conjugates were characterized by 1 percent Agarose gel, seen in Figure 4.48. Based on results, AuNP-Pep4 conjugation was not successful in each pH conditions while AuNP-Pep11 conjugation was successful at both pHs. When discussed all characterization data of AuNP-Pep4 and AuNP-Pep11 conjugates, it was concluded that AuNPs could be conjugated with Pep4 and Pep11 at pH 11.0.

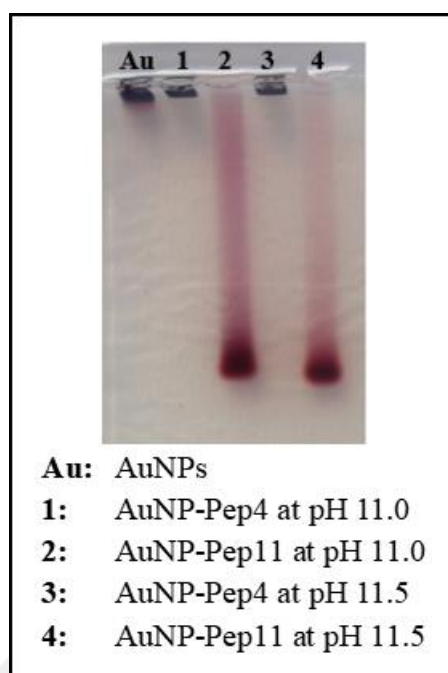


Figure 4.48. White light image of agarose gel loaded naked AuNPs, AuNP-Pep4 and AuNP-Pep11 conjugates.

#### ***4.2.2.5. Optimization of AuNP Conjugation with Pep5 and Pep12 and Their Characterization***

The spherical AuNPs of 13 nm diameter size were conjugated with 20  $\mu$ l of 1 mg/ml of seven amino acid length Pep5 (NH<sub>2</sub>-DGRGGGC-COOH) and Pep12 (NH<sub>2</sub>-CGGGRGD-COOH). The isoelectric point of peptides was 6.1. The AuNP aggregation did not occur after addition of Pep5 at basic conditions, especially after pH 11, and after addition of Pep12 when pH was 5.5 and higher. Therefore, in order to find the densest conjugation of Pep5 and Pep12 on the AuNP surfaces, the pH of AuNP suspensions were adjusted at 10.5, 11.0 and 11.5 with 0.05 NaOH. AuNPs were functionalized with 20  $\mu$ l of 1 mg/ml Pep5 when the pH of AuNP suspensions were at 10.5, 11.0 and 11.5 with three replicates, and conjugated with 20  $\mu$ l of 1 mg/ml Pep12 when the pH of AuNP suspensions were 5.9, 10.5, 11.0 and 11.5 with three replicates. As seen in Figure 4.49, no AuNP aggregation was observed after the functionalization indicating the stability of the suspension.



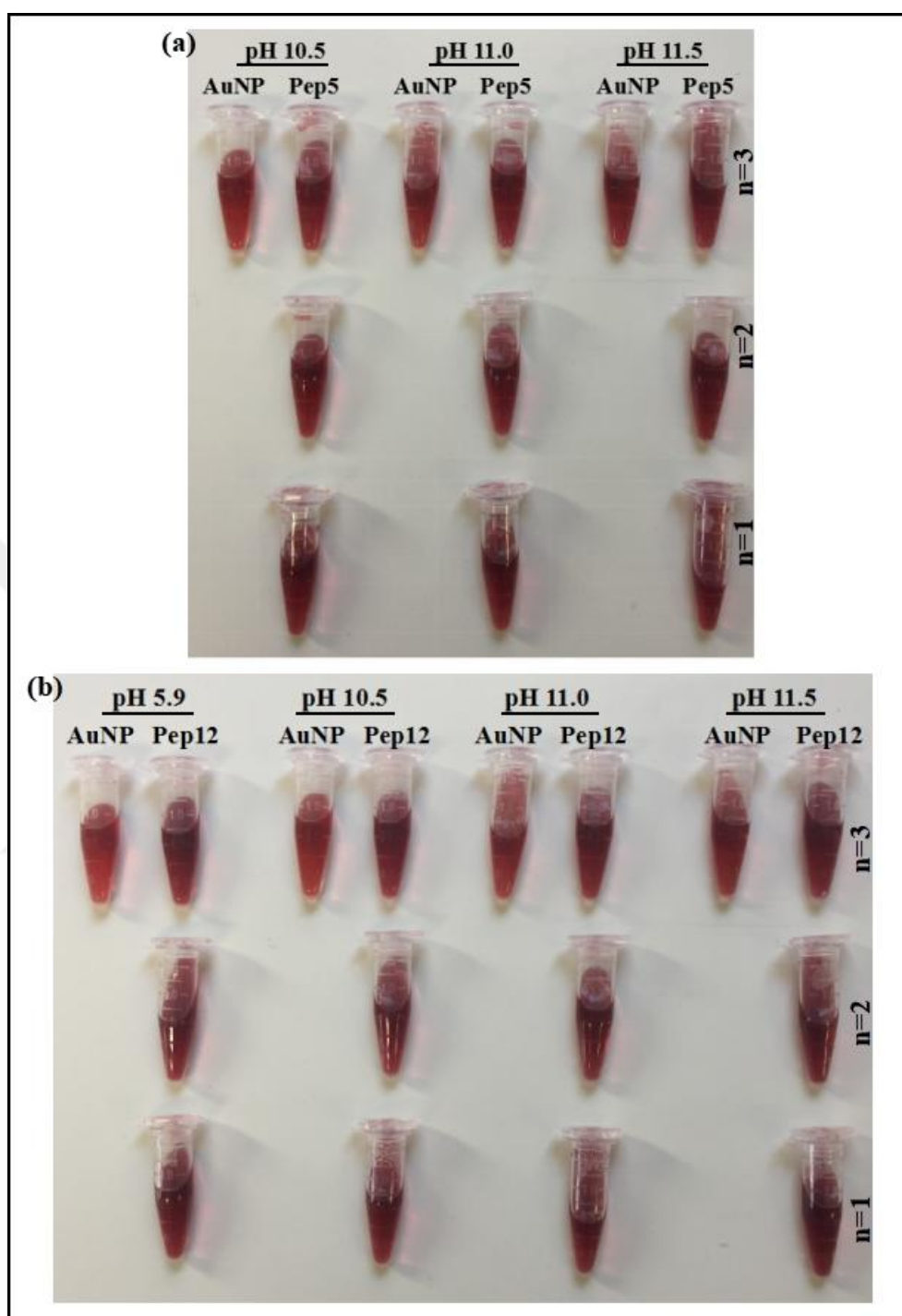


Figure 4.49. White light images of suspensions of (a) naked AuNPs and AuNPs modified with Pep5 at pH 10.5, 11.0 and 11.5 and (b) naked AuNPs and AuNPs modified with Pep12 at pH 5.9, 10.5, 11.0 and 11.5. “n” indicates replicate number.

The naked 13 nm AuNPs, AuNP-Pep5 and AuNP-Pep12 conjugates were characterized by UV/Vis spectroscopy, as seen in Figure 4.50. The SPR of 13 nm AuNPs was at 519 nm

whilst the AuNP-Pep5 conjugates had it at 522 nm. This 3 nm redshift was a proof that AuNPs could be conjugated with Pep5. Furthermore, the SPR of AuNP-Pep12 conjugates were at 523 or 524 nm. When the pH of AuNP suspension was 5.9, which was the original pH of the suspension, the conjugates had SPR at 524 nm. On the other hand, when the pH was adjusted at 10.5, 11.0 or 11.5, AuNP-Pep12 had it at 523 nm. Based on the result, it can be said that thanks to 4-5 nm redshift of SPR on UV/Vis spectra, AuNPs could be conjugated with Pep12 in each pHs, but the conjugation was better at original pH of AuNP suspension.

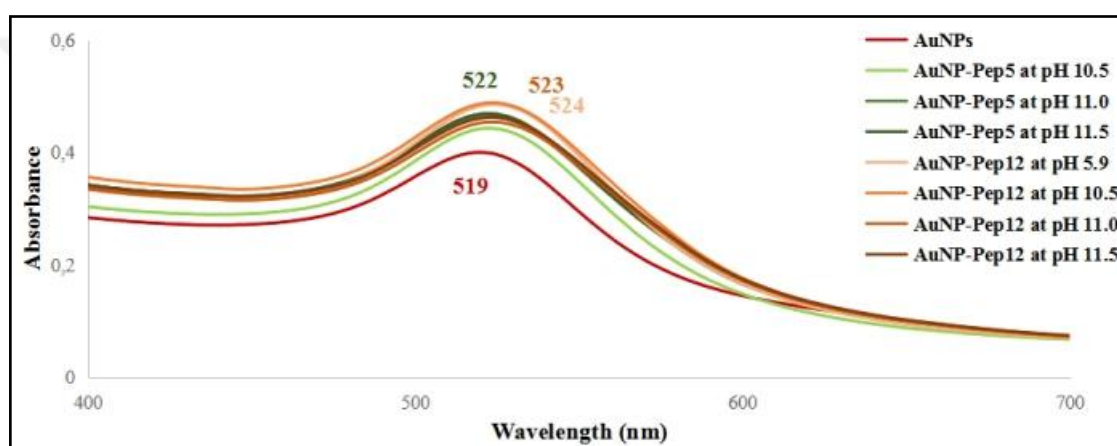


Figure 4.50. Comparative UV/Vis spectra of naked AuNPs, AuNP-Pep5 and AuNP-Pep12 conjugates.

The naked AuNPs, AuNP-Pep5 and AuNP-Pep12 conjugates were characterized by DLS. The hydrodynamic size and zeta potentials of naked AuNPs and the conjugates were measured three times. The average values with standard deviations of naked AuNPs and conjugates were given in Table 4.11. The average hydrodynamic size and zeta potential of naked AuNPs were 13.8 nm. After conjugation with Pep5 at different pHs, the sizes were various. Just the sizes of AuNP-Pep5 conjugated at pH 10.5 were higher than the others. Moreover, the zeta potential of naked AuNPs was -32.3 mV. AuNP-Pep5, conjugated at pH 10.5 and 11.0, had more positive zeta potential while AuNP-Pep5, conjugated at pH 11.5, had more negative than naked AuNPs. In addition, after conjugation with Pep12 at different pHs, the sizes and zeta potentials altered. The hydrodynamic sizes of all conjugates were larger than naked AuNPs, but the AuNP-Pep12 conjugated at pH 5.9 had

16.4 nm average size, which was the largest conjugate. The zeta potentials of all conjugates except that of conjugated at pH 11.5 were more positive than naked AuNPs. These all results claimed that AuNPs could be conjugated with Pep5 at pH 10.5 and with Pep12 at pH 5.9.

Table 4.11. Average hydrodynamic sizes and zeta potentials of naked AuNPs, AuNP-Pep5 and AuNP-Pep12 conjugates.

Sample	Size (nm)	Zeta Potential (mV)
AuNPs	13.8 ± 0.3	-32.3 ± 0.4
AuNP-Pep5 at pH 10.5	14.8 ± 0.3	-25.0 ± 0.7
AuNP-Pep5 at pH 11.0	13.0 ± 0.8	-26.5 ± 7.6
AuNP-Pep5 at pH 11.5	13.2 ± 0.8	-37.8 ± 1.6
AuNP-Pep12 at pH 5.9	16.4 ± 1.1	-25.7 ± 2.8
AuNP-Pep12 at pH 10.5	14.2 ± 0.9	-23.0 ± 2.3
AuNP-Pep12 at pH 11.0	14.4 ± 0.6	-23.1 ± 3.3
AuNP-Pep12 at pH 11.5	14.4 ± 0.5	-35.3 ± 5.6

The naked AuNPs, AuNP-Pep5 and AuNP-Pep12 conjugates were characterized by 1 percent Agarose gel electrophoresis, as seen in Figure 4.51. The naked AuNPs precipitated, could not run on the gel because of TAE buffer. On the other hand, AuNP-Peptide conjugated could run the gel since the peptide coating on the AuNPs surfaces were successful. AuNP-Pep5 conjugates, loaded in 2nd, 4th and 6th wells of the gel, were back than AuNP-Pep12 conjugates, loaded in the 1st, 3rd, 5th and 7th wells of the gel. The most dense band of AuNP-Pep5 was seen in the 2nd well, in which AuNP-Pep5 conjugated at pH 10.5 were loaded. When considered the band dense of AuNP-Pep12, it was determined that the bands in the 1st and 3rd wells were denser. According to the Agarose gel results, it can be said that AuNPs could be functionalized with Pep5 in the conditions of pH 10.5 and with Pep12 at 5.9 better.

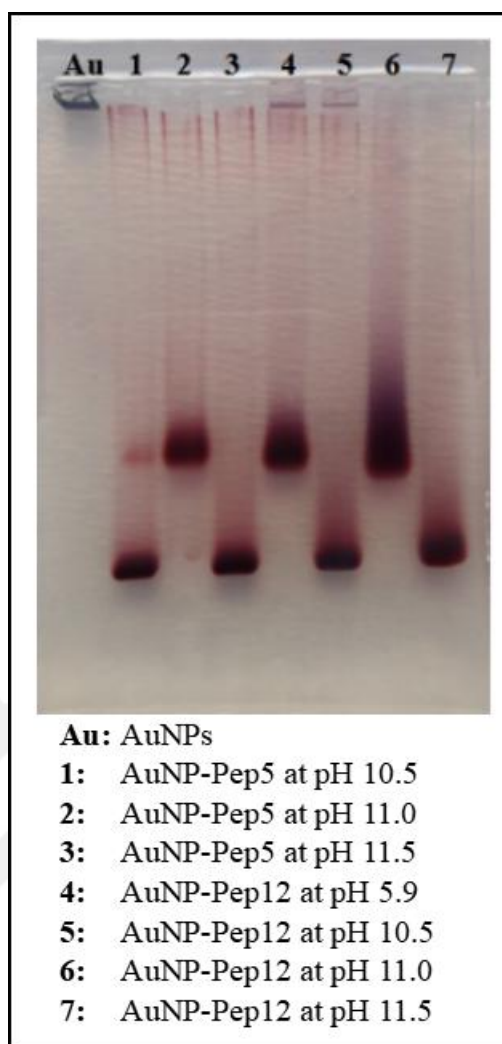


Figure 4.51. White light image of agarose gel loaded naked AuNPs, AuNP-Pep5 and AuNP-Pep12 conjugates.

#### ***4.2.2.6. Optimization of AuNP Conjugation with Pep6 and Pep13 and Their Characterization***

The spherical AuNPs of 13 nm diameter size were conjugated with 20  $\mu$ l of 1 mg/ml of seven amino acid length either Pep6 (NH<sub>2</sub>-DRGEEEC-COOH) or Pep13 (NH<sub>2</sub>-CGGGRGD-COOH). The isoelectric point of the peptides was 3.8. Based on results about the conjugation affinity of Pep6 on the surface of AuNPs at different pHs, no AuNP aggregation was occurred after addition of 20  $\mu$ l of 1 mg/ml Pep6 in the case of the pH of AuNP suspension was higher than 5.5 and after addition of 20  $\mu$ l of 1 mg/ml Pep13 in the

case of the pH of AuNP suspension was higher than 4.5. In order to find the best conjugation between 13 nm AuNPs and Pep6 or Pep13, it was decided that AuNPs could be functionalized with 20  $\mu$ l of 1 mg/ml Pep6 and Pep13 when the pH of AuNP suspensions was at 5.9, 9.5 and 11.5. 1 ml of 10 nM 13 nm AuNPs were functionalized with 20  $\mu$ l of 1 mg/ml Pep6 and Pep13 when the pH of AuNP suspensions were at 5.9, 9.5 and 11.5 with three replicates. As seen in Figure 4.52, no AuNP aggregation was observed after the conjugation indicating the stability of the suspension.

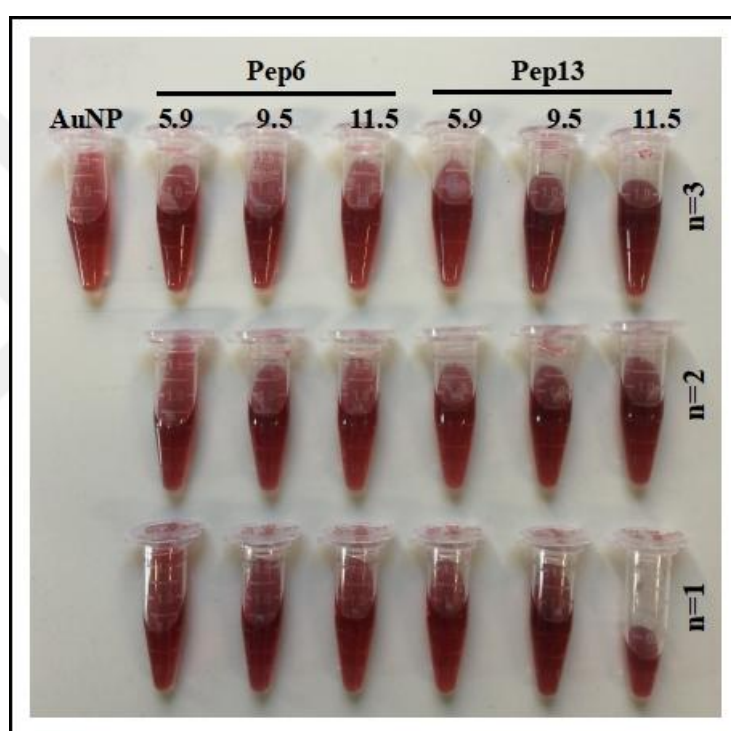


Figure 4.52. White light image of suspensions of naked AuNPs and AuNPs modified with either Pep6 or Pep13 at pH 5.9, 9.5 and 11.5. “n” indicates replicate number.

The naked 13 nm AuNPs, AuNP-Pep6 and AuNP-Pep13 conjugates were characterized by UV/Vis spectroscopy, as seen in Figure 4.53. The SPR of 13 nm AuNPs was at 519 nm whilst the AuNP-Pep6 and AuNP-Pep13 conjugates had it at 519, 521 or 522 nm. When the pH of AuNP suspension was 5.9, which was the original pH of the suspension, the conjugates had SPR at 522 nm. On the other hand, when the pH was adjusted at 9.5 or 11.5, the conjugates had it at 521 and 519 nm, respectively. Based on the result, it can be

concluded that AuNPs could be conjugated with Pep6 and Pep13 at only 5.9 and 9.5 pHs, but the conjugation was thought better at original pH of AuNP suspension.

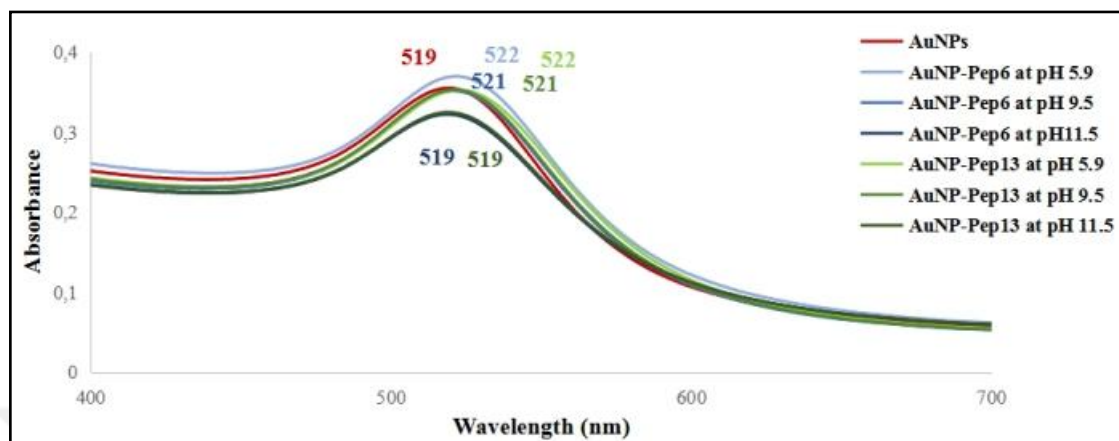


Figure 4.53. Comparative UV/Vis spectra of naked AuNPs, AuNP-Pep6 and AuNP-Pep13 conjugates.

The naked AuNPs, AuNP-Pep5 and AuNP-Pep12 conjugates were characterized by DLS. The hydrodynamic size and zeta potentials of naked AuNPs and the conjugates were measured three times by DLS. The average values with standard deviations of naked AuNPs and conjugates were given in Table 4.12. The average hydrodynamic size of naked AuNPs were 13.8 nm. After conjugation with Pep6 and Pep13 at different pHs, the sizes and zeta potentials altered. The sizes of only AuNP-Pep6 conjugated at pH 5.9 were larger than naked AuNPs, and the AuNP-Pep6 conjugated at pH 9.5 had 12.2 nm average size, which was the smallest conjugate. Moreover, the sizes of AuNP-Pep13, conjugated at pH, 5.9 were larger than naked AuNPs, but the AuNP-Pep13, conjugated at pH 11.5, had 0.7 nm average size. In addition, the zeta potential of AuNPs was measured as -32 mV whilst the zeta potentials of all conjugates except that of conjugated at pH 11.5 were more positive than naked AuNPs. These all results claimed that AuNPs could be conjugated with Pep6 at pH 5.9 and with Pep13 at pH 5.9 and 9.5.

Table 4.12. Average hydrodynamic sizes and zeta potentials of naked AuNPs, AuNP-Pep6 and AuNP-Pep13 conjugates.

Sample	Size (nm)	Zeta potential (mV)
AuNPs	13.8 ± 0.3	-32.0 ± 0.5
AuNP-Pep6 at pH 5.9	14.0 ± 0.9	-26.3 ± 0.6
AuNP-Pep6 at pH 9.5	12.2 ± 0.6	-13.0 ± 2.6
AuNP-Pep6 at pH11.5	13.6 ± 0.01	-81.7 ± 4.3
AuNP-Pep13 at pH 5.9	14.1 ± 0.4	-11.0 ± 1.6
AuNP-Pep13 at pH 9.5	12.8 ± 0.8	-29.0 ± 2.3
AuNP-Pep13 at pH 11.5	0.7 ± 0.01	-30.9 ± 1.9

The naked AuNPs, AuNP-Pep6 and AuNP-Pep13 conjugates were characterized by 1 percent Agarose gel electrophoresis, as seen in Figure 4.54. The naked AuNPs precipitated, could not run on the gel because of TAE buffer. However, AuNP-Peptides conjugated could run through the gel since the peptide could cover the AuNPs surfaces. AuNP-Pep6 conjugates were loaded in 1st, 2nd and 3rd wells of the gel and AuNP-Pep13 conjugates were loaded in the 4th, 5th and 6th wells of the gel. The most dense band of AuNP-Pep6 was seen in the 1st well, in which AuNP-Pep6 conjugated at pH 5.9 were loaded. When considered the band dense of AuNP-Pep12, it was determined that the bands in the 4th well was denser and homogeneous. According to the Agarose gel results, it can be said that AuNPs could be functionalized better with Pep6 and Pep13 in the conditions of pH 5.9.

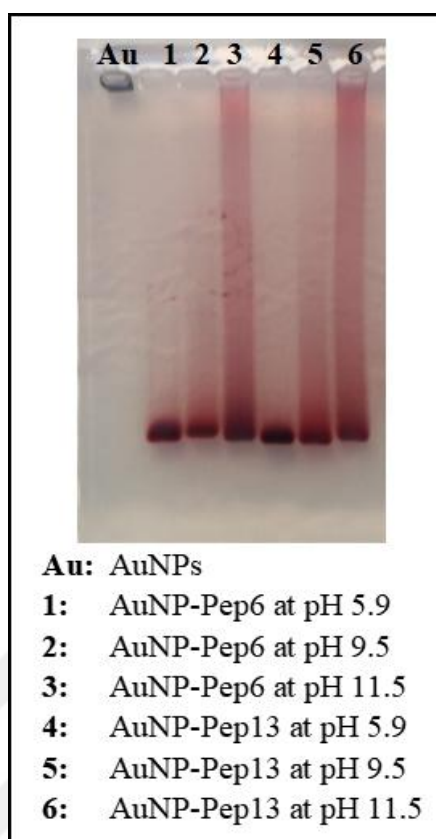


Figure 4.54. White light image of agarose gel loaded naked AuNPs, AuNP-Pep6 and AuNP-Pep13 conjugates.

#### ***4.2.2.7. Optimization of AuNP Conjugation with Pep7 and Pep14 and Their Characterization***

The spherical AuNPs of 13 nm diameter size were functionalized with Pep7 (NH<sub>2</sub>-DGRHHHC-COOH) and Pep14 (NH<sub>2</sub>-CGGGRGD-COOH). The isoelectric point of peptides was 7.4. According to the results about the conjugation affinity of Pep7 on the surface of AuNPs at different pHs, no AuNP aggregation was occurred after addition of 20  $\mu$ l of 1 mg/ml Pep6 in the case of the pH of AuNP suspension was higher than 10.5 and after addition of 20  $\mu$ l of 1 mg/ml Pep14 in the case of the pH of AuNP suspension was higher than 8.1. Due to determine the best conjugation between 13 nm AuNPs and Pep7 or Pep14, it was decided that AuNPs could be functionalized with 20  $\mu$ l of 1 mg/ml Pep7 when the pH of AuNP suspensions was at 10.5, 11.0 and 11.5, and with 20  $\mu$ l of 1 mg/ml



Pep14 when the pH of AuNP suspensions was at 8.4, 9.5 and 10.5 in three replicates. As seen in Figure 4.55, no AuNP aggregation was observed after the surface modification indicating the stability of the suspension.

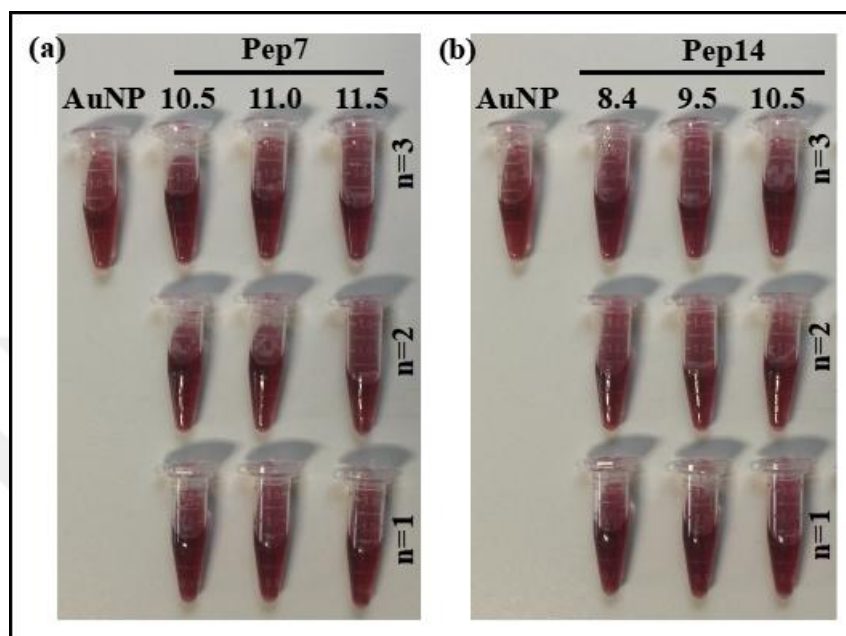


Figure 4.55. White light images of suspensions of (a) naked AuNPs and AuNPs modified with Pep7 at pH 10.5, 11.0 and 11.5 and (b) naked AuNPs and AuNP modified with Pep14 at pH 8.4, 9.5 and 10.5. “n” indicates replicate number.

The naked AuNPs, AuNP-Pep7 and AuNP-Pep14 conjugates were characterized by UV/Vis spectroscopy and the comparative spectra was given in Figure 4.56. The naked 13 nm AuNPs had SPR at 519 nm whereas AuNP-Pep7 conjugates had it at 521 and AuNP-Pep14 conjugates had at 523 nm. The 2-4 nm redshifts indicated the conjugation between AuNPs and peptides. Moreover, the shift was changed based on binding end of peptides.

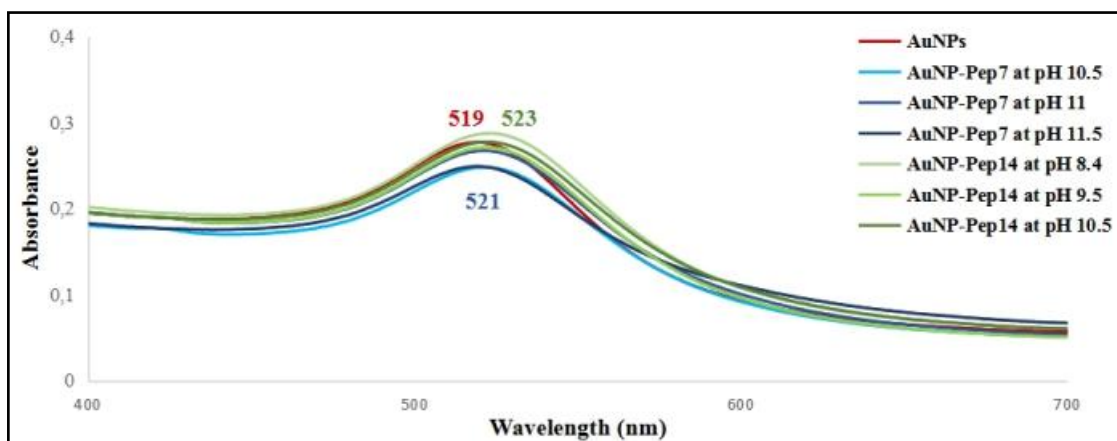


Figure 4.56. Comparative UV/Vis spectra of naked AuNPs, AuNP-Pep7 and AuNP-Pep14 conjugates.

The naked AuNPs, AuNP-Pep7 and AuNP-Pep14 conjugates were characterized by DLS. Their sizes were measured three times, and then averaged. The average sizes and zeta potentials of naked AuNPs, AuNP-Pep7 and AuNP-Pep14 conjugates could be listed in Table 4.13. The average hydrodynamic size of naked AuNPs was 11.6 nm while the sizes of conjugates were larger than naked AuNPs. The largest AuNP-Pep7 conjugates were seen in the condition of pH 10.5 whereas the largest AuNP-Pep14 conjugates were observed at pH 13.2. This determined that AuNPs could be conjugated with Pep7 at pH 10.5 and with Pep14 at pH 8.4. Due to agglomeration of AuNP-Pep7 and AuNP-Pep14 conjugates modified at higher pHs, their zeta potentials cannot be measured. Just, AuNP-Pep7 conjugates modified at pH 10.5 had more positive and AuNP-Pep14 conjugates modified at pH 8.4 had more negative zeta potentials when compared to naked AuNPs.

Table 4.13. Average hydrodynamic sizes and zeta potentials of naked AuNPs, AuNP-Pep7 and AuNP-Pep14 conjugates.

Sample	Size (nm)	Zeta potentials (mV)
AuNPs	11.6 ± 0.5	-23.1 ± 0.7
AuNP-Pep7 at pH 10.5	13.8 ± 1.5	-13.3 ± 0.5
AuNP-Pep7 at pH 11.0	227.7 ± 194.0	0.0
AuNP-Pep7 at pH 11.5	12.2 ± 3.3	0.0
AuNP-Pep14 at pH 8.4	13.2 ± 0.9	-27.9 ± 0.4
AuNP-Pep14 at pH 9.5	12.5 ± 0.7	0.0
AuNP-Pep14 at pH 10.5	12.3 ± 0.8	0.0

In order to observe the density of Pep7 and Pep14 on the AuNP surfaces, the naked AuNPs and conjugates were characterized by 1 percent Agarose gel electrophoresis, as seen Figure 4.57. The naked AuNPs could not run through the gel because of TAE buffer. Surprisingly, AuNP-Pep7 conjugates, which were observed as conjugated by UV/Vis and DLS, precipitated in the gel like naked AuNPs. The reason behind this could be that AuNPs could not be conjugated with Pep7 densely. On the other hand, AuNP-Pep14 conjugates could run through the gel and the one, conjugated at pH 8.4, had denser band. Based on the Agarose gel result, it can be said that the conjugation between AuNPs and Pep7 was not successful unlike others and AuNPs could be coated with Pep14 at pH 8.4 as best.

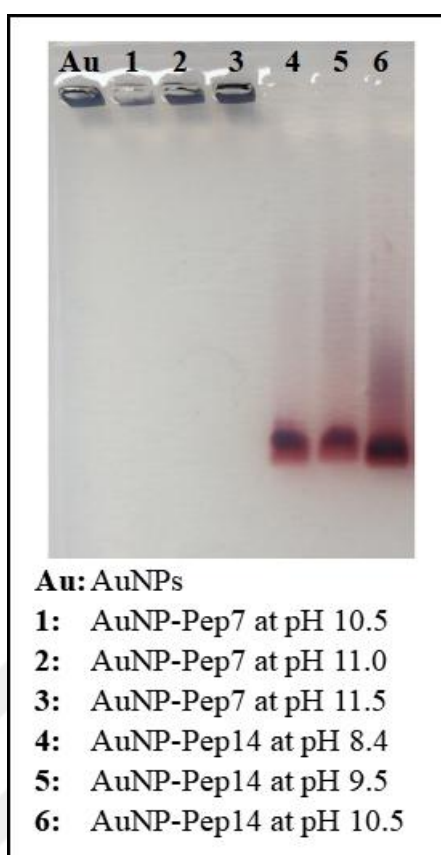


Figure 4.57. White light image of agarose gel loaded naked AuNPs, AuNP-Pep7 and AuNP-Pep14 conjugates.

#### ***4.2.2.8. Conjugation of AuNPs with Peptides and Their Characterization***

The spherical AuNPs of 13 nm diameter size were functionalized with fourteen peptides in their best conjugation conditions, listed above in Table 4.5, in order to see their characterization at total. AuNPs were functionalized with Pep6, Pep8, Pep9, Pep10, Pep12 and Pep13 at pH 5.9, which was the original pH of AuNP suspension, with Pep3 and Pep14 at pH 8.6, with Pep5 and Pep7 at pH 10.5, and lastly with Pep1, Pep2, Pep4 and Pep11 at pH 11.0.

1 ml of 10 nM 13 nm AuNPs were conjugated with 20  $\mu$ l of 1 mg/ml each peptide at best conjugation pH conditions in triplicates. The image of naked AuNPs and AuNP-Peptide conjugates' suspensions was given in Figure 4.58. As seen in the figure, no AuNP

aggregation was observed after the functionalization indicating the stability of the suspension.

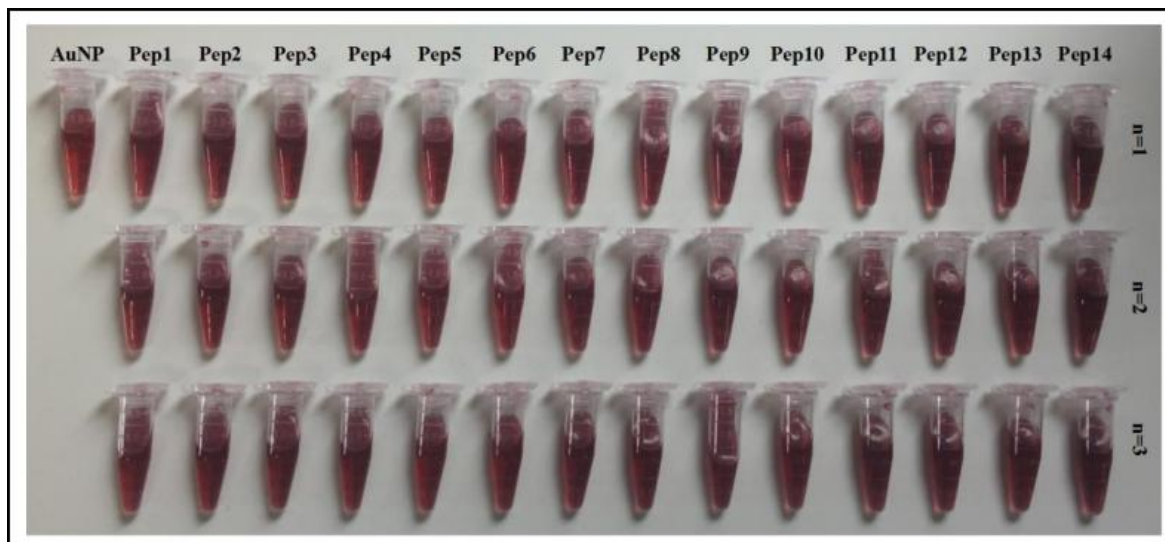


Figure 4.58. White light image of naked AuNPs and AuNP-Peptide conjugate suspensions. “n” indicates replicate number.

The naked AuNPs and AuNP-Peptide conjugates were characterized by UV/Vis spectroscopy. The comparative UV/Vis spectra of naked AuNPs and AuNP-Peptides was given in Figure 4.59. The SPR of naked AuNPs was at 519 nm while it was redshifted for all AuNP-Peptide conjugates. 1.0 nm redshifted was observed on the spectra of AuNP-Pep1, AuNP-Pep2, AuNP-Pep3 and AuNP-Pep5, while the SPR of AuNP-Pep4, AuNP-Pep10 and AuNP-Pep11 was redshifted 2 nm. In addition, 3 nm red-shift was seen on the spectra of AuNP-Pep6, AuNP-Pep7, AuNP-Pep8, AuNP-Pep9 and AuNP-Pep13. The longest shift, 4 nm, was occurred after conjugation with Pep12 and Pep14. As a conclusion, AuNP-Peptide conjugates showed unique properties, depending on their length, size, charge and binding end group to AuNP surfaces.

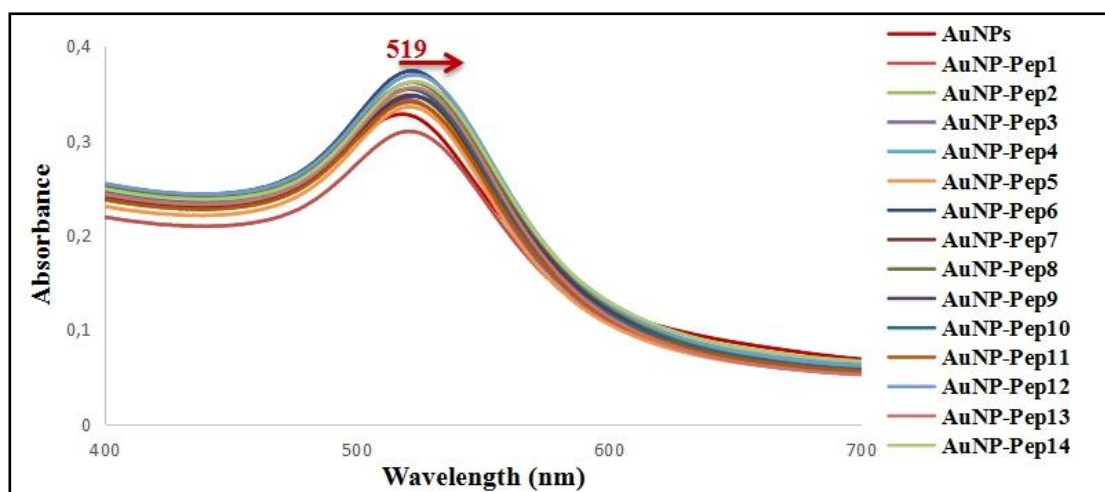


Figure 4.59. Comparative UV/Vis spectra of naked AuNPs and AuNP-Peptide conjugates.

The naked and peptide functionalized AuNPs were characterized by DLS. The hydrodynamic sizes and zeta potentials of naked AuNPs and AuNP-Peptide conjugates were measured three times. Their average sizes and zeta potentials with standard deviations were given in Table 4.14. The average hydrodynamic size of naked AuNPs was 11.9 nm. After conjugation with peptides, the average hydrodynamic sizes were grown and all conjugates were larger than naked AuNPs. This proved that AuNP surfaces could be coated with peptides since the size increase was a result of conjugation between AuNP and peptides.

Table 4.14. SPR on UV/Vis spectra, average hydrodynamic sizes and zeta potentials of naked AuNPs and AuNP-Peptide conjugates.

Sample	SPR (nm)	Size (nm)	Zeta potential (mV)
AuNPs	519	11.7 ± 0.7	-17.6 ± 0.6
AuNP-Pep1	520	13.0 ± 0.3	-35.9 ± 2.7
AuNP-Pep2	520	12.6 ± 0.9	-45.2 ± 3.1
AuNP-Pep3	520	12.3 ± 0.8	-27.0 ± 3.8
AuNP-Pep4	521	12.5 ± 1.0	-43.1 ± 3.1
AuNP-Pep5	520	12.8 ± 0.8	-36.6 ± 4.2
AuNP-Pep6	522	12.0 ± 0.5	-10.7 ± 1.8
AuNP-Pep7	522	13.1 ± 0.5	-46.6 ± 0.3
AuNP-Pep8	522	12.8 ± 1.2	-10.9 ± 0.3
AuNP-Pep9	522	13.0 ± 0.7	-11.6 ± 0.9
AuNP-Pep10	521	12.7 ± 0.8	-16.2 ± 0.9
AuNP-Pep11	521	12.8 ± 0.8	-18.2 ± 3.8
AuNP-Pep12	523	13.1 ± 0.6	-13.2 ± 3.8
AuNP-Pep13	522	13.6 ± 0.6	-11.7 ± 1.2
AuNP-Pep14	523	13.5 ± 0.7	-15.5 ± 0.4

When discussed the zeta potentials of AuNP-Peptide conjugates, the zeta potentials of AuNPs conjugated with Pep1 to Pep7, in which the free terminus was  $-NH_2$ , were more negative than naked AuNPs whereas AuNPs conjugated with Pep8-Pep14, in which the free terminus was  $-COOH$ , had more positive surface than the naked AuNPs, as schemed in Figure 60. The reason behind that was the interaction between the free citrate ions and free terminus groups of peptides, mentioned in the Figure 4.8 The  $-NH_2$  groups on the AuNPs interacted with the free citrate ions and made the surface more negative, however the  $-COOH$  groups on the surfaces repulsed the citrate ions and the surfaces were more positive when compared to the naked AuNPs. Moreover, the charge of peptides on AuNPs having  $-NH_2$  free terminus also affected the zeta potentials. The neutrally and positively charged peptides were more interacted with the free citrate ions than the negatively charged peptides, therefore the zeta potentials of neutrally and positively charged peptides caused more negative surface than negatively charged peptides. Additionally,  $-COOH$  free terminus of positively charged peptides on AuNPs resulted more negative surface when

compared to the naked AuNPs while the others had more positive surface. Based on zeta potential measurement results, it also demonstrated that the surfaces of AuNPs were functionalized with peptides so that their surface charges were various depending on the total charge and the free terminus of peptides.

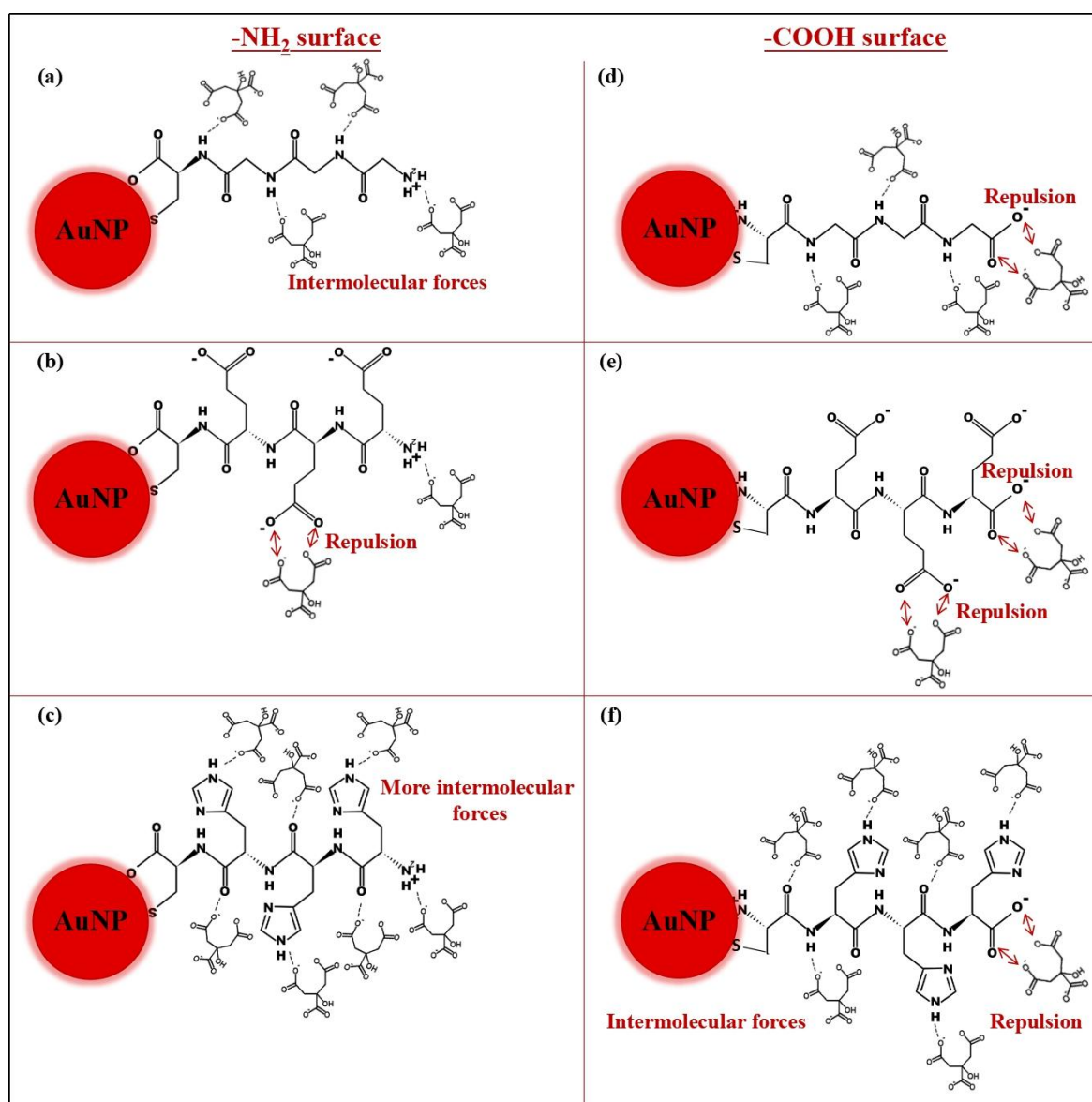


Figure 4.60. Schematic representation of interaction between the free citrate ions and reactive groups of (a,d) neutrally charged peptides, (b,e) negatively charged peptides and (c,f) positively charged peptides on AuNP surfaces.

The naked and peptide functionalized AuNPs were characterized by 1 percent Agarose gel electrophoresis in order to see the density of peptides on the AuNP surfaces in the



suspension. The image of the Agarose gel after run was shown in Figure 4.61. The naked AuNPs could not run on the gel because of aggregation caused by high salt content in TAE buffer. The all bands on the gels were dense and this displayed the success of the conjugation between AuNPs and peptides. AuNP-Pep4 and AuNP-Pep7 conjugates, which were rich in histidine, precipitated in the gel. On the other hand, AuNP-Pep11 and AuNP-Pep14, which were conjugated with Pep11 and Pep14 having reverse sequence of Pep4 and Pep7, could run through the gel. This result showed that AuNP surface functionalization with peptides were more related to binding end of peptide than isoelectric point of peptides, since Pep4 and Pep11 had same isoelectric point. In addition, AuNP-Pep5 and AuNP-Pep11 conjugates moved slowly in the gel and stayed at back. These conjugates were not in common in the case of sequence, size, zeta potential, charge and isoelectric point, however they showed similar behavior in the Agarose gel. Furthermore, based on the Agarose gel result, it was clearly understood that 20  $\mu$ l of 1 mg/ml peptides were coated the surfaces of nearly all AuNPs in 1 ml of 10 nM suspension and the location of cysteine in the peptide affected the conjugation.

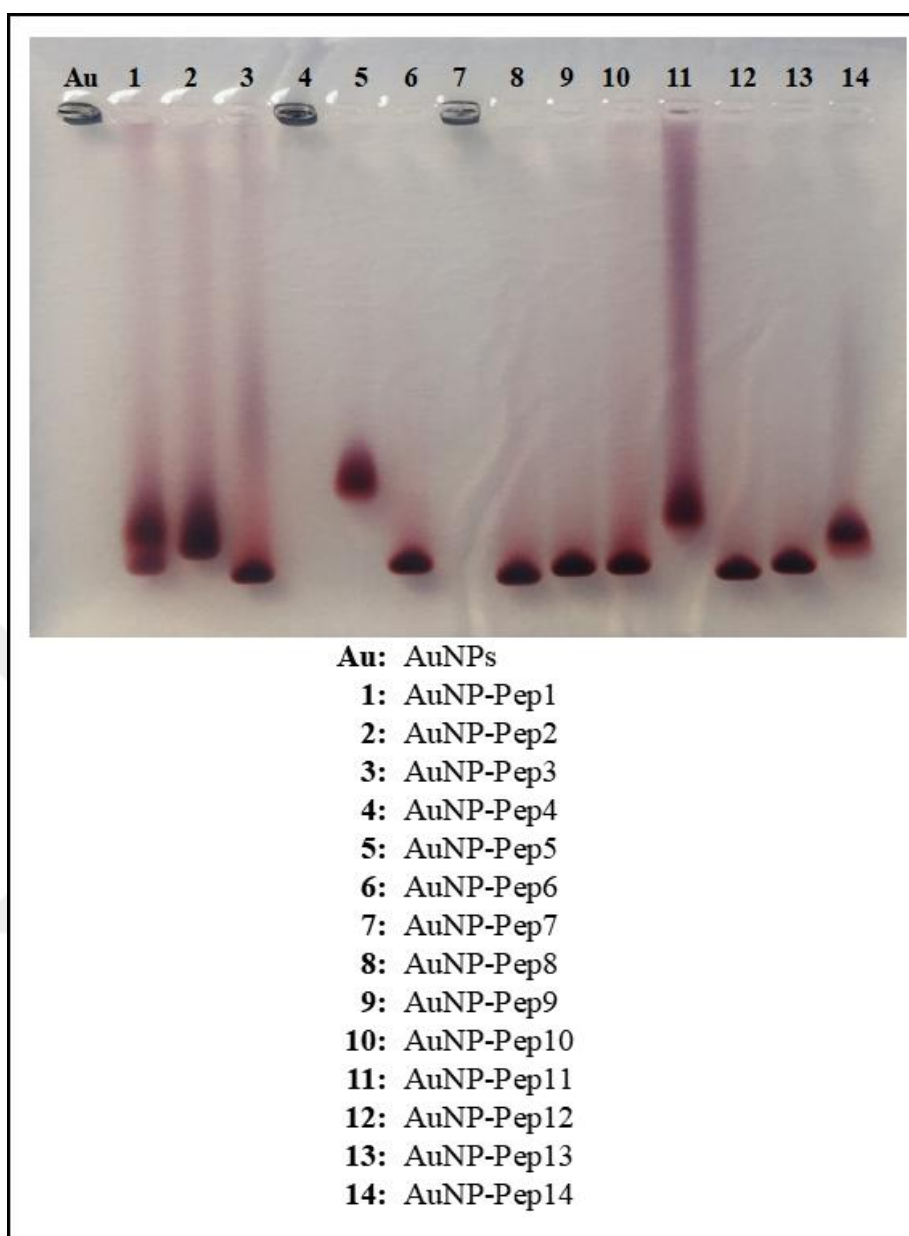


Figure 4.61. White light image of agarose gel, in which naked AuNPs and AuNP-Peptide conjugates were loaded.

The naked AuNPs and AuNP-Peptide conjugates were characterized by FTIR to identify chemical compounds in samples. The comparative FTIR spectra of naked AuNPs and AuNP-Peptide conjugates were given in Figure 4.62. According to the result, no information could be obtained in the FTIR spectrum of naked AuNPs. On the other hand, on the spectra of peptide functionalized AuNPs, there were some chemical information meaning amino acids and peptide bonds such as C-H stretching between  $2850\text{-}2900\text{ cm}^{-1}$ ,

C=O stretching of amide between 1640-1690  $\text{cm}^{-1}$ , N-H bending of amide between 1590-1640  $\text{cm}^{-1}$ , =C-CH<sub>3</sub> stretching at 1435  $\text{cm}^{-1}$ , C-N stretching between 1080-1250  $\text{cm}^{-1}$  and Amide I, representing C=O stretch and some N-H stretching characteristics [216]. These all information came from peptides proved that AuNPs could be coated with peptides, because amino acids can link each other by amide bond and on the spectra the information about amide bonds were collected.

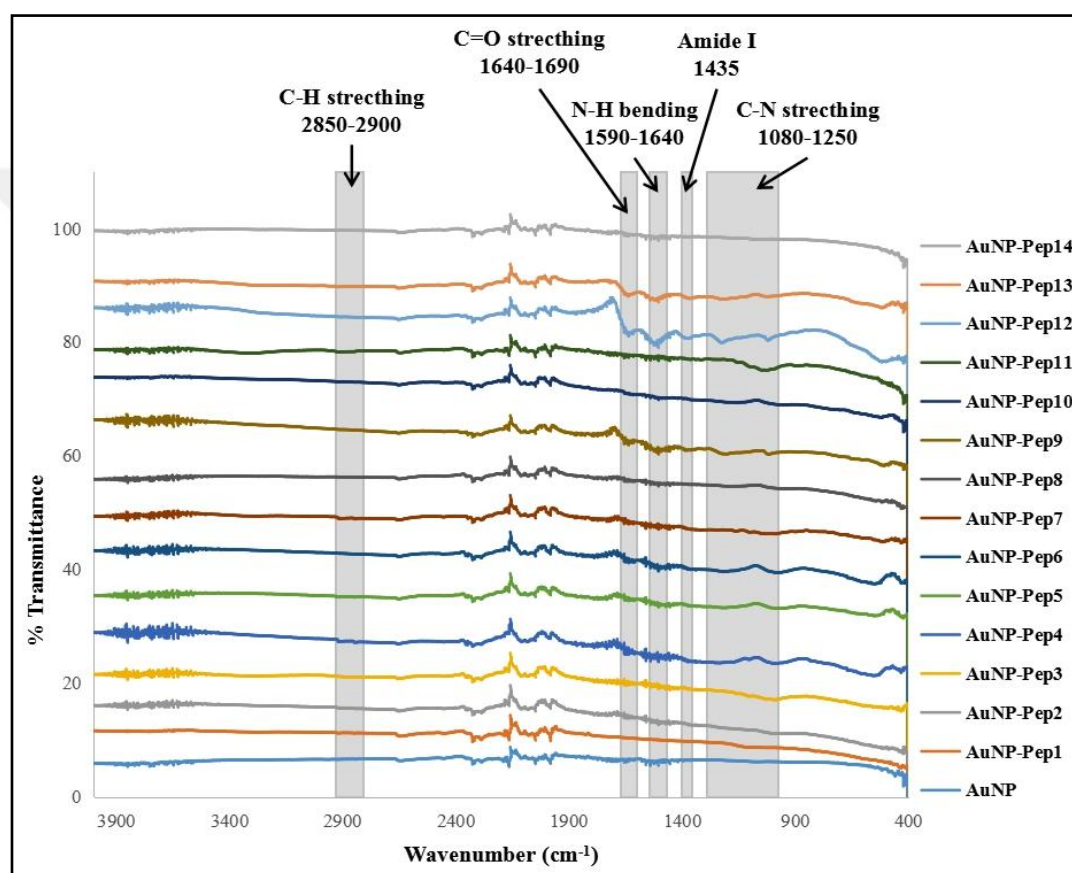


Figure 4.62. Comparative FTIR spectra of naked AuNPs and AuNP-Peptide conjugates.

The naked AuNPs and AuNP-Peptide conjugates were characterized by SERS since it could obtain the information about peptides chemically bound on AuNP surfaces. The comparative SERS spectra of naked AuNPs and AuNP-Peptide conjugates were presented in Figure 4.63. Based on SERS results, there existed significant differences between the spectra of naked AuNPs and AuNP-Peptides. The characteristic bands representing S-S disulfide stretching in proteins at 500-524  $\text{cm}^{-1}$ , C-S gauche conformation in amino acids at 638-650  $\text{cm}^{-1}$ , C-N stretching in proteins at 713-745  $\text{cm}^{-1}$ , deformative vibration of amine

groups at 817-840  $\text{cm}^{-1}$ , C-C stretching in  $\beta$  sheet of proteins at 853-954 and in aromatic ring formation at 977-1002  $\text{cm}^{-1}$ , C-N stretching of proteins at 1160-1185  $\text{cm}^{-1}$ , Amide III bonds at 1221-1322  $\text{cm}^{-1}$  and C-H formation in aromatic residues at 1331  $\text{cm}^{-1}$  [119]. These all peaks seen in the SERS spectra manifested the conjugation between AuNPs and peptides. Moreover, it was observed similar SERS spectra pattern between AuNPs conjugated with peptide couples, which had same amino acid sequence but in reverse order.

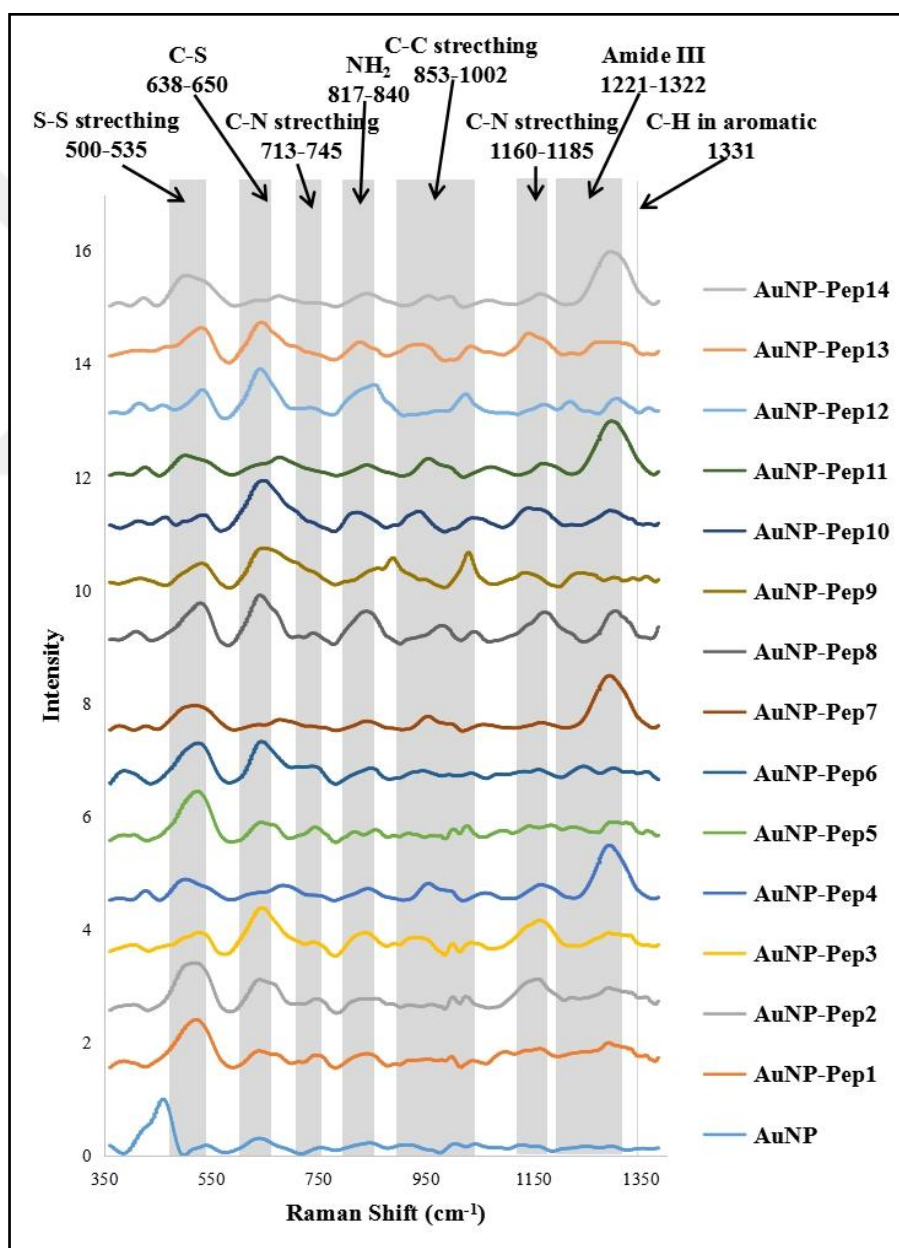


Figure 4.63. Comparative SERS spectra of naked AuNPs and AuNP-Peptide conjugates.

When the peaks on SERS spectra were analyzed, it was seen that some characteristic information about peptides on AuNP surfaces was acquired, as listed in Table 4.15 [222]. Amide III, C-C stretching and S-S disulfide stretching peaks were visible on all AuNP-Peptide spectra. On the other hand, C-S gauche conformation peak could not be taken on the spectra of AuNP-Pep4 and AuNP-Pep11, whose sequence was NH<sub>2</sub>-HHHC-COOH and NH<sub>2</sub>-CHHH-COOH. The peaks assigned as C-N stretching could not be analyzed on the spectra of functionalized with Pep10 and Pep13, which had NH<sub>2</sub>-CEEE-COOH and NH<sub>2</sub>-CEEERGD-COOH, and the peaks representing amino groups could not be seen in the AuNP-Pep9 and AuNP-Pep12, whose sequence was NH<sub>2</sub>-CGGG-COOH and NH<sub>2</sub>-CGGGRGD-COOH, respectively. In addition, C-H peak at 1331 cm<sup>-1</sup> was obtained in the few AuNP-Peptide spectra, whose sequences were reverse. As a consequence, it can be said that the characteristic spectral pattern of AuNP-Peptides in SERS spectra were collected.

Table 4.15. Peak assignments of SERS spectra of AuNP-Peptide conjugates.

Sample	1331 C-H	1221-1322 Amide III	1160-1185 C-N	835-1002 C-C	817-840 NH <sub>2</sub>	713-745 C-N	638-650 C-S	500-535 S-S
AuNP-Pep1		+	+	+	+	+	+	+
AuNP-Pep2	+	+	+	+	+	+	+	+
AuNP-Pep3	+	+	+	+	+	+	+	+
AuNP-Pep4		+	+	+	+			+
AuNP-Pep5		+	+	+	+	+	+	+
AuNP-Pep6	+	+	+	+	+	+	+	+
AuNP-Pep7		+	+	+	+	+	+	+
AuNP-Pep8		+	+	+	+	+	+	+
AuNP-Pep9	+	+		+			+	+
AuNP-Pep10	+	+		+	+		+	+
AuNP-Pep11		+	+	+	+			+
AuNP-Pep12		+	+	+		+	+	+
AuNP-Pep13		+		+	+		+	+
AuNP-Pep14		+	+	+	+	+	+	+

### 4.3. INVESTIGATION OF CELLULAR RESPONSE

The surface of AuNPs were systematically functionalized with carbohydrates and peptides and these modified AuNPs were incubated for 24 h with either healthy cell line, which was BEAS-2b cells (human lung bronchial epithelium cell line), and cancer cells lines, which were A549 cell (human lung cancer cells) and MDA-MB-231 cells (human breast carcinoma cells) in order to see the cellular response differences caused by metabolic activity variation of healthy/cancer cells. The cellular response was investigated by two ways: cytotoxicity and cell cycle arrest. Due to check the possible toxicity affect of surface modified AuNPs, WST-1 cell proliferation assay, Apoptosis/Necrosis assay and Clonogenic cell survival assay were applied. Furthermore, the changes on cell cycle of either healthy cells or cancer cells was investigated by ethanol fixated and PI stained cells by using flow cytometry. Based on optimization studies, the concentrations of NPs' exposure were determined as 0.1, 0.5, 1.0 and 2.5 nM. Surface modified AuNPs were incubated with healthy/cancer cells for 24 h and the cellular responses were investigated by observing cytotoxicity and cell cycle arrest explained molecular tests.

The study to investigate the cellular response to systematically modified AuNP surfaces was initiated with AuNP-Carbohydrate conjugates, then AuNP-Peptide conjugates were taken attention. Since the number of peptides to be used to cover AuNP surfaces were too many, the experiments were divided into four parts. In the first part, the cellular response to naked AuNPs, AuNP-Pep1 and AuNP-Pep8 (RGD sequenced peptides), in the second part, the cellular response to naked AuNPs, AuNP-Pep2, AuNP-Pep5, AuNP-Pep9, AuNP-Pep12 (Glycine rich peptides), in the third part, the cellular response to naked AuNPs, AuNP-Pep3, AuNP-Pep6, AuNP-Pep10, AuNP-Pep13 (Glutamic acid rich peptides) and in the last part, the cellular response to naked AuNPs, AuNP-Pep4, AuNP-Pep7, AuNP-Pep11, AuNP-Pep14 (Histidine rich peptides) was investigated by checking cytotoxicity and cell cycle progression. In the experiments, peptides were divided based on their rich amino acid type and its charge and the reverse order peptide and addition of RGD sequence to the peptide. There existed four peptides in each experiment set. By this way,

the effects of the peptide order and with or without RGD sequence at the peptide on cells were investigated.

Before investigation of cellular response to surface modified AuNPs, uptake of AuNPs into cells was pointed out by using flow cytometry. NPs uptaken by cells or attached to cell membrane increase the granulation of cell. The increment on cell granulation can be detected by the increase on side-scattered light (SSC) of flow cytometry technique [226]. Therefore, NP cellular uptake was determined by using flow cytometry. The results of uptake studies assisted to understand the cellular response to the AuNP surfaces.

Three tests were applied to analyze the cytotoxicity of the cells treated with surface modified AuNPs. WST-1 cell proliferation assay was used to measure the color change caused by the interaction between tetrazolium salts in the solution and mitochondria of living cells by using fluorescence microscopy [227]. This assay's result was affected by several mistakes such as cell number on the wells of the plates, adding more or less reagent into the wells, transferring more or less amount of reacted reagent into a new plate to be used analyze by microscopy. These all mistakes can change results and increase the standard deviation among the repeats. WST-1 cell proliferation test was utilized because of its easy protocol despite of these possible problems. On the other hand, in order to understand the cytotoxicity of surface modified AuNPs to the cells, another assays were necessary. The second applied assay to check the possible cytotoxicity of NPs was Apoptosis/Necrosis assay [228]. In this assay, the cells were stained with Annexin V and Propidium Iodide (PI) dyes, and then the stained cells were detected by flow cytometry. Annexin V is a protein that binds phosphatidylserine proteins, which switch their position from inside through the outer of cell membrane during apoptosis. By this way, apoptotic cells can be detected by Annexin V staining. PI also stains DNA strands. In the analysis of stained cells by flow cytometry, the cells stained by just Annexin V were evaluated as early apoptosis, the cells stained by both dyes were interpreted as late apoptosis and the cells stained by just PI were considered as necrosis. As a last toxicity assay, clonogenic cell survival assay, which is a sensitive technique, was performed to examine the colony

formation ability of a single cell in the treatment conditions. To investigate cell survival upon NP exposure is an essential phenotypic measurement to get information whether exposed NPs induced or prevented toxicity [229]. It was expected that the colony formation ability or formed cells colonies should decrease in parallel to increasing the concentration of NPs. Thanks to clonogenic cell survival assay, long term cytotoxicity of NPs can be evaluated.

The other cellular response upon NP exposure was the changes on cell cycle progression, which was detected by flow cytometry [230]. The investigation of cell cycle was considered significant since the applied NP dosage cannot create toxicity, but can affect the cell cycle. Therefore, the influence of biomacromolecules functionalized AuNPs on cell cycle was examined by using flow cytometry. In order to follow the cell cycle of the population, the cells were firstly 70 percent ethanol fixation, then stained with PI, and finally analyzed by flow cytometry. There exist three basic phases of cell cycle, G0/G1, S and G2/M. A cell doubles its DNA during proliferation. The DNA synthesis starts at S phase. The cells has double DNA at G2 phase and starts to divide into two at M phases. Thus, the cell cycle of the cells can be followed by measuring DNA content in the cells. At G0/G1 phase, the cells had 1x DNA, at S phase the cells had approximately 1.5x DNA and at G2/M phase the cells had 2x DNA. These PI stained cells can be differentiated by flow cytometry depending on their DNA content. In cell cycle studies, 20 000 cells were detected by flow cytometry as a population and remarked as 100 percent. Based on PI dye in the cells or another words DNA content in the cells, the percentage of the cells at G0/G1 or S or G2/M phases were calculated by software and the results were discussed.

#### **4.3.1. Cellular Response to AuNPs Modified With Carbohydrates**

The surfaces of AuNPs were functionalized with four specifically chosen carbohydrates, which were Glucose, Mannose, Lactose and Maltose, in order to create subtle differences on the AuNP surfaces. These small differences on AuNP surfaces after modification with Glucose, Mannose, Lactose and Maltose were visualized in Figure 4.64.



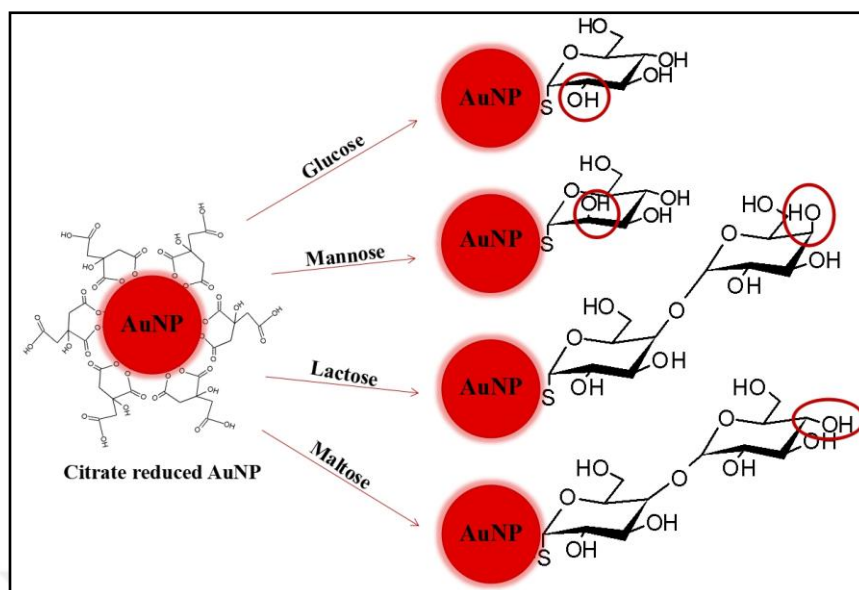


Figure 4.64. Subtle differences on AuNP surfaces after functionalization with thiolated Glucose, Mannose, Lactose and Maltose.

#### 4.3.1.1. Uptake Studies

SSC graphs of A549, BEAS-2b and MDA-MB-231 cells treated with 0.1, 0.5, 1 and 2.5 nM naked 13 nm AuNPs, AuNP-Glucose, AuNP-Mannose, AuNP-Lactose and AuNP-Maltose conjugates were given in Figure 4.65. The negative control cells of A549, BEAS-2b and MDA-MB-231 cells showed approximately 13, 5 and 4 percent granulation, respectively.

A549 cells significantly internalized only the high concentrations of AuNP-Lactose and AuNP-Maltose conjugates among others.

BEAS-2b cells internalized all AuNP-Carbohydrate conjugates when compared to untreated control cells. In addition, AuNP-Lactose and AuNP-Maltose penetrated into BEAS-2b cells more than others.

MDA-MB-231 cell uptaken only naked AuNPs. On the other hand, no significant granulation was detected MDA-MB-231 cells treated with AuNP-Carbohydrate conjugates.

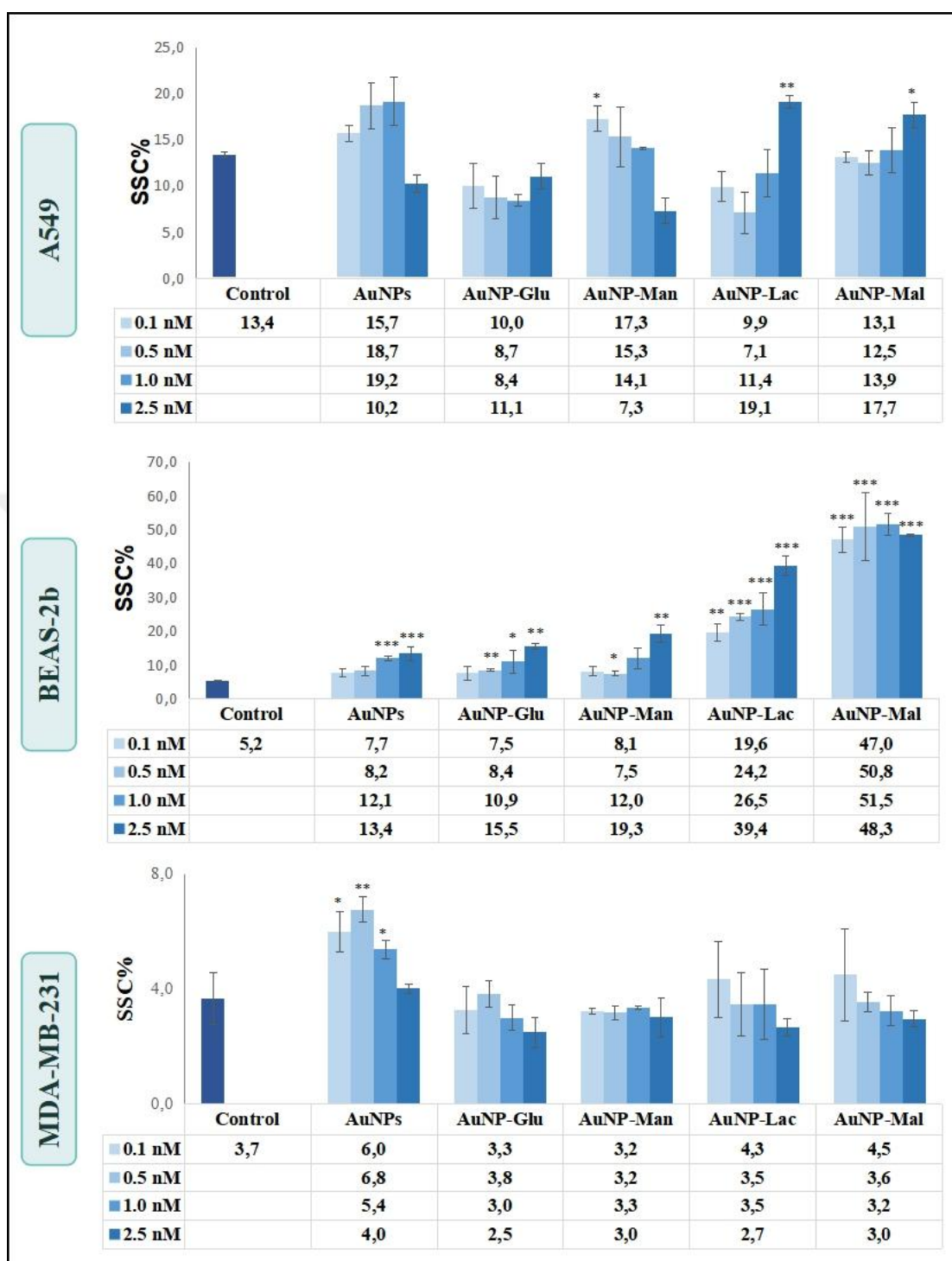


Figure 4.65. SSC graphs of A549, BEAS-2b and MDA-MB-231 cells treated with 0.1, 0.5, 1.0 and 2.5 nM naked 13 nm AuNPs and Glucose, Mannose, Lactose and Maltose Functionalized AuNPs. Statistically significant changes compared to negative control cells were calculated by two-paired Student's t test, and marked with stars, \* for  $p \leq 0.05$ , \*\* for  $p \leq 0.01$  and \*\*\* for  $p \leq 0.001$ .

#### ***4.3.1.2. WST-1 Cell Proliferation Assay***

WST-1 Cell Proliferation result of A549, BEAS-2b and MDA-MB-231 cells treated with 0.1, 0.5, 1.0 and 2.5 nM of naked 13 nm AuNPs and Glucose, Mannose, Lactose and Maltose Functionalized AuNPs was given in Figure 4.66. 10 percent DMSO was used as positive control and decreased the cell viability up to 5-10 percent for each cell types.

The cell viability of A549 cells affected by 2.5 nM of naked AuNPs, 0.1 and 0.5 nM of AuNP-Glucose and 1.0 and 2.5 nM of AuNP-Maltose while their epimers on AuNPs did not create any significant cytotoxic effect on A549 cells.

Neither naked AuNPs nor carbohydrate functionalized AuNPs created cytotoxicity to BEAS-2b cells. Moreover, the high concentrations of all NPs increased cell viability of BEAS-2b cells.

The cell viability of MDA-MB-231 cells was influenced by 0.5-2.5 nM of naked AuNPs and 0.1-0.5 nM of AuNP-Glucose conjugates. The toxicity induced by either naked AuNPs or AuNP-Glucose conjugates were concentration dependent, however toxicity of naked AuNPs increased whereas that of AuNP-Glucose decreased with the concentration increase.

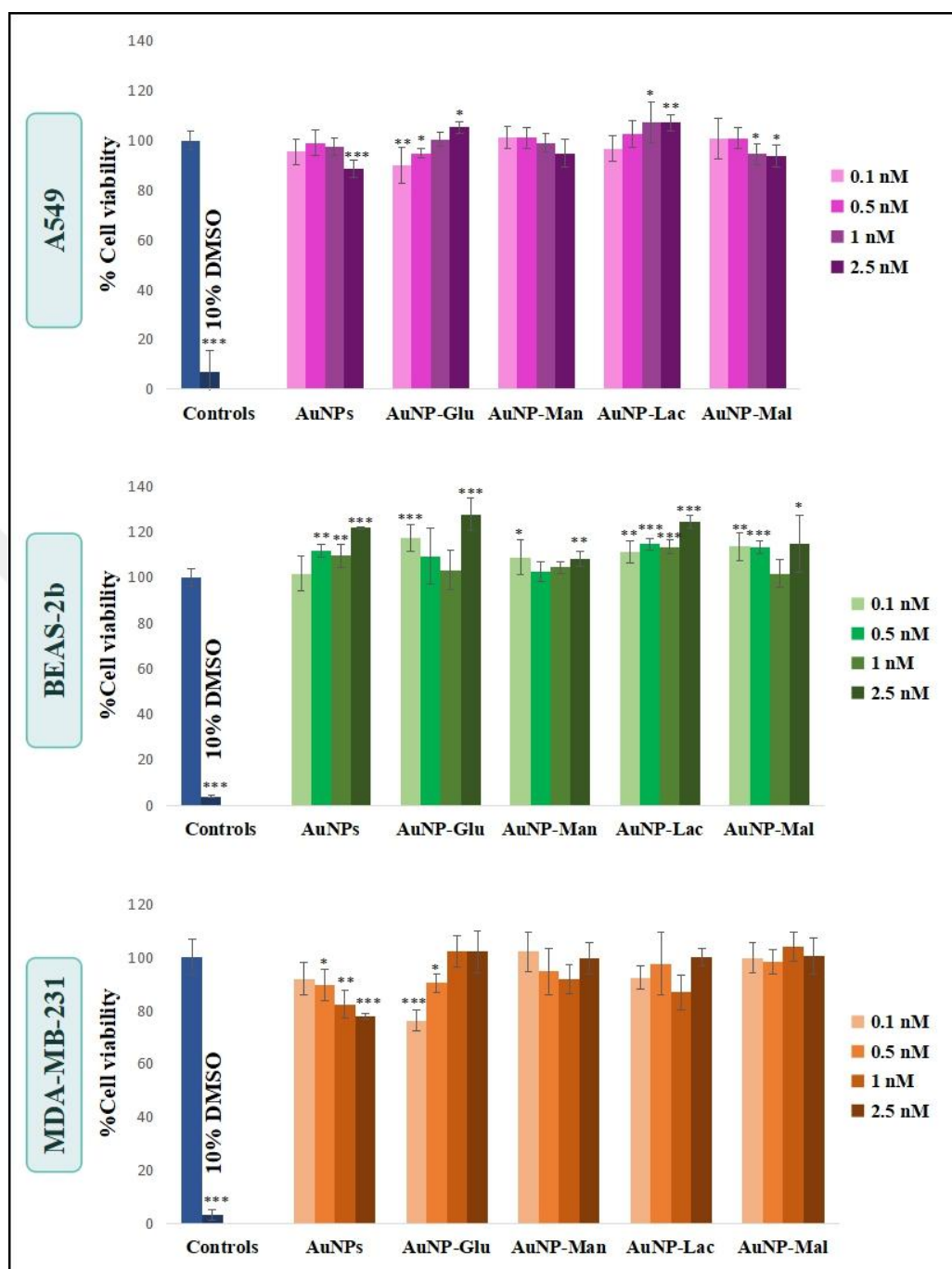


Figure 4.66. WST-1 Cell Proliferation result of A549, BEAS-2b and MDA-MB-231 cells treated with 0.1, 0.5, 1.0 and 2.5 nM of naked 13 nm AuNPs and Glucose, Mannose, Lactose and Maltose Functionalized AuNPs. The positive control was 10 percent DMSO. Statistically significant changes compared to negative control cells were calculated by two-paired Student's t test, and marked with stars, \* for  $p \leq 0.05$ , \*\* for  $p \leq 0.01$  and \*\*\* for  $p \leq 0.001$ .

#### ***4.3.1.3. Apoptosis/Necrosis Assay***

Apoptosis/necrosis assay result of A549, BEAS-2b and MDA-MB-231 cells treated with 0.1, 0.5, 1.0 and 2.5 nM of naked 13 nm AuNPs and Glucose, Mannose, Lactose and Maltose Functionalized AuNPs were given in Figure 4.67. The positive control was 10 percent DMSO and it induced apoptosis for A549 and BEAS-2b cells while necrosis for MDA-MB-231 cells.

The 0.1-1.0 nM of naked AuNPs, all concentrations of AuNP-Glucose and AuNP-Mannose, 0.1-1.0 nM of AuNP-Lactose resulted 5-10 percent A549 cells to get to necrosis while no significant toxicity was seen in A549 cells exposed to AuNP-Maltose.

AuNP-Glucose, AuNP-Lactose and AuNP-Maltose conjugates resulted apoptosis in BEAS-2b cells whereas no significant cytotoxicity was analyzed in BEAS-2b cells treated with AuNP-Mannose. In addition, approximately, the live cell percentage of BEAS-2b cells in population reduced to 80 percent after incubation with AuNP-Lactose.

MDA-MB-231 cells were affected the most among all cell types since 30-40 percent MDA-MB-231 cells went to necrosis after exposure to AuNP-Glucose and AuNP-Mannose. Moreover, only 2.5 nM of AuNP-Maltose and AuNP-Lactose elicited cytotoxicity and approximately 1-2 percent more MDA-MB-231 cells were induced to go to necrosis.

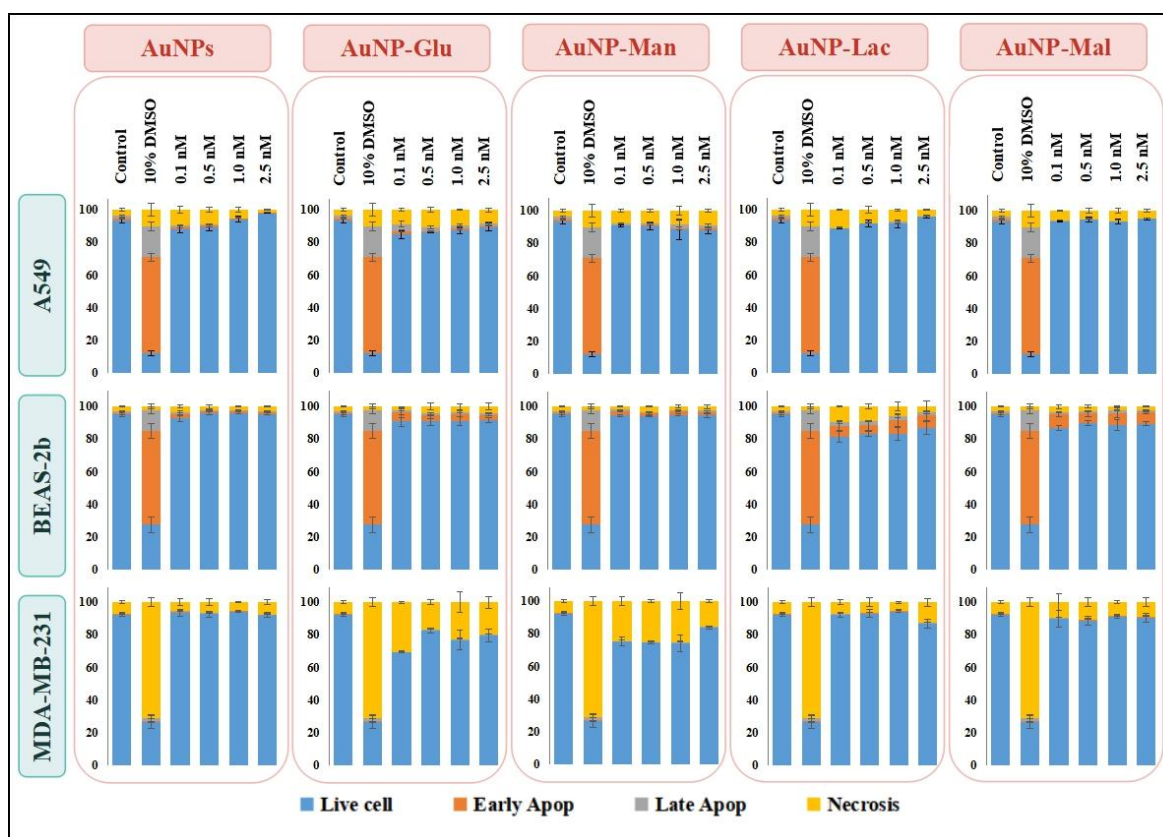


Figure 4.67. Apoptosis/necrosis assay result of A549, BEAS-2b and MDA-MB-231 cells treated with 0.1, 0.5, 1.0 and 2.5 nM of naked 13 nm AuNPs and Glucose, Mannose, Lactose and Maltose Functionalized AuNPs. The positive control was 10 percent DMSO.

#### 4.3.1.4. Clonogenic Assay

Clonogenic cell survival assay results of A549, BEAS-2b and MDA-MB-231 cells treated with increasing concentrations of either naked 13 nm AuNPs or Glucose, Mannose, Lactose and Maltose Functionalized AuNPs was seen in Figure 4.68. 10 percent DMSO was used as positive control and no colony formation was seen in all cell types in its presence.

A549 cells exposed to naked AuNPs and carbohydrate modified AuNPs can be referred as clonogenic since the seeded single A549 cells proliferated and produced a colony including a large number of cells to enable their integrity [231]. Based on results, A549 cells had

ability to survive in the conditions of 0.1-1.0 nM of either naked AuNPs or carbohydrate modified AuNPs exposure when compared to control untreated cells. Moreover, among carbohydrates modified AuNPs, there did not exist any significant differences about colony formation.

BEAS-2b cells treated with just 0.1 nM of all NPs were called as clonogenic as their colony formation ability was similar to negative control cells. Moreover, the cells exposed to other concentrations of AuNP-Lactose and AuNP-Maltose were visualized as unable to divide or able to go through one or two mitoses. On the other hand, BEAS-2b cells treated with higher doses of naked AuNPs, AuNP-Glucose and AuNP-Mannose could survive by forming colonies.

MDA-MB-231 cells treated with 0.1 nM of NPs were observed as clonogenic except the cells exposed to AuNP-Maltose. In addition, just 0.5-1.0 nM of NPs exposed cells could proliferate less when compared to negative control cells and the cells treated with 2.5 nM of NPs could not survive by forming colonies. It should be kept in mind that MDA-MB-231 cells exposed to AuNP-Maltose had the least ability to survive.

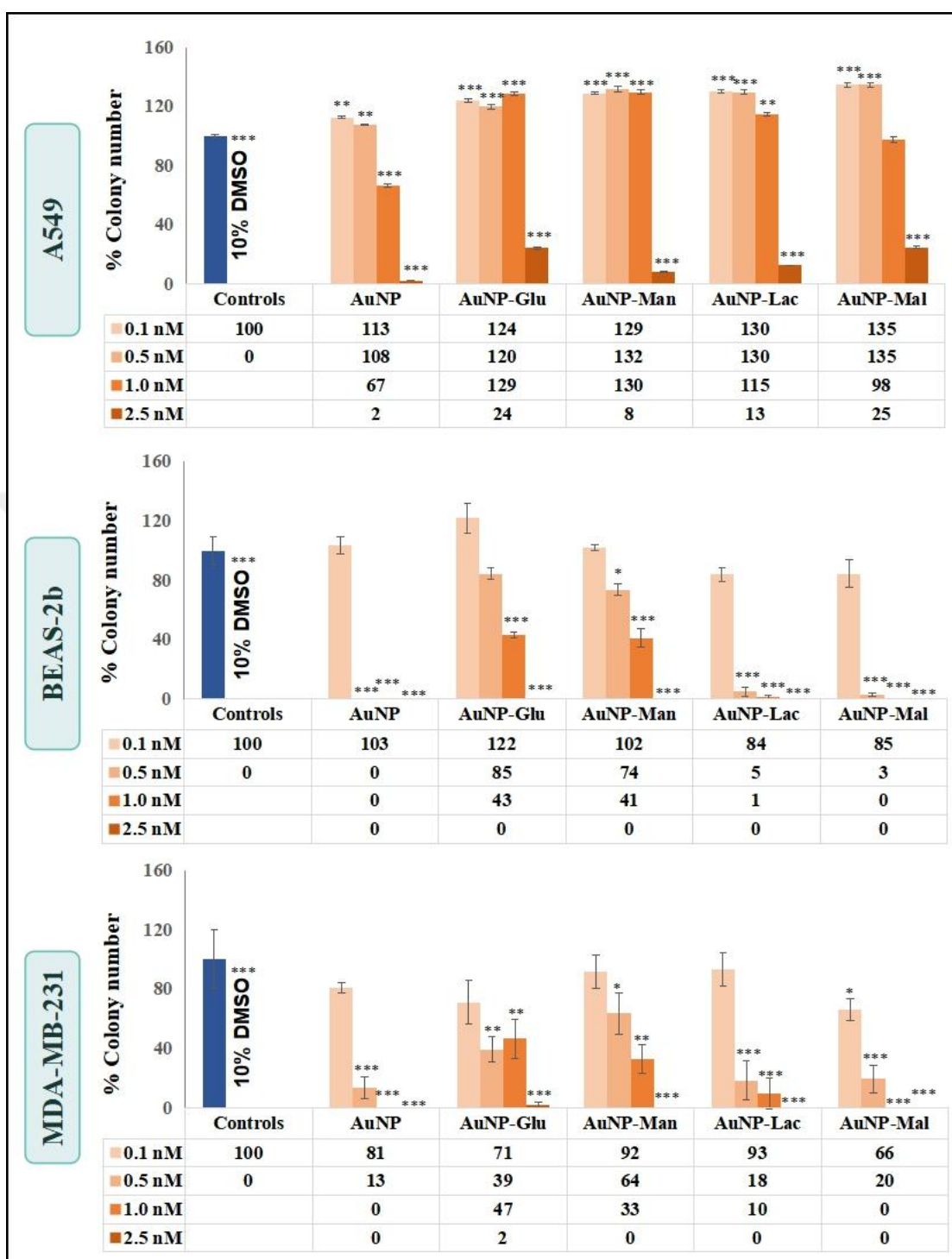


Figure 4.68. Clonogenic assay result of A549, BEAS-2b and MDA-MB-231 cells treated with 0.1, 0.5, 1.0 and 2.5 nM of naked 13 nm AuNPs and Glucose, Mannose, Lactose and Maltose Functionalized AuNPs. The positive control was 10 percent DMSO. Statistically significant changes compared to negative control cells were calculated by two-paired Student's t test, and marked with stars, \* for  $p \leq 0.05$ , \*\* for  $p \leq 0.01$  and \*\*\* for  $p \leq 0.001$ .



#### ***4.3.1.5. Cell Cycle Evaluation***

Cell cycle progression of A549, BEAS-2b and MDA-MB-231 cells treated with increasing concentrations of either naked 13 nm AuNPs or Glucose, Mannose, Lactose and Maltose functionalized AuNPs was seen in Figure 4.69. 0.1  $\mu$ M colchicine was used as positive control because it blocks cells at G2/M phase and it arrested 85-90 percent of all cell types at G2/M phase.

The cell cycle of A549 cells were blocked at G0/G1 phase after incubation with 0.1 nM of AuNP-Mannose and 2.5 nM of AuNP-Lactose whereas no significant change on cell cycle progression were investigated after treatment with naked AuNPs, AuNP-Glucose and AuNP-Maltose.

All carbohydrate functionalized AuNPs arrested approximately 90 percent of BEAS-2b cells at G0/G1 phase, except 0.1 nM concentration of AuNP-Maltose.

The 2.5 nM of AuNPs, 0.5-2.5 nM of AuNP-Glucose and 2.5 nM of AuNP-Mannose created G0/G1 phase arrest in MDA-MB-231 cells. In addition, the arrest caused by AuNP-Glucose was very dramatic since approximately 95 percent of MDA-MB-231 cells were blocked at G0/G1 phase.



Figure 4.69. Cell cycle progression of A549, BEAS-2b and MDA-MB-231 cells treated with 0.1, 0.5, 1.0 and 2.5 nM of naked 13 nm AuNPs and Glucose, Mannose, Lactose and Maltose Functionalized AuNPs. The positive control was 0.1 μM colchicine.

#### 4.3.1.6. Summary of Cellular Response to Carbohydrate Modified AuNPs

The cellular response to carbohydrate modified AuNPs was cell type, surface chemistry and NP concentration dependent. In other words, the cytotoxicity and the alteration on cell cycle progression created by same surface chemistry on NPs was various on three different cell types. Therefore, the cellular responses were discussed one by one:

A549 cells internalized AuNP-Lactose and AuNP-Maltose more among naked AuNPs and surface modified AuNPs. The cell viability of A549 cells were influenced quite few by Glucose, Mannose and Lactose modified AuNPs as 5-10 percent more A549 cells went to necrosis, however Maltose modified AuNPs created no significant cytotoxicity. Moreover, the result of clonogenic survival assay manifested that A549 cells could proliferate and

produce colonies upon NP exposure. Furthermore, the cell cycle of approximately 8 percent A549 cells were blocked at G0/G1 phase by 0.1 nM of AuNP-Mannose and 2.5 nM of AuNP-Lactose. Based on all results, it can be claimed that AuNPs conjugated with Glucose, Mannose, Lactose and Maltose could not create a severe cytotoxicity and cell cycle arrest on A549 cells. In addition, the orientation of -OH at second and fourth carbon on carbohydrates, which were Mannose (C2 epimer of Glucose, and Lactose (galactose, C4 epimer of Glucose) induced cytotoxicity and influenced significantly cell cycle progression of A549 cells.

BEAS-2b cells highly internalized all carbohydrate modified AuNPs, in particular Lactose and Maltose modified AuNPs. The Glucose, Lactose and Maltose coated AuNPs induced 3, 7 and 16 percent more BEAS-2b cells to go to apoptosis. Moreover, clonogenic survival assay results also showed that the cellular integrity of BEAS-2b cells were more affected by Lactose and Maltose conjugated AuNPs when compared to other carbohydrate coated AuNPs and these cells could not proliferate enough. However, these cytotoxicity clarified by two assays cannot be correlated with WST-1 assay result, which implied that no significant toxicity caused by naked AuNPs and AuNP-Carbohydrate conjugates was examined. Additionally, all carbohydrate conjugated AuNPs arrested approximately 90 percent BEAS-2b cells at G0/G1 phase excluding 0.1 nM of AuNP-Maltose. As a conclusion, the cell viability of BEAS-2b cells decreased after treatment with AuNP-Lactose and AuNP-Maltose and the cell cycle progression of BEAS-2b cells were dramatically blocked at G0/G1 phase because of high uptake of the conjugates by BEAS-2b cells. What is more, AuNPs conjugated with disaccharides, which were Maltose (double Glucose) and Lactose (Glucose and galactose) resulted more significant response in BEAS-2b cells when compared to others and it can be told that the free saccharides on Maltose and Lactose, which were C4 epimers, played an important role to create these mentioned cellular responses.

MDA-MB-231 cells internalized only naked AuNPs when compared to negative control cells. To discuss the cytotoxicity of MDA-MB-231 cells treated with either naked AuNPs

or carbohydrate modified AuNPs, three applied cytotoxicity assays less correlated with each other as WST-1 assay result showed that the naked AuNPs and AuNP-Glucose induced concentration dependent cytotoxicity, Apoptosis/necrosis assay result indicated that Glucose and Mannose coated AuNPs led 30-40 percent more MDA-MB-231 cells to go to necrosis, and clonogenic survival assay result demonstrated that the survival ability by forming colonies of MDA-MB-231 cells treated with AuNP-Carbohydrate conjugates were less and those of treated with AuNP-Maltose had no ability survive. In the light of all cytotoxicity assay results, it can summarized that Glucose and Mannose covered AuNPs were pioneer in the cytotoxicity of MDA-MB-231 cells. Moreover, the cell cycle progression of MDA-MB-231 cells exposed to AuNP-Glucose were dramatically arrested at G0/G1 phase, approximately the cell cycle of 95 percent MDA-MB-231 cells were influenced by AuNP-Glucose. Consequently, the cellular response of MDA-MB-231 cells to Glucose functionalized AuNPs was noteworthy among other carbohydrate modified AuNPs.

#### **4.3.2. Cellular Response to AuNPs Modified with RGD Sequenced Peptides**

Since the number of peptides used to modify AuNP surfaces were too much to test in the same experiment, they were divided into four group according to rich amino acid type in their sequences. The first group was selected as RGD sequenced peptides, which were Pep1 (NH<sub>2</sub>-DGRC-COOH) and Pep8 (NH<sub>2</sub>-CRGD-COOH). These peptides had same sequence, but in reverse order. After conjugation of AuNPs with these peptides, the free ends would be different, as seen Figure 4.70.

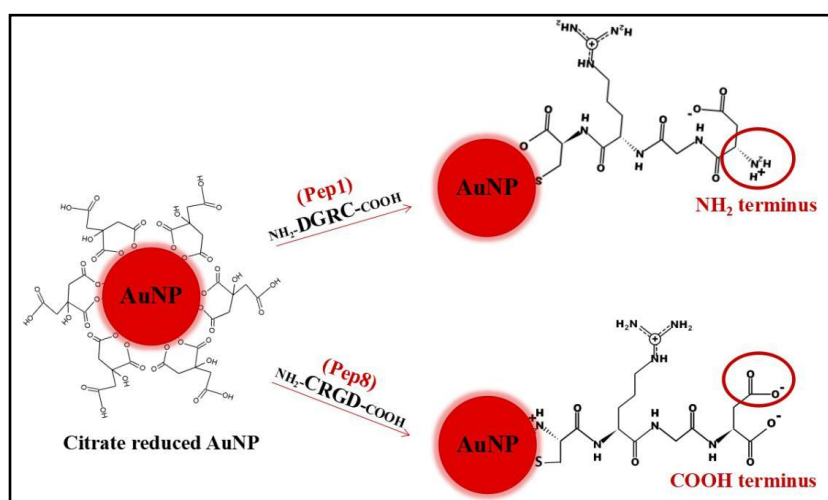


Figure 4.70. Subtle differences on AuNP surface after functionalization with Pep1 and Pep8.

#### 4.3.2.1. Uptake Studies

SSC graphs of A549, BEAS-2b and MDA-MB-231 cells treated with 0.1, 0.5, 1.0 and 2.5 nM naked 13 nm AuNPs, AuNP-Pep1 (AuNP-CRGD-NH<sub>2</sub>) and AuNP-Pep8 (AuNP-CRGD-COOH) conjugates was given in Figure 4.71. A549, BEAS-2b and MDA-MB-231 cells showed 6, 8 and 11 percent granulation in negative condition, respectively. The cellular uptake rates of NPs were cell dependent and type and concentration of NPs dependent.

A549 cells significantly internalized all concentrations of naked AuNPs and AuNP-Pep1 while just high concentrations of AuNP-Pep8. The order of NP uptake can be enumerated as AuNP-Pep1 > naked AuNPs > AuNP-Pep8. Consequently, among these three NPs, AuNPs having -NH<sub>2</sub> terminus penetrated the most into A549 cells.

BEAS-2b cells internalized just AuNP-Pep1 and AuNP-Pep8 conjugates. The most cellular uptake was investigated in 2.5 nM of AuNP-Pep8. It can be concluded that the cellular uptake of RGD sequenced peptides modified AuNPs were high in BEAS-2b cells.

MDA-MB-231 cells internalized just AuNP-Pep1 and AuNP-Pep8 conjugates like BEAS-2b cells, however the cellular uptake of AuNP-Pep1 was the most. To conclude, AuNPs having -NH<sub>2</sub> terminus were uptaken more by MDA-MB-231 cells.

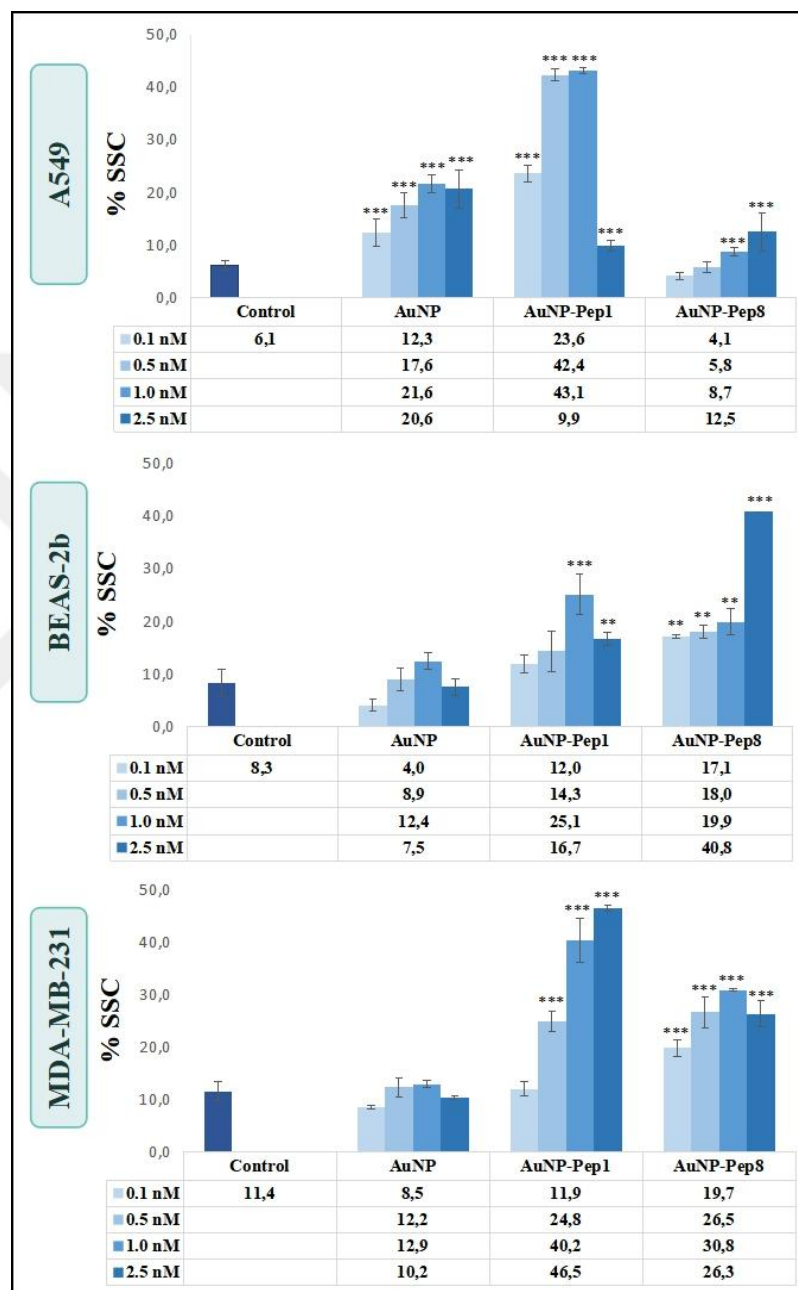


Figure 4.71. SSC graphs of A549, BEAS-2b and MDA-MB-231 cells treated with 0.1, 0.5, 1.0 and 2.5 nM of naked 13 nm AuNPs and Pep1 and Pep8 Functionalized AuNPs. Statistically significant changes compared to negative control cells were calculated by two-paired Student's t test, and marked with stars, \* for  $p \leq 0.05$ , \*\* for  $p \leq 0.01$  and \*\*\* for  $p \leq 0.001$ .

#### ***4.3.2.2. WST-1 Cell Proliferation Assay***

WST-1 Cell Proliferation results of A549, BEAS-2b and MDA-MB-231 cells treated with 0.1, 0.5, 1.0 and 2.5 nM of naked 13 nm AuNPs, AuNP-Pep1 and AuNP-Pep8 conjugates was given in Figure 4.72. 10 percent DMSO was used as positive control and it decreased the cell viability of all cell types up to 5-10 percent.

The naked AuNPs created no toxicity effect to A549 cells while AuNP-Pep1 conjugates at high concentrations significantly increased cell viability and AuNP-Pep8 at low concentrations led to decrease cell viability approximately up to 90 percent.

The cell viability of BEAS-2b cells was influenced by all NPs. In addition, neither naked AuNPs nor AuNPs modified with RGD sequenced peptides were significantly influenced the cell viability of BEAS-2b cells.

The cell viability of MDA-MB-231 cells were affected by naked AuNPs and AuNP-Pep8. It can be speculated that high concentrations of naked AuNPs and AuNP-Pep8 conjugates increased cell viability of MDA-MB-231 cells whereas AuNP-Pep1 did not affect it.

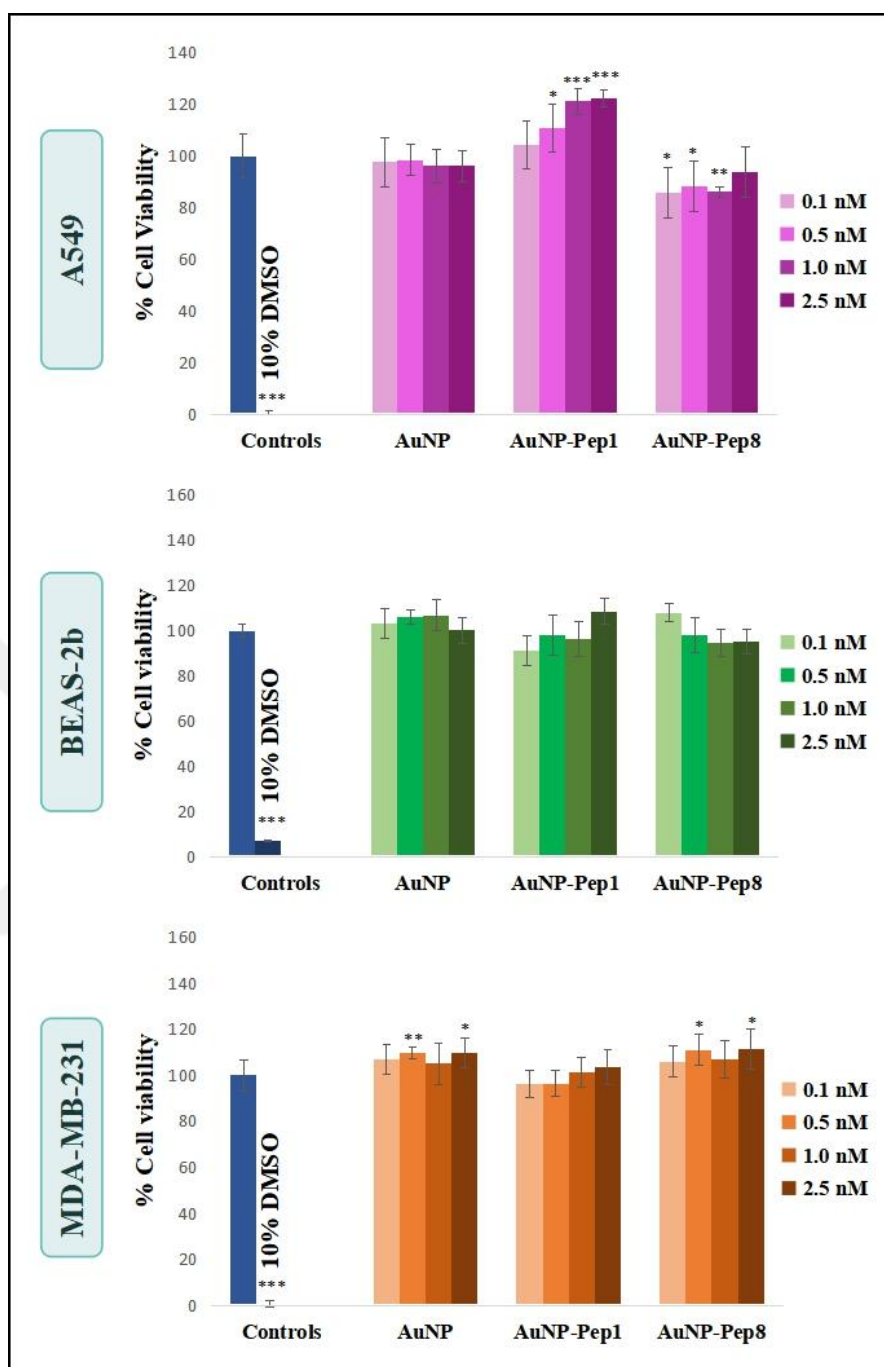


Figure 4.72. WST-1 cell proliferation assay results of A549, BEAS-2b and MDA-MB-231 cells treated with 0.1, 0.5, 1.0 and 2.5 nM of naked 13 nm AuNPs and Pep1 and Pep8 Functionalized AuNPs. Positive control was 10 percent DMSO. Statistically significant changes compared to negative control cells were calculated by two-paired Student's t test, and marked with stars, \* for  $p \leq 0.05$ , \*\* for  $p \leq 0.01$  and \*\*\* for  $p \leq 0.001$ .



#### ***4.3.2.3. Apoptosis/Necrosis Assay***

Apoptosis/necrosis assay results of A549, BEAS-2b and MDA-MB-231 cells treated with 0.1, 0.5, 1.0 and 2.5 nM of naked 13 nm AuNPs, AuNP-Pep1 and AuNP-Pep8 conjugates was given in Figure 4.73. 10 percent DMSO was utilized as positive control and induced A549 cells to early apoptosis, BEAS-2b cells to late apoptosis and MDA-MB-231 cells to necrosis.

The cell viability of A549 cells were affected by naked AuNPs and AuNP-Pep1. The naked AuNPs created cytotoxicity in A549 cells in parallel to decrease of their exposed concentration to cells as the cell viability reduced up to 50 percent after incubation with 1.0 nM. On the other side, AuNP-Pep1 conjugates caused cytotoxicity in A549 cells with respect to increment of their exposed concentration as the live cells decreased to 30 percent after treatment with 2.5 nM dose. Additionally, AuNP-Pep8 conjugates created no cytotoxicity in A549 cells.

By considering BEAS-2b cells, either naked AuNPs or AuNPs coated with RGD sequenced peptides led to a significant cytotoxicity.

Just 2.5 nM of AuNP-Pep1 conjugates exposure induced cytotoxicity in MDA-MB-231 cells while no important cytotoxic affect was seen in the case of treatment with naked AuNPs and AuNP-Pep8 conjugates.

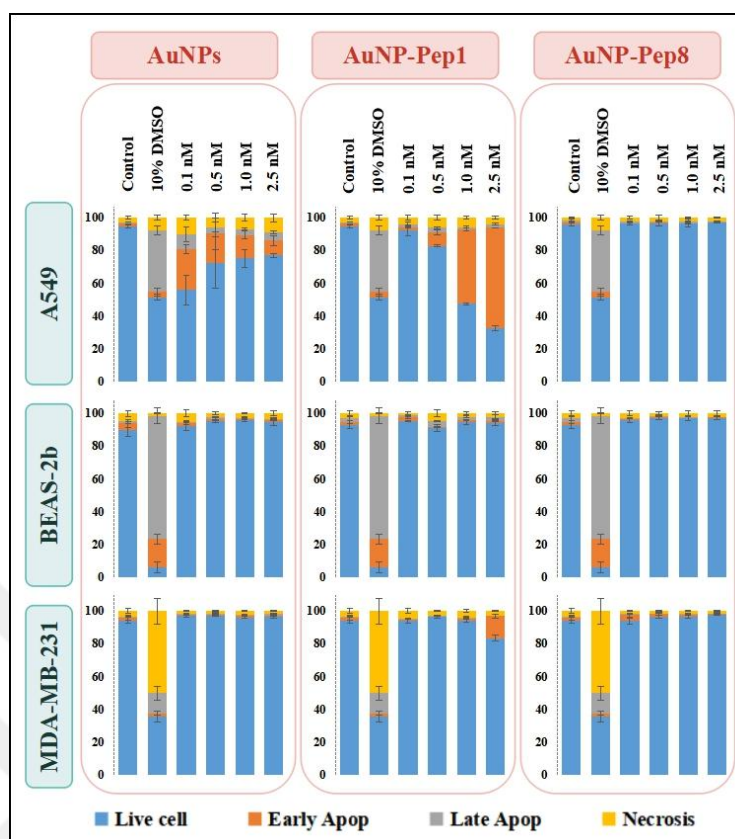


Figure 4.73. Apoptosis/Necrosis assay results of A549, BEAS-2b and MDA-MB-231 cells treated with 0.1, 0.5, 1.0 and 2.5 nM of naked 13 nm AuNPs and Pep1 and Pep8 Functionalized AuNPs. Positive control was 10 percent DMSO.

#### 4.3.2.4. Clonogenic Assay

Clonogenic assay results of A549, BEAS-2b and MDA-MB-231 cells treated with 0.1, 0.5, 1.0 and 2.5 nM of naked 13 nm AuNPs, AuNP-Pep1 and AuNP-Pep8 conjugates was given in Figure 4.74. 10 percent DMSO was utilized as positive control and the presence of DMSO in the medium resulted in no colony formation by all cell types.

After treatment with naked AuNPs, the formed colony number of A549 cells decreased, however they were called as clonogenic since they underwent more than 2-3 mitoses. When discussed A549 cells exposed to AuNPs modified RGD sequenced peptides, the cells could not survive in the presence of Pep1 whereas those of treated with Pep8 created more colonies than negative control.

BEAS-2b cells exposed to naked AuNPs could form significant colonies at only 0.1 nM concentration. Additionally, BEAS-2b cells treated with Pep1 up to 1.0 nM dose can be named as clonogenic since the single BEAS-2b cells generated colonies to survive in the mentioned condition. Nevertheless, BEAS-2b cells were investigated as unable to divide after treatment with Pep8.

MDA-MB-231 cells exposed to 0.1 nM naked AuNPs generated colonies while its other concentration decreased the cell proliferation. Moreover, Pep1 treated MDA-MB-231 cells formed more colonies to survive when compared to Pep8 treated cells and so Pep1 treated cells were called as clonogenic.

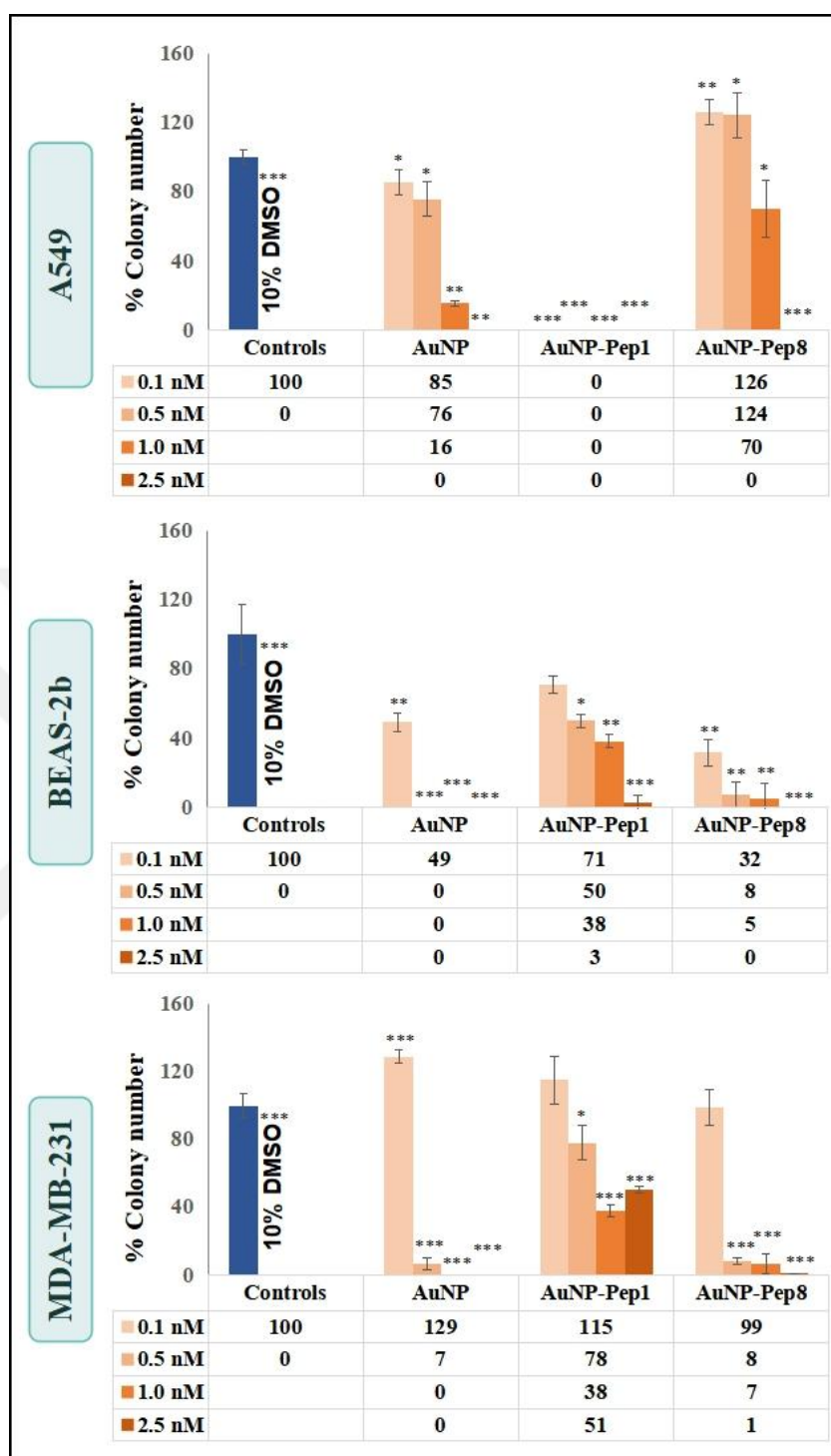


Figure 4.74. Clonogenic assay results of A549, BEAS-2b and MDA-MB-231 cells treated with 0.1, 0.5, 1.0 and 2.5 nM of naked 13 nm AuNPs and Pep1 and Pep8 Functionalized AuNPs. Positive control was 10 percent DMSO. Statistically significant changes compared to negative control cells were calculated by two-paired Student's t test, and marked with stars, \* for  $p \leq 0.05$ , \*\* for  $p \leq 0.01$  and \*\*\* for  $p \leq 0.001$ .

#### ***4.3.2.5. Cell Cycle Progression***

Cell cycle progression of A549, BEAS-2b and MDA-MB-231 cells treated with 0.1, 0.5, 1.0 and 2.5 nM of naked 13 nm AuNPs and AuNP-Pep1 and AuNP-Pep8 was seen in Figure 4.75. 0.1  $\mu$ M colchicine was used as positive control because it blocks cells at G2/M phase and it arrested 85-90 percent of all cell types at G2/M phase.

The cell cycle of A549 cells were significantly affected by naked AuNPs and AuNP-Pep1. The upper doses of naked AuNPs led more 10 percent A549 cells to arrest at G0/G1 phase. However, the most arrest on A549 cell cycle was investigated after treatment with 0.5 nM concentrations of AuNP-Pep1 conjugate as approximately 20 percent A549 cells treated with its 2.5 nM dose were blocked at G0/G1 phase. No remarkable change was demonstrated in AuNP-Pep8 exposed A549 cells.

The cell cycle of BEAS-2b cells were influenced by only AuNPs conjugated with RGD sequenced peptides. The concentrations higher than 0.5 nM of AuNP conjugates created a severe cell cycle arrest at G0/G1 phase in BEAS-2b cells.

AuNP-Pep1 resulted in an important cell cycle arrest at G0/G1 phase in MDA-MB-231 cells treated with the concentrations higher than 0.5 nM. On the other hand, no change was examined on the cell cycle progression of MDA-MB-231 cells exposed to either naked AuNPs or AuNP-Pep8 conjugates.

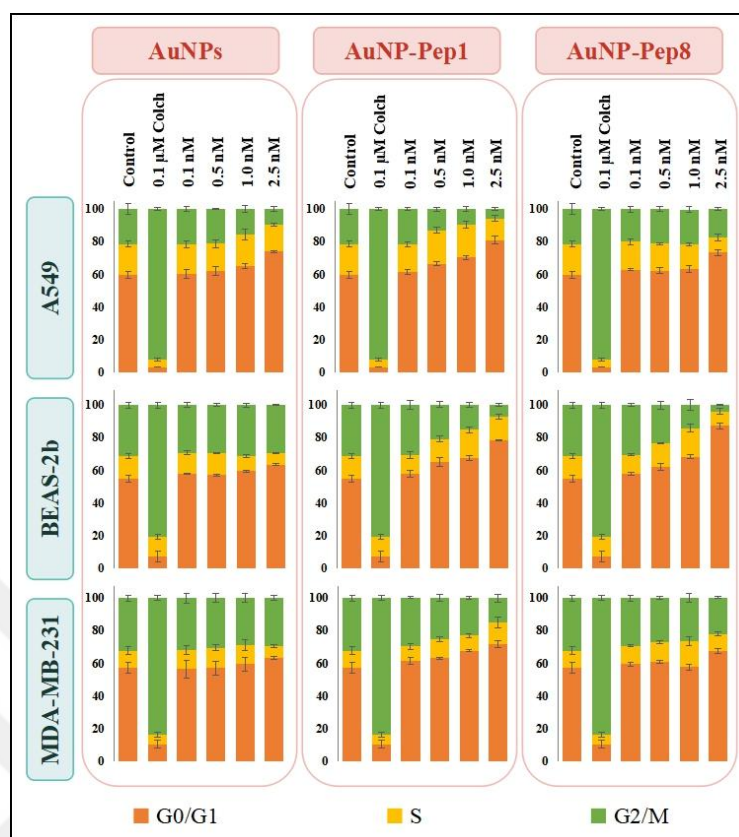


Figure 4.75. Cell cycle progression of A549, BEAS-2b and MDA-MB-231 cells treated with 0.1, 0.5, 1.0 and 2.5 nM of naked 13 nm AuNPs and Pep1 and Pep8 Functionalized AuNPs. Positive control was 0.1  $\mu$ M colchicine.

#### 4.3.2.6. Summary of Cellular Response to AuNPs Modified with RGD Sequenced Peptides

The cellular response to AuNPs modified with RGD sequenced peptides was dependent to the cell type, surface chemistry of NPs and NP exposure concentration. Therefore, the cytotoxicity and the changes on cell cycle process of three cell lines exposed to either naked AuNPs or AuNPs conjugated with RGD sequenced peptides were summarized one by one:

A549 cells significantly internalized either naked AuNPs and AuNP conjugated with RGD sequenced peptides. When quantitatively compared, AuNP-Pep1 penetrated the most, then naked AuNPs and lastly AuNP-Pep8. Furthermore, naked AuNPs and AuNP-Pep1 created

a severe NP concentration dependent cytotoxicity in A549 cells. The low concentrations of naked AuNPs created high cytotoxicity while high concentrations induced high cytotoxicity in A549 cells. The live cell percentage decreased up to 50 percent after treatment with 0.1 nM of naked AuNPs and reduced to 30 percent after treatment with 2.5 nM of AuNP-Pep1. Nevertheless, AuNP-Pep8 induced no significant cytotoxicity in A549 cells. These results were correlated not only clonogenic assay but also cell cycle evaluation. The cell cycle of A549 cells exposed to 2.5 nM of AuNPs and 1.0-2.5 nM of AuNP-Pep1 was arrested at G0/G1 phase. The treatment with 2.5 nM of naked AuNPs induced 10 percent more A549 cells to arrest at G0/G1 phase while 1.0-2.5 nM of AuNP-Pep1 exposure resulted to block 20 percent more A549 cells at G0/G1 phase. On the other hand, no significant alteration was investigated in cell cycle of A549 cells treated with AuNP-Pep8. Consequently, among these three AuNPs, AuNP-Pep1 penetrated the most into A549 cells and these results highlighted that this highly internalized naked AuNPs and AuNP-CRGD having -NH<sub>2</sub> terminus conjugate created a significant concentration dependent cytotoxicity and cell cycle arrest in A549 cells.

BEAS-2b cells only significantly internalized AuNPs modified with RGD sequenced peptides. Additionally, the most uptaken NPs by BEAS-2b cells were AuNP-Pep8. When considered the cytotoxicity of BEAS-2b cells, no significant cytotoxicity after treatment with naked AuNPs and AuNP conjugates was detected. On the other hand, the clonogenic assay results demonstrated that either naked AuNPs or AuNP-CRGD conjugates affected reproductive integrity of BEAS-2b cells since the single BEAS-2b cells could proliferate and produce colonies under NP treatment. What's more, the cell cycle arrest at G0/G1 phase was evaluated in BEAS-2b cells exposed to 0.5-2.5 nM of AuNP-Pep1 and AuNP-Pep8. This mentioned cell cycle arrest result in BEAS-2b cells was also correlated with clonogenic assay. As a result, AuNP-Pep1, having COOH terminus, were internalized more, however this phenomena did not change the cellular response of BEAS-2b cells.

MDA-MB-231 cells highly internalized AuNP-Pep1 and AuNP-Pep8, but in particularly AuNP-Pep1 like other cancer cell line A549. The cell viability and cell cycle progression

of MDA-MB-231 cells were affected by only AuNP-Pep1 conjugate. After treatment with 2.5 nM of AuNP-Pep1, the cell viability of MDA-MB-231 cells decreased to approximately 80 percent. The reason behind this toxicity can be because of high uptake of 2.5 nM of AuNP-Pep1 by MDA-MB-231 cells. Moreover, the cell cycle of MDA-MB-231 cells were arrested at G0/G1 phase upon exposure to the concentration higher than 0.5 nM of AuNP-Pep1. On the other hand, no significant change on cell viability and cell cycle progression was evaluated in MDA-MB-231 cells treated with either naked AuNPs or AuNP-Pep8. As a conclusion, MDA-MB-231 cells tend to internalize AuNP-Pep1 (AuNP-CRGD-NH<sub>2</sub>) more and so AuNPs having -NH<sub>2</sub> terminus created cytotoxicity and blocked MDA-MB-231 cells at G0/G1 phase.

#### **4.3.3. Cellular Response to AuNPs Modified Glycine Rich Peptides**

Due to create subtle differences on AuNP surfaces, AuNPs were conjugated with four glycine rich peptides, as second peptide group to be tested. These glycine rich peptides were designed as Pep2 (NH<sub>2</sub>-GGGC-COOH), Pep5 (NH<sub>2</sub>-DGRGGGC-COOH), Pep9 (NH<sub>2</sub>-CGGG-COOH) and Pep12 (NH<sub>2</sub>-CGGGRGD-COOH). Half of these neutrally charged peptides had same four amino acid length sequence, but in reverse order. The other seven amino acid length peptides had the same glycine amino acid rich sequence with addition of RGD sequence, again in reverse order. These small differences on AuNP surfaces after modification with these four glycine rich peptides were shown in Figure 4.76.



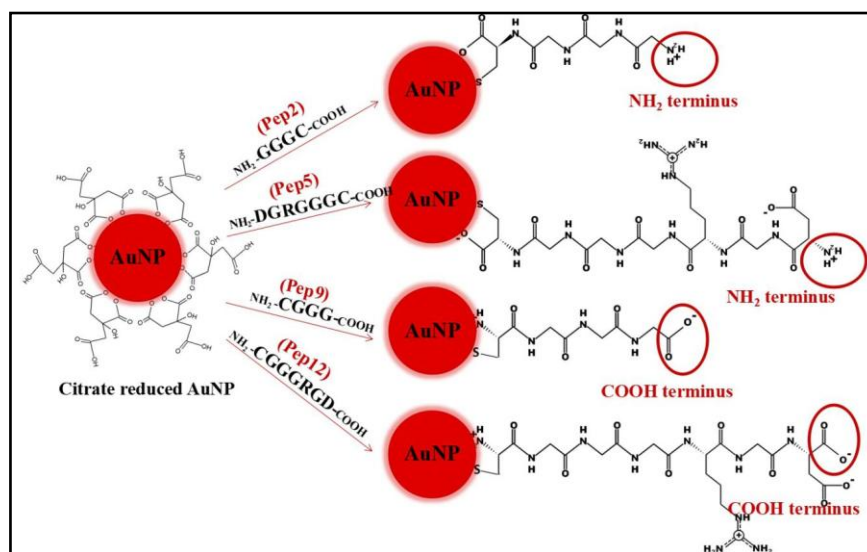


Figure 4.76. Subtle differences on AuNP surface after functionalization with Pep2, Pep5, Pep9 and Pep12.

#### 4.3.3.1. Uptake Studies

SSC graphs of A549, BEAS-2b and MDA-MB-231 cells treated with 0.1, 0.5, 1.0 and 2.5 nM naked 13 nm AuNPs, AuNP-Pep2, AuNP-Pep5, AuNP-Pep9 and AuNP-Pep12 conjugates was given in Figure 4.77. A549, BEAS-2b and MDA-MB-231 cells showed 6, 8 and 11 percent granulation in negative condition, respectively.

A549 cells internalized naked AuNPs in high amount when compared to AuNPs conjugated with glycine rich peptides. The cellular uptake of all AuNP conjugates were remarkable at high concentrations in A549 cells.

BEAS-2b cells highly internalized AuNP-Pep5, AuNP-Pep9 and AuNP-Pep12 conjugates at high concentrations, but no significant granulation in BEAS-2b cells caused by naked AuNPs and AuNP-Pep2 conjugates was detected when compared to negative cells.

MDA-MB-231 cells internalized AuNP-Pep5, AuNP-Pep9 and AuNP-Pep12 conjugates at all doses, however, no significant granulation was seen after treatment with naked AuNPs and AuNP-Pep2 conjugates.

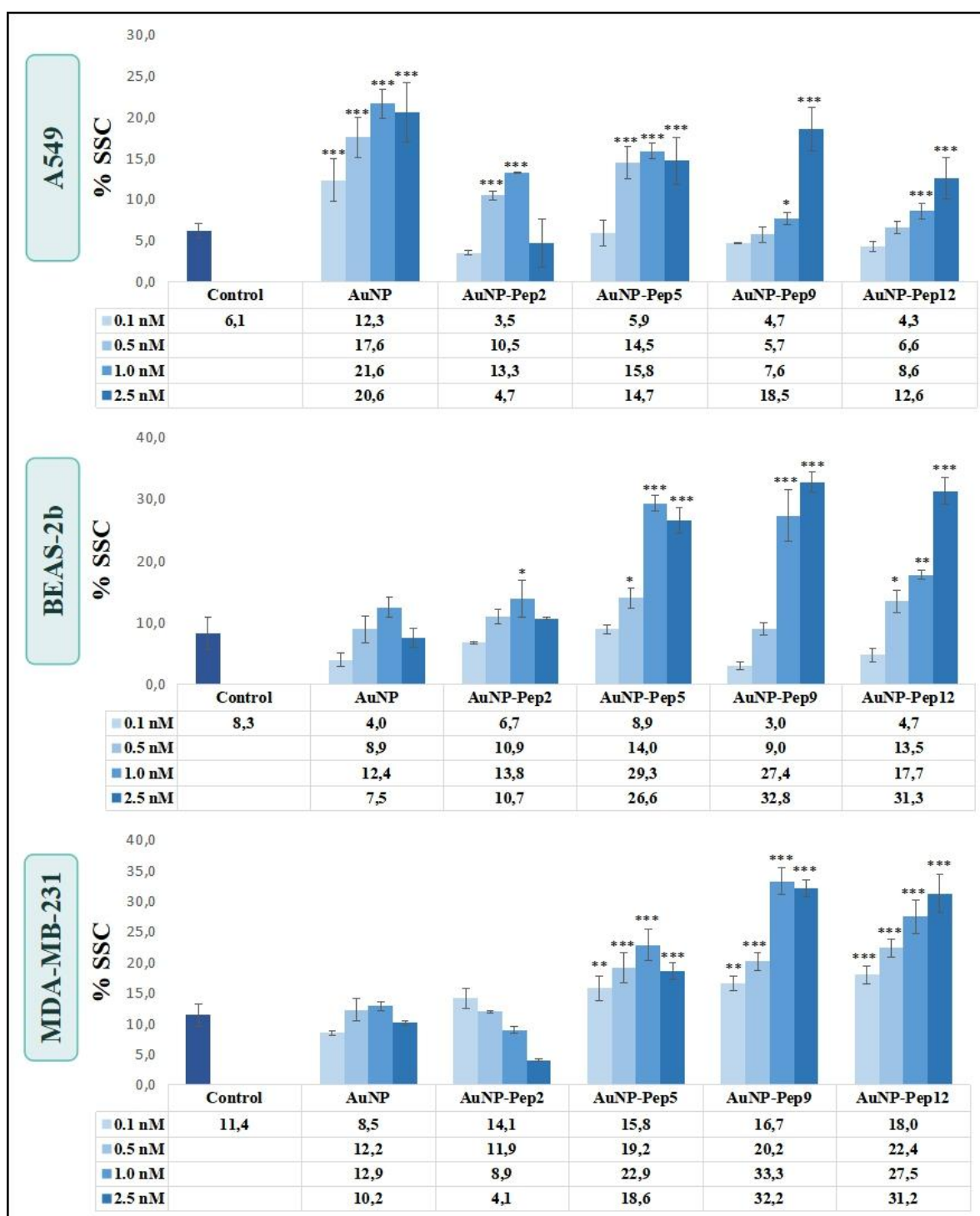


Figure 4.77. SSC graphs of A549, BEAS-2b and MDA-MB-231 cells treated with 0.1, 0.5, 1.0 and 2.5 nM of naked 13 nm AuNPs and Pep2, Pep5, Pep9 and Pep12 Functionalized AuNPs. Statistically significant changes compared to negative control cells were calculated by two-paired Student's t test, and marked with stars, \* for  $p \leq 0.05$ , \*\* for  $p \leq 0.01$  and \*\*\* for  $p \leq 0.001$ .

#### **4.3.3.2. WST-1 Cell Proliferation Assay**

WST-1 cell proliferation assay results of A549, BEAS-2b and MDA-MB-231 cells treated with 0.1, 0.5, 1.0 and 2.5 nM of naked 13 nm AuNPs, AuNP-Pep2, AuNP-Pep5, AuNP-Pep9 and AuNP-Pep12 conjugates was shown in Figure 4.78. The positive control was 10 percent DMSO and it decreased the cell viability of all cell lines up to 5-10 percent.

The cell viability of A549 cells increased after treatment with high doses of AuNP-Pep2 and all doses of AuNP-Pep5 and AuNP-Pep12 conjugates. Nevertheless, no significant alteration on the cell viability of A549 cells treated with naked AuNPs and AuNP-Pep9 was investigated.

The cell viability of BEAS-2b cells risen up after treatment with the high concentrations of AuNP-Pep2 and AuNP-Pep9 and the low concentrations of AuNP-Pep5. In addition, 0.1-0.5 nM of AuNP-Pep5 created cytotoxicity to BEAS-2b cells and the cell viability decreased to 80 percent.

It is noteworthy that MDA-MB-231 cells were more viable after incubation with 0.5-2.5 nM of naked AuNPs, 2.5 nM of AuNP-Pep5 and AuNP-Pep9 and 1.0-2.5 nM of AuNP-Pep12. Only 0.1 nM of AuNP-Pep9 conjugates created a few cytotoxicity in MDA-MB-231 cells.

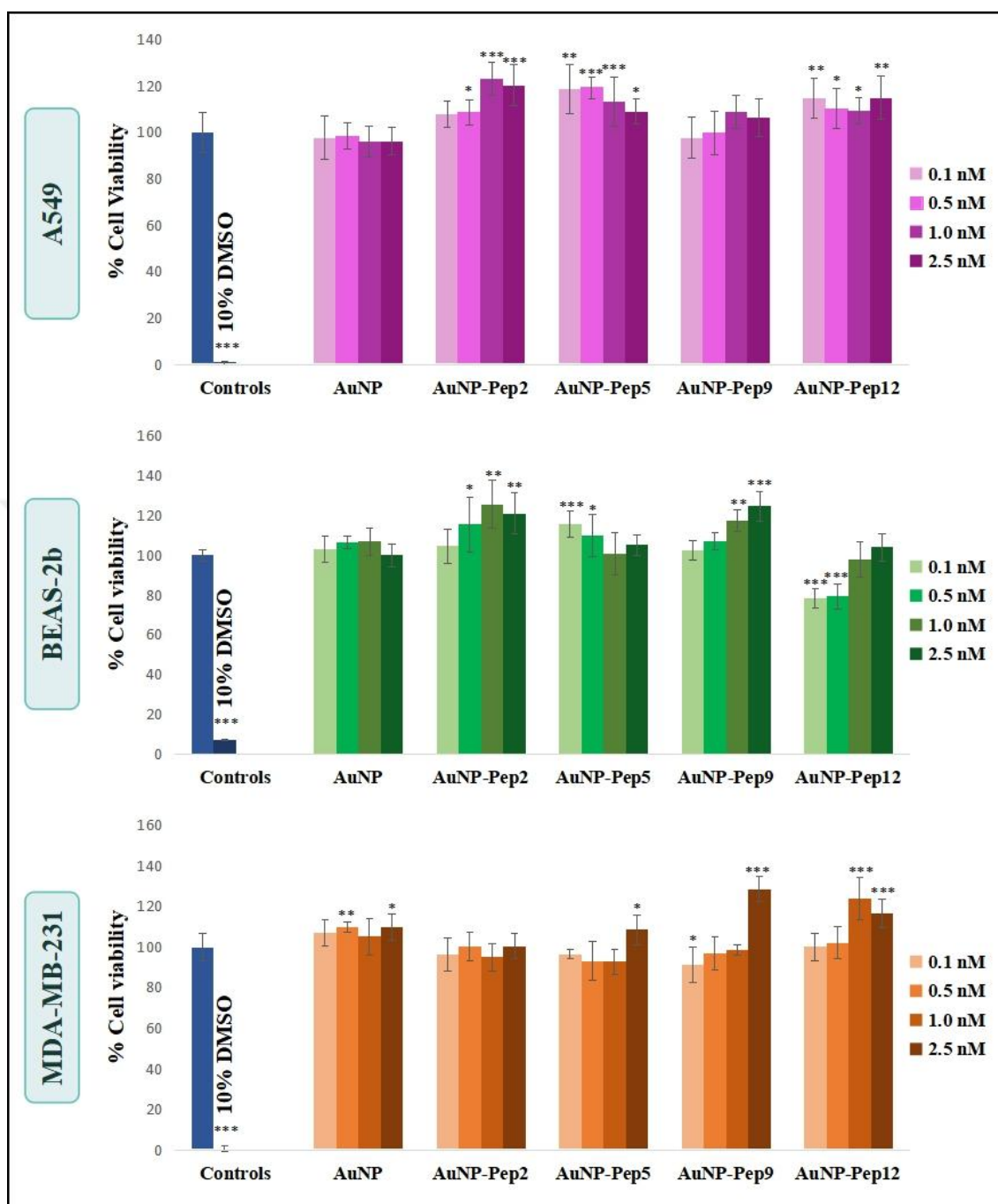


Figure 4.78. WST-1 cell proliferation assay results of A549, BEAS-2b and MDA-MB-231 cells treated with 0.1, 0.5, 1.0 and 2.5 nM of naked 13 nm AuNPs and Pep2, Pep5, Pep9 and Pep12 Functionalized AuNPs. Positive control was 10 percent DMSO. Statistically significant changes compared to negative control cells were calculated by two-paired Student's t test, and marked with stars, \* for  $p \leq 0.05$ , \*\* for  $p \leq 0.01$  and \*\*\* for  $p \leq 0.001$ .

#### ***4.3.3.3. Apoptosis/Necrosis Assay***

Apoptosis/Necrosis assay results of A549, BEAS-2b and MDA-MB-231 cells treated with 0.1, 0.5, 1.0 and 2.5 nM of naked 13 nm AuNPs, AuNP-Pep2, AuNP-Pep5, AuNP-Pep9 and AuNP-Pep12 conjugates was seen in Figure 4.79. 10 percent DMSO was used as positive control and it induced A549 cells to early apoptosis, BEAS-2b cells to late apoptosis and MDA-MB-231 cells to necrosis.

The cell viability of A549 cells were influenced by the naked AuNPs, AuNP-Pep2 and AuNP-Pep5. The cytotoxicity caused by naked AuNPs were dramatic and the lower concentrations created higher cytotoxicity. Additionally, AuNP-Pep2 and AuNP-Pep5 conjugates led approximately more 5-8 percent A549 cells to go to necrosis.

AuNP-Pep5 created a dramatic cytotoxicity in BEAS-2b cells. Along with increasing concentration of AuNP-Pep5, the cell viability reduced up to 5 percent. In addition, 0.1-1.0 nM of AuNP-Pep12 showed a less toxicity by induction of necrosis and decreased the viability up to approximately 90 percent in BEAS-2b cells.

The cell viability of MDA-MB-231 cells was affected by AuNP-Pep2, AuNP-Pep5 and AuNP-Pep9. Only 2.5 nM dose of AuNP-Pep2 and AuNP-Pep5 induced apoptosis in MDA-MB-231 cells and the cell viability decreased to approximately 75 and 55 percent, respectively. Additionally, the lowest concentration, 0.1 nM, of AuNP-Pep9 induced apoptosis in MDA-MB-231 cells.

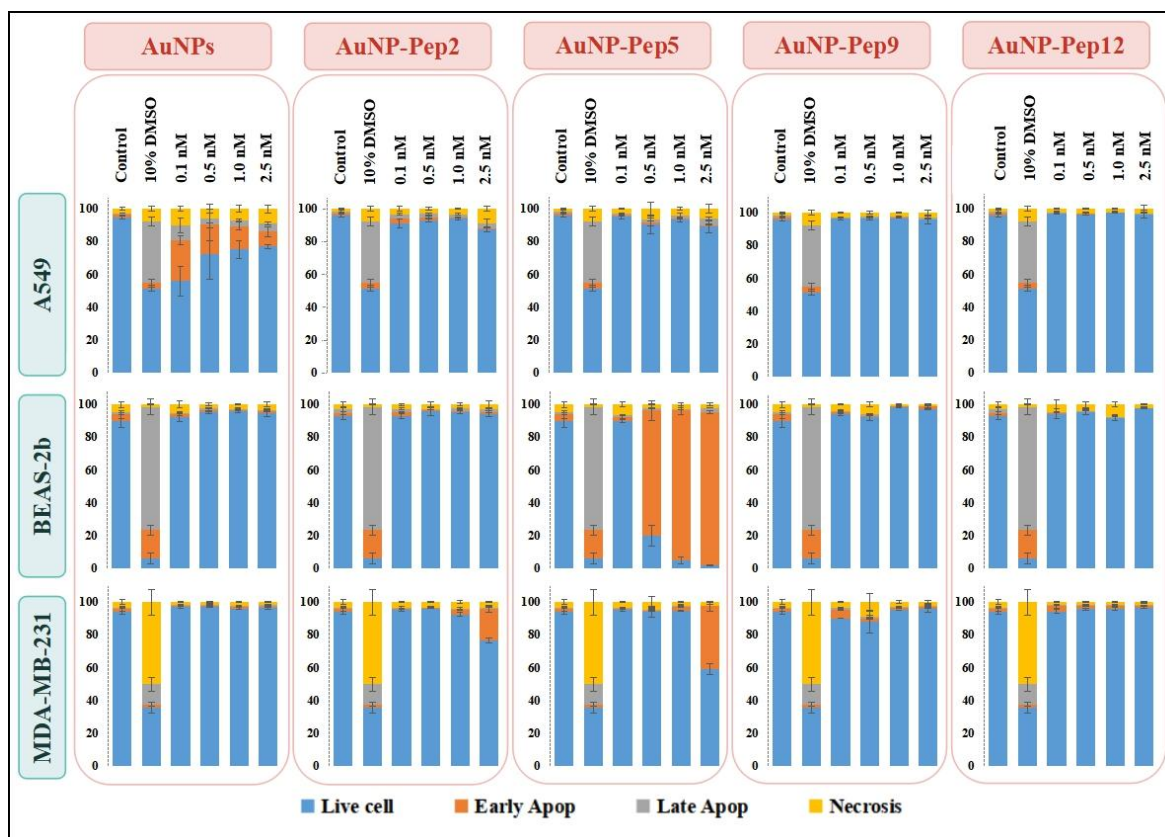


Figure 4.79. Apoptosis/Necrosis assay results of A549, BEAS-2b and MDA-MB-231 cells treated with 0.1, 0.5, 1.0 and 2.5 nM of naked 13 nm AuNPs and Pep2, Pep5, Pep9 and Pep12 Functionalized AuNPs. Positive control was 10 percent DMSO.

#### 4.3.3.4. Clonogenic Assay

Clonogenic cell survival assay results of A549, BEAS-2b and MDA-MB-231 cells treated with 0.1, 0.5, 1.0 and 2.5 nM of naked 13 nm AuNPs, AuNP-Pep2, AuNP-Pep5, AuNP-Pep9 and AuNP-Pep12 conjugates was shown in Figure 4.80. The positive control was 10 percent DMSO and no colony was formed in all cell types after its treatment.

A549 could survive in the incubation with each AuNPs, but generated less colonies than negative control. The survival ability by forming colony decreased from naked AuNPs to AuNP-Pep12 conjugate. Only A549 cells treated with 0.1 nM of AuNPs can be called as clonogenic.

BEAS-2b cells treated with AuNP-Pep5, AuNP-Pep9 and AuNP-Pep12 were called as clonogenic so that the cells proliferated upon their exposure. In addition, BEAS-2b cells treated with AuNP-Pep5 formed more colonies than negative control condition. On the other hand, the survival ability of BEAS-2b cells exposed to naked AuNPs and AuNP-Pep2 was less.

MDA-MB-231 cells treated with 0.1 nM of naked AuNPs, AuNP-Pep2 and AuNP-Pep9 were clonogenic since they generated similar number of colonies in comparison to untreated control. On the other hand, MDA-MB-231 cells exposed to higher concentrations of either naked AuNPs or all AuNPs modified with glycine rich peptides could not form enough colonies to survive, especially the cells treated with AuNP-Pep9 and AuNP-Pep12.

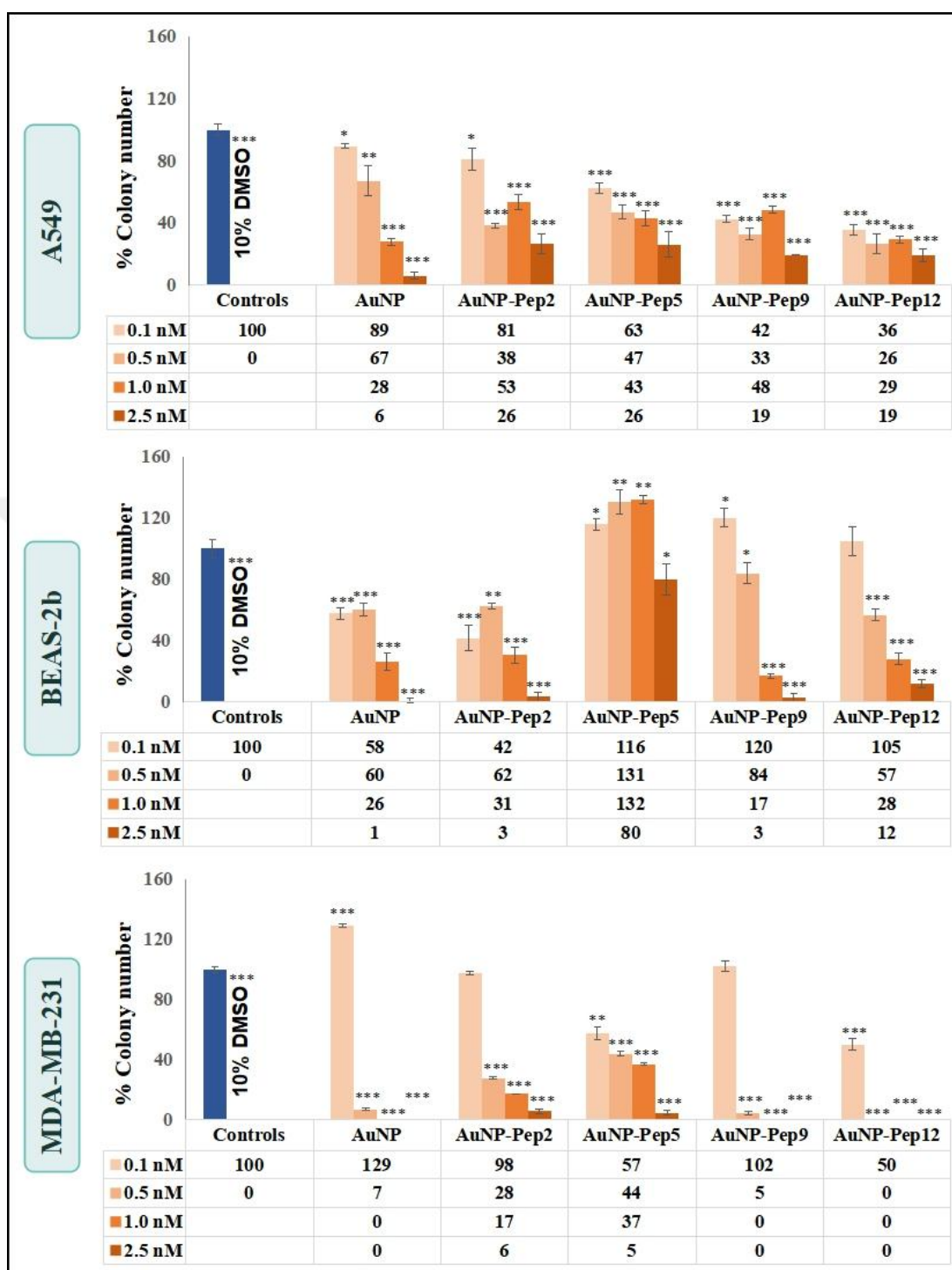


Figure 4.80. Clonogenic assay results of A549, BEAS-2b and MDA-MB-231 cells treated with 0.1, 0.5, 1.0 and 2.5 nM of naked 13 nm AuNPs and Pep2, Pep5, Pep9 and Pep12 Functionalized AuNPs. Positive control was 10 percent DMSO. Statistically significant changes compared to negative control cells were calculated by two-paired Student's t test, and marked with stars, \* for  $p \leq 0.05$ , \*\* for  $p \leq 0.01$  and \*\*\* for  $p \leq 0.001$ .



#### ***4.3.3.5. Cell Cycle Progression***

Cell cycle progression of A549, BEAS-2b and MDA-MB-231 cells treated with 0.1, 0.5, 1.0 and 2.5 nM of naked 13 nm AuNPs and AuNP-Pep2, AuNP-Pep5, AuNP-Pep9 and AuNP-Pep12 was seen in Figure 4.81. 0.1  $\mu$ M colchicine was used as positive control because it blocks cells at G2/M phase, and it arrested 85-90 percent of all cell types at G2/M phase.

The cell cycle of A549 cells was affected by either naked AuNPs or AuNPs modified with glycine rich peptides and the cell cycle arrest caused by them was NP concentration dependent. 1.0-2.5 nM of naked AuNPs arrested A549 cells at G0/G1 phase. 0.5 nM and higher concentrations of AuNP-Pep2 and AuNP-Pep5 conjugates created a significant G0/G1 and S phase arrest. Furthermore, 0.1 nM of AuNP-Pep9 induced a severe S phase arrest and 2.5 nM of AuNP-Pep12 blocked A549 cells at G0/G1 phase.

The cell cycle progression of BEAS-2b cells was influenced by only AuNP-Pep2 and AuNP-Pep5. The both conjugates created a concentration dependent cell cycle arrest as AuNP-Pep2 induced G0/G1 phase while AuNP-Pep5 blocked BEAS-2b cells at S phase.

The cell cycle of MDA-MB-231 cells was arrested by all glycine rich peptides conjugated AuNPs. The arrest caused by NPs was based on the concentration. 0.5 nM and higher dose of AuNP-Pep2 and AuNP-Pep5, only 2.5 nM of AuNP-Pep9 and 1.0 and 2.5 nM of AuNP-Pep12 blocked MDA-MB-231 cells at G0/G1 phase.

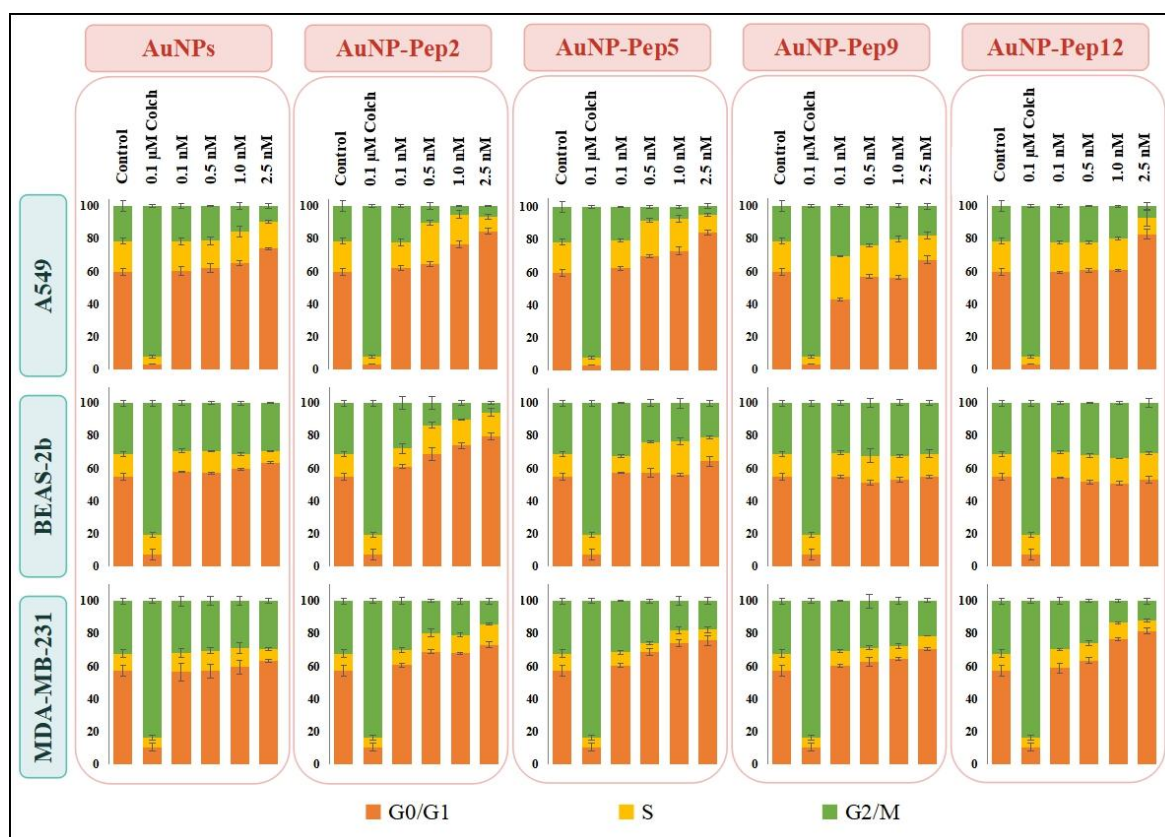


Figure 4.81. Cell cycle progression of A549, BEAS-2b and MDA-MB-231 cells treated with 0.1, 0.5, 1.0 and 2.5 nM of naked 13 nm AuNPs and Pep2, Pep5, Pep9 and Pep12 Functionalized AuNPs. Positive control was 0.1  $\mu$ M colchicine.

#### 4.3.3.6. Summary of Cellular Response to AuNPs Modified with Glycine Rich Peptides

The cellular response to AuNPs modified with glycine rich peptides was various and dependent to either cell type or surface chemistry and exposure concentration of NPs. Therefore, the cytotoxicity and the changes on cell cycle process of three cell lines treated with either naked AuNPs or AuNPs conjugated with glycine rich peptides were summarized one by one:

A549 cells highly internalized naked AuNPs when compared to AuNP-Peptide conjugates. The cell viability of A549 cells were dramatically affected by only naked AuNPs as the lower doses of naked AuNPs induced higher toxicity in A549 cells. Moreover, 5-8 percent more A549 cells went to necrosis after treatment with AuNP-Pep2 and AuNP-Pep5.

However, these results were not complementary with clonogenic assay because less colonies were formed after treatment with AuNP conjugates in comparison to untreated control. This meant that AuNP-Glycine conjugates influenced the reproductive integrity of A549 cells under NP treatment. Furthermore, the NP concentration dependent cell cycle arrest was investigated in A549 cells treated with naked AuNPs and AuNP-Peptide conjugates. Naked AuNPs and AuNP-Pep12 arrested the cell cycle of A549 cells at G0/G1 phase while AuNP-Pep2 and AuNP-Pep5 induced G0/G1 and S phase arrest and AuNP-Pep9 created a severe S phase arrest in A549 cells. As a result, naked AuNPs penetrated into A549 cell more and this highly internalization created a critical cytotoxicity. AuNP-Pep2 and AuNP-Pep5 conjugates, having  $-NH_2$  terminus, not also induced cytotoxicity in A549 cells but also arrested cells at G0/G1 and S phases. In addition, although AuNPs modified with AuNP-Pep9 and AuNP-Pep12, having  $-COOH$  terminus, did not result an important toxic affect in A549 cells, they induced the cell cycle progression of A549 cells significantly. It must be kept in mind that the end terminus type ( $-NH_2$  or  $-COOH$ ) and the presence of RGD sequence in glycine rich peptide demonstrated a various cell cycle arrest in A549 cells.

BEAS-2b cells significantly internalized AuNP-Pep5, AuNP-Pep9 and AuNP-Pep12 conjugates among all AuNPs. The cell viability of BEAS-2b cells were affected by AuNP-Pep5 and AuNP-Pep12 conjugates. AuNP-Pep5 induced a critical cytotoxicity in BEAS-2b cells even the percentage of live cells decreased to 5 percent upon exposure to 2.5 nM. AuNP-Pep12 in the range of 0.1-1.0 nM also created a less toxicity in BEAS-2b cells and this result was correlated by WST-1 assay result. Interestingly, in the presence of AuNP-Pep5 and partially AuNP-Pep9 the single BEAS-2b cells proliferated more and generated more colonies whereas other AuNP conjugates enabled the single BEAS-2b cells formed less colonies in comparison to untreated cells. Based on this clonogenic assay data, it was claimed that all AuNP-Glycine conjugates affected the reproductive integrity of BEAS-2b cells, but differently. AuNP-Pep5 and AuNP-Pep9 caused to lose the proliferation control while the others resulted in less proliferation. In addition, the cell cycle of BEAS-2b cells was arrested at G0/G1 phase by AuNP-Pep2 and at S phase by AuNP-Pep5. As a

conclusion, the cell viability of BEAS-2b cells were affected by AuNP-Pep5, having -NH<sub>2</sub> terminus and including RGD sequence, the most, and the cell cycle progression of BEAS-2b cells was critically blocked at G<sub>0</sub>/G<sub>1</sub> phase by AuNP-Pep2, having -NH<sub>2</sub> terminus. In the light of these results, the cellular response of BEAS-2b cells to -NH<sub>2</sub> surface of AuNPs modified with glycine rich peptides was remarkable.

MDA-MB-231 cells highly internalized AuNP-Pep5, AuNP-Pep9 and AuNP-Pep12 conjugates and the uptake was concentration dependent. The cell viability of MDA-MB-231 cells was influenced by AuNP-Pep2, AuNP-Pep5 and AuNP-Pep9 as 0.5 nM of AuNP-Pep2 and AuNP-Pep5 decreased the cell viability up to 75 and 55 percent, respectively, and 0.1 nM of AuNP-Pep9 induced apoptosis, which was correlated by WST-1 cell viability results. On the other hand, the survival ability by forming colonies of the single MDA-MB-231 cells was found insufficient due to the less proliferation number of the cells and this data showed that the reproductive integrity of MDA-MB-231 cells were more influenced by AuNP-Glycine conjugates. Moreover, the all AuNPs conjugated with glycine rich peptides arrested MDA-MB-231 cells at G<sub>0</sub>/G<sub>1</sub> phase and it was concentration dependent. Consequently, the high doses of AuNP-Pep2 and AuNP-Pep5, having -NH<sub>2</sub> terminus, and lowest dose of AuNP-Pep9, having -COOH terminus, induced apoptosis in MDA-MB-231 cells and all glycine rich peptide functionalized AuNPs resulted G<sub>0</sub>/G<sub>1</sub> phase cell cycle arrest in MDA-MB-231 cells.

#### **4.3.4. Cellular Response to AuNPs Modified with Glutamic Acid Rich Peptides**

Because of generating subtle differences on AuNP surfaces, AuNPs were conjugated with four glutamic acid rich peptides, as third peptide group to be tested. These glutamic acid rich peptides were designed as Pep3 (NH<sub>2</sub>-EEEC-COOH), Pep6 (NH<sub>2</sub>-DGREEEC-COOH), Pep10 (NH<sub>2</sub>-CEEE-COOH) and Pep13 (NH<sub>2</sub>-CEEERGD-COOH). Half of these negatively charged peptides had same four amino acid length sequence, but in reverse order. The other seven amino acid length peptides had the same glutamic acid rich sequence with addition of RGD sequence, again in reverse order. These small differences

on AuNP surfaces after modification with these four glutamic acid rich peptides were shown in Figure 4.82.

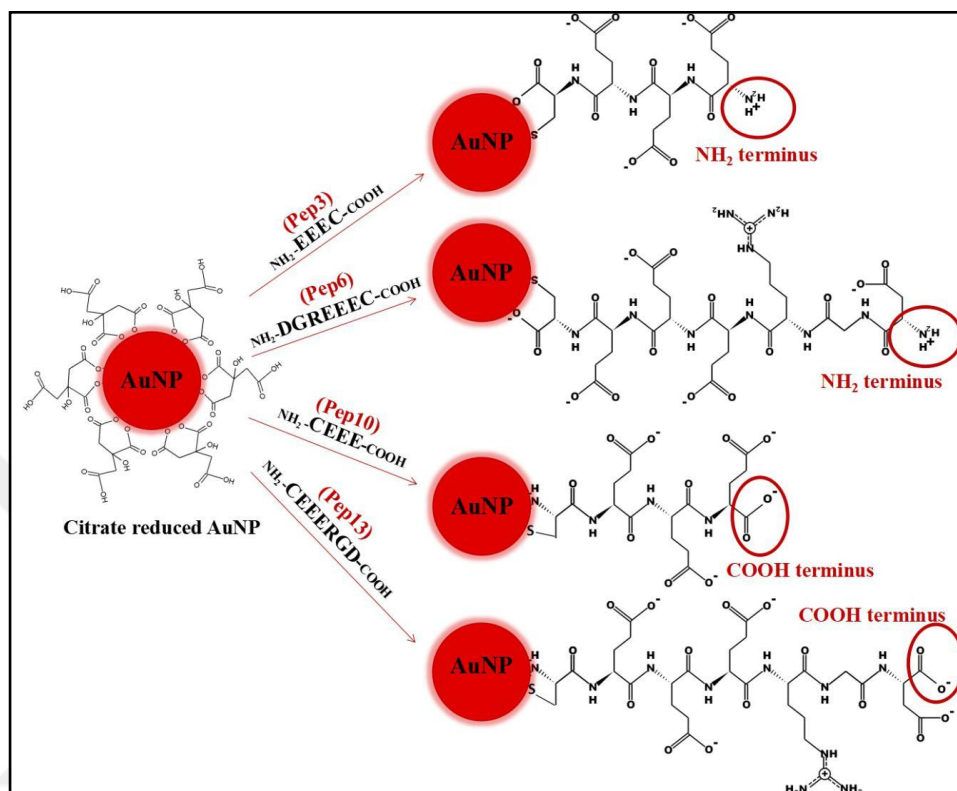


Figure 4.82. Subtle differences on AuNP surface after functionalization with Pep3, Pep6, Pep10 and Pep13.

#### 4.3.4.1. Uptake Studies

SSC graphs of A549, BEAS-2b and MDA-MB-231 cells treated with 0.1, 0.5, 1.0 and 2.5 nM naked 13 nm AuNPs, AuNP-Pep3, AuNP-Pep6, AuNP-Pep10 and AuNP-Pep13 conjugates was given in Figure 4.83. A549, BEAS-2b and MDA-MB-231 cells showed 6, 8 and 11 percent granulation in negative condition, respectively.

A549 cells internalized naked AuNPs in high amount when compared to AuNPs conjugated with glutamic acid rich peptides. To discuss the cellular uptake of glutamic acid rich peptides modified AuNPs, the granulation of 2.5 nM of AuNP-Pep10 and AuNP-Pep13 was analyzed significantly more in A549 cells in comparison to negative cells.

BEAS-2b cells internalized significantly 0.5-2.5 nM doses of all AuNPs modified with glutamic acid peptides. Additionally, the cellular uptake of AuNP-Pep10 and AuNP-Pep13 in BEAS-2b cells was the most among others.

MDA-MB-231 cells internalized AuNP-Pep3, AuNP-Pep10 and AuNP-Pep13 at all exposed doses, however, no significant granulation was seen after treatment with naked AuNPs and AuNP-Pep6 conjugates. Moreover, the penetration of AuNP-Pep10 and AuNP-Pep13 in MDA-MB-231 cells was more than AuNP-Pep3.



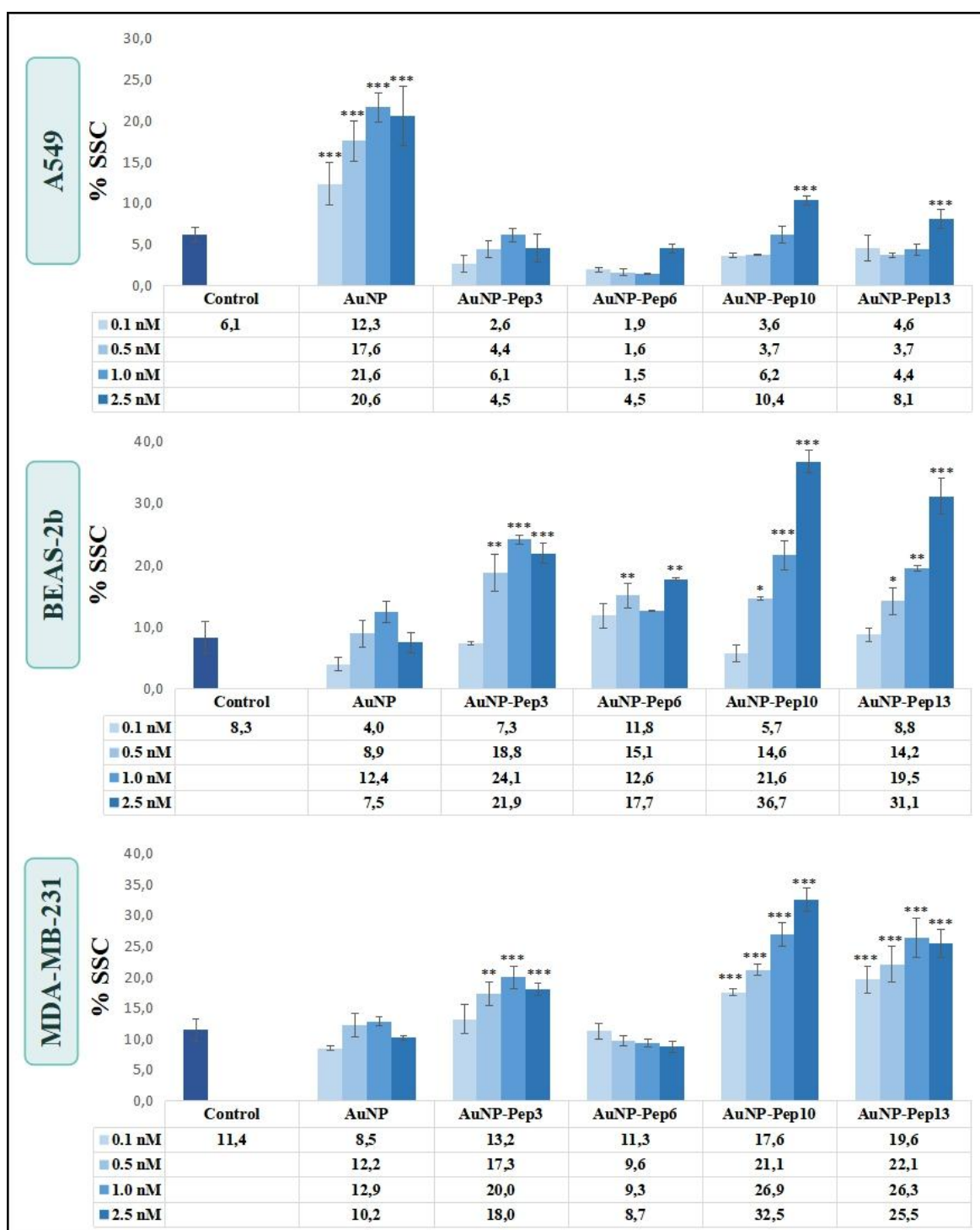


Figure 4.83. SSC graphs of A549, BEAS-2b and MDA-MB-231 cells treated with 0.1, 0.5, 1.0 and 2.5 nM of naked 13 nm AuNPs and Pep3, Pep6, Pep10 and Pep13 Functionalized AuNPs. Statistically significant changes compared to negative control cells were calculated by two-paired Student's t test, and marked with stars, \* for  $p \leq 0.05$ , \*\* for  $p \leq 0.01$  and \*\*\* for  $p \leq 0.001$ .

#### ***4.3.4.2. WST-1 Cell Proliferation Assay***

WST-1 cell proliferation assay results of A549, BEAS-2b and MDA-MB-231 cells treated with 0.1, 0.5, 1.0 and 2.5 nM of naked 13 nm AuNPs, AuNP-Pep3, AuNP-Pep6, AuNP-Pep10 and AuNP-Pep13 conjugates was shown in Figure 4.84. The positive control was 10 percent DMSO and it decreased the cell viability of all cell lines up to 5-10 percent.

The cell viability of A549 cells treated with all doses of AuNP-Pep3 and high doses of AuNP-Pep6 and AuNP-Pep10 conjugates was increased whereas only 0.1 nM of AuNP-Pep13 conjugates decreased the cell viability up to approximately 90 percent and created cytotoxicity to A549 cells.

The cell viability of BEAS-2b cells treated with 0.1-2.5 nM of AuNP-Pep3 and AuNP-Pep6 conjugates and 1.0-2.5 nM of AuNP-Pep13 was significantly higher than untreated control cells. Nevertheless, 0.1 nM of AuNP-Pep10 conjugates created a significant cytotoxicity in BEAS-2b cells and the live cell percentage of BEAS-2b cells reduced to 90 percent.

AuNP-Pep3 and AuNP-Pep6 conjugates at 2.5 nM and all exposed doses of AuNP-Pep10 increased the cell viability of MDA-MB-231 cells. Just 0.5 nM of AuNP-Pep3 and 0.1 nM of AuNP-Pep13 created a few cytotoxicity to MDA-MB-231 cells.



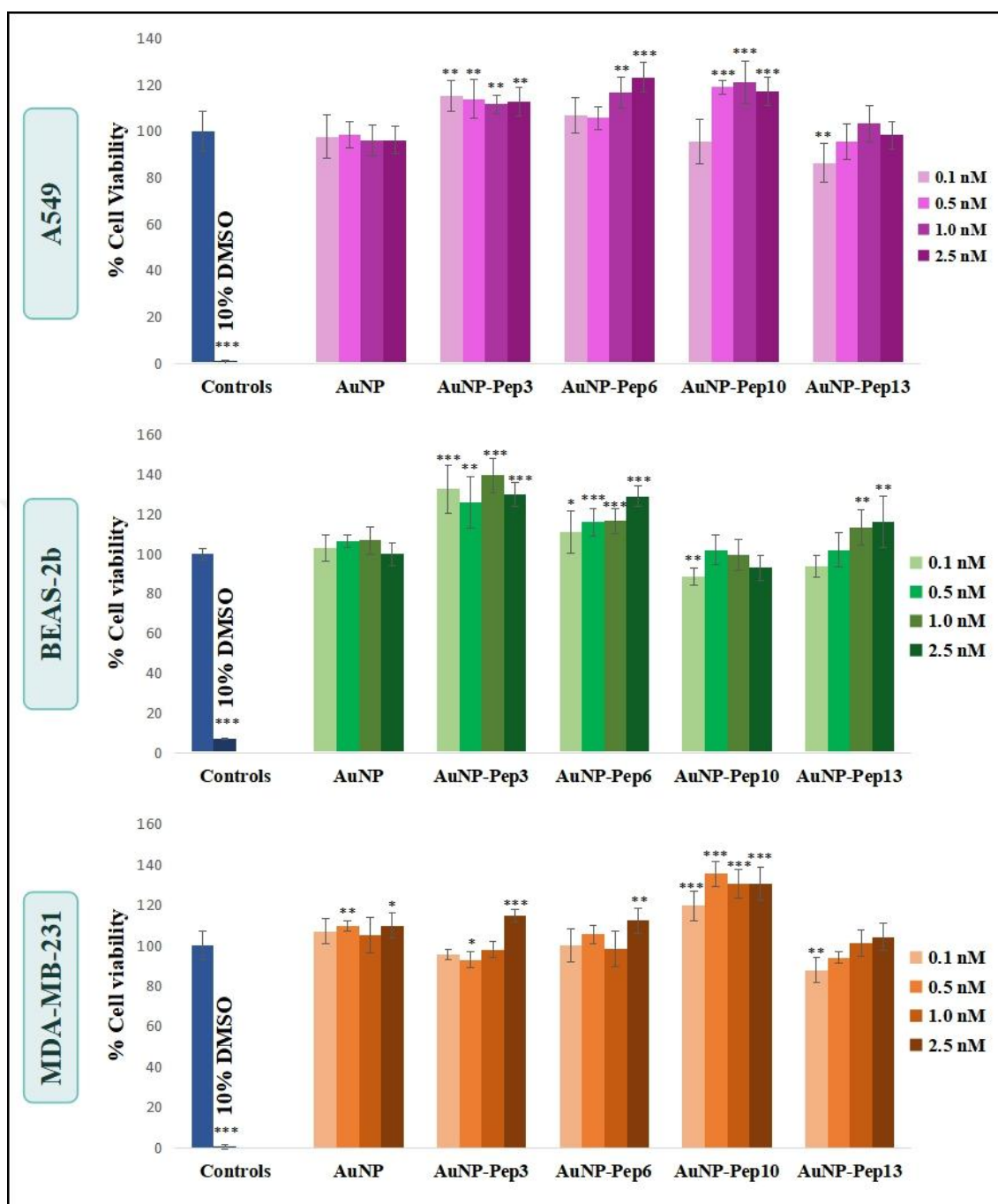


Figure 4.84. WST-1 cell proliferation assay results of A549, BEAS-2b and MDA-MB-231 cells treated with 0.1, 0.5, 1.0 and 2.5 nM of naked 13 nm AuNPs and Pep3, Pep6, Pep10 and Pep13 Functionalized AuNPs. Positive control was 10 percent DMSO. Statistically significant changes compared to negative control cells were calculated by two-paired Student's t test, and marked with stars, \* for  $p \leq 0.05$ , \*\* for  $p \leq 0.01$  and \*\*\* for  $p \leq 0.001$ .

#### ***4.3.4.3. Apoptosis/Necrosis Assay***

Apoptosis/Necrosis assay results of A549, BEAS-2b and MDA-MB-231 cells treated with 0.1, 0.5, 1.0 and 2.5 nM of naked 13 nm AuNPs, AuNP-Pep3, AuNP-Pep6, AuNP-Pep10 and AuNP-Pep13 conjugates was seen in Figure 4.85. 10 percent DMSO was used as positive control and it induced A549 cells to early apoptosis, BEAS-2b cells to late apoptosis and MDA-MB-231 cells to necrosis.

The naked AuNPs created a severe apoptosis in A549 cells as the lower concentrations created higher cytotoxicity and AuNP-Pep13 led approximately 5 percent more A549 cells to go to necrosis.

Neither naked 13 nm AuNPs nor AuNPs modified with glutamic acid rich peptides resulted a significant cytotoxicity in BEAS-2b cells.

The cell viability of MDA-MB-231 cells was influenced by only AuNP-Pep3. This conjugate induced a dramatic apoptosis in MDA-MB-231 cells such that the cell viability decreased up to 10 percent in the condition of 2.5 nM treatment.

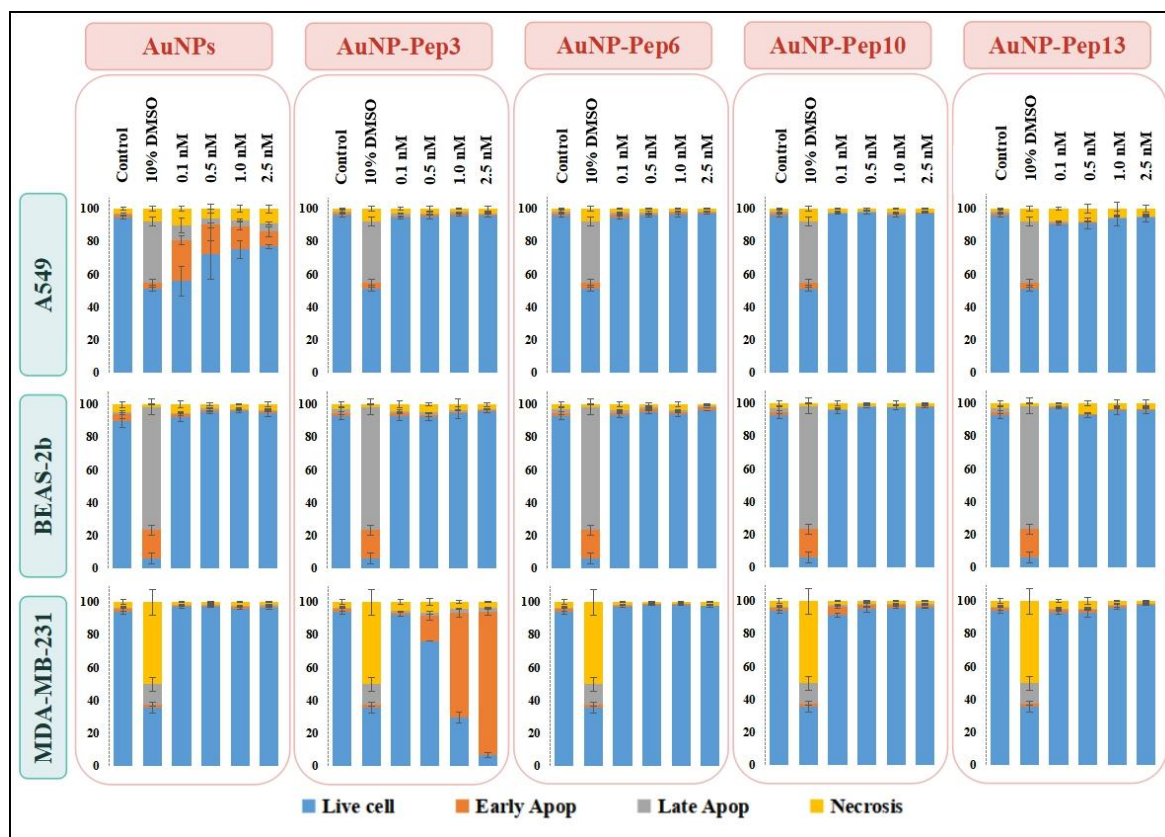


Figure 4.85. Apoptosis/Necrosis assay results of A549, BEAS-2b and MDA-MB-231 cells treated with 0.1, 0.5, 1.0 and 2.5 nM of naked 13 nm AuNPs and Pep3, Pep6, Pep10 and Pep13 Functionalized AuNPs. Positive control was 10 percent DMSO.

#### 4.3.4.4. Clonogenic Assay

Clonogenic cell survival assay results of A549, BEAS-2b and MDA-MB-231 cells treated with 0.1, 0.5, 1.0 and 2.5 nM of naked 13 nm AuNPs, AuNP-Pep3, AuNP-Pep6, AuNP-Pep10 and AuNP-Pep13 conjugates was shown in Figure 4.86. The positive control was 10 percent DMSO and one colony of A549 cells was formed and no colony was formed in other cell types after treatment with 10 percent DMSO.

A549 cells could survive after treatment with each NPs, except AuNP-Pep3 conjugates, however the single A549 cells exposed to 2.5 nM of NPs generated less colonies than negative control. During AuNP-Pep3 conjugates treatment, single A549 cells did not form colonies to survive.

BEAS-2b cells treated with the lowest concentration of naked AuNPs and AuNPs conjugated with glutamic acid rich peptides were clonogenic since they survived by forming colonies. Nevertheless, the colony formation ability of BEAS-2b cells treated with these AuNPs decreased with respect to increasing doses of NPs, especially at 2.5 nM dose. The least colony formation ability was observed for AuNP-Pep3 conjugates.

MDA-MB-231 cells had the least ability to form colonies in the treatment with AuNPs modified with glutamic acid rich peptides. The colony formation was observed only in the treatment with their low concentrations of NPs. MDA-MB-231 cells survived by forming colonies after treatment with AuNP-Pep3 and AuNP-Pep6 conjugates while no colony was formed at 0.5 nM and upper doses of AuNP-Pep10 and AuNP-Pep13 conjugates.

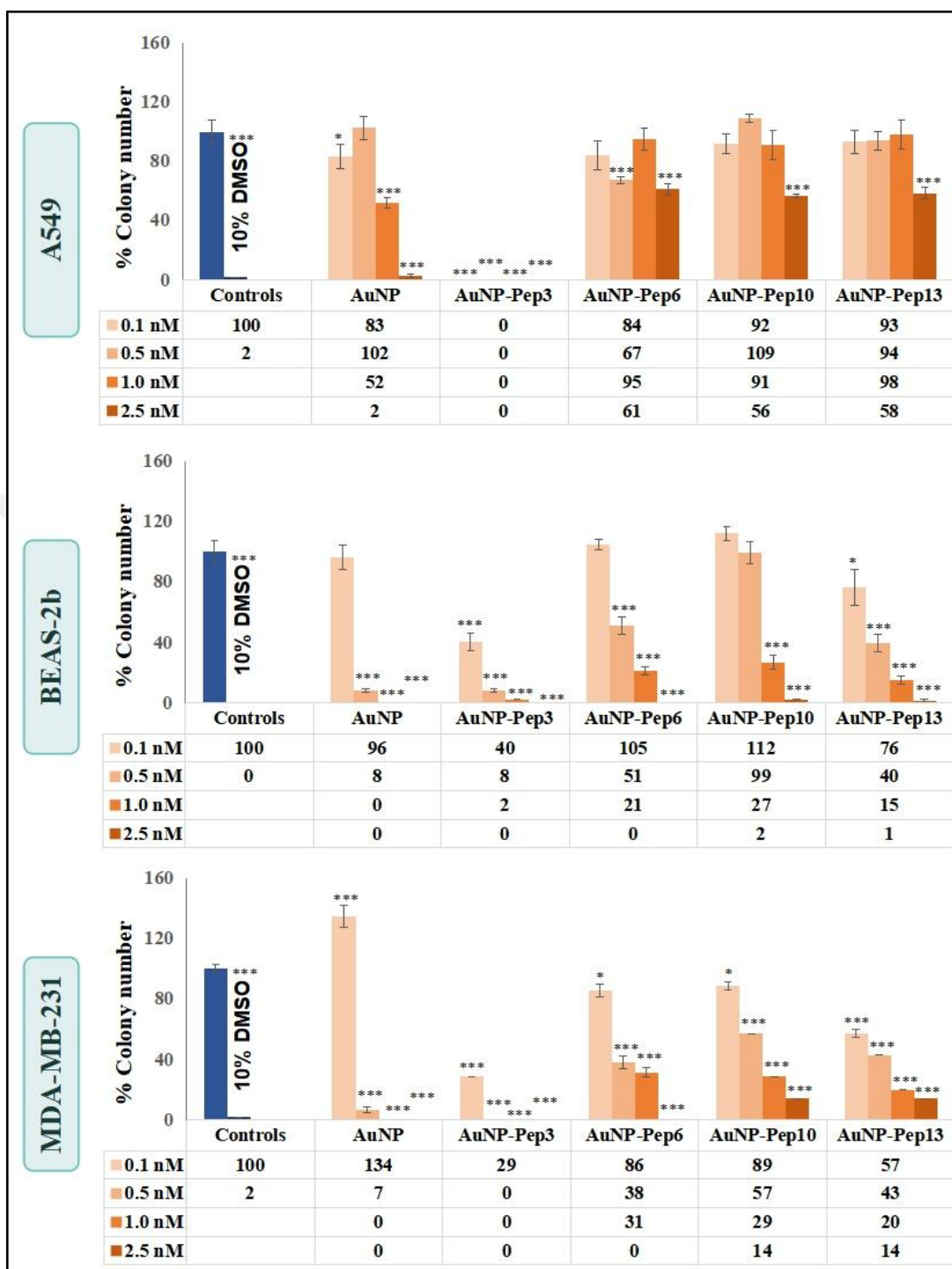


Figure 4.86. Clonogenic assay results of A549, BEAS-2b and MDA-MB-231 cells treated with 0.1, 0.5, 1.0 and 2.5 nM of naked 13 nm AuNPs and Pep3, Pep6, Pep10 and Pep13 Functionalized AuNPs. Positive control was 10 percent DMSO. Statistically significant changes compared to negative control cells were calculated by two-paired Student's t test, and marked with stars, \* for  $p \leq 0.05$ , \*\* for  $p \leq 0.01$  and \*\*\* for  $p \leq 0.001$ .

#### ***4.3.4.5. Cell Cycle Progression***

Cell cycle progression of A549, BEAS-2b and MDA-MB-231 cells treated with 0.1, 0.5, 1.0 and 2.5 nM of naked 13 nm AuNPs and AuNP-Pep3, AuNP-Pep6, AuNP-Pep10 and AuNP-Pep13 was seen in Figure 4.87. 0.1  $\mu$ M colchicine was used as positive control because it blocks cells at G2/M phase and it arrested 85-90 percent of all cell types at G2/M phase.

The cell cycle progression of A549 cells were affected by the higher concentrations of all AuNPs. The naked AuNPs and AuNP-Pep6 arrested A549 cells at G0/G1 phase after treatment with 1.0 and 2.5 nM dose whereas just 2.5 nM of other AuNP conjugates induced G0/G1 phase cell cycle arrest in A549 cells.

The cell cycle of BEAS-2b cells were significantly influenced by only AuNP-Pep3 and AuNP-Pep13 conjugates. 1.0 and 2.5 nM concentrations of AuNP-Pep3 arrested BEAS-2b cells at G0/G1 phase although 2.5 nM of AuNP-Pep13 induced S phase cell cycle arrest in BEAS-2b cells.

The cell cycle of MDA-MB-231 cells were arrested at G0/G1 phase after treatment with AuNP-Pep3 and AuNP-Pep6. The arrest caused by AuNP-Pep3 was concentration dependent as the concentrations higher than 0.5 nM created a significant cell cycle arrest whereas just 2.5 nM of AuNP-Pep6 induced G0/G1 phase blockage.



Figure 4.87. Cell cycle progression of A549, BEAS-2b and MDA-MB-231 cells treated with 0.1, 0.5, 1.0 and 2.5 nM of naked 13 nm AuNPs and Pep3, Pep6, Pep10 and Pep13 Functionalized AuNPs. Positive control was 0.1  $\mu$ M colchicine.

#### 4.3.4.6. Summary of Cellular Response to AuNPs Modified with Glutamic Acid Rich Peptides

The cellular response to AuNPs modified with glutamic rich peptides was based on cell type, surface chemistry and NP concentration. Therefore, the cytotoxicity and the changes on cell cycle process of three cell lines treated with either naked AuNPs or AuNP-Glutamic acid conjugates were explained one by one:

A549 cells significantly internalized naked AuNPs in comparison to AuNPs modified with glutamic acid peptides. Among AuNP conjugates, AuNP-Pep10 and AuNP-Pep13 having -COOH surfaces at 2.5 nM concentration penetrated more into A549 cells. The cell viability of A549 cells was affected by naked AuNPs and AuNP-Pep13. The naked AuNPs induced

a severe apoptosis and the lower doses resulted higher toxicity while AuNP-Pep13 induced apoptosis and reduced the cell viability of A549 cells up to 90 percent. In addition, the single A549 cells could not proliferate by forming colonies under treatment of AuNP-Pep3. It was claimed that AuNP-Pep3 affected the reproductive integrity of A549 cells. The cell cycle of A549 cells was arrested at G0/G1 phase after treatment with not only naked AuNPs but also AuNPs functionalized with glutamic acid peptides, however the blockage at cell cycle was NP concentration dependent. As a conclusion, citrate reduced naked AuNPs were internalized more in A549 cells and this high uptake created a significant cytotoxicity in A549 cells. Additionally, AuNP-Pep13 having -COOH surface with RGD sequence also affected the cell viability. AuNP-Pep3 having -NH<sub>2</sub> surface inhibited proliferation of single A549 cells under exposure. Although only naked AuNPs, AuNP-Pep3 and AuNP-Pep13 influenced the cell viability and survival ability of A549 cells, naked AuNPs and AuNPs conjugated with glutamic acid rich peptides affected the cell cycle progression of A549 cells in a NP concentration dependent manner.

The conjugation of AuNPs with glutamic acid rich peptides enabled higher uptake by BEAS-2b cells when compared to untreated cells and the naked AuNPs treated cells. Among AuNP-Glutamic acid conjugates, AuNP-Pep10 and AuNP-Pep13, which had -COOH surfaces, were internalized more by BEAS-2b cells. Furthermore, neither naked 13 nm AuNPs nor AuNPs modified with glutamic acid rich peptides induced a severe cytotoxicity in BEAS-2b cells. Nevertheless, the colony formation ability of BEAS-2b cells decreased with respect to increasing doses of NPs, especially at 2.5 nM dose and AuNP-Pep3 conjugates. This result demonstrated that AuNP conjugates affected DNA integrity of BEAS-2b cells during proliferation, the most by AuNP-Pep3, even though they were analyzed as nontoxic. In addition, the cell cycle of BEAS-2b cells was arrested by AuNP-Pep3 and AuNP-Pep13 significantly as higher concentrations of AuNP-Pep3, having -NH<sub>2</sub> surface, hindered BEAS-2b cells to pass through S phase and 2.5 nM of highly uptaken AuNP-Pep13, having RGD sequence and -COOH surfaces, blocked the cells at S phase. These results also confirmed the clonogenic assay results, thus non-toxic AuNP-Glutamic acid conjugates affected DNA integrity and so the cell cycle. As a



conclusion, AuNP-Glutamic acid conjugates having -COOH surfaces were internalized by BEAS-2b cells and although all AuNP conjugates were analyzed as non-toxic, AuNP-Pep3, having -NH<sub>2</sub> surface, and AuNP-Pep13, having RGD sequence and -COOH surfaces, affected the DNA integrity and so cell proliferation and cell cycle of BEAS-2b cells.

MDA-MB-231 cells highly internalized AuNP-Pep3, AuNP-Pep10 and AuNP-Pep13 but no significant uptake was detected after incubation with either naked AuNPs or AuNP-Pep6. In addition, AuNP-Pep10 and AuNP-Pep13 having -COOH surface penetrated the most into MDA-MB-231 cells. The cell viability of MDA-MB-231 cells was severely affected by only AuNP-Pep3 as the live cell percentage decreased up to 10 percent after treatment with 2.5 nM. MDA-MB-231 cells showed low survival ability by forming colonies upon AuNP-Glutamic acid conjugates exposure when compared to other cell types. The severe cytotoxicity caused by AuNP-Pep3 was also detected by clonogenic assay result since the single MDA-MB-231 cells treated with AuNP-Pep3 could not proliferate and form colonies under all exposed concentrations. Furthermore, the cell cycle of MDA-MB-231 cells was influenced after treatment with just AuNP-Pep3 and AuNP-Pep6, additionally the dose higher than 0.5 nM of AuNP-Pep3 and just 2.5 nM of AuNP-Pep6 arrested the cells at G0/G1 phase. As a result, even though AuNP-Pep10 and AuNP-Pep13 having -COOH surfaces were highly uptaken into MDA-MB-231 cells, no significant cellular response caused by them was investigated. On the other hand, AuNP-Pep3 (AuNP-CEEE-NH<sub>2</sub>) not only induced a severe toxicity but also caused a concentration dependent G0/G1 cell cycle arrest in MDA-MB-231 cells. At last but not the least, the NH<sub>2</sub> terminus on AuNP-Glutamic acid conjugates created a significant cellular response in MDA-MB-231 cells.

#### **4.3.5. Cellular Response to AuNPs Modified with Histidine Rich Peptides**

In order to make subtle differences on AuNP surfaces, AuNPs were conjugated with four histidine rich peptides, as fourth and last peptide group to be tested. These histidine rich

peptides were designed as Pep4 ( $\text{NH}_2\text{-HHHC-COOH}$ ), Pep7 ( $\text{NH}_2\text{-DGRHHHC-COOH}$ ), Pep11 ( $\text{NH}_2\text{-CHHH-COOH}$ ) and Pep14 ( $\text{NH}_2\text{-CHHHRGD-COOH}$ ). Half of these positively charged peptides had same four amino acid length sequence, but in reverse order. The other seven amino acid length peptides had the same histidine rich sequence with addition of RGD sequence, again in reverse order. These small differences on AuNP surfaces after modification with these four histidine rich peptides were shown in Figure 4.88.

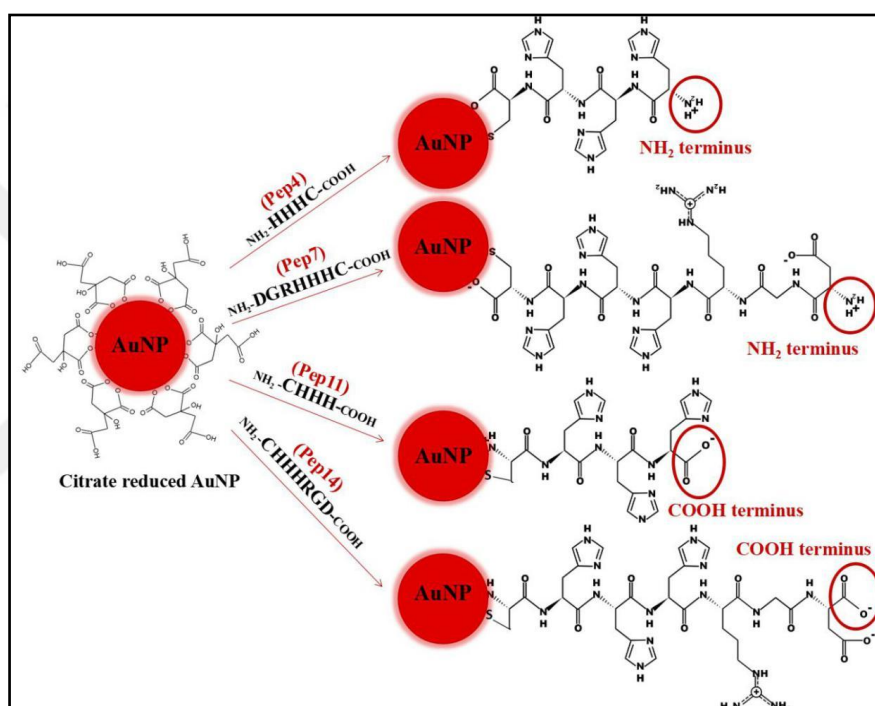


Figure 4.88. Subtle differences on AuNP surfaces after functionalization with Pep4, Pep7, Pep11 and Pep14.

#### 4.3.5.1. Uptake Studies

SSC graphs of A549, BEAS-2b and MDA-MB-231 cells treated with 0.1, 0.5, 1.0 and 2.5 nM naked 13 nm AuNPs, AuNP-Pep4, AuNP-Pep7, AuNP-Pep11 and AuNP-Pep14 conjugates were given in Figure 4.89. A549, BEAS-2b and MDA-MB-231 cells showed 6, 8 and 11 percent granulation in negative condition, respectively.

A549 cells highly internalized naked AuNPs and AuNP-Pep7. Moreover, the cellular uptake of all applied concentrations of AuNP-Pep10 and high concentrations of AuNP-Pep13 was also significantly high in A549 cells when compared to negative cells.

AuNP-Pep14 were highly penetrated into BEAS-2b cells. It is also noteworthy that AuNP-Pep7 and AuNP-Pep11 were also uptaken by BEAS-2b cells but in less amount.

MDA-MB-231 cells significantly internalized AuNP-Pep7 and AuNP-Pep11, however the uptake of naked AuNPs and other AuNP conjugates demonstrated similar uptake rate with negative control condition.



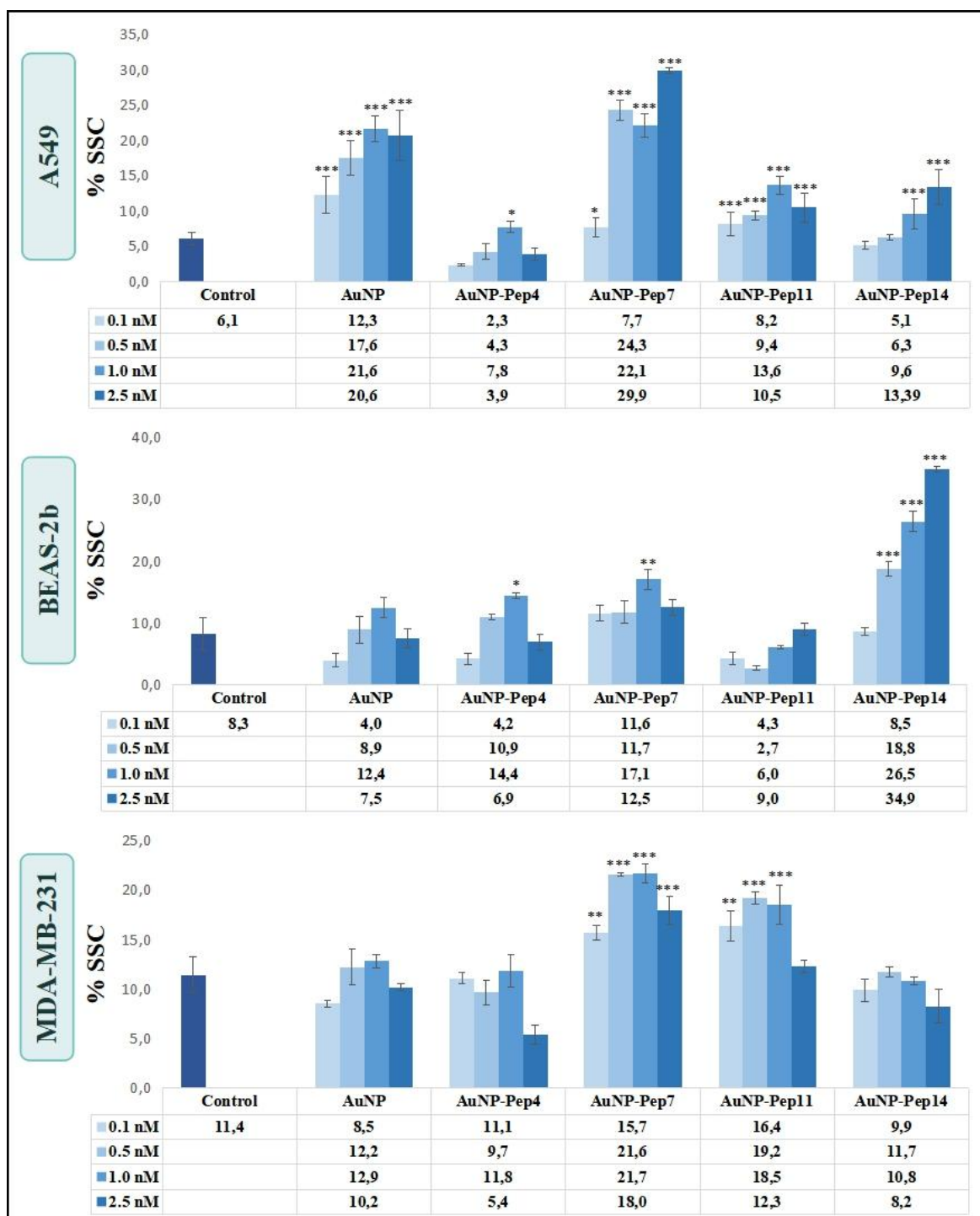


Figure 4.89. SSC graphs of A549, BEAS-2b and MDA-MB-231 cells treated with 0.1, 0.5, 1.0 and 2.5 nM of naked 13 nm AuNPs and Pep4, Pep7, Pep11 and Pep14 Functionalized AuNPs. Statistically significant changes compared to negative control cells were calculated by two-paired Student's t test, and marked with stars, \* for  $p \leq 0.05$ , \*\* for  $p \leq 0.01$  and \*\*\* for  $p \leq 0.001$ .

#### ***4.3.5.2. WST-1 Cell Proliferation Assay***

WST-1 cell proliferation assay results of A549, BEAS-2b and MDA-MB-231 cells treated with 0.1, 0.5, 1.0 and 2.5 nM of naked 13 nm AuNPs, AuNP-Pep4, AuNP-Pep7, AuNP-Pep11 and AuNP-Pep14 conjugates was shown in Figure 4.90. The positive control was 10 percent DMSO and it decreased the cell viability of cells up to 5-10 percent.

The cell viability of A549 cells was affected by AuNP-Pep4, AuNP-Pep7 and AuNP-Pep11 conjugates as the 0.5-2.5 nM of AuNP-Pep4 and all exposed concentrations of AuNP-Pep11 increased the cell viability of A549 cells whereas AuNP-Pep7 induced cytotoxicity and decreased the viability to approximately 95 percent.

The cell viability of BEAS-2b cells was influenced by all AuNP-Histidine conjugates, however in a different way. A significant increase on the cell viability was investigated after exposure to 0.5 and 1.0 nM of AuNP-Pep4, 1.0-2.5 nM of AuNP-Pep11 and 0.1-2.5 nM of AuNP-Pep14 conjugates. Nevertheless, 0.1 nM of AuNP-Pep4 and AuNP-Pep11 and 0.1 and 0.5 nM of AuNP-Pep7 created a severe cytotoxicity in BEAS-2b cells.

The cell viability of MDA-MB-231 cells was affected after treatment with either naked AuNPs or AuNP-Histidine conjugates excluding AuNP-Pep14. 2.5 nM of AuNP-Pep4, 0.1 nM of AuNP-Pep7 and all exposed doses of AuNP-Pep11 conjugates increased cell viability of MDA-MB-231 cells while 0.1-0.5 nM of AuNP-Pep4 conjugates indicated a significant cytotoxicity to MDA-MB-231 cells.

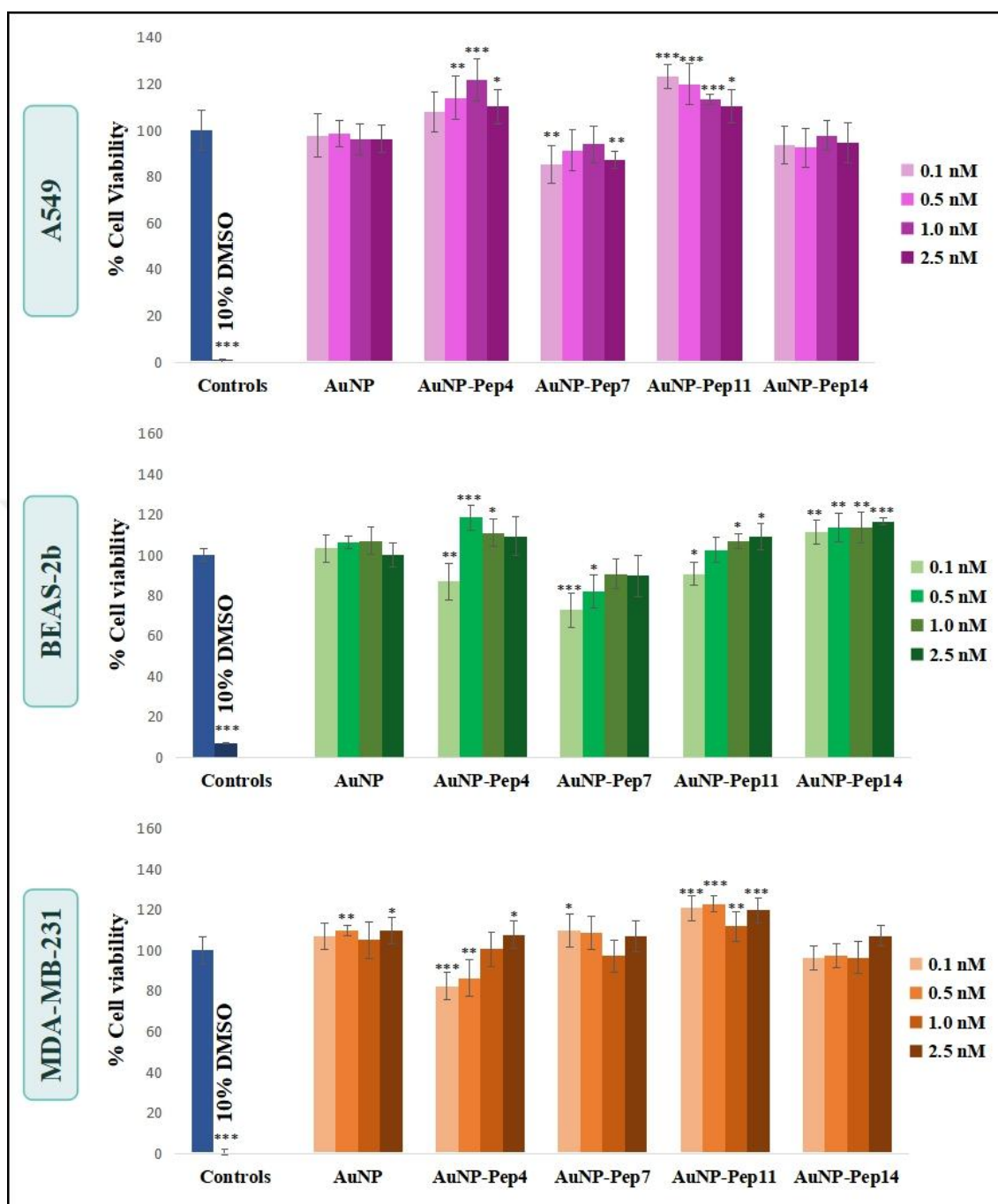


Figure 4.90. WST-1 proliferation assay results of A549, BEAS-2b and MDA-MB-231 cells treated with 0.1, 0.5, 1.0 and 2.5 nM of naked 13 nm AuNPs and Pep4, Pep7, Pep11 and Pep14 Functionalized AuNPs. Positive control was 10 percent DMSO. Statistically significant changes compared to negative control cells were calculated by two-paired Student's t test, and marked with stars, \* for  $p \leq 0.05$ , \*\* for  $p \leq 0.01$  and \*\*\* for  $p \leq 0.001$ .

#### ***4.3.5.3. Apoptosis/Necrosis Assay***

Apoptosis/Necrosis assay results of A549, BEAS-2b and MDA-MB-231 cells treated with 0.1, 0.5, 1.0 and 2.5 nM of naked 13 nm AuNPs, AuNP-Pep4, AuNP-Pep7, AuNP-Pep11 and AuNP-Pep14 conjugates was seen in Figure 4.91. 10 percent DMSO was used as positive control and it induced A549 cells to early apoptosis, BEAS-2b cells to late apoptosis and MDA-MB-231 cells to necrosis.

The naked AuNPs and AuNP-Pep11 conjugates created cytotoxicity in A549 cells. The lower concentrations of naked AuNPs created higher cytotoxicity and just 0.1 nM of AuNP-Pep11 conjugates led approximately 10 percent more A549 cells to go to necrosis.

AuNP-Pep11 conjugates induced a concentration dependent apoptosis in BEAS-2b cells and so the cell viability of BEAS-2b cells decreased to 25 percent after treatment with 2.5 nM of AuNP-Pep11.

AuNPs modified with histidine rich peptides influenced the cell viability of MDA-MB-231 cells more when compared to other cell lines. All conjugates created cytotoxicity, however AuNP-Pep7, AuNP-Pep11 and AuNP-Pep14 conjugates induced a dramatic apoptosis in MDA-MB-231 cells such that the cell viability decreased up to 5-25 percent in the condition of 2.5 nM treatment.

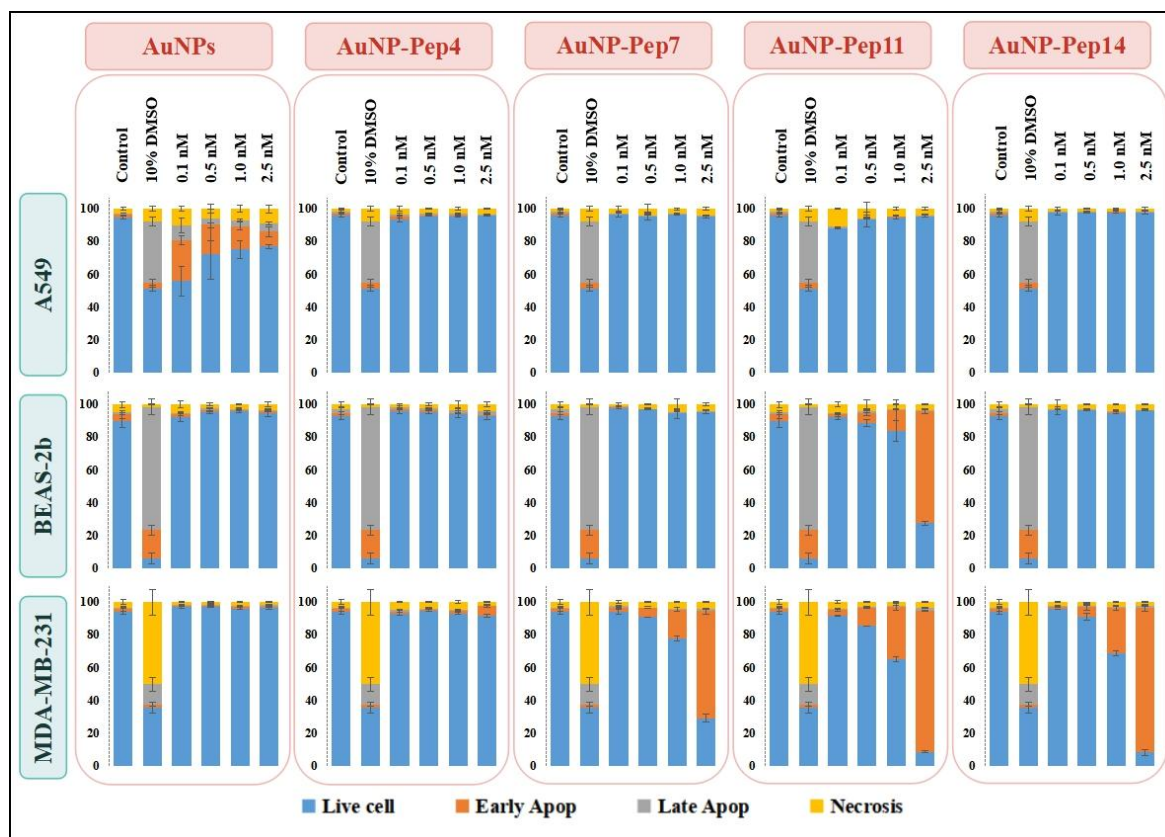


Figure 4.91. Apoptosis/Necrosis assay results of A549, BEAS-2b and MDA-MB-231 cells treated with 0.1, 0.5, 1.0 and 2.5 nM of naked 13 nm AuNPs and Pep4, Pep7, Pep11 and Pep14 Functionalized AuNPs. Positive control was 10 percent DMSO.

#### 4.3.5.4. Clonogenic Assay

Clonogenic cell survival assay results of A549, BEAS-2b and MDA-MB-231 cells treated with 0.1, 0.5, 1.0 and 2.5 nM of naked 13 nm AuNPs, AuNP-Pep4, AuNP-Pep7, AuNP-Pep11 and AuNP-Pep14 conjugates was shown in Figure 4.92. The positive control was 10 percent DMSO and one colony of MDA-MB-231 cells was formed and no colony was formed in other cell types after treatment with 10 percent DMSO.

The single A549 cells treated with 0.1 and 0.5 nM of AuNP-Pep7 and 0.1.0 nM of AuNP-Pep11 conjugates generated more colonies when compared to negative cells, which meant that these surface modifications resulted loss of proliferation control of A549 cells and so



increased the cell viability. No colony was observed in A549 cells exposed to high doses of AuNP-Pep4 and the highest dose of AuNP-Pep11 conjugates.

BEAS-2b cells survived by forming colonies at low doses of NPs, except AuNP-Pep4 conjugates, however the colony formation ability decreased with respect to increasing doses of NPs, especially at 2.5 nM dose. No colony formation ability of single BEAS-2b cells was observed for AuNP-Pep4 conjugates.

MDA-MB-231 cells had the least ability to form colonies in the treatment with AuNPs modified with histidine acid rich peptides, since colony formation was observed only in the treatment with their low concentrations of naked AuNPs, AuNPep7, AuNP-Pep11 and AuNP-Pep14 conjugates. They cannot survive after treatment with AuNP-Pep4 conjugates by forming colonies.

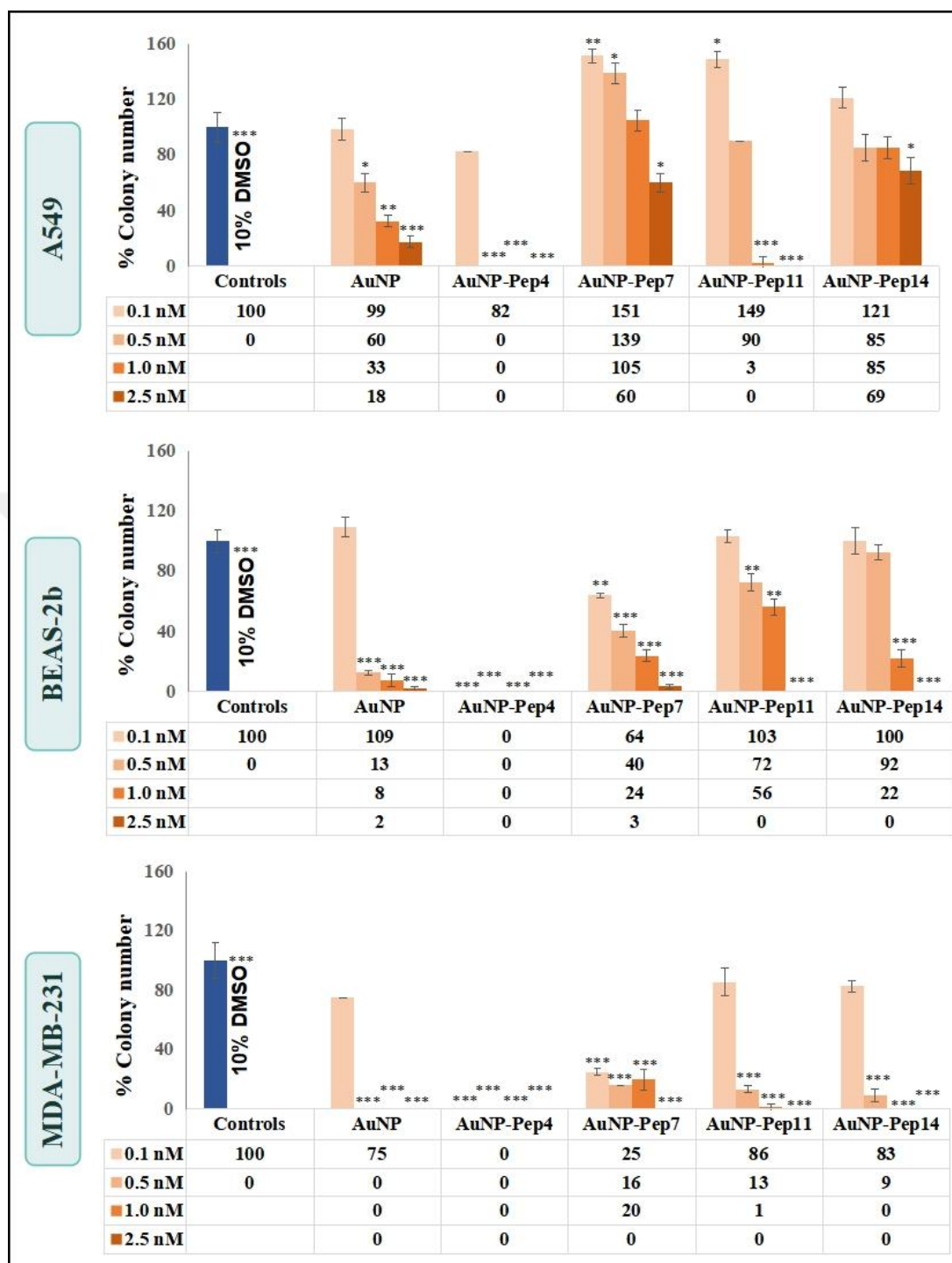


Figure 4.92. Clonogenic assay results of A549, BEAS-2b and MDA-MB-231 cells treated with 0.1, 0.5, 1.0 and 2.5 nM of naked 13 nm AuNPs and Pep4, Pep7, Pep11 and Pep14 Functionalized AuNPs. Positive control was 10 percent DMSO. Statistically significant changes compared to negative control cells were calculated by two-paired Student's t test, and marked with stars, \* for  $p \leq 0.05$ , \*\* for  $p \leq 0.01$  and \*\*\* for  $p \leq 0.001$ .

#### ***4.3.5.5. Cell Cycle Progression***

Cell cycle progression of A549, BEAS-2b and MDA-MB-231 cells treated with 0.1, 0.5, 1.0 and 2.5 nM of naked 13 nm AuNPs and AuNP-Pep4, AuNP-Pep7, AuNP-Pep11 and AuNP-Pep14 was seen in Figure 4.93. 0.1  $\mu$ M colchicine was used as positive control because it blocks cells at G2/M phase and it arrested 85-90 percent of all cell types at G2/M phase.

The cell cycle of A549 cells were influenced by either naked AuNPs or AuNPs modified with histidine rich peptides. 1.0 and 2.5 nM of naked AuNPs, 2.5 nM of AuNP-Pep11 and 1.0 and 2.5 nM of AuNP-Pep14 arrested A549 cells at G0/G1 phase whereas 0.5-2.5 nM of AuNP-Pep4 and AuNP-Pep7 induced a significant G0/G1 and S phase arrest in A549 cells. Moreover, the arrest caused by NPs were concentration dependent as the higher concentrations resulted higher cell cycle arrest in A549 cells.

The cell cycle of BEAS-2b cells were blocked by only AuNPs functionalized with histidine rich peptides. 1.0 and 2.5 nM of AuNP-Pep4, 2.5 nM of AuNP-Pep11 and 1.0 and 2.5 nM of AuNP-Pep14 arrested BEAS-2b cells at G0/G1 phase while AuNP-Pep7 conjugates at 0.5-2.5 nM concentrations created G0/G1 and S phase arrest.

The cell cycle of MDA-MB-231 cells were affected by histidine rich peptides conjugated AuNPs. 1.0 and 2.5 nM of AuNP-Pep4 and 2.5 nM of AuNP-Pep11 and AuNP-Pep14 arrested MDA-MB-231 cells at G0/G1 phase while 0.5-2.5 nM of AuNP-Pep7 induced G0/G1 and S phase arrest in MDA-MB-231 cells. Despite of different AuNPs created a same cell cycle arrest, the different amount of MDA-MB-231 cells were affected.

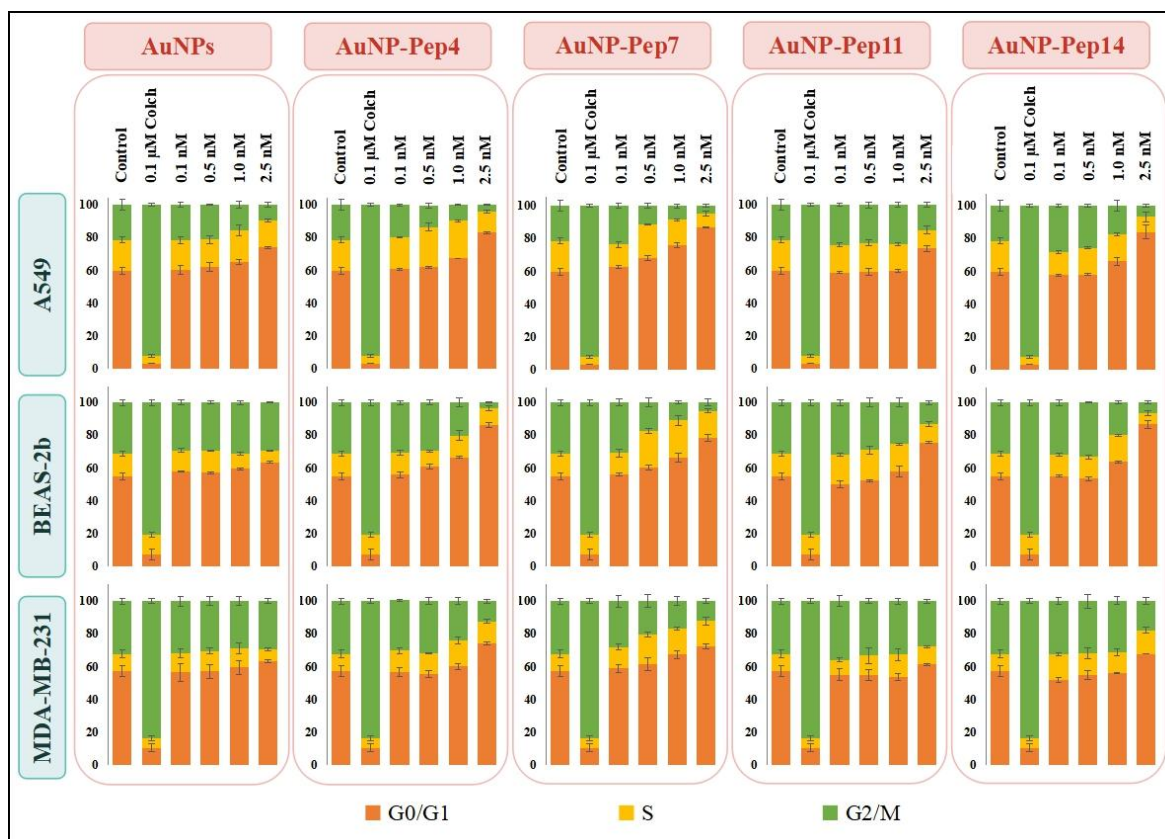


Figure 4.93. Cell cycle progression of A549, BEAS-2b and MDA-MB-231 cells treated with 0.1, 0.5, 1.0 and 2.5 nM of naked 13 nm AuNPs and Pep4, Pep7, Pep11 and Pep14 Functionalized AuNPs. Positive control was 0.1  $\mu$ M colchicine.

#### 4.3.5.6. Summary of Cellular Response to AuNPs Modified with Histidine Rich Peptides

The cellular response to AuNPs conjugated with histidine peptides was based on surface chemistry, cell type and NP concentration. Therefore, the cytotoxicity and the arrests on cell cycle progression of three cell lines treated with either naked AuNPs or AuNP-Histidine conjugates were criticized one by one:

A549 cells significantly internalized naked AuNPs and AuNP-Histidine conjugates, excluding AuNP-Pep4 in comparison to untreated control cells. Additionally, AuNP-Pep7 (AuNP-CHHHRGD-COOH) penetrated into the cells the most and RGD sequence on the peptide enabled higher cellular uptake. Based on WST-1 cell proliferation results, the cell viability of A549 cells reduced up to 95 percent after incubation with AuNP-Pep4, AuNP-

Pep7 and AuNP-Pep11 conjugates and this cell proliferation reduction was NP concentration dependent. Moreover, Apoptosis/Necrosis assay demonstrated that the naked 13 nm AuNPs and AuNP-Pep11 induced cytotoxicity in A549 cells. The naked AuNPs created a higher cytotoxicity at their low concentrations while the cell viability of A549 cells treated with 0.1 nM of AuNP-Pep11 decreased to approximately 90 percent. Furthermore, the single A549 cells formed more colonies than untreated control cells after treatment with AuNP-Pep7 and AuNP-Pep11 while they formed no colony after treatment with AuNP-Pep4. These three AuNP surfaces led A549 cells to lose their proliferation control and then affected the cell integrity. When discussed the cell cycle progression of A549 cells, either naked AuNPs or AuNP-Histidine conjugates affected the cell cycle, however the arrest was dependent on surface modification and NP concentration. AuNP-Pep11 and AuNP-Pep14, having -COOH surfaces, blocked A549 cells at G0/G1 phase whereas AuNP-Pep4 and AuNP-Pep7, having -NH<sub>2</sub> surfaces, arrested the cells at G0/G1 and S phase. As a conclusion, histidine rich peptides coated AuNPs were significantly internalized by A549 cells, except AuNP-Pep4 having -NH<sub>2</sub> surface. On the other hand, AuNP-Pep7, which had RGD sequence at -NH<sub>2</sub> terminus when compared to AuNP-Pep4, penetrated into A549 cells the most. This result indicated that RGD sequence increased the cellular uptake in A549 cells. As second conclusion, AuNP-Histidine conjugates did not induce a severe toxic affect to A549 cells, however especially AuNP-Pep4, AuNP-Pep7 and AuNP-Pep11 influenced the reproductive integrity of A549 cells. At last but not least, the cell cycle of A549 cells were arrested upon AuNP-Histidine conjugates and it was surface chemistry and NP concentration dependent.

BEAS-2b cells significantly internalized AuNP-Pep14 conjugate among all AuNPs. The cell viability of BEAS-2b cells decreased after treatment with 0.1 nM of AuNP-Pep4, AuNP-Pep7 and AuNP-Pep11 conjugates. These conjugates created a significant cytotoxicity in BEAS-2b cells at that dose. Based on Apoptosis/Necrosis assay results, only AuNP-Pep11 induced a concentration dependent apoptosis in BEAS-2b cells and the cell viability reduced up to 25 percent at their 2.5 nM dose. Moreover, AuNP-Pep4, AuNP-Pep7 and AuNP-Pep11 affected the reproductive integrity of BEAS-2b cells because the

single BEAS-2b cells could not proliferate and form colonies under treatment with these conjugates. Additionally, the integrity of BEAS-2b cells was influenced by AuNP-Pep4 the most since no colony was formed upon their exposure. What is more, AuNP-Histidine conjugates arrested the cell cycle process of BEAS-2b cells, however the arrest was concentration of NP and surface chemistry dependent. Although AuNP-Pep4, AuNP-Pep11 and AuNP-Pep14 induced cell cycle arrest at G0/G1 phase, AuNP-Pep7 blocked BEAS-2b cells at G0/G1 and S phases. Consequently, even though BEAS-2b cells internalized AuNP-Pep14 conjugates as most, the other AuNP-Histidine conjugates induced cytotoxicity and affected the reproductive integrity, especially AuNP-Pep11 having -COOH surfaces. In addition to the conclusion, all AuNP-Histidine conjugates resulted severe cell cycle arrests, which were dependent on NP concentration and subtle differences on peptides.

MDA-MB-231 cells tended to significantly internalize only AuNP-Pep7 and AuNP-Pep11 conjugates among others. The cell viability of MDA-MB-231 cells decreased upon AuNP-Pep4 exposure based on WST-1 cell proliferation data. On the other hand, Apoptosis/Necrosis assay result demonstrated that AuNP-Pep7, AuNP-Pep11 and AuNP-Pep14 conjugates induced a dramatic cytotoxicity in MDA-MB-231 cells even the cell viability reduced up to 5-25 percent at their 2.5 nM dose. Moreover, all AuNP-Histidine conjugates influenced the reproductive integrity of MDA-MB-231 cells since the single MDA-MB-231 cells could not produce colonies to survive under treatment with these conjugates. Especially, AuNP-Pep4 prevented the proliferation of the cells and the single cells could form no colonies. This was correlated with WST-1 assay data. Additionally, the cell cycle of MDA-MB-231 cells were influenced by all AuNP-Histidine conjugates, however the effect was NP surface and concentration dependent. AuNP-Pep4, AuNP-Pep11 and AuNP-Pep14 arrested MDA-MB-231 cells at G0/G1 phase whereas AuNP-Pep7 blocked the cells at G0/G1 and S phases. Consequently, despite of the fact that MDA-MB-231 cells internalized just AuNP-Pep7 and AuNP-Pep11, AuNP-Pep4 caused severe cellular responses as AuNP-Pep4 (AuNP-CHHH-NH<sub>2</sub>) affected the proliferation and reproductive integrity while the others induced severe apoptosis in MDA-

MB-231 cells and also, the cell cycle progression of MDA-MB-231 cells exposed to AuNP-Histidine conjugates was dependent on NP concentration and subtle differences on surface chemistry.



## 5. CONCLUSION AND FUTURE PERSPECTIVES

Nanomedicine is the application of nanosized nanomaterials in medicine. The interfaces between the engineered NPs and living systems play a critical role to explain the cellular responses. Therefore, the nature of these interactions between the NP surfaces and living systems should be determined to design safer NPs to be used in a wide range of technological applications. At that point, the cellular response to NP surface chemistry should be investigated to clarify their potential use in medicine. Thus, in this thesis, it was aimed to systematically investigate the cellular response of living cells to the subtle surface chemistry changes on AuNPs conjugated with custom designed carbohydrates and peptides. The spherical AuNPs of 13 nm diameter size were used as model NPs because of their unique optical properties, ease of synthesis and easy surface chemistry. In order to create subtle differences on AuNP surfaces, AuNPs were conjugated with custom designed four carbohydrates, Glucose and Mannose as mono saccharides and epimers at C2, and Lactose and Maltose as di saccharides and are epimers at C4, and fourteen peptides, which were varied in length, charge, sequence with or without RGD and free terminus whether -NH<sub>2</sub> or -COOH end. The cellular responses to these small chemical differences on the AuNP surfaces were examined on three cell lines; A549 cells (human carcinoma), BEAS-2b cells (human bronchial cell line) and MDA-MB-231 cells (human breast cancer cell line) by considering cellular uptake, cytotoxicity, reproductive integrity and cell cycle progression.

In order to generate small chemical differences on AuNP surfaces, fourteen peptides were designed by taking into account of their charge, length, sequence with or without RGD, isoelectric points and free terminus end whether -NH<sub>2</sub> or -COOH group. Considering the peptide sequences from -NH<sub>2</sub> to -COOH end, the first amino acid in the sequences of seven peptides coded as Pep1 to Pep7, was cysteine whereas cysteine was the last amino acid in the other peptides coded as Pep8 to Pep14. The results showed that that cysteine had a critical role in bioconjugation of AuNPs with peptides. The peptides tended to bind on



AuNP surfaces via -SH groups on cysteine because of its dominant affinity in comparison to -NH<sub>2</sub> and -COOH groups. This tendency completely changed the reaction conditions. Therefore, AuNPs could be functionalized with the peptide couples, which had same sequence but in reverse order, at different pH conditions. Even though the effect of isoelectric point of peptides on conjugation was explained as an important factor in the literature, the presence of cysteine as a first amino acid in a peptide alters that norm. With the knowledge of affinity order of -SH, -NH<sub>2</sub> and -COOH groups for AuNP surfaces, -SH group governs the binding side of the peptides on AuNP surfaces. The peptides that had a cysteine residue at the -NH<sub>2</sub> end were immobilized on AuNP surfaces both -SH group of cysteine and -NH<sub>2</sub> group at free end of the peptide. On the other hand, when the cysteine was located at the -COOH terminus, the peptide binds to the AuNP surfaces through -SH group of cysteine and -COOH group at free end. When both types of peptides coat the surface of AuNPs, the surface charge changes depending on the binding orientations of the peptides. When the AuNPs are conjugated with the peptides coded from Pep1 to Pep7, the functional group on the surface is -NH<sub>2</sub>, with the peptides coded as Pep8-Pep14, it is -COOH.

The citrate reduced AuNPs were significantly internalized by all cell lines. They caused severe apoptosis and significant cell cycle arrest in only A549 cells. On the other hand, just the reproductive integrity of BEAS-2b and MDA-MB-231 cells was influenced under 0.5-2.5 nM AuNPs exposure.

AuNP-Carbohydrate conjugates induced varying cellular responses in three cell lines. AuNP-Mannose (C2 epimer of Glucose) and AuNP-Lactose (Galactose as free unit on the surface and C4 epimer of Glucose) induced cytotoxicity and influenced the cell cycle progression of A549 cells. However, AuNP-Lactose and AuNP-Maltose conjugates, on which the free units were C4 epimers, caused a significant apoptosis and G<sub>0</sub>/G<sub>1</sub> phase cell cycle arrest in BEAS-2b cells. Moreover, Glucose and Mannose functionalized AuNPs, which were C2 epimers, caused a deleterious effect on cellular viability of MDA-MB-231 cells and also just AuNP-Glucose conjugates arrested MDA-MB-231 cells at G<sub>0</sub>/G<sub>1</sub> phase.

Consequently, the cellular response of three cell lines varied according to -OH orientation differences at second or fourth carbon of these chosen carbohydrates.

AuNPs functionalized with two RGD peptides resulted in various cellular responses in three cell lines. AuNP-CRGD having -NH<sub>2</sub> terminus was highly uptaken by A549 cells and this created a significant concentration dependent cytotoxicity and G<sub>0</sub>/G<sub>1</sub> phase cell cycle arrest in A549 cells. Although both AuNP-CRGD conjugates did not cause any cytotoxicity in BEAS-2b cells, they influenced the reproductive integrity and the cell cycle progression, but much by AuNP-CRGD conjugates possessing -COOH surfaces. Additionally, MDA-MB-231 cells tend to internalize both AuNP-CRGD conjugates, however, only AuNPs having -NH<sub>2</sub> terminus at 2.5 nM concentration created substantial cytotoxicity and cell cycle arrest in MDA-MB-231 cells. It can be concluded that highly internalized AuNP-CRGD-NH<sub>2</sub> influenced the cancer cells while the healthy cell line was significantly affected by AuNP-CRGD-COOH.

The free terminus (-NH<sub>2</sub> or -COOH) and the presence of RGD sequence in AuNP-Glycine conjugates demonstrated varying cellular response in three cell lines. AuNP-CGGG-NH<sub>2</sub> and AuNP-CGGGRGD-NH<sub>2</sub> led to cytotoxicity and crucial G<sub>0</sub>/G<sub>1</sub> and S phases arrests in A549 cells; whereas, those of possessing -COOH surfaces affected significantly reproductive integrity and cell cycle progression in A549 cells. Moreover, the AuNP-Glycine conjugates having -NH<sub>2</sub> surfaces triggered the significant cytotoxicity and cell cycle arrest in BEAS-2b cells even the cell viability of BEAS-2b cells treated with AuNP-CGGGRGD-NH<sub>2</sub> dramatically decreased down to 5 percent at 2.5 nM dose. Furthermore, 1.0-2.5 nM of AuNP-Glycine conjugates having -NH<sub>2</sub> terminus and 0.1-0.5 nM of AuNP-CGGG-COOH terminus induced a severe apoptosis in MDA-MB-231 cells and all glycine rich peptide functionalized AuNPs resulted G<sub>0</sub>/G<sub>1</sub> phase cell cycle arrest in MDA-MB-231 cells. In conclusion, AuNPs-Glycine conjugates having -NH<sub>2</sub> surfaces caused significant cytotoxicity and cell cycle alteration in A549 and BEAS-2b cells while all AuNP-Glycine conjugates resulted in different cellular responses in MDA-MB-231 cells.

The cells treated with glutamic acid rich peptides modified AuNPs showed various cellular responses dependent to free terminus type and presence of RGD in the peptides. Just AuNP-CEEERGD-COOH conjugates created significant cytotoxicity in A549 cells while only AuNP-CEEE-NH<sub>2</sub> conjugates showed harmful effect to the reproductive integrity of A549 cells. Nevertheless, all AuNP-Glutamic acid conjugates induced G0/G1 phase cell cycle arrest in A549 cells, which was concentration dependent. Even though all AuNP-Glutamic acid conjugates were remarkably uptaken by BEAS-2b cells, they showed no significant cytotoxicity in BEAS-2b cells. In addition, AuNP-CEEE-NH<sub>2</sub> and AuNP-CEEERGD-COOH conjugates affected the DNA integrity, cell proliferation and cell cycle of BEAS-2b cells. Despite of higher uptake of AuNP-CEEE and AuNP-CEEERGD conjugates possessing -COOH surfaces, they caused no remarkable cellular response in MDA-MB-231 cells. However, AuNP-CEEE-NH<sub>2</sub> not only created a severe apoptosis but also induced a concentration dependent G0/G1 cell cycle arrest in MDA-MB-231 cells. Consequently, AuNP-CEEE-NH<sub>2</sub> and AuNP-CEEERGD-COOH conjugates among all AuNP-Glutamic acid conjugates affected the cellular uptake, cytotoxicity, reproductive integrity and cell cycle progression of A549, BEAS-2b and MDA-MB-231 cells, however the effects were cell type dependent.

The varying cellular responses of A549, BEAS-2b and MDA-MB-231 cells to AuNP-Histidine conjugates having -NH<sub>2</sub> or -COOH surfaces and RGD sequence. AuNP-Histidine conjugates did not result a toxic affect to A549 cells, except 0.1 nM of AuNP-CHHH-COOH, however AuNP-CHHH-NH<sub>2</sub>, AuNP-CHHHRGD-NH<sub>2</sub> and AuNP-CHHH-COOH affected the reproductive integrity of A549 cells. Furthermore, all AuNP-Histidine conjugates demonstrated NP concentration dependent cell cycle arrest in A549 cells. Although BEAS-2b cells internalized AuNP-CHHHRGD-COOH conjugates as most, the other AuNP-Histidine conjugates, especially AuNP-CHHH-COOH, induced cytotoxicity and loss of the reproductive integrity. In addition, all AuNP-Histidine conjugates induced NP concentration dependent severe cell cycle arrests in BEAS-2b cells. MDA-MB-231 cells significantly internalized AuNP-Histidine conjugates having -COOH surfaces among others. However, all AuNP-Histidine conjugates caused severe cellular responses as

AuNP-CHHH-NH<sub>2</sub> affected the proliferation and reproductive integrity while the others induced severe apoptosis in MDA-MB-231 cells. Additionally, the cell cycle progression of MDA-MB-231 cells exposed to AuNP-Histidine conjugates was dependent on NP concentration. Consequently, the cellular response of A549, BEAS-2b and MDA-MB-231 cells to AuNP-Histidine conjugates was diversified based on free terminus the presence of RGD sequence at peptide on AuNP surfaces, NP concentration and cell line type.

Finally, this study showed that the small chemistry differences on AuNP surfaces caused varying cellular uptake, cytotoxicity, reproductive integrity and cell cycle arrests. In addition, these cellular responses were directly associated with NP concentration and cell type.

The evaluation of cellular response with the surface chemistry change at proteomics level can be further pursued to understand the cellular response in depth. The formation of protein corona is strongly influenced by the surface chemistry of NPs. Thus, in a similar fashion, subtle chemical changes generated on the NPs can influence the density of proteins on the NPs, thus their cellular uptake. This can be another point for further investigation. Moreover, cytotoxicity of the NPs with varying surface chemistry can be evaluated from other perspectives such as ROS in order to obtain more molecular insight for NPs behavior in the living systems and enrich the knowledge about cellular response to subtle changes on surface chemistry.

## REFERENCES

1. Prasad PN. *Introduction to biophotonics*. Hoboken, New Jersey: John Wiley & Sons; 2004.
2. Algar WR, Prasuhn DE, Stewart MH, Jennings TL, Blanco-Canosa JB, Dawson PE, et al. The controlled display of biomolecules on nanoparticles: A challenge suited to bioorthogonal chemistry. *Bioconjugate Chemistry*. 2011;22(5):825-58.
3. Perrault SD, Chan WCW. Synthesis and surface modification of highly monodispersed, spherical gold nanoparticles of 50-200 nm. *Journal of the American Chemical Society*. 2009;131(47):17042-3.
4. Nikoobakht B, El-Sayed MA. Preparation and growth mechanism of gold nanorods (NRs) using seed-mediated growth method. *Chemistry of Materials*. 2003;15(10):1957-62.
5. Cui Y, Wei Q, Park H, Lieber CM. Nanowire nanosensors for highly sensitive and selective detection of biological and chemical species. *Science*. 2001;293(5533):1289-92.
6. Coleman JN, Lotya M, O'Neill A, Bergin SD, King PJ, Khan U, et al. Two-dimensional nanosheets produced by liquid exfoliation of layered materials. *Science*. 2011;331(6017):568-71.
7. Hao F, Nehl CL, Hafner JH, Nordlander P. Plasmon resonances of a gold nanostar. *Nano Letters*. 2007;7(3):729-32.
8. Chen J, Saeki F, Wiley BJ, Cang H, Cobb MJ, Li Z-Y, et al. Gold nanocages: Bioconjugation and their potential use as optical imaging contrast agents. *Nano Letters*. 2005;5(3):473-7.

9. Teng X and Yang H. Synthesis of platinum multipods: An induced anisotropic growth. *Nano Letters*. 2005;5(5):885-91.
10. Ozin GA. Nanochemistry: Synthesis in diminishing dimensions. *Advanced Materials*. 1992;4(10):612-49.
11. Prasad PN. *Introduction to nanomedicine and nanobioengineering*. Hoboken, New Jersey: John Wiley & Sons; 2012.
12. Prasad PN. *Nanophotonics*. Hoboken, New Jersey: John Wiley & Sons; 2004.
13. Burda C, Chen X, Narayanan R, El-Sayed MA. Chemistry and properties of nanocrystals of different shapes. *Chemical Reviews*. 2005;105(4):1025-102.
14. Yu H, Li L, Zhang Y. Silver nanoparticle-based thermal interface materials with ultra-low thermal resistance for power electronics applications. *Scripta Materialia*. 2012;66(11):931-4.
15. Zhu G, Lin ZH, Jing Q, Bai P, Pan C, Yang Y, et al. Toward large-scale energy harvesting by a nanoparticle-enhanced triboelectric nanogenerator. *Nano Letters*. 2013;13(2):847-53.
16. Grande L, Chundi VT, Wei D, Bower C, Andrew P, Ryhaenen T. Graphene for energy harvesting/storage devices and printed electronics. *Particuology*. 2012;10(1):1-8.
17. Allia P, Barrera G, Tiberto P, Nardi T, Leterrier Y, Sangermano M. Fe<sub>3</sub>O<sub>4</sub> nanoparticles and nanocomposites with potential application in biomedicine and in communication technologies: Nanoparticle aggregation, interaction, and effective magnetic anisotropy. *Journal of Applied Physics*. 2014;116(11):113903-12.
18. Dykman L, Khlebtsov N. Gold nanoparticles in biology and medicine: Recent advances and prospects. *Acta Naturae*. 2011;3(2):34-55.

19. Nam J, Won N, Bang J, Jin H, Park J, Jung S, et al. Surface engineering of inorganic nanoparticles for imaging and therapy. *Advanced Drug Delivery Reviews*. 2013;65(5):622-48.
20. Oberdick SD, Abdelgawad A, Moya C, Mesbahi-Vasey S, Kepaptsoglou D, Lazarov VK, et al. Spin canting across core/shell  $\text{Fe}_3\text{O}_4/\text{Mnx Fe}_{3-x}\text{O}_4$  nanoparticles. *Scientific Reports*. 2018;8(1):3425-36.
21. Sapsford KE, Algar WR, Berti L, Gemmill KB, Casey BJ, Oh E, et al. Functionalizing nanoparticles with biological molecules: Developing chemistries that facilitate nanotechnology. *Chemical Reviews*. 2013;113(3):1904-2074.
22. Thanh NT, Green LA. Functionalisation of nanoparticles for biomedical applications. *Nano Today*. 2010;5(3):213-30.
23. Miyata K, Christie RJ, Kataoka K. Polymeric micelles for nano-scale drug delivery. *Reactive Functional Polymers*. 2011;71(3):227-34.
24. Dubertret B, Skourides P, Norris DJ, Noireaux V, Brivanlou AH, Libchaber A. *In vivo* imaging of quantum dots encapsulated in phospholipid micelles. *Science*. 2002;298(5599):1759-62.
25. Fröhlich E. The role of surface charge in cellular uptake and cytotoxicity of medical nanoparticles. *International Journal of Nanomedicine*. 2012;7:5577-91.
26. Chen G, Roy I, Yang C, Prasad PN. Nanochemistry and nanomedicine for nanoparticle-based diagnostics and therapy. *Chemical Reviews*. 2016;116(5):2826-85.
27. Moghimi SM, Hunter AC, Murray JC. Nanomedicine: Current status and future prospects. *The FASEB Journal*. 2005;19(3):311-30.
28. Fornaguera C, García-Celma M. Personalized nanomedicine: A revolution at the nanoscale. *Journal of Personalized Medicine*. 2017;7(4):12-31.

29. Allen TM, Cullis PR. Drug delivery systems: Entering the mainstream. *Science*. 2004;303(5665):1818-22.
30. Cormode DP, Jarzyna PA, Mulder WJ, Fayad ZA. Modified natural nanoparticles as contrast agents for medical imaging. *Advanced Drug Delivery Reviews*. 2010;62(3):329-38.
31. Chen G, Qiu H, Prasad PN, Chen X. Upconversion nanoparticles: Design, nanochemistry, and applications in theranostics. *Chemical Reviews*. 2014;114(10):5161-214.
32. Goldberg M, Langer R, Jia X. Nanostructured materials for applications in drug delivery and tissue engineering. *Journal of Biomaterials Science, Polymer Edition*. 2007;18(3):241-68.
33. Gamrad L, Rehbock C, Krawinkel J, Tumursukh B, Heisterkamp A, Barcikowski S. Charge balancing of model gold-nanoparticle-peptide conjugates controlled by the peptide's net charge and the ligand to nanoparticle ratio. *The Journal of Physical Chemistry C*. 2014;118(19):10302-13.
34. Kopp M, Kollenda S, Epple M. Nanoparticle–protein interactions: Therapeutic approaches and supramolecular chemistry. *Accounts of Chemical Research*. 2017;50(6):1383-90.
35. Narayanan J, Sharma MK, Ponmariappan S, Sarita, Shaik M, Upadhyay S. Electrochemical immunosensor for botulinum neurotoxin type-E using covalently ordered graphene nanosheets modified electrodes and gold nanoparticles-enzyme conjugate. *Biosensors and Bioelectronics*. 2015;69:249-56.
36. Jazayeri MH, Amani H, Pourfatollah AA, Pazoki-Toroudi H, Sedighimoghaddam B. Various methods of gold nanoparticles (GNPs) conjugation to antibodies. *Sensing and Bio-Sensing Research*. 2016;9:17-22.



37. Park SY, Lytton-Jean AKR, Lee B, Weigand S, Schatz GC, Mirkin CA. DNA-programmable nanoparticle crystallization. *Nature*. 2008;451:553.
38. Farokhzad OC, Jon S, Khademhosseini A, Tran TN, LaVan DA, Langer R. Nanoparticle-aptamer bioconjugates. *A New Approach for Targeting Prostate Cancer Cells*. 2004;64(21):7668-72.
39. Earhart C, Jana NR, Erathodiyil N, Ying JY. Synthesis of carbohydrate-conjugated nanoparticles and quantum dots. *Langmuir*. 2008;24(12):6215-9.
40. Liu Y, Li K, Pan J, Liu B, Feng SS. Folic acid conjugated nanoparticles of mixed lipid monolayer shell and biodegradable polymer core for targeted delivery of Docetaxel. *Biomaterials*. 2010;31(2):330-8.
41. Tang M, Zhou M, Huang Y, Zhong J, Zhou Z, Luo K. Dual-sensitive and biodegradable core-crosslinked HPMA copolymer-doxorubicin conjugate-based nanoparticles for cancer therapy. *Polymer Chemistry*. 2017;8(15):2370-80.
42. Weissleder R, Kelly K, Sun EY, Shtatland T, Josephson L. Cell-specific targeting of nanoparticles by multivalent attachment of small molecules. *Nature Biotechnology*. 2005;23:1418-1423.
43. Maiti KK, Dinish US, Fu CY, Lee JJ, Soh KS, Yun SW, et al. Development of biocompatible SERS nanotag with increased stability by chemisorption of reporter molecule for *in vivo* cancer detection. *Biosensors and Bioelectronics*. 2010;26(2):398-403.
44. De M, Rana S, Akpınar H, Miranda OR, Arvizo RR, Bunz UH, et al. Sensing of proteins in human serum using conjugates of nanoparticles and green fluorescent protein. *Nature Chemistry*. 2009;1:461-5.
45. Sapsford KE, Tyner KM, Dair BJ, Deschamps JR, Medintz IL. Analyzing nanomaterial bioconjugates: A review of current and emerging purification and characterization techniques. *Analytical Chemistry*. 2011;83(12):4453-88.

46. Soo Choi H, Liu W, Misra P, Tanaka E, Zimmer JP, Itty Ipe B, et al. Renal clearance of quantum dots. *Nature Biotechnology*. 2007;25(10):1165-70.
47. Yee C, Kataby G, Ulman A, Prozorov T, White H, King A, et al. Self-assembled monolayers of alkanesulfonic and phosphonic acids on amorphous iron oxide nanoparticles. *Langmuir*. 1999;15(21):7111-5.
48. Park S, Hamad-Schifferli K. Nanoscale interfaces to biology. *Current Opinion in Chemical Biology*. 2010;14(5):616-22.
49. Lynch I, Cedervall T, Lundqvist M, Cabaleiro-Lago C, Linse S, Dawson KA. The nanoparticle–protein complex as a biological entity; a complex fluids and surface science challenge for the 21st century. *Advances in Colloid and Interface Science*. 2007;134-135:167-74.
50. Medintz IL, Clapp AR, Brunel FM, Tiefenbrunn T, Tetsuo Uyeda H, Chang EL, et al. Proteolytic activity monitored by fluorescence resonance energy transfer through quantum-dot–peptide conjugates. *Nature Materials*. 2006;5:581-9.
51. Aubin-Tam ME, Hamad-Schifferli K. Structure and function of nanoparticle–protein conjugates. *Biomedical Materials*. 2008;3(3):034001-17.
52. Clapp AR, Medintz IL, Fisher BR, Anderson GP, Mattoussi H. Can luminescent quantum dots be efficient energy acceptors with organic dye donors? *Journal of the American Chemical Society*. 2005;127(4):1242-50.
53. Delehanty JB, Boeneman K, Bradburne CE, Robertson K, Medintz IL. Quantum dots: A powerful tool for understanding the intricacies of nanoparticle-mediated drug delivery. *Expert Opinion on Drug Delivery*. 2009;6(10):1091-112.
54. Lammers T, Hennink WE, Storm G. Tumour-targeted nanomedicines: principles and practice. *British Journal of Cancer*. 2008;99(3):392-7.
55. Hermanson GT. *Bioconjugate techniques*. Cambridge: Academic press; 2013.

56. Song J, Park S, Kim S, Im K, Park N. Electrostatic interaction driven gold nanoparticle assembly on three-dimensional triangular pyramid DNA nanostructures. *New Journal of Chemistry*. 2017;41(18):9590-3.
57. Guo J, Filpponen I, Su P, Laine J, Rojas OJ. Attachment of gold nanoparticles on cellulose nanofibrils via click reactions and electrostatic interactions. *Cellulose*. 2016;23(5):3065-75.
58. Schneider G, Decher G. From functional core/shell nanoparticles prepared via layer-by-layer deposition to empty nanospheres. *Nano Letters*. 2004;4(10):1833-9.
59. Hinterwirth H, Kappel S, Waitz T, Prohaska T, Lindner W, Lämmerhofer M. Quantifying thiol ligand density of self-assembled monolayers on gold nanoparticles by inductively coupled plasma–mass spectrometry. *ACS Nano*. 2013;7(2):1129-36.
60. Daniel MC, Astruc D. Gold nanoparticles: Assembly, supramolecular chemistry, quantum-size-related properties, and applications toward biology, catalysis, and nanotechnology. *Chemical Reviews*. 2004;104(1):293-346.
61. Mirkin CA, Letsinger RL, Mucic RC, Storhoff JJ. A DNA-based method for rationally assembling nanoparticles into macroscopic materials. *Nature*. 1996;382:607-9.
62. Blanco-Canosa JB, Wu M, Susumu K, Petryayeva E, Jennings TL, Dawson PE, et al. Recent progress in the bioconjugation of quantum dots. *Coordination Chemistry Reviews*. 2014;263-264:101-37.
63. Moo-Kwang S, Byunghoon K, Nam-Kyung Y, Myeong-Hoon K, Jisun K, Seungmin H, et al. Synthesis of Fe<sub>3</sub>O<sub>4</sub>@nickel–silicate core–shell nanoparticles for His-tagged enzyme immobilizing agents. *Nanotechnology*. 2016;27(49):495705-13.
64. Keleştemur S, Altunbek M, Culha M. Influence of EDC/NHS coupling chemistry on stability and cytotoxicity of ZnO nanoparticles modified with proteins. *Applied Surface Science*. 2017;403:455-63.

65. Giorgi-Coll S, Blunt-Foley H, Hutchinson PJ, Carpenter KLH. Heparin-gold nanoparticles for enhanced microdialysis sampling. *Analytical Bioanalytical Chemistry*. 2017;409(21):5031-42.
66. Lesch HP, Kaikkonen MU, Pikkarainen JT, Ylä-Herttua S. Avidin-biotin technology in targeted therapy. *Expert Opinion on Drug Delivery*. 2010;7(5):551-64.
67. Wilchek M, Bayer EA, Livnah O. Essentials of biorecognition: The (strept)avidin–biotin system as a model for protein–protein and protein–ligand interaction. *Immunology Letters*. 2006;103(1):27-32.
68. van der Meer SB, Knuschke T, Frede A, Schulze N, Westendorf AM, Epple M. Avidin-conjugated calcium phosphate nanoparticles as a modular targeting system for the attachment of biotinylated molecules *in vitro* and *in vivo*. *Acta Biomaterialia*. 2017;57:414-25.
69. Veszelka S, Mészáros M, Kiss L, Kóta Z, Páli T, Hoyk Z, et al. Biotin and glutathione targeting of solid nanoparticles to cross human brain endothelial cells. *Current Pharmaceutical Design*. 2017;23(28):4198-205.
70. Kuku G, Saricam M, Akhatova F, Danilushkina A, Fakhrullin R, Culha M. Surface-enhanced Raman scattering to evaluate nanomaterial cytotoxicity on living cells. *Analytical Chemistry*. 2016;88(19):9813-20.
71. Panahi Y, Farshbaf M, Mohammadhosseini M, Mirahadi M, Khalilov R, Saghfi S, et al. Recent advances on liposomal nanoparticles: Synthesis, characterization and biomedical applications. *Artificial Cells, Nanomedicine, and Biotechnology*. 2017;45(4):788-99.
72. Bronstein LM, Shifrina ZB. Nanoparticles in dendrimers: From synthesis to application. *Nanotechnologies in Russia*. 2009;4(9):576-608.

73. Tyrrell ZL, Shen Y, Radosz M. Fabrication of micellar nanoparticles for drug delivery through the self-assembly of block copolymers. *Progress in Polymer Science*. 2010;35(9):1128-43.
74. Bhatia S. *Nanoparticles types, classification, characterization, fabrication methods and drug delivery applications*. Natural Polymer Drug Delivery Systems: Springer; 2016:33-93.
75. Banga RJ, Krovi SA, Narayan SP, Sprangers AJ, Liu G, Mirkin CA, et al. Drug-loaded polymeric spherical nucleic acids: enhancing colloidal stability and cellular uptake of polymeric nanoparticles through DNA surface-functionalization. *Biomacromolecules*. 2017;18(2):483-9.
76. Du Y, Zhang D, Liu H, Lai R. Thermochemotherapy effect of nanosized As<sub>2</sub>O<sub>3</sub>/Fe<sub>3</sub>O<sub>4</sub> complex on experimental mouse tumors and its influence on the expression of CD44v6, VEGF-C and MMP-9. *BMC Biotechnology*. 2009;9(1):84-95.
77. Dykman L, Khlebtsov N. *Gold nanoparticles in biomedical applications*. Boca Raton, Florida: CRC Press; 2017.
78. Daraee H, Eatemadi A, Abbasi E, Fekri Aval S, Kouhi M, Akbarzadeh A. Application of gold nanoparticles in biomedical and drug delivery. *Artificial Cells, Nanomedicine, and Biotechnology*. 2016;44(1):410-22.
79. Antonii F. Panacea aurea-auro potabile. *Bibliopolio Frobeniano: Hamburg*.1618:205.
80. De Planis CD. *Traicté de la vraye, unique, grande, et universelle médecine des anciens dite des recens, or potable*. Paris, François Targa; 1633.
81. Helcher HH. *Aurum potabile, oder gold-tinctur*. Breslau, Leipzig, J. Herbord Klossen; 1712.
82. Faraday M. X. The bakerian lecture: Experimental relations of gold (and other metals) to light. *Philosophical Transactions of the Royal Society of London*. 1857;147:145-81.

83. Mie G. Beiträge zur optik trüber medien, speziell kolloidaler metallösungen. *Annalen der Physik*. 1908;330(3):377-445.
84. Hayat MA. *Colloidal gold: Principles, Methods, and Applications*. San Diego: Academic Press; 1989.
85. Zsigmondy R. Die chemische natur des cassiusschen goldpurpurs. *Justus Liebigs Annalen der Chemie*. 1898;301(2-3):361-87.
86. Svedberg T. *Die methoden zur herstellung kolloider lösungen anorganischer stoffe: Ein hand-und hilfsbuch für die chemie und industrie der kolloide*. Dresden: T. Steinkopff; 1909.
87. Bhattacharya R, Mukherjee P. Biological properties of “naked” metal nanoparticles. *Advanced Drug Delivery Reviews*. 2008;60(11):1289-306.
88. Ochsner EH. *Colloidal gold in inoperable cancer*. Clinical Medicine and Surgery: Chicago; 1935.
89. Rogoff EE, Romano R, Hahn EW. The prevention of ehrlich ascites tumor using intraperitoneal colloidal 198Au: Dose vs. size of inoculum. *Radiology*. 1975;114(1):225-6.
90. Page Faulk W, Malcolm Taylor G. Communication to the editors: An immunocolloid method for the electron microscope. *Immunochemistry*. 1971;8(11):1081-3.
91. Lee J, Han S, Lee J, Choi M, Kim C. Stimuli-responsive  $\alpha$ -helical peptide gatekeepers for mesoporous silica nanocarriers. *New Journal of Chemistry*. 2017;41(15):6969-72.
92. Sonay AY, Keseroglu K and Culha M. 2D Gold nanoparticle structures engineered through DNA tiles for delivery and therapy. *Nano Biomedicine & Engineering*. 2012; 4(1):17-22.
93. Kim CK, Ghosh P and Rotello VM. Multimodal drug delivery using gold nanoparticles. *Nanoscale*. 2009; 1(1):61-67.

94. Kyriazi ME, Giust D, El-Sagheer AH, Lackie PM, Muskens OL, Brown T, et al. Multiplexed mRNA sensing and combinatorial-targeted drug delivery using DNA-Gold nanoparticle dimers. *ACS Nano*. 2018;12(4):3333-40.
95. Lee K, Lee H, Bae KH, Park TG. Heparin immobilized gold nanoparticles for targeted detection and apoptotic death of metastatic cancer cells. *Biomaterials*. 2010;31(25):6530-6.
96. Jiang Y, Shi M, Liu Y, Wan S, Cui C, Zhang L, et al. Aptamer/AuNP biosensor for colorimetric profiling of exosomal proteins. *Angewandte Chemie International Edition*. 2017;56(39):11916-20.
97. Priyadarshini E, Pradhan N. Gold nanoparticles as efficient sensors in colorimetric detection of toxic metal ions: A review. *Sensors and Actuators B: Chemical*. 2017;238:888-902.
98. Scott AW, Garimella V, Calabrese CM, Mirkin CA. Universal biotin-PEG-linked gold nanoparticle probes for the simultaneous detection of nucleic acids and proteins. *Bioconjugate Chemistry*. 2017;28(1):203-11.
99. Petkova GA, Záruba K, Žvátora P, Král V. Gold and silver nanoparticles for biomolecule immobilization and enzymatic catalysis. *Nanoscale Research Letters*. 2012;7(1):287.
100. Ran B, Zheng W, Dong M, Xianyu Y, Chen Y, Wu J, et al. Peptide-mediated controllable cross-linking of gold nanoparticles for immunoassays with tunable detection range. *Analytical Chemistry*. 2018;90(13):8234-40.
101. Carlos FF, Veigas B, Matias AS, Doria G, Flores O, Baptista PV. Allele specific LAMP-gold nanoparticle for characterization of single nucleotide polymorphisms. *Biotechnology Reports (Amsterdam, Netherlands)*. 2017;16:21-5.

102. Turkevich J, Stevenson PC, Hillier J. A study of the nucleation and growth processes in the synthesis of colloidal gold. *Discussions of the Faraday Society*. 1951;11(0):55-75.
103. Link S, Mohamed MB, El-Sayed MA. Simulation of the optical absorption spectra of gold nanorods as a function of their aspect ratio and the effect of the medium dielectric constant. *The Journal of Physical Chemistry B*. 1999;103(16):3073-7.
104. Sahoo GP, Basu S, Samanta S, Misra A. Microwave-assisted synthesis of anisotropic gold nanocrystals in polymer matrix and their catalytic activities. *Journal of Experimental Nanoscience*. 2015;10(9):690-702.
105. Nehl CL, Liao H, Hafner JH. Optical properties of star-shaped gold nanoparticles. *Nano Letters*. 2006;6(4):683-8.
106. Sun Y, Xia Y. Mechanistic study on the replacement reaction between silver nanostructures and chloroauric acid in aqueous medium. *Journal of the American Chemical Society*. 2004;126(12):3892-901.
107. Huang X, El-Sayed IH, Qian W, El-Sayed MA. Cancer cell imaging and photothermal therapy in the near-infrared region by using gold nanorods. *Journal of the American Chemical Society*. 2006;128(6):2115-20.
108. Vasilev K, Zhu T, Wilms M, Gillies G, Lieberwirth I, Mittler S, et al. Simple, one-step synthesis of gold nanowires in aqueous solution. *Langmuir*. 2005;21(26):12399-403.
109. Minati L, Cheng CL, Lin YC, Hees J, Lewes-Malandrakis G, Nebel CE, et al. Synthesis of novel nanodiamonds–gold core shell nanoparticles. *Diamond and Related Materials*. 2015;53:23-8.
110. Lu W, Arumugam SR, Senapati D, Singh AK, Arbnesi T, Khan SA, et al. Multifunctional oval-shaped gold-nanoparticle-based selective detection of breast



- cancer cells using simple colorimetric and highly sensitive two-photon scattering assay. *ACS Nano*. 2010;4(3):1739-49.
111. Frens G. Controlled nucleation for the regulation of the particle size in monodisperse gold suspensions. *Nature Physical Science*. 1973;241(105):20-22.
112. Brust M, Walker M, Bethell D, Schiffrin DJ, Whyman R. Synthesis of thiol-derivatised gold nanoparticles in a two-phase Liquid–Liquid system. *Journal of The Chemical Society, Chemical Communications*. 1994(7):801-2.
113. Perrault SD, Walkey C, Jennings T, Fischer HC, Chan WC. Mediating tumor targeting efficiency of nanoparticles through design. *Nano Letters*. 2009;9(5):1909-15.
114. Martin MN, Basham JI, Chando P, Eah SK. Charged gold nanoparticles in non-polar solvents: 10-min synthesis and 2D self-assembly. *Langmuir*. 2010;26(10):7410-7.
115. Navarro JRG, Lerouge F, Cepraga C, Micouin G, Favier A, Chateau D, et al. Nanocarriers with ultrahigh chromophore loading for fluorescence bio-imaging and photodynamic therapy. *Biomaterials*. 2013;34(33):8344-51.
116. Santos SA, Pinto RJ, Rocha SM, Marques PA, Neto CP, Silvestre AJ, et al. Unveiling the chemistry behind the green synthesis of metal nanoparticles. *ChemSusChem*. 2014;7(9):2704-11.
117. Thakkar KN, Mhatre SS, Parikh RY. Biological synthesis of metallic nanoparticles. *Nanomedicine: Nanotechnology, Biology and Medicine*. 2010;6(2):257-62.
118. Eustis S, El-Sayed MA. Why gold nanoparticles are more precious than pretty gold: Noble metal surface plasmon resonance and its enhancement of the radiative and nonradiative properties of nanocrystals of different shapes. *Chemical Society Reviews*. 2006;35(3):209-17.

119. Jain PK, Lee KS, El-Sayed IH and El-Sayed MA. Calculated absorption and scattering properties of gold nanoparticles of different size, shape, and composition: Applications in biological imaging and biomedicine. *The Journal of Physical Chemistry B*. 2006;110(14):7238-7248.
120. Patra CR, Bhattacharya R, Mukhopadhyay D, Mukherjee P. Fabrication of gold nanoparticles for targeted therapy in pancreatic cancer. *Advanced Drug Delivery Reviews*. 2010;62(3):346-61.
121. Su KH, Wei QH, Zhang X, Mock JJ, Smith DR and Schultz S. Interparticle coupling effects on plasmon resonances of nanogold particles. *Nano Letters*. 2003;3(8):1087-1090.
122. Gold Nanoparticle Properties: Cytodiagnostics; 2019 [cited 2019 30 January]. Available from: <http://www.cytodiagnostics.com/store/pc/Gold-Nanoparticle-Properties-d2.htm>.
123. Radwan SH, Azzazy HME. Gold nanoparticles for molecular diagnostics. *Expert Review of Molecular Diagnostics*. 2009;9(5):511-24.
124. Altunbek M, Kuku G, Culha M. Gold nanoparticles in single-cell analysis for surface enhanced Raman scattering. *Analytical Chemistry*. 2016;21(12):1617-34.
125. Lee K-S, El-Sayed MA. Dependence of the enhanced optical scattering efficiency relative to that of absorption for gold metal nanorods on aspect ratio, size, end-cap shape, and medium refractive index. *The Journal of Physical Chemistry B*. 2005;109(43):20331-8.
126. Akhatova F, Danilushkina A, Kuku G, Saricam M, Culha M, Fakhrullin R. Simultaneous intracellular detection of plasmonic and non-plasmonic nanoparticles using dark-field hyperspectral microscopy. *Bulletin of the Chemical Society of Japan*. 2018;91(11):1640-5.

127. Wang H, Huff TB, Zweifel DA, He W, Low PS, Wei A, et al. *In vitro* and *in vivo* two-photon luminescence imaging of single gold nanorods. *Proceedings of the National Academy of Sciences of the United States of America*. 2005;102(44):15752-6.
128. Adler DC, Huang S-W, Huber R, Fujimoto JG. Photothermal detection of gold nanoparticles using phase-sensitive optical coherence tomography. *Optics Express*. 2008;16(7):4376-93.
129. Mallidi S, Larson T, Tam J, Joshi PP, Karpouk A, Sokolov K, et al. Multiwavelength photoacoustic imaging and plasmon resonance coupling of gold nanoparticles for selective detection of cancer. *Nano Letters*. 2009;9(8):2825-31.
130. Kumar A, Ma H, Zhang X, Huang K, Jin S, Liu J, et al. Gold nanoparticles functionalized with therapeutic and targeted peptides for cancer treatment. *Biomaterials*. 2012;33(4):1180-9.
131. Guo Y, Wang Z, Qu W, Shao H, Jiang X. Colorimetric detection of mercury, lead and copper ions simultaneously using protein-functionalized gold nanoparticles. *Biosensors and Bioelectronics*. 2011;26(10):4064-9.
132. Luo XL, Xu JJ, Du Y, Chen HY. A glucose biosensor based on chitosan–glucose oxidase–gold nanoparticles biocomposite formed by one-step electrodeposition. *Analytical Biochemistry*. 2004;334(2):284-9.
133. Hurst SJ, Lytton-Jean AKR, Mirkin CA. Maximizing DNA loading on a range of gold nanoparticle sizes. *Analytical Chemistry*. 2006;78(24):8313-8.
134. de la Fuente JM, Penadés S. Glyconanoparticles: Types, synthesis and applications in glycoscience, biomedicine and material science. *Biochimica et Biophysica Acta (BBA) - General Subjects*. 2006;1760(4):636-51.

135. Katz E, Sheeney-Haj-Ichia L, Willner I. Electrical contacting of glucose oxidase in a redox-active rotaxane configuration. *Angewandte Chemie International Edition*. 2004;43(25):3292-300.
136. Ulman A. Formation and structure of self-Assembled monolayers. *Chemical Reviews*. 1996;96(4):1533-1554.
137. Lévy R, Thanh NTK, Doty RC, Hussain I, Nichols RJ, Schiffrin DJ, et al. Rational and combinatorial design of peptide capping ligands for gold nanoparticles. *Journal of the American Chemical Society*. 2004;126(32):10076-84.
138. Love JC, Estroff LA, Kriebel JK, Nuzzo RG, Whitesides GM. Self-assembled monolayers of thiolates on metals as a form of nanotechnology. *Chemical Reviews*. 2005;105(4):1103-70.
139. Templeton AC, Wuelfing WP, Murray RW. Monolayer-protected cluster molecules. *Accounts of Chemical Research*. 2000;33(1):27-36.
140. Luedtke W, Landman U. Structure, dynamics, and thermodynamics of passivated gold nanocrystallites and their assemblies. *The Journal of Physical Chemistry B*. 1996;100(32):13323-9.
141. Hostetler MJ, Wingate JE, Zhong CJ, Harris JE, Vachet RW, Clark MR, et al. Alkanethiolate gold cluster molecules with core diameters from 1.5 to 5.2 nm: Core and monolayer properties as a function of core size. *Langmuir*. 1998;14(1):17-30.
142. Israelachvili JN. Intermolecular and surface forces. In: Israelachvili JN, editor. *Intermolecular and surface forces (Third Edition)*. Boston: Academic Press; 2011.
143. Wuelfing WP, Templeton AC, Hicks JF, Murray RW. Taylor dispersion measurements of monolayer protected clusters: a physicochemical determination of nanoparticle size. *Analytical Chemistry*. 1999;71(18):4069-74.

144. Di Marco M, Shamsuddin S, Razak KA, Aziz AA, Devaux C, Borghi E, et al. Overview of the main methods used to combine proteins with nanosystems: Absorption, bioconjugation, and encapsulation. *International Journal of Nanomedicine*. 2010;5(1):37-49.
145. Bartczak D, Kanaras AG. Preparation of peptide-functionalized gold nanoparticles using one pot EDC/Sulfo-NHS coupling. *Langmuir*. 2011;27(16):10119-23.
146. Gao J, Huang X, Liu H, Zan F, Ren J. Colloidal stability of gold nanoparticles modified with thiol compounds: bioconjugation and application in cancer cell imaging. *Langmuir*. 2012;28(9):4464-71.
147. Manson J, Kumar D, Meenan BJ, Dixon D. Polyethylene glycol functionalized gold nanoparticles: the influence of capping density on stability in various media. *Gold Bulletin*. 2011;44(2):99-105.
148. Tang XL, Jiang P, Ge GL, Tsuji M, Xie SS, Guo YJ. Poly (N-vinyl-2-pyrrolidone)(PVP)-capped dendritic gold nanoparticles by a one-step hydrothermal route and their high SERS effect. *Langmuir*. 2008;24(5):1763-8.
149. García-Calvo J, García-Calvo V, Vallejos SI, García FIC, Avella M, García J-M, et al. Surface coating by gold nanoparticles on functional polymers: On-demand portable catalysts for suzuki reactions. *ACS Applied Materials Interfaces*. 2016;8(38):24999-5004.
150. Mitra M, Kandalam M, Rangasamy J, Shankar B, Maheswari UK, Swaminathan S, et al. Novel epithelial cell adhesion molecule antibody conjugated polyethyleneimine-capped gold nanoparticles for enhanced and targeted small interfering RNA delivery to retinoblastoma cells. *Molecular Vision*. 2013;19(1):1029-38.

151. Shan C, Yang H, Han D, Zhang Q, Ivaska A, Niu L. Graphene/AuNPs/chitosan nanocomposites film for glucose biosensing. *Biosensors Bioelectronics*. 2010;25(5):1070-4.
152. Powers KW, Palazuelos M, Moudgil BM, Roberts SM. Characterization of the size, shape, and state of dispersion of nanoparticles for toxicological studies. *Nanotoxicology*. 2007;1(1):42-51.
153. Warheit DB. Debunking some misconceptions about nanotoxicology. *Nano Letters*. 2010;10(12):4777-82.
154. Krug HF, Wick P. Nanotoxicology: An interdisciplinary challenge. *Angewandte Chemie International Edition*. 2011;50(6):1260-78.
155. Aioub M, Austin LA, El-Sayed MA. Chapter 2 - Gold nanoparticles for cancer diagnostics, spectroscopic imaging, drug delivery, and plasmonic photothermal therapy. In: Grumezescu AM, editor. *Inorganic frameworks as smart nanomedicines*: William Andrew Publishing. 2018:41-91.
156. Peckys DB, de Jonge N. Visualizing gold nanoparticle uptake in live cells with liquid scanning transmission electron microscopy. *Nano Letters*. 2011;11(4):1733-8.
157. Jans H, Liu X, Austin L, Maes G, Huo Q. Dynamic light scattering as a powerful tool for gold nanoparticle bioconjugation and biomolecular binding studies. *Analytical Chemistry*. 2009;81(22):9425-32.
158. Rahme K, Nolan MT, Doody T, McGlacken GP, Morris MA, O'Driscoll C, et al. Highly stable PEGylated gold nanoparticles in water: applications in biology and catalysis. *RSC Advances*. 2013;3(43):21016-24.
159. Amendola V, Meneghetti M. Size evaluation of gold nanoparticles by UV-vis spectroscopy. *The Journal of Physical Chemistry C*. 2009;113(11):4277-85.

160. Dulkeith E, Ringler M, Klar TA, Feldmann J, Muñoz Javier A, Parak WJ. Gold nanoparticles quench fluorescence by phase induced radiative rate suppression. *Nano Letters*. 2005;5(4):585-9.
161. O'Brien MN, Jones MR, Brown KA, Mirkin CA. Universal noble metal nanoparticle seeds realized through iterative reductive growth and oxidative dissolution reactions. *Journal of the American Chemical Society*. 2014;136(21):7603-6.
162. Irrgang J, Ksienczyk J, Lapiene V, Niemeyer CM. Analysis of non-covalent bioconjugation of colloidal nanoparticles by means of atomic force microscopy and data clustering. *ChemPhysChem*. 2009;10(9-10):1483-91.
163. Ong Q, Luo Z, Stellacci F. Characterization of ligand shell for mixed-ligand coated gold nanoparticles. *Accounts of Chemical Research*. 2017;50(8):1911-9.
164. Karpel RL, da Silva Liberato M, Campeiro JD, Bergeon L, Szychowski B, Butler A, et al. Design and characterization of crotonamine-functionalized gold nanoparticles. *Colloids and Surfaces B: Biointerfaces*. 2018;163:1-8.
165. Mamat C, Pretze M, Gott M, Köckerling M. Synthesis, dynamic NMR characterization and XRD studies of novel N,N'-substituted piperazines for bioorthogonal labeling. *Beilstein Journal of Organic Chemistry*. 2016;12:2478-89.
166. Topete A, Alatorre-Meda M, Iglesias P, Villar-Alvarez EM, Barbosa S, Costoya JA, et al. Fluorescent drug-loaded, polymeric-based, branched gold nanoshells for localized multimodal therapy and imaging of tumoral cells. *ACS Nano*. 2014;8(3):2725-38.
167. Azadeh A, Bijan R, Tahereh Tohidi M, Zeinab B, Saeede Ranjbari B. Surface plasmon resonance coupled circular dichroism of DNA-gold nanorods assembly. *Journal of Physics D: Applied Physics*. 2014;47(31):315401-7.
168. Anand K, Gengan RM, Phulukdaree A, Chuturgoon A. Agroforestry waste *Moringa oleifera* petals mediated green synthesis of gold nanoparticles and their anti-cancer

- and catalytic activity. *Journal of Industrial and Engineering Chemistry*. 2015;21:1105-11.
169. Sharma R, Holland GP, Solomon VC, Zimmermann H, Schiffenhaus S, Amin SA, et al. NMR Characterization of ligand binding and exchange dynamics in triphenylphosphine-capped gold nanoparticles. *The Journal of Physical Chemistry C*. 2009;113(37):16387-93.
170. Aillon KL, Xie Y, El-Gendy N, Berkland CJ, Forrest ML. Effects of nanomaterial physicochemical properties on *in vivo* toxicity. *Advanced Drug Delivery Reviews*. 2009;61(6):457-66.
171. Juneja R, Roy I. *In vitro* techniques to investigate the oxidative effects of quantum dots. In: Armstrong D, Bharali DJ, editors. *Oxidative stress and nanotechnology: Methods and protocols*. Totowa, NJ: Humana Press; 2013: 265-77.
172. May S, Hirsch C, Rippl A, Bohmer N, Kaiser JP, Diener L, et al. Transient DNA damage following exposure to gold nanoparticles. *Nanoscale*. 2018;10(33):15723-35.
173. Zhang L, Gu F, Chan J, Wang A, Langer R, Farokhzad O. Nanoparticles in medicine: Therapeutic applications and developments. *Clinical Pharmacology & Therapeutics*. 2008;83(5):761-9.
174. Park MV, Neigh AM, Vermeulen JP, de la Fonteyne LJ, Verharen HW, Briedé JJ, et al. The effect of particle size on the cytotoxicity, inflammation, developmental toxicity and genotoxicity of silver nanoparticles. *Biomaterials*. 2011;32(36), 9810-9817.
175. Brigger I, Dubernet C, Couvreur P. Nanoparticles in cancer therapy and diagnosis. *Advanced Drug Delivery Reviews*. 2012;64:24-36.



176. Xia T, Kovoichich M, Brant J, Hotze M, Sempf J, Oberley T, et al. Comparison of the abilities of ambient and manufactured nanoparticles to induce cellular toxicity according to an oxidative stress paradigm. *Nano Letters*. 2006;6(8):1794-807.
177. Carlson C, Hussain SM, Schrand AM, K. Braydich-Stolle L, Hess KL, Jones RL, et al. Unique cellular interaction of silver nanoparticles: Size-dependent generation of reactive oxygen species. *The Journal of Physical Chemistry B*. 2008;112(43):13608-19.
178. Wagner SC, Roskamp M, Pallerla M, Araghi RR, Schlecht S, Kokschi B. Nanoparticle-induced folding and fibril formation of coiled-coil-based model peptides. *Small*. 2010;6(12):1321-8.
179. Gao W, Xu K, Ji L, Tang B. Effect of gold nanoparticles on glutathione depletion-induced hydrogen peroxide generation and apoptosis in HL7702 cells. *Toxicology Letters*. 2011;205(1):86-95.
180. Arvizo RR, Miranda OR, Thompson MA, Pabelick CM, Bhattacharya R, Robertson JD, et al. Effect of nanoparticle surface charge at the plasma membrane and beyond. *Nano Letters*. 2010;10(7):2543-8.
181. Yan J, Zhang G, Hu Y, Ma Y. Effect of luteolin on xanthine oxidase: Inhibition kinetics and interaction mechanism merging with docking simulation. *Food Chemistry*. 2013;141(4):3766-73.
182. Verma A, Stellacci F. Effect of surface properties on nanoparticle–cell interactions. *Small*. 2010;6(1):12-21.
183. Wilson CL, Natarajan V, Hayward SL, Khalimonchuk O, Kidambi S. Mitochondrial dysfunction and loss of glutamate uptake in primary astrocytes exposed to titanium dioxide nanoparticles. *Nanoscale*. 2015;7(44):18477-88.

184. Rauch J, Kolch W, Laurent S, Mahmoudi M. Big signals from small particles: Regulation of cell signaling pathways by nanoparticles. *Chemical Reviews*. 2013;113(5):3391-406.
185. Park EJ, Yi J, Chung KH, Ryu DY, Choi J, Park K. oxidative stress and apoptosis induced by titanium dioxide nanoparticles in cultured BEAS-2B cells. *Toxicology Letters*. 2008;180(3):222-9.
186. Bhabra G, Sood A, Fisher B, Cartwright L, Saunders M, Evans WH, et al. Nanoparticles can cause DNA damage across a cellular barrier. *Nature Nanotechnology*. 2009;4(12):876-83.
187. Chompoosor A, Saha K, Ghosh PS, Macarthy DJ, Miranda OR, Zhu ZJ, et al. The role of surface functionality on acute cytotoxicity, ROS generation and DNA damage by cationic gold nanoparticles. *Small*. 2010;6(20):2246-9.
188. Chen M, von Mikecz A. Formation of nucleoplasmic protein aggregates impairs nuclear function in response to SiO<sub>2</sub> nanoparticles. *Experimental Cell Research*. 2005;305(1):51-62.
189. AshaRani PV, Low Kah Mun G, Hande MP, Valiyaveettil S. Cytotoxicity and genotoxicity of silver nanoparticles in human cells. *ACS Nano*. 2009;3(2):279-90.
190. Mahmoudi M, Saeedi-Eslami SN, Shokrgozar MA, Azadmanesh K, Hassanlou M, Kalhor HR, et al. Cell "vision": Complementary factor of protein corona in nanotoxicology. *Nanoscale*. 2012;4(17):5461-8.
191. Jia YP, Ma BY, Wei XW, Qian ZY. The *in vitro* and *in vivo* toxicity of gold nanoparticles. *Chinese Chemical Letters*. 2017;28(4):691-702.
192. Boisselier E, Astruc D. Gold nanoparticles in nanomedicine: Preparations, imaging, diagnostics, therapies and toxicity. *Chemical Society Reviews*. 2009;38(6):1759-82.

193. Sung JH, Ji JH, Park JD, Song MY, Song KS, Ryu HR, et al. Subchronic inhalation toxicity of gold nanoparticles. *Particle Fibre Toxicology*. 2011;8(1):16-35.
194. Pan Y, Neuss S, Leifert A, Fischler M, Wen F, Simon U, et al. Size-dependent cytotoxicity of gold nanoparticles. *Small*. 2007;3(11):1941-9.
195. Goodman CM, McCusker CD, Yilmaz T, Rotello VM. Toxicity of gold nanoparticles functionalized with cationic and anionic side chains. *Bioconjugate Chemistry*. 2004;15(4):897-900.
196. Dube DH, Bertozzi CR. Glycans in cancer and inflammation – potential for therapeutics and diagnostics. *Nature Reviews Drug Discovery*. 2005;4(6):477–488.
197. Hakomori S. Glycosylation defining cancer malignancy: New wine in an old bottle. *Proceedings of the National Academy of Sciences of the United States of America*. 2002;99:10231–10233.
198. Kim YJ, Varki A. Perspectives on the significance of altered glycosylation of glycoproteins in cancer. *Glycoconjugate Journal*. 1997;14:569–576.
199. Rana S, Bajaj A, Mout R and Rotello VM. Monolayer coated gold nanoparticles for delivery applications. *Advanced Drug Delivery Reviews*. 2012;64(2): 200-216.
200. Rojo J, Diaz V, de la Fuente JM, Segura I, Barrientos AG, Riese HH, Bernade A, Penades S. Gold glyconanoparticles as new tools in antiadhesive therapy. *ChemBioChem*. 2004;5:291–297.
201. Ojeda R, de Paz JL, Barrientos AG, Martin-Lomas M, Penades S. Preparation of multifunctional glyconanoparticles as a platform for potential carbohydrate-based anticancer vaccines. *Carbohydrate Resources*. 2007;342,448–459.
202. Wang C, Li X, Wang Y, Liu Z, Fu L and Hu L. Enhancement of radiation effect and increase of apoptosis in lung cancer cells by thio-glucose-bound gold nanoparticles

- at megavoltage radiation energies. *Journal of Nanoparticle Research*. 2013;15(5):1642-53.
203. Suavarna S, Das U, Sunil KC, Mishra S, Sudarshan M, Saha KD, Dey S, Chakraborty A, Narayana Y. Synthesis of a novel glucose capped gold nanoparticle as a better theranostic candidate. *PloS One*. 2017;12(6):0178202-16.
204. Kawazoe N, Guoping C. Gold nanoparticles with different charge and moiety induce differential cell response on mesenchymal stem cell osteogenesis. *Biomaterials*. 2015;54: 226-236.
205. Arvizo RR, Miranda OR, Thompson M A, Pabelick CM, Bhattacharya R, Robertson J D et al. Effect of nanoparticle surface charge at the plasma membrane and beyond. *Nano Letters*. 2010;10(7): 2543-2548.
206. Goodman CM, McCusker CD, Yilmaz, T and Rotello VM. Toxicity of gold nanoparticles functionalized with cationic and anionic side chains. *Bioconjugate Chemistry*. 2004; 15(4): 897-900.
207. Nogueira DR, Mitjans M, Rolim C, Vinardell MP. Mechanisms underlying cytotoxicity induced by engineered nanomaterials: A review of *in vitro* studies. *Nanomaterials*. 2014;4(2):454-84.
208. Soenen SJ, De Cuyper M. Assessing cytotoxicity of (iron oxide-based) nanoparticles: an overview of different methods exemplified with cationic magnetoliposomes. *Contrast Media Molecular Imaging*. 2009;4(5):207-19.
209. Granchi D, Ciapetti G, Savarino L, Cavedagna D, Donati ME, Pizzoferrato A. Assessment of metal extract toxicity on human lymphocytes cultured *in vitro*. *Journal of Biomedical Materials Research: An Official Journal of The Society for Biomaterials and The Japanese Society for Biomaterials*. 1996;31(2):183-91.

210. Wörle-Knirsch JM, Pulskamp K, Krug HF. Oops they did it again! Carbon nanotubes hoax scientists in viability assays. *Nano Letters*. 2006;6(6):1261-8.
211. Suska F, Gretzer C, Esposito M, Emanuelsson L, Wennerberg A, Tengvall P, et al. *In vivo* cytokine secretion and NF- $\kappa$ B activation around titanium and copper implants. *Biomaterials*. 2005;26(5):519-27.
212. Kroll A, Pillukat MH, Hahn D, Schnekenburger J. Current *in vitro* methods in nanoparticle risk assessment: Limitations and challenges. *European Journal of Pharmaceutics Biopharmaceutics*. 2009;72(2):370-7.
213. Haiss W, Thanh NTK, Aveyard J, Fernig DG. Determination of size and concentration of gold nanoparticles from UV-Vis spectra. *Analytical Chemistry*. 2007;79(11):4215-21.
214. Bernardes GJ, Gamblin DP, Davis BG. The direct formation of glycosyl thiols from reducing sugars allows one-pot protein glycoconjugation. *Angewandte Chemie*. 2006;118(24):4111-5.
215. Tournebize J, Sapin-Minet A, Bartosz G, Leroy P, Boudier A. Pitfalls of assays devoted to evaluation of oxidative stress induced by inorganic nanoparticles. *Talanta*. 2013;116(1):753-63.
216. Ding L, Ji Q, Qian R, Cheng W, Ju H. Lectin-based nanoprobe functionalized with enzyme for highly sensitive electrochemical monitoring of dynamic carbohydrate expression on living cells. *Analytical Chemistry*. 2010;82(4):1292-8.
217. Reynolds AJ, Haines AH, Russell DA. Gold glyconanoparticles for mimics and measurement of metal ion-mediated carbohydrate-carbohydrate interactions. *Langmuir*. 2006;22(3):1156-63.
218. Lin CC, Yeh YC, Yang CY, Chen CL, Chen GF, Chen CC, et al. Selective binding of mannose-encapsulated gold nanoparticles to type 1 pili in *Escherichia coli*. *Journal of the American Chemical Society*. 2002;124(14):3508-9.

219. De la Fuente JM, Barrientos AG, Rojas TC, Rojo J, Cañada J, Fernández A, et al. Gold glyconanoparticles as water-soluble polyvalent models to study carbohydrate interactions. *Angewandte Chemie International Edition*. 2001;40(12):2257-61.
220. Thygesen MB, Jensen KJ. Carbohydrate-modified gold nanoparticles. *Carbohydrate Nanotechnology*. Hoboken, New Jersey: John Wiley & Sons; 2015.
221. Nakamoto K. Infrared and Raman spectra of inorganic and coordination compounds. *Handbook of Vibrational Spectroscopy*. Hoboken, New Jersey: John Wiley & Sons; 2006.
222. Talari ACS, Movasaghi Z, Rehman S, Rehman IU. Raman spectroscopy of biological tissues. *Applied Spectroscopy Reviews*. 2015;50(1):46-111.
223. Zong J, Cobb SL, Cameron NR. Peptide-functionalized gold nanoparticles: Versatile biomaterials for diagnostic and therapeutic applications. *Biomaterials Science*. 2017;5(5):872-86.
224. Agyei D, Danquah MK. Industrial-scale manufacturing of pharmaceutical-grade bioactive peptides. *Biotechnology Advances*. 2011;29(3):272-7.
225. Sperling RA, Rivera Gil P, Zhang F, Zanella M, Parak WJ. Biological applications of gold nanoparticles. *Chemical Society Reviews*. 2008;37(9):1896-908.
226. Ibuki Y, Toyooka T. Nanoparticle uptake measured by flow cytometry. In: Reineke J, editor. *Nanotoxicity: Methods and protocols*. Totowa, NJ: Humana Press; 2012:157-66.
227. Berridge MV, Tan AS. Trans-plasma membrane electron transport: A cellular assay for NADH- and NADPH-oxidase based on extracellular, superoxide-mediated reduction of the sulfonated tetrazolium salt WST-1. *Protoplasma*. 1998;205(1):74-82.

228. Vermes I, Haanen C, Steffens-Nakken H, Reutellingsperger C. A novel assay for apoptosis Flow cytometric detection of phosphatidylserine expression on early apoptotic cells using fluorescein labelled Annexin V. *Journal of Immunological Methods*. 1995;184(1):39-51.
229. Valiathan C, McFaline JL, Samson LD. A rapid survival assay to measure drug-induced cytotoxicity and cell cycle effects. *DNA Repair*. 2012;11(1):92-8.
230. Galbraith DW, Harkins KR, Maddox JM, Ayres NM, Sharma DP, Firoozabady E. Rapid flow cytometric analysis of the cell cycle in intact plant tissues. *Science*. 1983;220(4601):1049-51.
231. Munshi A, Hobbs M, Meyn RE. Clonogenic cell survival assay. *Chemosensitivity*. Switzerland: Springer; 2005:21-8.